On the road to personalized immunotherapy:

an unexpected journey

Chiara M. Cattaneo

On the road to personalized immunotherapy: an unexpected journey

The road goes ever on and on

Down the door where it began

Chiara Maria Cattaneo

ISBN: 978-94-6419-181-3
Printed by: Gildeprint
Layout: Chiara Maria Cattaneo
Cover design: Chiara Maria Cattaneo

On the road to personalized immunotherapy: an unexpected journey

Op weg naar gepersonaliseerde immunotherapie: een onverwachte reis

(met een samenvatting in het Nederlands)

Proefschrift

ter verkrijging van de graad van doctor aan de
Universiteit Utrecht
op gezag van de rector magnificus, prof.dr. H.R.B.M. Kummeling,
ingevolge het besluit van het college voor promoties
in het openbaar te verdedigen op
donderdag 15 april 2021 des middags te 12.45 uur

door

Chiara Maria Cattaneo

geboren op 17 oktober 1991
te Rho (MI), Italië

Promotor:

Prof. Dr. E. E. Voest

CONTENTS

1

General introduction and outline of the thesis

"As the anecdotes coalesce into data, there's another layer, too, a sense of paradigms shifting. Immunotherapy marks an entirely different way of treating cancer —by targeting the immune system, not the tumor itself. Oncologists, a grounded-in-reality bunch, say a corner has been turned and we won't be going back."

With these words, back in 2013, Science named cancer immunotherapy the scientific breakthrough of the year (Couzin-Frankel et al., 2013).

Cancer immunotherapy has truly transformed the treatment for advanced cancers. In the past decade immunotherapy successes moved from being extraordinary anecdotes - how unforgettable the result of a single treatment in the metastatic melanoma setting shown by (Chapman et al., 2015) - to solid and stable reality. Checkpoint inhibitors have successfully been used for treatment of multiple tumors: melanoma, non-small cell lung cancer, head and neck squamous cell carcinoma, renal cell carcinoma, Hodgkin lymphoma, urothelial cancer, gastric cancer, primary mediastinal B-cell lymphoma, Merkel cell carcinoma, hepatocellular cancer, cervical cancer and colorectal cancer, only to cite a few (Meric-Bernstam et al., 2020). However, even in the most immune-responsive tumor types, durable responses to checkpoint inhibitors are rare events, and success rates show great variation, spanning from ~15%, when used in monotherapy, to ~60%, when used in combination (Larkin et al, 2015; Larkin et al., 2019).

To further improve the efficacy of current cancer immunotherapies, it is necessary to find ways to predict which patient is most likely to respond or not to the treatment, who is likely to eventually relapse, which resistance mechanisms will arise and, most importantly, how to overcome these mechanisms. These challenges highlight the need for a pre-clinical model system that allows to interrogate the interaction between tumor cells and immune cells, in an unbiased manner, for the individual patient. In this thesis we embrace these challenges, trying to find a comprehensive solution.

In **chapter 2** we present a new model system for the study of direct interactions between tumor and immune cells for the individual patients. By co-culturing peripheral blood mononuclear lymphocytes (PBMCs) and autologous tumor organoids we are able to generate a tumor-reactive T cell population for a subset of colorectal cancer (CRC)

and non-small cell lung cancer (NSCLC) patients. We also demonstrate that these T cells are specifically able to recognize and kill tumor organoids, while ignoring autologous healthy colon or airway organoids. We speculate this new platform could be used as a new technology to dissect the different aspects of tumor-immune interactions and for the generation of a patient specific T cell product.

In **chapter 3** we describe the co-culture platform in details, highlighting the pros and cons of our method of generating tumor reactive T cells compared to pre-existing methods.

In **chapter 4** we investigate the physiological value of the platform, exploring the hypothesis that it could be used to predict patient response to immunotherapy. We show a perfect correlation between the ability to generate patient specific tumor-reactive T cells and clinical outcome of anti-PD-1 blocking therapy for a subset of colorectal cancer (CRC) and non-small cell lung cancer (NSCLC) patients. We also demonstrate the feasibility of using the co-culture system to monitor response to immunotherapy over time, during treatment. We also provide a critical point of view, highlighting the intrinsic limitations of the use of tumor organoids as a model system for such a predictive purpose.

In **chapter 5** we use the co-culture system to generate and analyze models of primary or acquired resistance to immunotherapy. To be specific, Werner helicase (WRN) has been identified as a specific synthetic-lethal target in mismatch repair-deficient (dMMR)/ microsatellite instability-high (MSI-H) cancers. We demonstrate that WRN dependency is retained in diverse models of primary and acquired resistance to targeted, chemo- and checkpoint inhibitor therapy, providing a strong rationale for the clinical development of specific small-molecule inhibitors targeting WRN.

In **chapter 6** we focus on a better understanding of the tumor-reactive T cells we induced through co-culturing tumor organoids and autologous PBMCs. We present HANSolo, HLA-Agnostic Neoantigen Screening, a high-throughput genetic platform for personalized discovery of $CD4^+$ and $CD8^+$ T cell-recognized (neo)antigens. We

demonstrate that, by using patient-matched immortalized B cells, that encode a library consisting of all non-synonymous tumor-specific mutations, as APCs, we can enable the unbiased screening of T cell specificities across all MHC-I and -II alleles of individual patients.

A general discussion of the research presented in this thesis can be found in **chapter 7.**

REFERENCES

- Couzin-Franjel J. (2013). Cancer Immunotherapy. Science. 342, 1432-1433
- Chapman P.B., D'angelo S.P. and Wholchock J.D. (2015) Rapid Eradication of a Bulky Melanoma Mass with One Dose of Immunotherapy. NEJM. 372, 2073-2074
- Larkin J., Chiarion-Sileni V., Gonzalez R., Grob J.J., et al. (2015) Combined Nivolumab and Ipilimumab or Monotherapy in Untreated Melanoma. NEJM. 373, 23-34.
- Larkin J., Chiarion-Sileni V., Gonzalez R., Grob J.J., et al. (2019) Five-Year Survival with Combined Nivolumab and Ipilimumab in Advanced Melanoma. NEJM. 381, 1535-1546
- Meric-Bernstam F., Larkin J., Tabernero J., Bonini C. (2020) Enhancing anti-tumour efficacy with immunotherapy combinations. The Lancet.

2

Generation of tumor-reactive T cells by coculture of peripheral blood lymphocytes and tumor organoids

Dijkstra K.K.[1,*], **Cattaneo C.M.[1,*]**, Weeber F.[1], Chalabi M.[1,2], van de Haar J.[1], Fanchi L.F.[1], Slagter M.[1], van Der Velden D.[1], Kaing S.[1], Kelderman S.[1], van Rooij N.[1], van Leerdam M.E.[2], Depla A.[3], Smit E.F.[4], Hartemink K.J.[5], de Groot R.[6], Wolders M.C.[6], Sachs N.[8], Snaebjornsson P.[9], Monkhorst K.[9], Haanen J.[1], Clevers H.[8,10,11], Schumacher T.N.[1,11,#], Voest E.E[1,#].

*,# These authors contributed equally

[1]Department of Molecular Oncology and Immunology, The Netherlands Cancer Institute, Antoni van Leeuwenhoek Hospital

[2]Department of Gastroenterologic Oncology, the Netherlands Cancer Institute, Antoni van Leeuwenhoek Hospital

[3]Department of Gastroenterology and Hepatology, EC Slotervaart Hospital

[4]Department of Thoracic Oncology, the Netherlands Cancer Institute, Antoni van Leeuwenhoek Hospital

[5]Department of Surgery, the Netherlands Cancer Institute, Antoni van Leeuwenhoek Hospital

[6]Department of Hematopoeisis, Sanquin Research

[7]Landsteiner Laboratory, Amsterdam Medical Center

[8]Hubrecht Institute, University Medical Center Utrecht

[9]Department of Pathology, the Netherlands Cancer Institute, Antoni van Leeuwenhoek Hospital

[10]Princess Maxima Center for Pediatric Oncology

[11]Oncode Institute

Cell. 2018 Sept 6; (174): 1-13

ABSTRACT

Cancer immunotherapies have shown substantial clinical activity for a subset of patients with epithelial cancers. Still, technological platforms to study cancer T-cell interactions for individual patients and understand determinants of responsiveness are presently lacking. Here, we establish and validate a platform to induce and analyse tumor-specific T cell responses to epithelial cancers in a personalized manner. We demonstrate that co-cultures of autologous tumor organoids and peripheral blood lymphocytes can be used to enrich tumor-reactive T cells from peripheral blood of patients with mismatch repair-deficient colorectal cancer and non-small-cell lung cancer. Furthermore, we demonstrate that these T cells can be used to assess the efficiency of killing of matched tumor organoids. This platform provides an unbiased strategy for the isolation of tumor-reactive T cells and provides a means by which to assess the sensitivity of tumor cells to T cell-mediated attack at the level of the individual patient.

INTRODUCTION

The use of antibodies against immune checkpoints, such as CTLA-4 and PD-1/PD-L1, has shown clear clinical benefit for patients with advanced cancer, including melanoma, non-small-cell lung cancer (NSCLC), and mismatch repair-deficient (dMMR) colorectal cancer (CRC) (Larkin et al., 2015; Garon et al., 2015; Borghaei et al., 2015; Le et al., 2015, 2017; Overman et al., 2017, 2018). Furthermore, the adoptive transfer of ex-vivo-expanded autologous tumor-infiltrating lymphocytes (TILs) has shown impressive clinical responses in melanoma (Rosenberg and Restifo, 2015) and an early clinical signal in cervical cancer (Stevanovic et al., 2015). Despite these encouraging results, a large fraction of patients does not respond to current immunotherapies. Treatment failure may be explained at many different levels that include a low number of immunogenic antigens, defective antigen presentation, and/or the expression of alternative immune checkpoint molecules (Blank et al., 2016; Dijkstra et al., 2016; Pitt et al., 2016; Sharma et al., 2017). Given the large variety in mechanisms of immune evasion by cancers, it is presently challenging to predict whether an individual patient will be sensitive to immunotherapy, what mechanism is likely to underlie resistance, and what alternative treatment could potentially overcome resistance. Platforms to allow the unbiased and systematic analysis of T cell-mediated tumor recognition on an individual patient basis would greatly contribute to our understanding of the critical factors that determine a successful anti-tumor immune response. Traditionally, ex vivo systems to analyze T cell-tumor interaction have to a very large extent focused on cutaneous melanoma, both because of the availability of robust approaches to expand tumor-infiltrating T cells for this disease (Rosenberg and Restifo, 2015), and because of the relative ease with which melanoma cell lines can be obtained. Importantly however, with the now widespread clinical development and clinical use of immunotherapy for major epithelial cancers, it is critical to develop technology to dissect T cell-mediated tumor recognition in these tumor types. Traditionally, this effort has been limited by both the low success rate of establishing primary tumor cell lines of epithelial cancers, such as NSCLC and CRC (success rate of 10% or lower) (Dangles-Marie et al., 2007; Zheng et al., 2011), and the limited feasibility of obtaining matched tumor-reactive T cell populations.

We set out to evaluate the feasibility of an autologous T cell tumor organoid co-culture platform for individual patients. Tumor organoids are three-dimensional primary tumor cell cultures that retain the histological and mutational features of the original tumor. Organoids can be established from surgical tumor resections (e.g., success rate for CRC of 60%–90%) (van de Wetering et al., 2015; Schütte et al., 2017) and from needle biopsies of metastases (e.g., success rate for CRC of ~70%) (Weeber et al., 2015). In this effort, we wished to establish two things: first, whether tumor-reactive T cells can be obtained by co-culture of peripheral blood lymphocytes (PBLs) with matched tumor organoids; second, whether such T cells can be used to assess the efficiency of tumor cell killing. The use of peripheral blood as a source of tumor-reactive T cells could provide an easily accessible alternative to TILs (Verdegaal et al., 2011).

Here, we provide proof of concept that co-culture of tumor organoids with PBLs forms an unbiased strategy to obtain tumor- reactive T cells from patients with dMMR CRC and NSCLC that kill tumor organoids from the same patient. Our findings provide proof of principle for the generation of a novel class of tumor-specific T cell products, derived from peripheral blood, and provide a means to assess the sensitivity of tumor cells to T cell-mediated attack at the level of the individual patient.

RESULTS

Characterization of a Panel of dMMR CRC Organoids

To evaluate whether tumor-reactive T cells can be enriched by PBLs via stimulation with autologous tumor organoids, we established a clinical protocol that allowed us to withdraw blood and obtain tumor tissue from patients with CRC. We focused on dMMR CRC, given its high mutational load (Cancer Genome Atlas Network, 2012) and frequent response to anti-PD-1 therapy (Le et al., 2015, 2017; Overman et al., 2017, 2018). Fresh tumor tissue was obtained from resection specimens or core-needle biopsies and used for the establishment of organoids. Mismatch repair deficiency was evaluated by an independent pathologist based on expression of mismatch repair proteins according to standard diagnostic criteria (Table 1; the STAR Methods). In line with prior data (Weeber et al., 2015; van de Wetering et al., 2015; Schütte et al., 2017), the success rate of growing tumor organoids from these sources was ~60%. Organoids were expanded from weekly to biweekly passaging at 1:2 to 1:5 split ratios and cryopreserved in low passage master bio-banks within 2–9 weeks after derivation. Organoids can be recovered from frozen stocks and expanded for several months to large numbers without loss of proliferative capacity. We established a panel of 15 tumor organoids from 13 different patients with dMMR CRC (Table 1).

The organoids morphologically reflected the original tumor they were derived from (Figures 1A and S1). Whole-exome sequencing (WES) of tumor organoids showed a high mutational burden (median = 1,938 non-synonymous mutations per tumor, range 795– 2,877), well in the range previously reported for hypermutated CRC (Figure 1B) (TCGA, 2012; Vogelstein et al., 2013). Mutations typically associated with hypermutated CRC (TCGA, 2012) were also represented in these organoids (Figure 1C; Table S1). Considering that loss of major histocompatibility complex class I (MHC class I) occurs in up to 60% of dMMR CRC (Dierssen et al., 2007), we screened for MHC class I expression after stimulation with interferon-gamma (IFNg) and identified 9 MHC-class-I-proficient tumor organoids from eight patients (62% of organoid samples) (Figures 1D and S2). MHC class I expression of tumor organoids correlated with immunohistochemistry data of MHC class I expression of the tumor they were derived from (Spearman $r = 0.78$; $p = 0.01$) (Figure S2; Table S2). Most importantly, tumor organoids classified as MHC class I deficient were always derived from MHC class I deficient tumors, indicating that loss of MHC class I is not a general feature of organoid culture.

Table 1. Characteristics of dMMR CRC Samples

Sample	Sex	Age	Tumor Location	Stage	Primary tumor/Metastasis	Biopsy/Resection	Absent MMR stains
CRC-1	F	68	Colon	I	Primary tumor	Resection	MLH1/PMS2
CRC-2	M	65	Colon	III	Primary tumor	Resection	MSH6
CRC-3	F	65	Colon	II	Primary tumor	Resection	MLH1/PMS2
CRC-4	F	75	Colon	III	Primary tumor	Resection	MLH1/PMS2
CRC-5	F	73	Rectum	I	Primary tumor	Resection	MSH6
CRC-6P	F	67	Colon	IV	Primary tumor	Resection	MLH1/PMS2
CRC-6M	F	67	Peritoneum	IV	Metastasis	Resection	MLH1/PMS2
CRC-7	F	62	Colon	III	Primary tumor	Resection	MLH1/PMS2
CRC-8P	M	50	Colon	IV	Primary tumor	Resection	MLH1/PMS2
CRC-8M	M	50	Liver	IV	Metastasis	Resection	MLH1/PMS2
CRC-9	F	51	Lymph node (neck)	IV	Metastasis	Biopsy	MLH1/PMS2
CRC-10	F	66	Liver	IV	Metastasis	Biopsy	MLH1/PMS2 (partial loss of MSH6)
CRC-11	F	66	Peritoneum	IV	Metastasis	Biopsy	MLH1/PMS2
CRC-12	F	74	Colon	I	Primary tumor	Resection	MLH1/PMS2
CRC-13	F	70	Colon	II	Primary tumor	Biopsy	MLH1/PMS2

MLH1, mutL homolog 1; PMS2, PMS1 homolog 2, mismatch repair system component; MSH2, mutS homolog 2; MSH6, mutS homolog 6; F, female; and M, male.

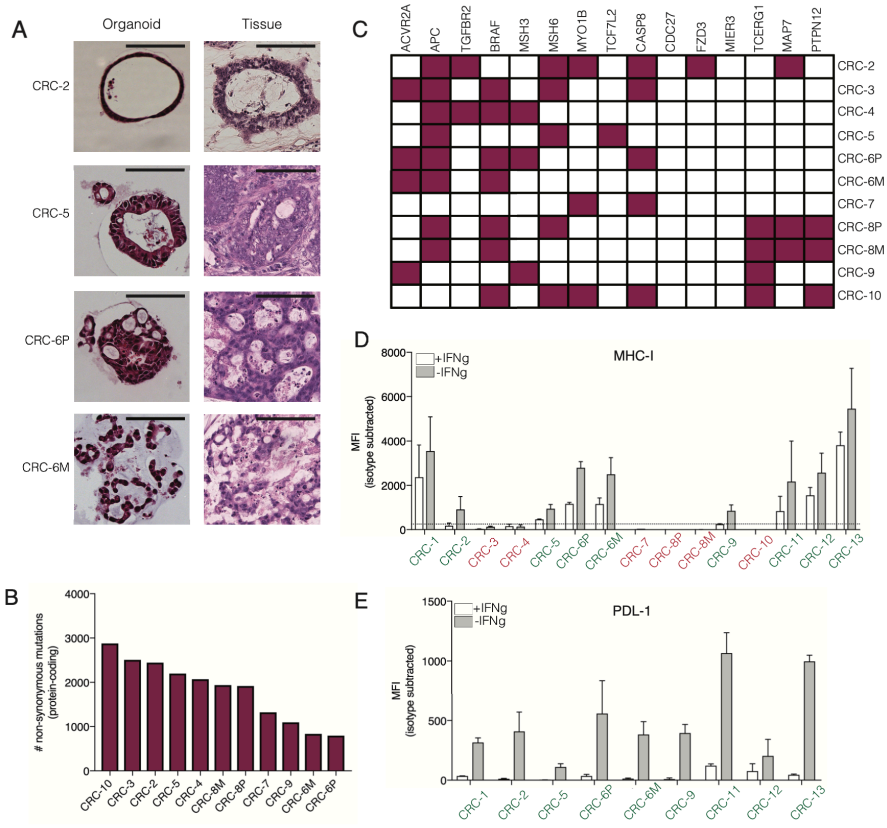

Figure 1. Characterization of a Panel of dMMR CRC Organoids

(A) H&E staining of tumor organoids and original tumor tissue. Organoids show morphology similar to the architecture of the original tumor. CRC-2 organoids demonstrates cystic tubules similar to mucin-filled glands of the primary tumor. CRC-5 organoids and primary tumors comprise tubular glands with layered epithelium. Organoid CRC-6P comprises complex cribriform glands also seen in the primary tumor. Organoid CRC-6M consists of irregular trabecular structures and poorly formed glands, similar to the metastasis. Scale bar 100 mm.

(B) Mutational load of tumor organoids as determined by the number of non-synonymous mutations per tumor exome.

(C) Mutation status of genes significantly mutated in hypermutated colorectal cancer according to TCGA (2012). Mutated genes are indicated in purple.

(D) Cell-surface MHC class I expression as determined by flow cytometry. Organoids were stimulated with 200 ng/mL IFNg for 24 hr or were left unstimulated. Bar graphs indicate median fluorescence intensity (MFI) of anti-HLA-A, -B, and -C-PE minus MFI of isotype control. Tumor organoids with MFI < 250 above isotype control (dashed line) were classified as MHC class I deficient (indicated in red). Error bars represent SEM of at least two independent experiments.

(E) Cell-surface PD-L1 expression as determined by flow cytometry. Organoids were stimulated with 200 ng/mL IFNg for 24 hr or were left unstimulated. Bar graphs indicate median fluorescence intensity (MFI) of anti-PD-L1-APC minus MFI of isotype control. Error bars represent SEM of at least two independent experiments.

Induction of Tumor Reactivity in Circulating T Cells by Co-culture with Autologous Tumor Organoids

To test whether tumor organoids may be used to obtain tumor reactive T cells, we selected MHC class I proficient tumor organoids and focused on the peripheral blood compartment as a source of T cells with a lower degree of exhaustion. Prior to co-culture with autologous T cells, tumor organoids were pre-stimulated with IFNg to enhance antigen presentation. IFNg exposure also led to the induction of PD-L1, a negative regulator of T cell activation (Figure 1E), and to counteract any inhibitory effect of PD-L1 during T cell activation, we added blocking antibodies to PD-1. Plate-bound anti-CD28 and interleukin-2 (IL-2) were added to provide co-stimulation and to support T cell proliferation, respectively. Peripheral blood mononuclear cells (PBMCs) were isolated from patients with dMMR CRC and stimulated weekly with autologous tumor organoids (Figure 2A). To tumor recognition by $CD8^+$ T cells was evaluated at baseline and after 2 weeks of co-culture by staining for IFNg and the degranulation marker CD107a.

In 4 of 8 (50%) patients with MHC class I^+ tumor organoids, stimulation with autologous tumor organoids induced both IFNg secretion and CD107a upregulation in $CD8^+$ T cells after 2 weeks of co-culture (Figures 2B and 2C). Responses were never observed in MHC class I deficient lines (data not shown). The magnitude of the response varied between patients, including small, but reproducible, responses of 1%–3% tumor-reactive $CD8^+$ T cells, as well as a patient of whom ~50% of all $CD8^+$ T cells were tumor reactive. The high reactivity for CRC-9 suggested the presence of a pre-existing tumor-reactive T cell population. We therefore evaluated tumor reactivity of T cells before co-culture with tumor organoids (i.e., directly after isolation from blood). A substantial proportion of $CD8^+$ T cells from patient CRC-9 was already tumor reactive, and this population increased approximately 10-fold in frequency upon 2 weeks of co-culture (Figures 2D and 2E). In contrast, T cells from patients CRC-11, CRC-12, and CRC-13 did not show any detectable tumor reactivity before organoid co-culture (Figure 2E), indicating that T cell organoid co-culture systems also can be used to expand previously undetectable tumor-reactive T cell populations.

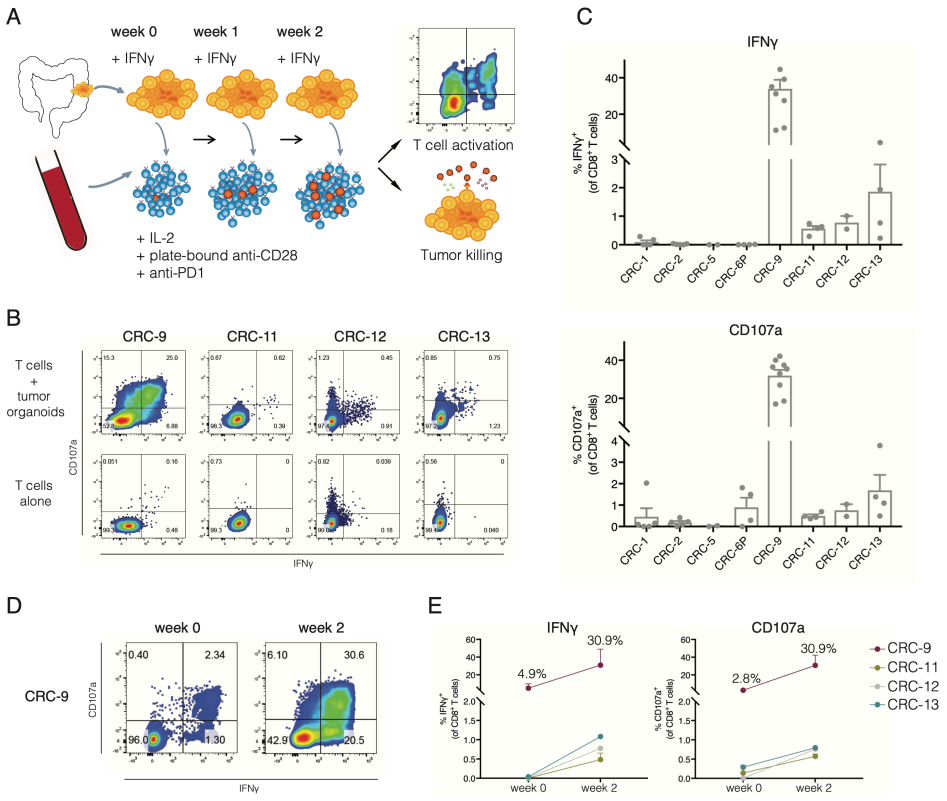

Figure 2. Induction of Tumor Reactivity in Circulating T Cells by Co-culture with Autologous Tumor Organoids

(A) Experimental workflow. Tumor organoids were established from dMMR CRC (resections or biopsies of primary tumors or metastases) and stimulated with IFNg for 24 hr prior to co-culture with peripheral blood lymphocytes (PBLs) from the same patient. PBLs were stimulated weekly with fresh tumor cells. After 2 weeks of co-culture, T cell effector functions and sensitivity of tumor organoids to T-cell-mediated killing were evaluated using flow cytometry.

(B) Representative flow cytometry plots gated on $CD8^+$ T cells tested for reactivity against autologous organoids after 2 weeks of co-culture with autologous tumor organoids.

(C) Quantification of organoid-induced IFNg production and CD107a cell-surface expression of $CD8^+$ T cells obtained by 2-week co-culture with autologous tumor organoids. The background (spontaneous IFNg production or CD107a expression) is subtracted from the signal. Error bars represent SEM of at least two biological replicates. Dots indicate biological replicates.

(D) Flow cytometry plots gated on $CD8^+$ T cells of patient CRC-9 tested for reactivity against autologous organoids directly after PBL isolation or after 2 weeks of co-culture with autologous tumor organoids.

(E) Quantification of organoid-induced IFNg production and CD107a cell-surface expression of $CD8^+$ T cells directly after PBL isolation or obtained by 2-week co-culture with autologous tumor organoids. The background (spontaneous IFNg production or CD107a expression) is subtracted from the signal. Error bars represent SEM of n = 2 biological replicates for CRC-9 and CRC-11. n = 1 for CRC-12 and CRC-13 (low amount of blood available).

Induction of Tumor Reactivity in Circulating T Cells from Patients with NSCLC

We then assessed whether our strategy to obtain tumor-reactive T cell populations from peripheral blood by organoid co-culture also could be applied to non-small cell lung cancer. As compared to dMMR CRC, mutational burden of NSCLC is approximately 5-fold lower (Vogelstein et al., 2013; Govindan et al., 2012) and response to PD-1/PD-L1 blockade is restricted to approximately 20% of patients (Garon et al., 2015; Borghaei et al., 2015). We generated NSCLC organoids from six patients (Figures 3A and S3; Table S3), using a method similar to that established for CRC organoids (Sachs et al., 2018). Sample NSCLC-3 contained both normal airway epithelial organoids that grew as cystic thin-walled organoids and tumor organoids that showed a more solid morphology. To select for tumor organoids, we applied the MDM-2 inhibitor Nutlin-3a to selectively grow out p53 mutant cells of this sample, resulting in a pure tumor organoid population (Sachs et al., 2018). All NSCLC organoids were MHC class I proficient and expressed various levels of PD-L1 upon stimulation with IFNg (Figures 3B and 3C). In vitro exposure of PBMCs to autologous tumor organoids resulted in the expansion of tumor-reactive $CD8^+$ populations in two of these patients after 2 weeks of co-culture (Figures 3D and 3E). Notably, none of these responses could be consistently detected before co-culture with organoids (Figure 3F). Collectively, these data demonstrate the feasibility of inducing patient-specific tumor-reactive T cell responses by co-culture of PBMCs and autologous tumor organoids in two epithelial tumor types.

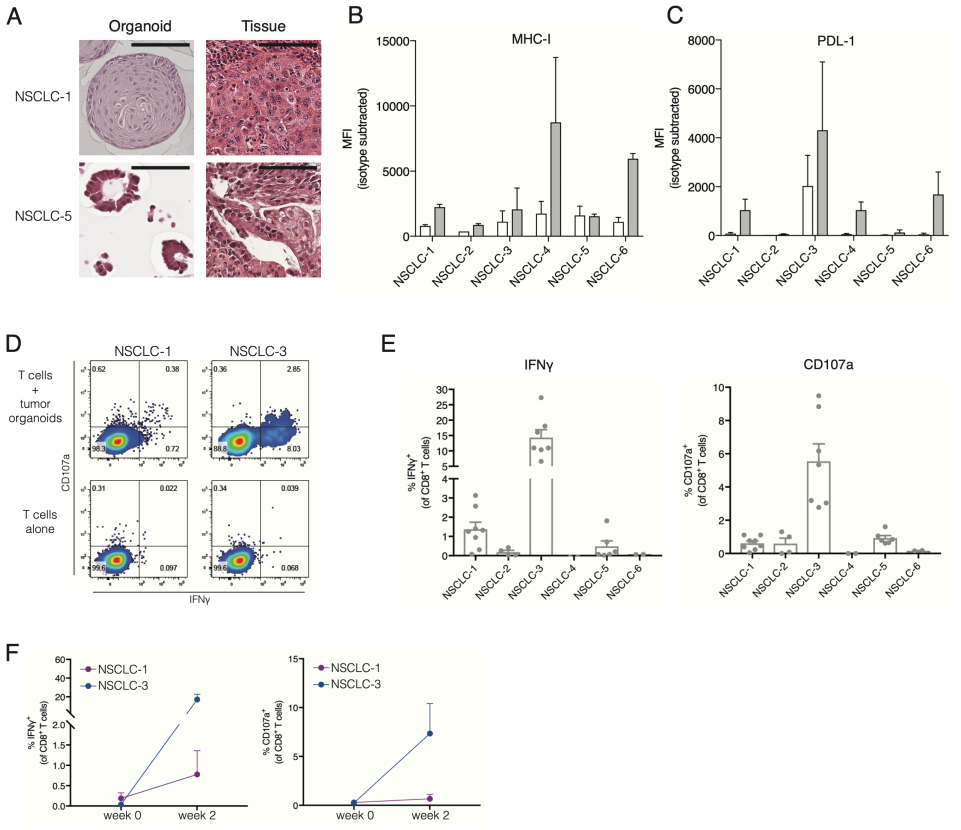

Figure 3. Induction of Tumor Reactivity in Circulating T Cells from Patients with NSCLC

(A) H&E staining of tumor organoids and original tumor tissue. Organoids show morphology similar to the architecture of the original tumor. NSCLC-1 organoids consists of large cells forming a solid mass, similar to the primary tumor. NSCLC-5 organoids comprise tubular glands similar to the original tumor. Scale bar, 100 mm.

(B and C) Cell-surface MHC class I **(B)** and PD-L1 **(C)** expression as determined by flow cytometry. Organoids were stimulated with 200 ng/mL IFNg for 24 hr or were left unstimulated. Bar graphs indicate median fluorescence intensity (MFI) of anti-HLA-A, -B, and -C-PE or anti-PD-L1-APC minus MFI of isotype control. Error bars represent SEM of two independent experiments.

(D) Representative flow cytometry plots gated on $CD8^+$ T cells tested for reactivity against autologous organoids after 2 weeks of co-culture with autologous tumor organoids.

(E) Quantification of organoid-induced IFNg production and CD107a cell-surface expression of $CD8^+$ T cells obtained by 2-week co-culture with autologous tumor organoids. The background (spontaneous IFNg production or CD107a expression) is subtracted from the signal. Error bars represent SEM of at least two biological replicates. Dots indicate biological replicates.

(F) Quantification of organoid-induced IFNg production and CD107a cell-surface expression of $CD8^+$ T cells directly after PBL isolation, or obtained by 2-week co-culture with autologous tumor organoids. The background (spontaneous IFNg production or CD107a expression) is subtracted from the signal. Error bars represent SEM of n = 2 biological replicates.

See also Figure S3 and Table S3.

Specificity of Organoid-Reactive T Cell Responses

Next, we wished to evaluate whether the T cell responses induced by organoid co-culture are truly tumor-specific or should be considered artefacts of organoid culture or IFNg treatment. Specifically, while IFNg enhances antigen processing and presentation, it also induces expression of a large number of genes, potentially allowing the formation of T cell responses against (self-)antigens not expressed in the absence of IFNg. To evaluate the dependency of tumor organoid-reactive T cell responses on IFNg, we compared T cell expression of the activation marker CD137 upon stimulation with tumor organoids that were either pre-stimulated with IFNg or left untreated (Figure 4A). For 4 of 5 cases tested, similar $CD8^+$ T cell responses were induced toward tumor organoids regardless of IFNg pre-stimulation. To more directly assess whether the induced T cell responses were specific for tumor antigens, we tested whether T cells also responded to stimulation with organoids of autologous normal tissue, and whether T cells responded to stimulation with autologous tumor digest. To assess restriction of T cell reactivity to the tumor organoid used for T cell induction, we established normal colon or lung organoids from two patients (CRC-12 and NSCLC-3). In addition, we generated organoids of a synchronous mismatch repair-proficient (pMMR) CRC from patient CRC-13, from whom we also had obtained a dMMR CRC. In all cases, T cell reactivity was restricted to the tumor organoids to which reactivity had been induced in the 2-week co-culture with PBLs; i.e., no reactivity was observed against normal tissue or pMMR CRC organoids (Figures 4B–4G).

For two patients, single-cell digest of autologous tumor tissue was also available to stimulate organoid-reactive T cells (Figures 4F and 4G). T cells reactive to NSCLC-3 organoids were also reactive to tumor digest but not to normal lung digest. In contrast, T cells reactive to NSCLC-1 organoids did not produce IFNg upon stimulation with autologous tumor digest. While the relatively low level of reactivity toward NSCLC-1 organoids limits the ability to detect subtle reactivity toward tumor digest, at this stage we cannot rule out that T cell reactivity in this sample is directed against organoid-specific targets. Taken together with the experiments in which we evaluated reactivity toward control organoids, this indicates that for 3 out of 4 tested samples, induced $CD8^+$ T cell responses are tumor specific. At the same time, it also highlights the value of generating organoids from non-malignant tissue that can serve as controls.

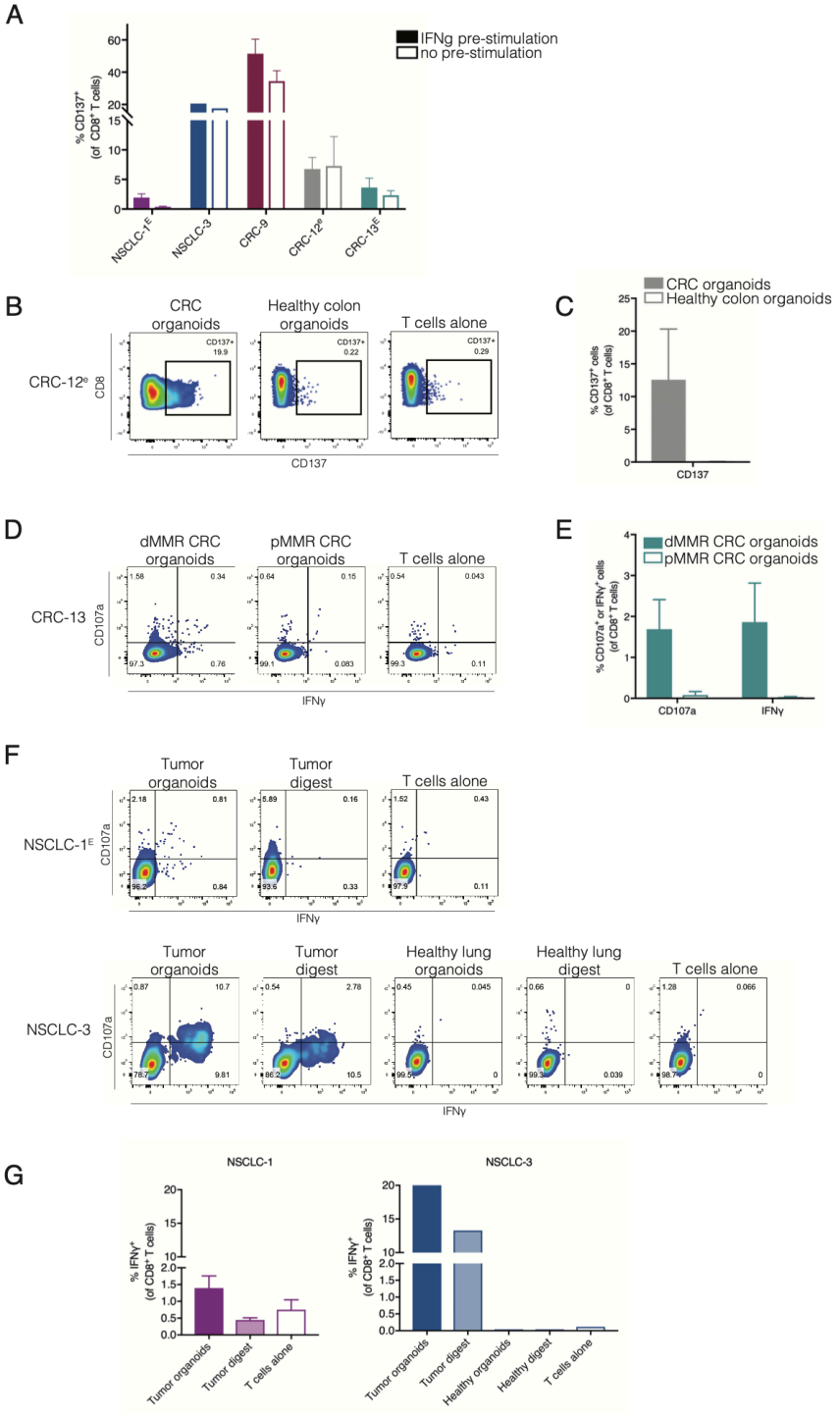
A
IFNg pre-stimulation
no pre-stimulation
% CD137+ (of CD8+ T cells)
NSCLC-1E
NSCLC-3
CRC-9
CRC-12e
CRC-13E
B
CRC organoids
Healthy colon organoids
T cells alone
CRC-12e
CD8
CD137
C
CRC organoids
Healthy colon organoids
% CD137+ cells (of CD8+ T cells)
CD137
D
dMMR CRC organoids
pMMR CRC organoids
T cells alone
CRC-13
CD107a
IFNγ
E
dMMR CRC organoids
pMMR CRC organoids
% CD107a+ or IFNγ+ cells (of CD8+ T cells)
CD107a
IFNγ
F
Tumor organoids
Tumor digest
T cells alone
NSCLC-1E
CD107a
IFNγ
Tumor organoids
Tumor digest
Healthy lung organoids
Healthy lung digest
T cells alone
NSCLC-3
CD107a
IFNγ
G
NSCLC-1
NSCLC-3
% IFNγ+ (of CD8+ T cells)
Tumor organoids
Tumor digest
T cells alone
Healthy organoids
Healthy digest

Figure 4. Specificity of Organoid-Reactive T Cell Responses *(previous page)*

T cells were obtained by 2-week co-culture with autologous tumor organoids. To increase the number of T cells available for testing, where indicated (by a lowercase "e") tumor-reactive T cells were then expanded using a rapid expansion protocol (Dudley et al., 2003), in some cases preceded by CD137-based enrichment of tumor-reactive cells (indicated by an uppercase "E").

(A) T cells were challenged with organoids pre-stimulated with 200 ng/mL IFNg for 24 hr or with unstimulated organoids and evaluated for expression of the activation marker CD137. Background (percentage positive cells in T cells alone control) is subtracted from signal. Error bars represent SEM of at least two biological replicates.
(B) Representative flow cytometry plots of $CD8^+$ T cells stimulated with either tumor organoids or healthy colon organoids.
(C) Quantification of CD137 expression by $CD8^+$ T cells stimulated with either tumor organoids or healthy colon organoids. The background (the percentage of positive cells in T cells alone control) is subtracted from the signal. Error bars represent SEM of two biological replicates. One of the replicates for T cells stimulated with tumor organoids is the same as data in (A).
(D) Representative flow cytometry plots of $CD8^+$ T cells obtained by 2 weeks of co-culture with mismatch repair-deficient (dMMR) CRC organoids that were restimulated with either dMMR CRC organoids or mismatch repair proficient (pMMR) CRC organoids.
(E) Quantification of organoid-induced IFNg production and CD107a cell-surface expression of $CD8^+$ T cells obtained by 2 weeks of co-culture with dMMR CRC organoids that were restimulated with either dMMR CRC organoids or mismatch repair-proficient (pMMR) CRC organoids. The background (the percentage of positive cells in T cells alone control) is subtracted from the signal. Error bars represent SEM of four biological replicates. Data for T cells stimulated with dMMR CRC organoids is the same as data in Figure 2A.
(F) Representative flow cytometry plots of $CD8^+$ T cells stimulated with tumor digest, normal lung digest, NSCLC organoids, or healthy lung organoids.
(G) Quantification of IFNg production of $CD8^+$ T cells stimulated with tumor digest, normal lung digest, NSCLC organoids, or healthy lung organoids. Error bars represent SD of technical replicates.

$CD4^+$ T Cell Reactivity against Xenogeneic Tissue Culture Components

In addition to tumor-reactive $CD8^+$ T cell responses, we occasionally observed variable $CD4^+$ T cell responses upon stimulation with tumor organoids (Figure 5A). Notably, $CD4^+$ T cell reactivity was not restricted to tumor organoids but, in some cases, was also directed against control organoids (organoids of normal tissue or of the synchronous pMMR CRC from patient CRC-13) (Figure 5B).

Since we only observed cross-reactivity to control organoids for $CD4^+$ T cells and not for $CD8^+$ T cells, we hypothesised this may be directed against foreign antigens derived from the extracellular environment. Organoids are cultured in murine basement

membrane matrix (Geltrex), and consequently murine antigens could be presented to T cells. To address this hypothesis, we generated monocyte-derived dendritic cells (moDCs) from PBMCs of patient CRC-1 and loaded these with Geltrex or irradiated cells of tumor or healthy colon organoids. CD4+ T cell reactivity was only induced by stimulation with Geltrex-loaded DCs or organoids grown in Geltrex (Figure 5C). In addition, reactivity was largely abolished when organoids were grown in the absence of Geltrex for 3 days (Figures 5C and S4). This indicates that co-culture systems involving Geltrex can induce CD4+ T cell reactivity not directed against tumor antigens. Of note, strategies to expand organoids in synthetic matrices have been described recently (Gjorevski et al., 2016) and could serve as alternatives to bypass reactivity to animal antigen.

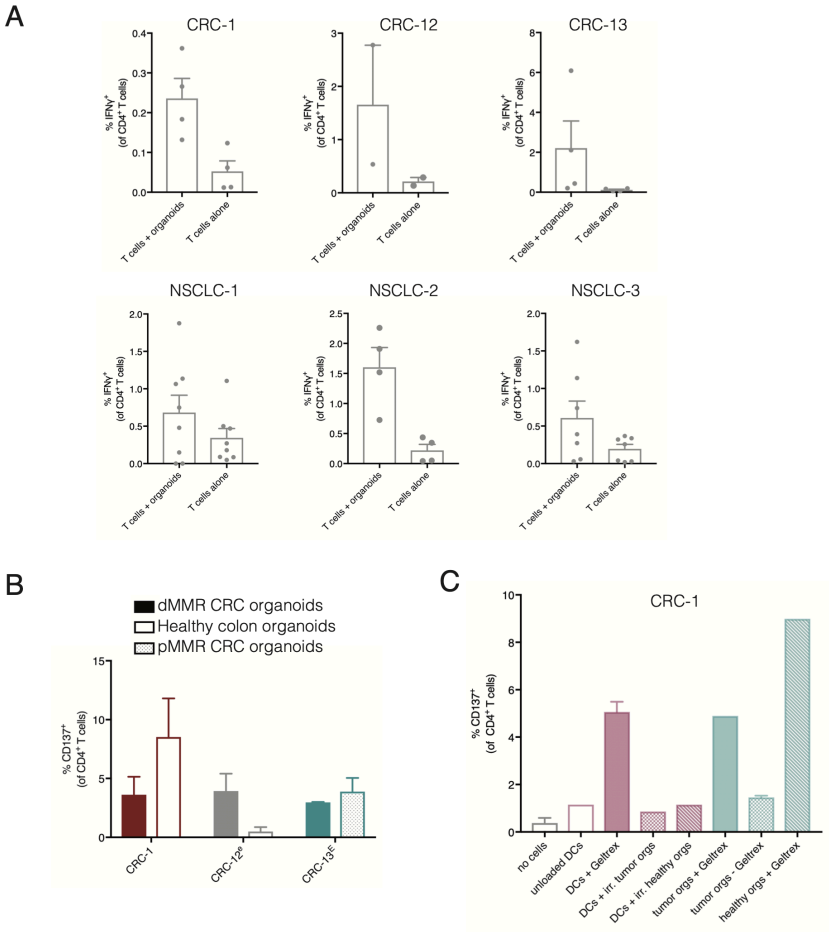

Figure 5. CD4+ T Cell Reactivity against Xenogeneic Tissue Culture Components *(previous page)*

(A) Quantification of spontaneous and organoid-induced IFNg production by CD4+ T cells obtained by 2-week co-culture with autologous tumor organoids. Error bars represent SEM of at least two biological replicates.
(B) Quantification of CD137 expression by CD4+ T cells upon re-stimulation with the tumor organoids used for induction, normal colon organoids, or organoids of a pMMR CRC from the same patient. T cells were obtained by 2-week co-culture with autologous tumor organoids and where indicated (lower case e) further expanded using a rapid expansion protocol (Dudley et al., 2003), in some cases preceded by CD137-based enrichment of tumor-reactive cells (indicated by upper case E). Error bars represent SEM of at least two biological replicates.
(C) Quantification of CD137 expression by CD4+ T cells after stimulation with unloaded or Geltrex-loaded monocyte-derived dendritic cells (DCs), irradiated tumor cells, or organoids cultured with or without Geltrex. Error bars represent SD of technical replicates.
See also Figure S4.

Tumor Organoids Are Killed by Autologous Tumor- Reactive T Cells

Having established the feasibility of inducing autologous tumor- reactive CD8+ T cell products for a substantial fraction of patients, we next aimed to determine whether organoid systems can be used to assess the efficiency of tumor destruction by these T cells. To determine this, we co-cultured tumor organoids with autologous tumor-reactive T cell populations for 3 days and quantified the number of live tumor cells by flow cytometry. For all samples tested, exposure of tumor organoids to autologous T cells led to substantially reduced survival (Figure 6A). Addition of MHC class I blocking antibodies rescued tumor cell survival, demonstrating the presence of an antigen-specific CD8+ T cell response. To visualize the cytolytic activity of tumor-reactive T cells, we labeled NSCLC-1 organoids with a tracer dye and imaged them in the presence of a green fluorescent apoptosis probe detecting active caspase-3/7 (‘‘caspase-3/7 probe’’) (Figure 6B). Addition of autologous T cells led to reduced organoid size and was accompanied by widespread apoptosis.

To provide further evidence for the specificity of tumor cell killing by autologous T cells, we performed parallel cytotoxicity assays with tumor and healthy organoids of NSCLC-3. T cells were first expanded using the rapid expansion protocol previously established to generate TIL products for adoptive cell therapy (Dudley et al., 2003). T cells efficiently

killed tumor organoids, but did not affect survival of healthy organoids (Figure 6C). Live imaging showed strong T cell mediated killing of tumor organoids when incubated with autologous T cells (Figures 6D and S5; Video S1). Tumor organoids cultured without T cells (Video S2) or with T cells in the presence of blocking antibodies to MHC class I and MHC class II (Video S3) continued to proliferate. As a further control, healthy organoids continued proliferation regardless of the presence of T cells (Figures 6D and S5; Videos S4, S5, and S6). Taken together, these data demonstrate that organoids of epithelial tumors can be used to measure the rate of destruction by autologous T cells. This platform should provide a valuable tool to compare e.g., the relative contribution of different cancer (neo-)antigens to T-cell-mediated killing, assess how the genetic state of tumor cells influences sensitivity to T cell attack, and test the value of strategies to increase this sensitivity.

Figure 6. Tumor Organoids Are Killed by Autologous Tumor-Reactive T Cells *(next page)*

T cells were obtained by 2-week co-culture with autologous tumor organoids and, where indicated (by a lowercase "e"), further expanded using a rapid expansion protocol (Dudley et al., 2003), in some cases preceded by CD137-based enrichment of tumor-reactive cells (indicated by an uppercase "E").

(A) Quantification of organoid killing upon T cell co-culture. After 3 days of co-culture, organoids were dissociated into single cells and the number of live cells was quantified using flow cytometry in the presence of counting beads. Where indicated, MHC class I or MHC class II was blocked with W6/32 or Tü39 antibody, respectively. *$p < 0.05$; **$p < 0.01$; and ***$p < 0.001$; Student's t test. Error bars represent SEM of at least two biological replicates.

(B) Microphotographs of NSCLC-1 organoids 72 hr after culture with or without T cells in the presence of a green-fluorescent caspase-3/7 probe. Organoids were labeled with CellTrace Yellow (magenta) prior to co-culture. Note the appearance of apoptotic (green) cells upon addition of T cells. When MHC class I and MHC class II are blocked, T cells cluster around organoids but apoptosis is reduced and organoids remain larger in size.

(C) Quantification of killing of matched NSCLC and healthy lung organoids like in (A). Representative of two independent experiments. Error bars represent SD of technical replicates.

(D) Microphotograph images of NSCLC-3 healthy and tumor organoids 72 hr after culture with or without T cells in the presence of a green fluorescent caspase-3/7 probe.

See also Figure S5 and Videos S1, S2, S3, S4, S5, and S6.

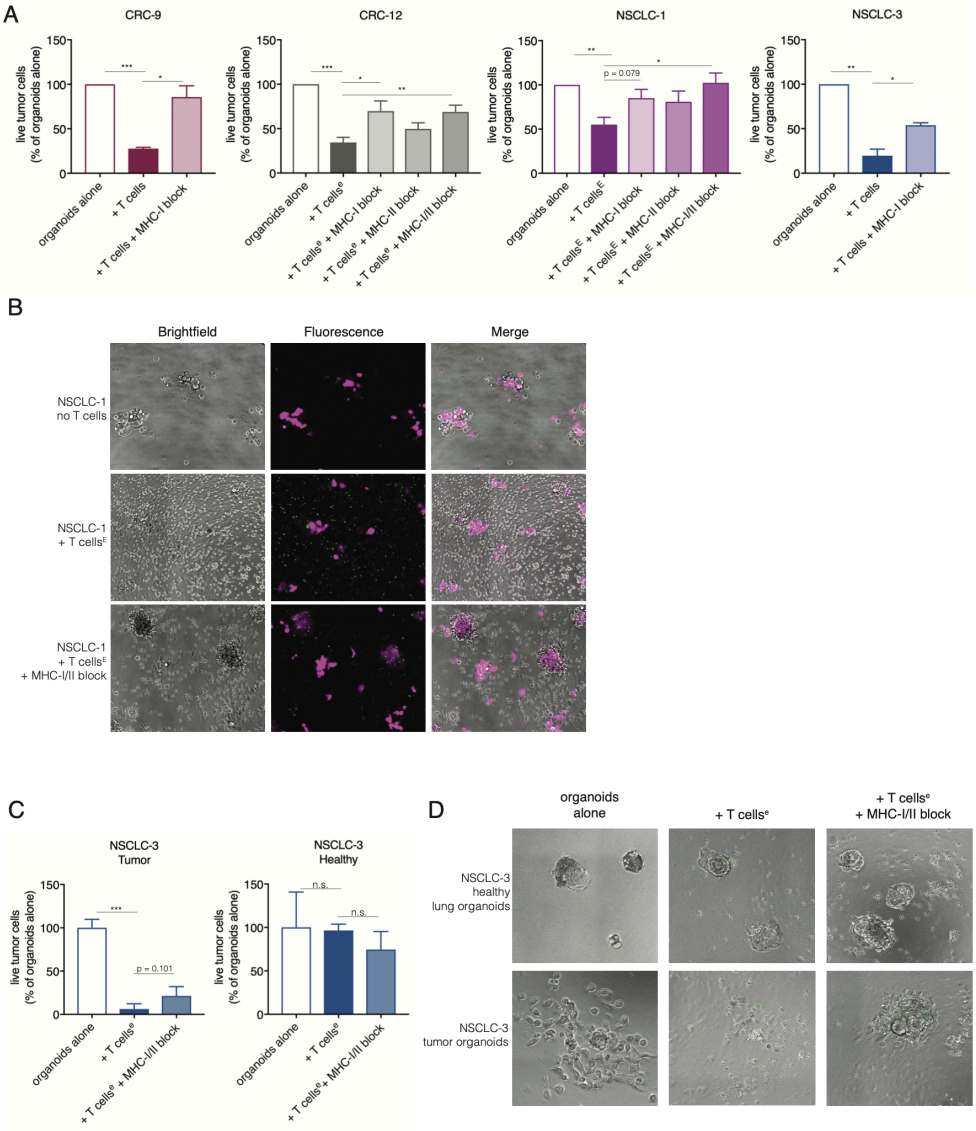
A
CRC-9
CRC-12
NSCLC-1
NSCLC-3
live tumor cells (% of organoids alone)
organoids alone
+ T cells
+ T cells + MHC-I block
+ T cells^e
+ T cells^e + MHC-I block
+ T cells^e + MHC-II block
+ T cells^e + MHC-I/II block
+ T cells^E
+ T cells^E + MHC-I block
+ T cells^E + MHC-II block
+ T cells^E + MHC-I/II block
p = 0.079
B
Brightfield
Fluorescence
Merge
NSCLC-1 no T cells
NSCLC-1 + T cells^E
NSCLC-1 + T cells^E + MHC-I/II block
C
NSCLC-3 Tumor
NSCLC-3 Healthy
p = 0.101
n.s.
D
organoids alone
+ T cells^e
+ T cells^e + MHC-I/II block
NSCLC-3 healthy lung organoids
NSCLC-3 tumor organoids

DISCUSSION

The potential of patient-specific model systems for the implementation of personalized medicine in the field of targeted therapy is considered substantial (Horvath et al., 2016). We speculate that the value of patient-specific model systems will prove even higher in the field of immuno-oncology, given the inherent diversity in human leukocyte antigen (HLA) and T cell receptor (TCR) genes, the private nature of the neo-antigens that are expressed in human cancers, and the multifactorial nature of T cell-mediated tumor destruction. Much of our current under- standing of T cell recognition in human cancer has been based on work in melanoma, and robust systems to measure T cell tumor interactions in a patient-specific manner, to our knowledge, have not been described for epithelial cancers. Here, we provide proof of concept that tumor organoids can be used to establish individualized ex vivo model systems to support T cell-based therapies and to study the interactions between T cells and tumor cells.

We foresee two major applications for the platform that we describe. First, it will allow one to mechanistically dissect the pathways that determine tumor cell sensitivity and resistance to immunotherapy. Second, it opens the possibility to generate patient-specific T cell products in an unbiased manner. With respect to the former application, the ability to establish tumor organoid cultures from very limited amounts of tumor (such as needle biopsies), combined with the potential to expand circulating tumor-reactive T cells from peripheral blood, provides a minimally invasive means to interrogate tumor sensitivity to immunotherapy for individual patients at different time points during treatment. For patients who initially responded to treatment with immune checkpoint inhibitors but eventually relapse, the establishment of co-cultures based on paired (tumor and blood) biopsies before and after relapse should provide a unique assay system for the functional dissection of the underlying cause of relapse. Recent genetic studies on paired biopsies have demonstrated the power of such an approach in a small set of melanoma patients who relapsed while on anti-PD1 therapy, demonstrating the acquisition of JAK1/2 mutations as one cause of resistance (Zaretsky et al., 2016). It will be of interest to determine whether a similar reduced sensitivity to T cell attack by JAK1/2 mutations is selected for in epithelial cancers. In addition to the analysis of natural and therapy-induced variation in tumor cell sensitivity to T cell pressure, there is increasing interest in the use of small molecules and antibodies to enhance tumor cell

sensitivity to T cell attack (Patel and Minn, 2018). Parallel tumor organoid T cell cultures in the presence or absence of drugs of interest should form a straightforward system to identify suitable candidates for combination with immunotherapy.

With respect to the second potential application of this platform, the ability to expand circulating tumor-reactive T cells by co-culture with tumor organoids provides a clinically feasible strategy for the generation of patient-specific T cell products for adoptive T cell transfer. This approach bypasses the need for samples derived from resection specimens to isolate tumor-infiltrating lymphocytes. In our proof-of-concept study, tumor-reactive $CD8^+$ T cells were expanded from the circulation in 4 of 13 dMMR CRC patients (31%) and 2 of 6 NSCLC patients (33%). When considering only MHC-class- I-proficient dMMR CRC patients, tumor-reactive T cells were induced in 50% of samples, highlighting the need for strategies to revert or bypass MHC I loss as an immune escape mechanism. Larger sample sizes will be needed to more precisely define the success rate of this approach. Moreover, in this study we focused on tumor types with high mutational load, and it will be important to determine whether the feasibility of inducing tumor-reactive T cells can be extended to poorly immunogenic cancers, such as mismatch repair-proficient CRC. In parallel, efforts to further increase the success rate of this approach could focus on strategies to improve selection of circulating tumor-reactive T cells, e.g., based on PD-1 expression by T cells (Gros et al., 2016).

METHODS

Contact for reagent and resource sharing

Further information and requests for resources and reagents should be directed to and will be fulfilled by the Lead Contact, Emile E. Voest (e.voest@nki.nl).

Reagents obtained under material transfer agreement (MTA) include producer lines for conditioned medium of Wnt-3a, Noggin (MTA with Hubrecht Institute) and R-spondin-1 (MTA with Calvin Kuo, Stanford).

Patient material, including tissue and organoids, are available for sharing as defined in the signed informed consent (study NL48824.031.14), and as approved by the local Medical Ethical Committee. Deposition of DNA sequencing data in publicly available databases is regulated by the informed consent that participants to this study signed.

Experimental model and subject details

Human subjects

The study (NL48824.031.14) was approved by the Medical Ethical Committee of the Netherlands Cancer Institute – Antoni van Leeuwenhoek hospital and written informed consent was obtained from all patients. Peripheral blood and tumor tissue were obtained from patients with a confirmed diagnosis of colorectal or non-small cell lung cancer. Mismatch repair deficiency was confirmed by immunohistochemical staining for the mismatch repair proteins MSH2, MSH6, MLH1 and PMS2 in routine assessment by a pathologist (see Immunohistochemistry).

Organoid culture

Tumor tissue was obtained either by 18G core needle biopsy or by surgical resection. Tumor tissue was processed for organoid culture within 24 hr. CRC organoids were established essentially as described in van de Wetering et al., 2015. NSCLC organoids were cultured using similar methods; a detailed protocol is accessible at bioRxiv (Sachs et al., 2018). Briefly, tumor tissue derived from needle biopsies was mechanically dissociated into small tumor pieces using needles and embedded in Geltrex (Geltrex

LDEV-free reduced growth factor basement membrane extract, GIBCO). Tumor tissue derived from surgical resections was cut into small pieces and enzymatically digested using 1.5 mg/mL collagenase II (Sigma-Aldrich), 10 mg/mL hyaluronidase type IV (Sigma-Aldrich) and 10 mM Y-27632 (Sigma-Aldrich) before embedding in Geltrex. After Geltrex solidification for 20 min at 37 C, cells were overlaid with human CRC or non-small cell lung cancer (NSCLC) organoid medium (van de Wetering et al., 2015; Sachs et al., 2018). Human CRC organoids medium is composed of Ad-DF+++ (Advanced DMEM/F12 (GIBCO) supplemented with 2 mM Ultra- glutamine I (Lonza), 10 mM HEPES (GIBCO), and 100/100 U/ml Pencillin/Streptomycin (GIBCO)), 10% Noggin-conditioned medium, 20% R-spondin1-conditioned medium, 1x B27 supplement without vitamin A (GIBCO), 1.25 mM N-Acetylcysteine (Sigma-Aldrich), 10 mM nicotinamide (Sigma-Aldrich), 50 ng/mL human recombinant EGF (Peprotech), 500 nM A83-01 (Tocris), 3 mM SB202190 (Cayman Chemicals) and 10 nM prostaglandin E2 (Cayman Chemicals). Human wild-type colon organoid medium is identical to CRC medium, except that 50% Wnt3a-conditioned medium is added. Human NSCLC and normal airway organoid medium is composed of Ad-DF+++, 10% Noggin-conditioned medium, 10% R-spondin1-conditioned medium, 1x B27 supplement, 1.25 mM N-Acetylcystein, 10 mM nicotinamide, 25 ng/mL human recombinant FGF-7 (Peprotech), 100 ng/mL human recombinant FGF-10 (Peprotech), 500 nM A83-01, 1 mM SB202190, 5 mM Y-27632. R-spondin1-conditioned medium was produced from 293T-HA-Rspol-Fc producer cell lines (obtained from C. Kuo, Stanford), Wnt3a-conditioned medium from L-Wnt3a cells and Noggin-conditioned medium from HEK293-mNoggin-Fc cell lines (both kind gift from J. den Hertog, Utrecht). In the first two weeks of organoid culture, 1x Primocin (Invivogen) was added to prevent microbial contamination. Organoids were passaged approximately every week by incubating in TrypLE Express (GIBCO) for 5-10 min at 37 C to dissociate organoids to single cells and replating in fresh Geltrex. After passaging, 10 mM Y-27632 was added to CRC medium for the first 2-3 days. Organoids were cryopreserved in 10% FCS/DMSO or Recovery Cell Culture Freezing Medium (ThermoFisher) as master and working biobanks. Organoids < passage 30 were used in experiments. To rule out overgrowth by healthy lung organoids for NSCLC organoids derived from intrapulmonal lesions, hematoxylin and eosin stained sections of tumor organoids (see Immunohistochemistry) were evaluated by a pathologist to determine tumor status of organoids. To prevent overgrowth by healthy lung organoids, for patient NSCLC-3, p53

mutant organoids were selected by culturing in the presence of 5 mM Nutlin-3 (Cayman Chemicals). Organoids were regularly checked for mycoplasma contamination using the MycoAlert Mycoplasma Detection Kit (Lonza).

Peripheral blood lymphocytes

The peripheral blood mononuclear cells (PBMC) fraction was isolated from peripheral blood by Ficoll-Paque density gradient separation and cryopreserved until later use.

Organoid line authentication

DNA was isolated from master and working biobanks of organoids and patient-matched peripheral blood using a DNEasy kit (QIAGEN). Samples were genotyped using a Taqman-based SNParray targeting 26 SNPs (Hartwig Medical Foundation, Amsterdam). An identity score was calculated as described by (Tanabe et al., 1999) and (Liang-Chu et al., 2015). When comparing two samples, for each locus where both samples had called alleles, the number of distinct alleles in each individual sample, as well as the number of shared alleles was computed. These were summed across all loci and an identity score was computed defined as

$$\frac{2x \text{ the number of shared alleles}}{\text{total distinct alleles sample 1} + \text{total distinct alleles sample 2}}$$

A threshold of 0.9 of the summed identity score was defined as a cut-off and organoid lines that did not match to autologous blood were discarded.
Two samples (NSCLC-3 and NSCLC-5), showed identity scores < 0.9 in comparison with autologous blood, but showed exclusively heterozygous to homozygous changes in the tumor, suggesting loss of heterozygosity due to copy number aberrations. We authenticated these lines by performing HLA-typing by PCR (Sanquin, Amsterdam) or based on whole genome sequencing data by Optitype (Szolek et al., 2014).

Methods details

Organoid – lymphocyte co-culture

Culture media for PBMC was composed of RPMI 1640 (GIBCO), supplemented with 2 mM Ultraglutamine I, 1:100 penicillin/streptomycin and 10% male human AB serum (Sigma-Aldrich) (''T cell medium''). One day before co-culture, PBMC were thawed in pre-warmed (37 C) T cell medium (human serum was replaced with FCS during thawing) and incubated for 15 min with 25 U/mL benzonase (Merck). After washing, cells were resuspended at 2-3*10^6 cells/mL in T cell medium supplemented with 150 U/mL IL-2 and cultured overnight at 37 C. Prior to co-culture, tumor organoids were stimulated overnight with 200 ng/mL human recombinant IFNg (Peprotech). 96-well U-bottom plates were coated with 5 mg/mL anti-CD28 (clone CD28.2, eBioscience) and kept overnight at 4 C.

The next day, tumor organoids were dissociated to single cells with TrypLE Express and resuspended in T cell medium. Anti-CD28- coated plates were washed twice with PBS and PBMC were seeded at a density of 10^5 cells/well and stimulated with single cell-dissociated organoids at a 20:1 effector:target ratio. Co-cultures were performed in the presence of 150 U/mL IL-2 and 20 mg/mL anti-PD-1-blocking antibody (kindly donated by Merus, Utrecht). Half of the medium, including IL-2 and anti-PD-1, was refreshed two to three times per week. Every week, PBMC were collected, counted, and replated at 10^5 cells/well, and re-stimulated with fresh tumor organoids.

Flow cytometry

For evaluation of MHC-I and PD-L1 expression by tumor organoids, organoids were dissociated to single cells using TrypLE Express, with or without overnight pre-incubation with 200 ng/mL IFNg. Tumor cells were washed in FACS buffer (PBS + 5 mM EDTA + 1% bovine serum antigen) and stained with mouse anti-human HLA-A,B,C-PE (BD Bioscience) or anti-CD274-APC (eBioscience) anti- bodies, or isotype controls (PE mouse IgG1, kappa (BD) and APC mouse IgG1 kappa (eBioscience)) for 30 min at 4 C. Cells were washed twice with FACS buffer and DAPI was added to exclude dead cells prior to recording at a Becton Dickinson Fortessa or LSRII flow cytometer.

For evaluation of tumor reactivity, 10^5 PBMC were restimulated with tumor organoids at a 2:1 effector: target ratio and seeded in anti-CD28-coated plates in the presence of 20

mg/mL anti-PD-1 and co-cultured for 5 hr. Mouse anti-human CD107a-PE antibodies (BD) were added at the start of co-culture. Golgi-Plug (1:1000, BD) and Golgi-Stop (1:1500, BD) was added after 1 hr and co-culture continued for an additional 4 hr. Cells were washed twice in FACS buffer and stained with the following antibodies: anti-CD3-PerCP-Cy5.5 (BD), anti-CD4-FITC (BD), anti-CD8-BV421 (BD), and near-IR viability dye (Life technologies) for 30 min at 4 C. Cells were washed twice in FACS buffer, fixed, and stained for intracellular IFNg (anti-IFNg-APC, BD) using the Cytofix/Cytoperm kit (BD), according to manufacturer's instructions. PBMC stimulated with 50 ng/mL phorbol 12-myristate 13-acetate (PMA, Sigma- Aldrich) and 1 mg/mL ionomycin (Sigma-Aldrich) served as positive controls and PBMC cultured without tumor stimulation as negative controls. In some experiments, PBMC and tumor cells were co-cultured for 24 hr before staining with anti-CD3- PerCP-Cy5.5, anti-CD4-FITC, anti-CD8-PB, anti-CD137-APC (BD) and near-IR viability dye.

Rapid expansion of unselected T cells or tumor-reactive sublines

T cells from patient CRC-12, NSCLC-1 and NSCLC-3 were co-cultured for two weeks with autologous tumor organoids and expanded for two weeks in the presence of irradiated (40 Gy, Gamma Cell-40) pooled PBMC from three healthy donors (1:200 T cell:feeder ratio), 3000 U/mL IL-2 and 30 ng/mL anti-human CD3 (OKT-3, eBioscience). After 5-7 days, medium, including IL-2, was refreshed every 2-3 days. For expansion of tumor-reactive sublines, T cells were sorted on the basis of CD137 expression 24 hours after stimulation with tumor organoids, using a CD137 Microbead Kit (Miltenyi) following manufacturer's instructions and expanded as described above.

Organoid killing assays

To determine the sensitivity of tumor organoids to T cell-mediated killing, flat-bottom non-tissue culture-treated plates were coated with 5 mg/mL anti-CD28 and kept at 4 C overnight prior to co-culture. Organoids were stimulated with 200 ng/mL IFNg for 24h prior to co-culture. The next day, organoids were isolated from Geltrex by density gradient separation. Part of the organoids were dissociated to single cells and counted using a hemocytometer. This was used to infer the number of tumor cells per tumor organoid to allow co-culture of organoids and T cells at a 5:1 effector:target ratio. Next, tumor organoids were resuspended in T cell medium. T cells were collected after two

weeks of co-culture with tumor organoids and resuspended in T cell medium. Anti-CD28-coated plates were washed twice with PBS and organoids were seeded in triplicate without T cells or with $5*10^5$ autologous T cells obtained by two weeks of organoid co-culture. To block MHC class I and II, organoids were pre-incubated for 30 min with 50 mg/mL pan-MHC-I blocking antibody W6/32, or pan-MHC-II blocking antibody Tü39 (blocking antibody remained present throughout the co-culture). To facilitate visualization, organoids were in some cases stained with 1 mM of CellTrace Yellow (Invitrogen) and T cells with 100 nM CellTrace FarRed (Invitrogen) in PBS for 20 min at 37 C followed by blocking with human serum and washing in PBS. At the start of co-culture, a green-fluorescent caspase 3/7 probe that binds DNA upon cleavage by caspase 3/7 (referred to as ''caspase 3/7 probe'') (Biotium) was added at 1:2000 dilution to visualize cells undergoing apoptosis.

After 3 days of co-culture, organoids and PBMC were collected and dissociated into single cells with TrypLE Express, combined with regular resuspension and vortexing. Care was taken to limit the reaction until the moment organoids were fully dissociated. 7.46 mm AccuCount blank counting beads (Spherotech) were added to each well, cells were washed in FACS buffer and stained with anti-CD3-AF700 (Invitrogen) and anti-CD326-PE-Cy7 (Biolegend) for 30 min at 4 C. Organoids or T cells labeled with CellTrace dyes were not stained with antibodies. Cells were washed twice and stained with DAPI to mark dead cells prior to flow cytometric recording.

Immunohistochemistry

Organoids were recovered from Geltrex by density gradient separation (centrifugation at 300 g, 5 min, 4 C in cold basal organoid culture medium) when they reached an approximate diameter of 100 mm, fixed in 4% paraformaldehyde for 30 min at room temperature or overnight at 4 C, pelleted, and embedded in paraffin blocks. In some cases, organoids were isolated from Geltrex using 10 mg/mL dispase type II (Sigma) or Cell Recovery Solution (Corning). Immunohistochemistry of samples was performed on a BenchMark Ultra autostainer (Ventana Medical Systems). Briefly, paraffin sections were cut at 3 mm, heated at 75C for 28 min and deparaffinized in the instrument with EZ prep solution (Ventana Medical Systems). Heat-induced antigen retrieval was carried out using Cell Conditioning 1 (CC1, Ventana Medical Systems) for 32 min at 95C. P53 was detected using clone DO-7 (1:7000 dilution, 32 min at 37C, Agilent Technologies), and

MHC-I using clone HCA2 (1:5000 dilution, 32 min at 37C, Nordic Mubio) and clone HC10 (1:20000 dilution, 32 min at 37C, Nordic Mubio). For HCA2 signal amplification was applied using the Optiview Amplification Kit (4 min, Ventana Medical Systems). Bound antibody was detected using the OptiView DAB Detection Kit (Ventana Medical Systems). Slides were counterstained with Hematoxylin and Bluing Reagent (Ventana Medical Systems). For assessment of mismatch repair status, immunohistochemistry was performed according to standard protocols for the Ventana automated immunostainer. (MLH1, clone M1, Roche; MSH2, clone G219-1129, Roche; MSH6, clone EP49, Abcam; PMS2, clone EP51, Agilent Technologies).

Whole exome DNA sequencing

At least 200 ng of genomic DNA was extracted from CRC organoids and patient-matched PBMC using a DNEasy kit (QIAGEN). After exome capture (Integrated DNA Technologies probe set), whole-exome sequencing was performed on an Illumina HiSeq DNA analyzer using 100 bp paired-end reads.

T cell recognition assays of Geltrex

Tumor or healthy organoids were isolated from Geltrex using 10 mg/mL dispase type II (Sigma) and cultured in organoid medium for three days with 10 mM Y-27632 (Cayman Chemicals) in 6-well plates. In some cases, two days later, 100 mL/well Geltrex was added to organoids. After three days, organoids were used in tumor recognition assays as described under flow cytometry. Monocytes were sorted on the basis of CD14 on a MoFlo Astrios flow cytometer and cultured in GMP DC medium (CellGenix) with 800 U/mL GM-CSF and 400 U/mL IL-4 (CellGenix). Five days after differentiation, DCs were matured with GM-CSF, IL-4, IL-6 (1 ng/mL), IL-1b (1 ng/mL), TNFa (1 ng/mL) and PGE1 (0.5 mg/mL). DCs were seeded at $2*10^4$ cells/well and loaded with Geltrex or 40 Gy dissociated and irradiated tumor or healthy organoid cells ($2*10^4$ cells/well). Two days later, $1*10^5$ T cells were added to each well and cultured for 24h. T cells were assayed for CD137 expression as described under flow cytometry.

Quantification and statistical analysis

Whole exome DNA sequencing data

Reads were aligned to a reference genome (GRCh38). Somatic single nucleotide variations and indels were called using Somatic Sniper (Larson et al., 2012) and SomaticIndelDetector (GATK; McKenna et al., 2010), respectively. Variants were annotated using snpEff (Cingolani et al., 2012), version 4.3. Extra-exonic and synonymous variants were removed from further analyses. Mutational load was defined as the number of non-synonymous mutations per tumor exome. The occurrence of mutations in genes recurrently mutated in hypermutated CRC was based on the top 15 most frequently recurring significantly mutated genes according to TCGA 2012.

Live imaging

During organoid killing assays, cells were co-cultured for 3 days and imaged using a charge coupled device (CCD) camera equipped with a Zeiss AxioCam MRm camera fitted to a Zeiss Axio Observer Z1 inverted microscope. Tile scans were performed every 20 to 30 min followed by tile stitching after recording using Zen software. Videos were generated from the stitched tiles or regions of interest after background subtraction using ImageJ software version 1.50i (Schneider et al., 2012).

Flow cytometry

Flow cytometry data were analyzed using FlowJo version 10.

Statistical analysis

Data were analyzed using GraphPad Prism version 7. Group sizes and definition of error bars is indicated in figure legends. In indicated bar graphs, background is subtracted from signal and negative values set to zero. Statistical analysis was performed using a two-tailed Student's t test. p values < 0.05 were considered significant; significance values are indicated as * ($p < 0.05$), ** ($p < 0.01$) and *** ($p < 0.001$).

Data and software availability

Whole-exome DNA sequencing data are available in Table S1.

SUPPLEMENTAL INFORMATION

Supplemental Information includes five figures, three tables, and six videos and can be found with this article online at https://doi.org/10.1016/j.cell. 2018.07.009.

ACKNOWLEDGMENTS

We thank Suzanne van der Kolk, Judith Westra, Louisa Hoes, and Luuk Schipper for help with patient inclusion. We acknowledge Martijn van Baalen, Anita Pfauth, and Frank van Diepen for assistance in flow cytometry. We thank Marjolijn Mertz, Lenny Brocks, and Bram van den Broek for help in live imaging experiments. We would like to acknowledge Dennis Peters and Ingrid Hofland from the NKI-AVL Core Facility Molecular Pathology & Biobanking (CFMPB) for supplying NKI-AVL Biobank material and lab support. DNA sequencing was performed by Marja Nieuwland, Roel Kluin, and Ron Kerkhoven. We thank Marc van de Wetering and Hubrecht Organoid Technology (HUB) for advice on organoid cultures. We would like to thank Merus for provision of anti-PD-1. Thanks to Marije Marsman, Steven van Houtvin, Hylke Galema, and Koen Verhoef for support in technology transfer. Stef van Lieshout, Ewart de Bruijn, and Edwin Cuppen (Hartwig Medical Foundation) performed authentication of organoid lines. Thanks to Salo Ooft, Chelsea McLean, Christina Stangl, Louisa Hoes, Luuk Schipper, Maarten Ligtenberg, David Vredevoogd, Julia Boshuijzen, Wouter Scheper, Joost van den Berg, Renate de Boer, Christian Blank, and Daniel Peeper for input in the design of experiments. This work was supported by the NWO Gravitation Program (NWO; 2012-2022) (to E.E.V. on behalf of CancerGenomics.nl), a KWF grant (HUBR2014-7006) (to E.E.V.), the KWF Queen Wilhelmina Award (NKI 2013-6122) (to T.S.), and ERC AdG SENSIT (to T.S.).

AUTHOR CONTRIBUTIONS

K.K.D. designed, performed, and analyzed the experiments and wrote the manuscript. C.M.C. designed, performed, and analyzed the experiments. F.W. designed the clinical protocol, and F.W., M.C., D.L.v.d.V., M.E.v.L., A.D., E.F.S., J.H., and K.J.H. organized patient inclusion. L.F.F., S. Kelderman, and N.v.R. designed the co-culture experiments. J.v.d.H., L.F., and M.S. analyzed the DNA sequencing data. S. Kaing cultured the tumor organoids. M.C.W. and R.d.G. provided material for, and designed reactivity tests against, tumor digest. N.S. and H.C. provided the protocols for organoid culture. P.S. and K.M. analyzed the histology data. T.N.S. and E.E.V. supervised the study.

DECLARATION OF INTERESTS

H.C. is an inventor on several patents related to organoid technology. N.S. re- ports grants from the Netherlands Organization for Scientific Research, during the conduct of the study; others come from Vertex Pharmaceuticals Incorporated, outside the submitted work. In addition, N.S. has a patent (PCT/EP2015/ 077990) with royalties paid to Stichting HUB and a patent (PCT/EP2015/ 077988) with royalties paid to Stichting HUB.

REFERENCES

- Blank, C.U., Haanen, J.B., Ribas, A., and Schumacher, T.N. (2016). CANCER IMMUNOLOGY. The ''cancer immunogram''. Science 352, 658–660.
- Borghaei, H., Paz-Ares, L., Horn, L., Spigel, D.R., Steins, M., Ready, N.E., Chow, L.Q., Vokes, E.E., Felip, E., Holgado, E., et al. (2015). Nivolumab versus docetaxel in advanced nonsquamous non-small-cell lung cancer. N. Engl. J. Med. 373, 1627–1639.
- Cancer Genome Atlas Network (2012). Comprehensive molecular characterization of human colon and rectal cancer. Nature 487, 330–337.
- Cingolani, P., Platts, A., Wang, L., Coon, M., Nguyen, T., Wang, L., Land, S.J., Lu, X., and Ruden, D.M. (2012). A program for annotating and predicting the effects of single nucleotide polymorphisms, SnpEff: SNPs in the genome of Drosophila melanogaster strain w1118; iso-2; iso-3. Fly (Austin) 6, 80–92.
- Dangles-Marie, V., Pocard, M., Richon, S., Weiswald, L.B., Assayag, F., Saulnier, P., Judde, J.G., Janneau, J.L., Auger, N., Validire, P., et al. (2007). Establishment of human colon cancer cell lines from fresh tumors versus xenografts: comparison of success rate and cell line features. Cancer Res. 67, 398–407.
- Dierssen, J.W., de Miranda, N.F., Ferrone, S., van Puijenbroek, M., Cornelisse, C.J., Fleuren, G.J., van Wezel, T., and Morreau, H. (2007). HNPCC versus sporadic microsatellite-unstable colon cancers follow different routes toward loss of HLA class I expression. BMC Cancer 7, 33–43.
- Dijkstra, K.K., Voabil, P., Schumacher, T.N., and Voest, E.E. (2016). Genomics- and transcriptomics-based patient selection for cancer treatment with immune checkpoint inhibitors: a review. JAMA Oncol. 2, 1490–1495.
- Dudley, M.E., Wunderlich, J.R., Shelton, T.E., Even, J., and Rosenberg, S.A. (2003). Generation of tumor-infiltrating lymphocyte cultures for use in adoptive transfer therapy for melanoma patients. J. Immunother. 26, 332–342.
- Garon, E.B., Rizvi, N.A., Hui, R., Leighl, N., Balmanoukian, A.S., Eder, J.P., Patnaik, A., Aggarwal, C., Gubens, M., Horn, L., et al.; KEYNOTE-001 Investigators (2015). Pembrolizumab for the treatment of non-small-cell lung cancer. N. Engl. J. Med. 372, 2018–2028.
- Gjorevski, N., Sachs, N., Manfrin, A., Giger, S., Bragina, M.E., Ordó ñ ez-Morá, P., Clevers, H., and Lutolf, M.P. (2016). Designer matrices for intestinal stem cell and organoid culture. Nature 539, 560–564.
- Govindan, R., Ding, L., Griffith, M., Subramanian, J., Dees, N.D., Kanchi, K.L., Maher, C.A., Fulton, R., Fulton, L., Wallis, J., et al. (2012). Genomic landscape of non-small cell lung cancer in smokers and never-smokers. Cell 150, 1121–1134.
- Gros, A., Parkhurst, M.R., Tran, E., Pasetto, A., Robbins, P.F., Ilyas, S., Prick- ett, T.D., Gartner, J.J., Crystal, J.S., Roberts, I.M., et al. (2016). Prospective identification of neoantigen-specific lymphocytes in the peripheral blood of melanoma patients. Nat. Med. 22, 433–438.

- Horvath, P., Aulner, N., Bickle, M., Davies, A.M., Nery, E.D., Ebner, D., Montoya, M.C., Ostling, P., Pietiäinen, V., Price, L.S., et al. (2016). Screening out irrelevant cell-based models of disease. Nat. Rev. Drug Discov. 15, 751–769.
- Larkin, J., Chiarion-Sileni, V., Gonzalez, R., Grob, J.J., Cowey, C.L., Lao, C.D., Schadendorf, D., Dummer, R., Smylie, M., Rutkowski, P., et al. (2015). Combined nivolumab and ipilimumab or monotherapy in untreated melanoma. N. Engl. J. Med. 373, 23–34.
- Larson, D.E., Harris, C.C., Chen, K., Koboldt, D.C., Abbott, T.E., Dooling, D.J., Ley, T.J., Mardis, E.R., Wilson, R.K., and Ding, L. (2012). SomaticSniper: identification of somatic point mutations in whole genome sequencing data. Bioinformatics 28, 311–317.
- Le, D.T., Uram, J.N., Wang, H., Bartlett, B.R., Kemberling, H., Eyring, A.D., Skora, A.D., Luber, B.S., Azad, N.S., Laheru, D., et al. (2015). PD-1 blockade in tumors with mismatch-repair deficiency. N. Engl. J. Med. 372, 2509–2520.
- Le, D.T., Durham, J.N., Smith, K.N., Wang, H., Bartlett, B.R., Aulakh, L.K., Lu, S., Kemberling, H., Wilt, C., Luber, B.S., et al. (2017). Mismatch repair deficiency predicts response of solid tumors to PD-1 blockade. Science 357, 409–413.
- Liang-Chu, M.M.Y., Yu, M., Haverty, P.M., Koeman, J., Ziegle, J., Lee, M., Bourgon, R., and Neve, R.M. (2015). Human biosample authentication using the high-throughput, cost-effective SNPtrace(TM) system. PLoS ONE 10, e0116218.
- McKenna, A., Hanna, M., Banks, E., Sivachenko, A., Cibulskis, K., Kernytsky, A., Garimella, K., Altshuler, D., Gabriel, S., Daly, M., and DePristo, M.A. (2010). The Genome Analysis Toolkit: a MapReduce framework for analyzing next-generation DNA sequencing data. Genome Res. 20, 1297–1303.
- Overman, M.J., McDermott, R., Leach, J.L., Lonardi, S., Lenz, H.J., Morse, M.A., Desai, J., Hill, A., Axelson, M., Moss, R.A., et al. (2017). Nivolumab in patients with metastatic DNA mismatch repair-deficient or microsatellite instability-high colorectal cancer (CheckMate 142): an open-label, multicentre, phase 2 study. Lancet Oncol. 18, 1182–1191.
- Overman, M.J., Lonardi, S., Wong, K.Y.M., Lenz, H.J., Gelsomino, F., Aglietta, M., Morse, M.A., Van Cutsem, E., McDermott, R., Hill, A., et al. (2018). Durable clinical benefit with nivolumab plus ipilimumab in DNA mismatch repair-deficient/microsatellite instability-high metastatic colorectal cancer. J. Clin. Oncol. 36, 773–779.
- Patel, S.A., and Minn, A.J. (2018). Combination cancer therapy with immune checkpoint blockade: mechanisms and strategies. Immunity 48, 417–433.
- Pitt, J.M., Vé tizou, M., Daillè re, R., Roberti, M.P., Yamazaki, T., Routy, B., Lep- age, P., Boneca, I.G., Chamaillard, M., Kroemer, G., and Zitvogel, L. (2016). Resistance mechanisms to immune checkpoint blockade in cancer: tumor- intrinsic and –extrinsic factors. Immunity 44, 1255–1269.
- Rosenberg, S.A., and Restifo, N.P. (2015). Adoptive cell transfer as personalized immunotherapy for human cancer. Science 348, 62–68.
- Sachs, N., Zomer-van Ommen, D.D., Papaspyropoulos, A., Heo, I., Bottinger, L., Klay, D., Weeber, F., Huelsz-Prince, G., Lakobachvili, N., Viveen, M.C., et al. (2018). Long-term expanding human airway organoids for disease modeling. bioRxiv,. https://doi.org/10.1101/318444.

- Schneider, C.A., Rasband, W.S., and Eliceiri, K.W. (2012). NIH Image to ImageJ: 25 years of image analysis. Nat. Methods 9, 671–675.
- Schütte, M., Risch, T., Abdavi-Azar, N., Boehnke, K., Schumacher, D., Keil, M., Yildiriman, R., Jandrasits, C., Borodina, T., Amstislavskiv, V., et al. (2017). Molecular dissection of colorectal cancer in pre-clinical models identifies biomarkers predicting sensitivity to EGFR inhibitors. Nat. Commun. 8, 14262.
- Sharma, P., Hu-Lieskovan, S., Wargo, J.A., and Ribas, A. (2017). Primary, adaptive, and acquired resistance to cancer immunotherapy. Cell 168, 707–723.
- Stevanovic, S., Draper, L.M., Langhan, M.M., Campbell, T.E., Kwong, M.L., Wunderlich, J.R., Dudley, M.E., Yang, J.C., Sherry, R.M., Kammula, U.S., et al. (2015). Complete regression of metastatic cervical cancer after treatment with human papillomavirus-targeted tumor-infiltrating T cells. J. Clin. Oncol. 33, 1543–1550.
- Szolek, A., Schubert, B., Mohr, C., Sturm, M., Feldhahn, M., and Kohlbacher, O. (2014). OptiType: precision HLA typing from next-generation sequencing data. Bioinformatics 30, 3310–3316.
- Tanabe, H., Takada, Y., Minegishi, D., Kurematsu, M., Masui, T., and Mizu- sawa, H. (1999). Cell line individualization by STR multiplex system in the cell bank found cross-contamination between ECV304 and EJ-1/T24. Tiss. Cult. Res. Commun. 18, 329–338.
- van de Wetering, M., Francies, H.E., Francis, J.M., Bounova, G., Iorio, F., Pronk, A., van Houdt, W., van Gorp, J., Taylor-Weiner, A., Kester, L., et al. (2015). Prospective derivation of a living organoid biobank of colorectal cancer patients. Cell 161, 933–945.
- Verdegaal, E.M., Visser, M., Ramwadhdoebé , T.H., van der Minne, C.E., van Steijn, J.A., Kapiteijn, E., Haanen, J.B., van der Burg, S.H., Nortier, J.W., and Osanto, S. (2011). Successful treatment of metastatic melanoma by adoptive transfer of blood-derived polyclonal tumor-specific $CD4^+$ and $CD8^+$ T cells in combination with low-dose interferon-alpha. Cancer Immunol. Immunother. 60, 953–963.
- Vogelstein, B., Papadopoulos, N., Velculescu, V.E., Zhou, S., Diaz, L.A., Jr., and Kinzler, K.W. (2013). Cancer genome landscapes. Science 339, 1546–1558.
- Weeber, F., van de Wetering, M., Hoogstraat, M., Dijkstra, K.K., Krijgsman, O., Kuilman, T., Gadellaa-van Hooijdonk, C.G., van der Velden, D.L., Peeper, D.S., Cuppen, E.P., et al. (2015). Preserved genetic diversity in organoids cultured from biopsies of human colorectal cancer metastases. Proc. Natl. Acad. USA 112, 13308–13311.
- Zaretsky, J.M., Garcia-Diaz, A., Shin, D.S., Escuin-Ordinas, H., Hugo, W., Hu- Lieskovan, S., Torrejon, D.Y., Abril-Rodriguez, G., Sandoval, S., Barthly, L., et al. (2016). Mutations associated with acquired resistance to PD-1 blockade in melanoma. N. Engl. J. Med. 375, 819–829.
- Zheng, C., Sun, Y.H., Ye, X.L., Chen, H.Q., and Ji, H.B. (2011). Establishment and characterization of primary lung cancer cell lines from Chinese population. Acta Pharmacol. Sin. 32, 385–392.

SUPPLEMENTARY MATERIAL

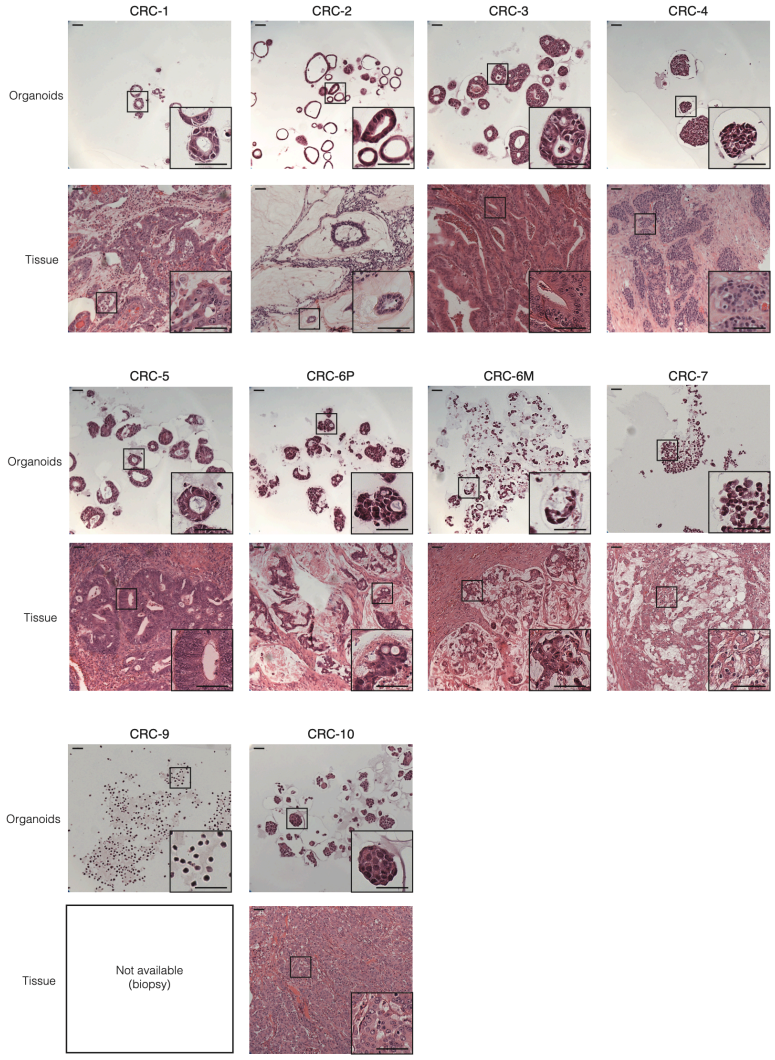

Figure S1. Hematoxylin and Eosin Stainings of Tumor Organoids and Original Mismatch Repair Deficient Colorectal Cancers, ***Related to Figure 1***

Excised tumor pieces or tumor organoids derived thereof were fixed, paraffin-embedded and stained with hematoxylin and eosin. Inserts show higher magnification images of boxed area. Scale bar, 50 mm.

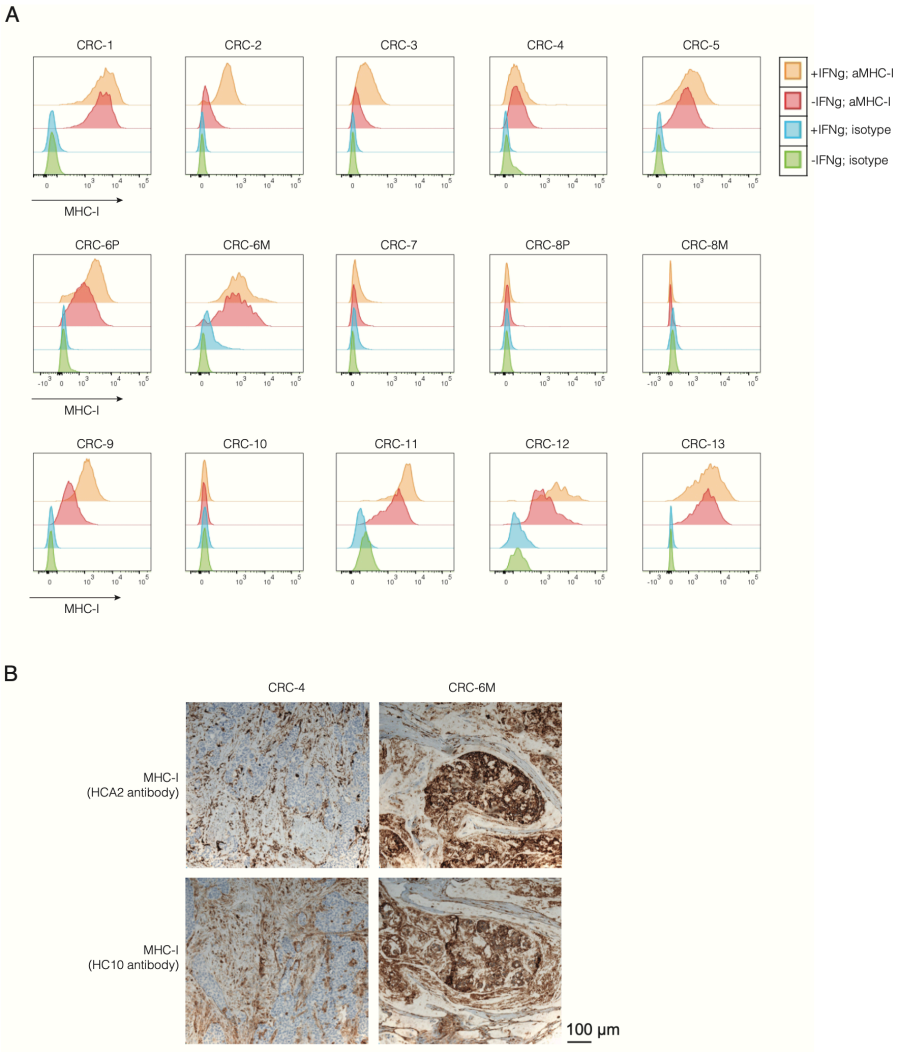

Figure S2. MHC-I Expression of Mismatch Repair Deficient Colorectal Cancer Organoids and Original Tumors, Related to *Figure 1*

(A) Cell surface MHC-I expression of mismatch repair deficient colorectal cancer organoids as determined by flow cytometry. Organoids were stimulated with 200 ng/mL IFNg for 24 hr or left unstimulated. Histograms indicate fluorescence intensity of anti-HLA-A,B,C-PE or isotype control antibodies.

(B) Excised tumor pieces were fixed and paraffin-embedded, and sequential slides were stained with HCA2 and HC10 antibodies against MHC-I. Representative staining of MHC-I proficient (CRC-6M) and deficient (CRC-4) tumors. CRC-4 shows positive MHC-I staining in stroma but absence of signal in the tumor mass. CRC-6M contains MHC-I positive tumor cells grouped in islands. Scale bar, 100 mm.

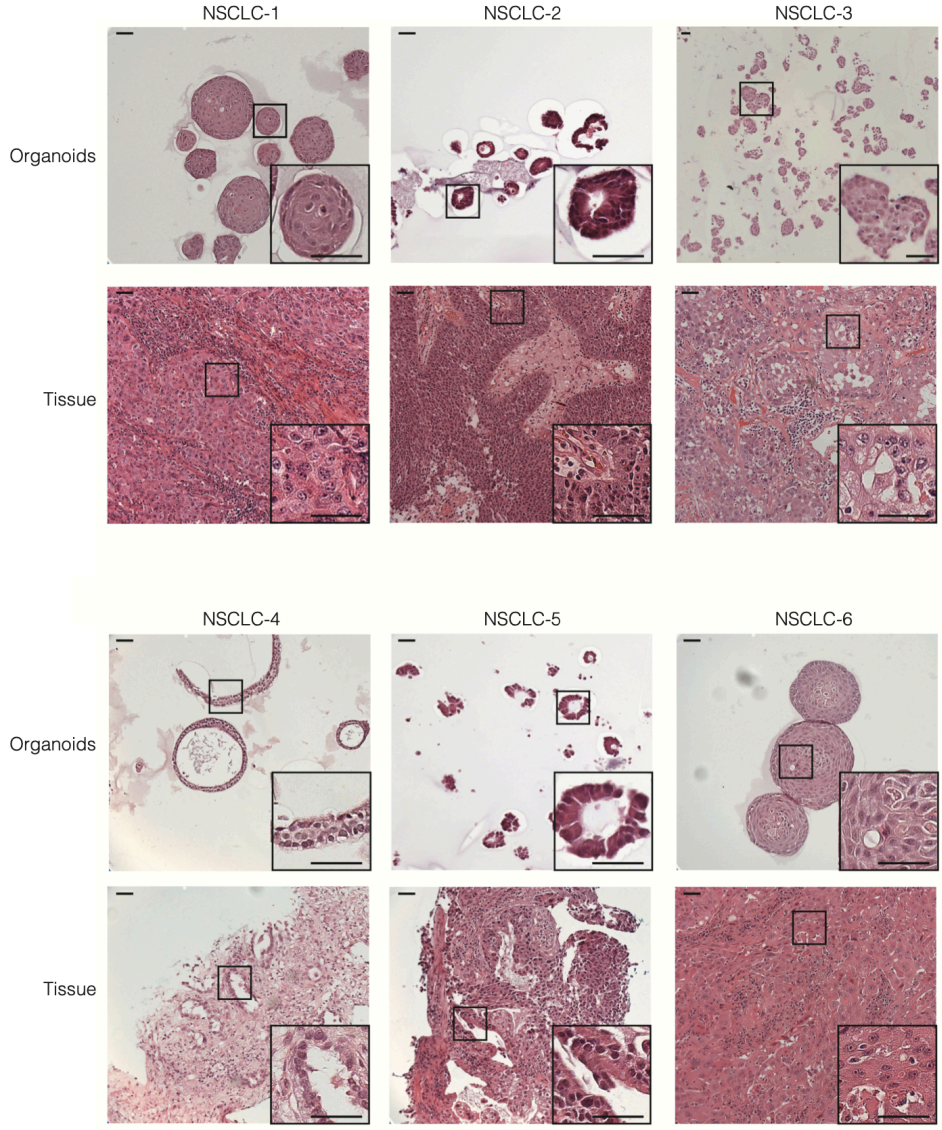

Figure S3. Hematoxylin and Eosin Stainings of Tumor Organoids and Original Non-small-cell Lung Cancers, Related to *Figure 3*

Excised tumor pieces or tumor organoids derived thereof were fixed, paraffin-embedded and stained with hematoxylin and eosin. Inserts show higher magnification images of boxed area. Scale bar, 50 mm.

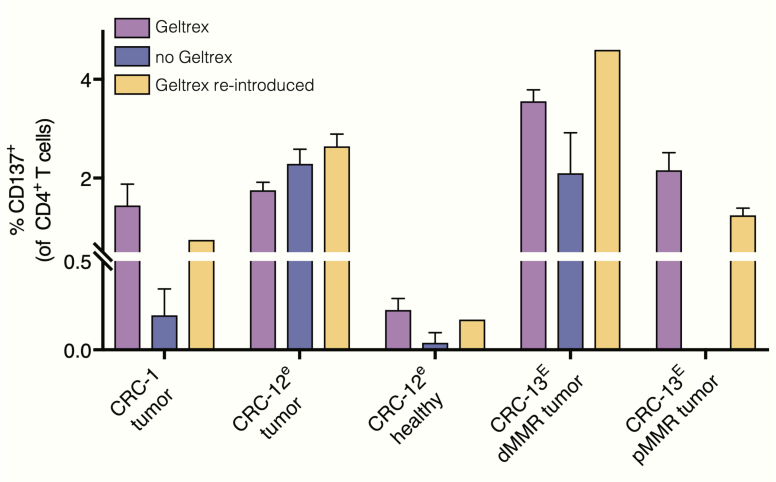

Figure S4. CD4+ Reactivity against Geltrex, Related to *Figure 5*

Quantification of CD137+ CD4+ T cells after stimulation of T cells with organoids cultured under standard conditions (with Geltrex), cultured for 3 days without Geltrex, or cultured for 3 days without Geltrex with Geltrex re-introduced 1 day before T cell challenge. T cells were obtained by two week co-culture with autologous tumor organoids and where indicated (lower case e) further expanded using a rapid expansion protocol (Dudley et al., 2003), in some cases preceded by CD137-based enrichment of tumor-reactive cells (indicated by upper case E). Error bars indicate SEM of at least 2 biological replicates.

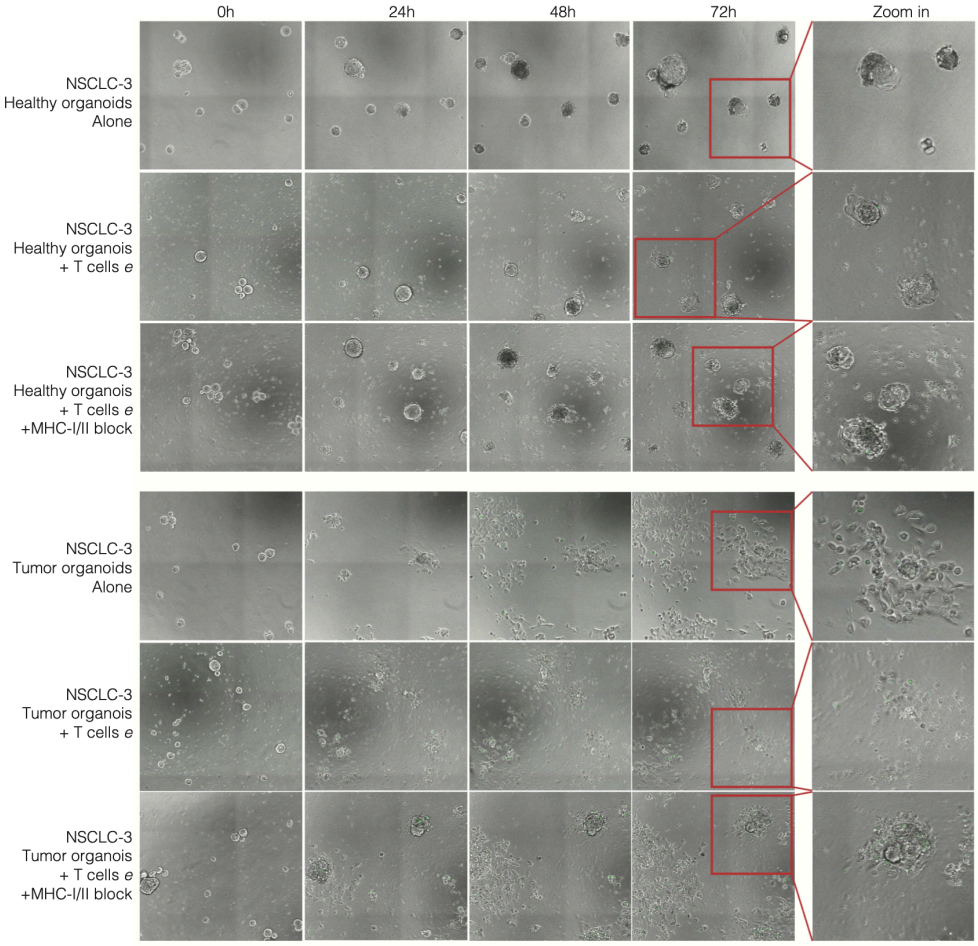

Figure S5. Time Course Imaging of NSCLC-3 Organoids Targeted by Tumor-Reactive T Cells, Related to *Figure 6*

Microphotograph images of NSCLC-3 organoids at indicated time points of culture with or without T cells in the presence of a green-fluorescent caspase 3/7 probe. Where indicated, MHC-I and MHC-II were blocked with W6/32 and Tü39 antibodies, respectively. T cells are obtained by two weeks of co-culture with autologous tumor organoids followed by rapid expansion (indicated by upper case e).

Supplementary Table 1 and Supplementary Videos 1-6 are available in the online version of this manuscript

Table S1. Whole exome sequencing of colorectal cancer organoids, related to *Figure 1*.
DNA isolated from mismatch repair deficient colorectal cancer organoids and matched PBMCs was analyzed by whole exome sequencing.

Video S1. NSCLC-3 tumor organoids co-cultured with autologous tumor-reactive T cells, related to *Figure 6*.
Time-lapse bright-field and fluorescence microscopy of NSCLC-3 tumor organoids exposed to autologous T cells obtained by two weeks of co-culture with autologous tumor organoids followed by rapid expansion. Note the destruction of tumor organoids by surrounding T cells and appearance of apoptotic cells visualized by a green-fluorescent caspase 3/7 probe. Video duration: 3 days.

Video S2. NSCLC-3 tumor organoids cultured without T cells, related to *Figure 6.*
Time-lapse bright-field and fluorescence microscopy of NSCLC-3 tumor organoids cultured without T cells in the presence of a green-fluorescent caspase 3/7 probe. Note proliferation of tumor cells that spread out onto the plate toward the end of the assay. Video duration: 3 days.

Video S3. NSCLC-3 tumor organoids cultured with autologous tumor-reactive T cells in the presence of MHC-I and MHC-II blocking antibodies, related to *Figure 6.*
Time-lapse bright-field and fluorescence microscopy of NSCLC-3 tumor organoids exposed to autologous T cells, in the presence of a green-fluorescent caspase 3/7 probe. T cells were obtained by two weeks of co-culture with autologous tumor organoids followed by rapid expansion. MHC-I and MHC-II were blocked with W6/32 and Tü39 antibodies, respectively. Note absence of killing and continued proliferation of tumor cells. Video duration: 3 days.

Video S4. NSCLC-3 healthy lung organoids co-cultured with autologous tumor-reactive T cells, related to *Figure 6.*
Time-lapse bright-field and fluorescence microscopy of NSCLC-3 healthy lung organoids exposed to autologous T cells, in the presence of a green-fluorescent caspase 3/7 probe. T cells were obtained by two weeks of co-culture with autologous tumor organoids followed by rapid expansion. Note that organoids are unaffected by presence of T cells. Video duration: 3 days.

Video S5. NSCLC-3 healthy lung organoids cultured without T cells, related to *Figure 6*.
Time-lapse bright-field and fluorescence microscopy of NSCLC-3 healthy lung organoids cultured without T cells, in the presence of a green-fluorescent caspase 3/7 probe. Video duration: 3 days.

Video S6. NSCLC-3 healthy lung organoids cultured with autologous tumor-reactive T cells in the presence of MHC-I and MHC-II blocking antibodies, related to *Figure 6.*
Time-lapse bright-field and fluorescence microscopy of NSCLC-3 healthy lung organoids exposed to autologous T cells, in the presence of a green-fluorescent caspase 3/7 probe. T cells were obtained by two weeks of co-culture with autologous tumor organoids followed by rapid expansion. MHC-I and MHC-II were blocked with W6/32 and Tü39 antibodies, respectively. Video duration: 3 days.

Table S2. Comparison of MHC-I expression of tumor organoids and original tumors, related to *Figure 1*.

Excised tumor pieces were fixed and paraffin-embedded, and slides were stained with the HCA2 or HC10 antibody against MHC-I. Tumor slides were scored by a pathologist for staining intensity, with the percentage of tumor cells negative or strongly, moderately or weakly positive for MHC-I indicated in the table. The score for each individual staining is calculated by multiplying the percentage of tumor cells strongly (3), moderately (2), or weakly (1) positive with the number indicated in brackets, and summing the outcome. The composite IHC score (average of the HCA2 and HC10 scores) is compared to mean fluorescence intensity (MFI) of anti-HLA-A,B,C-PE staining (isotype control MFI subtracted) of tumor organoids.

	HCA2					HC10					Comparison	
	Strong (%)	Moderate (%)	Weak (%)	Negative (%)	Score HCA2	Strong (%)	Moderate (%)	Weak (%)	Negative (%)	Sore HC10	Tumor slides composite score HCA2/HC10 (IHC)	Tumor organoids (MFI)
CRC-1	30	0	0	70	**90**	70	20	10	0	**260**	**175**	**2368**
CRC-3	0	0	0	100	**0**	0	1	10	89	**12**	**6**	**23**
CRC-4	0	0	1	99	**1**	0	0	1	99	**1**	**1**	**154**
CRC-5	0	0	0	100	**0**	0	0	15	85	**15**	**8**	**461**
CRC-6M	35	25	20	20	**175**	30	25	20	15	**160**	**168**	**1158**
CRC-6P	70	20	10	0	**260**	65	30	5	0	**260**	**260**	**1165**
CRC-7	0	0	0	100	**0**	0	0	0	100	**0**	**0**	**1**
CRC-8M	0	2	8	90	**12**	0	0	0	100	**0**	**6**	**0**
CRC-8P	2	0	5	93	**11**	2	0	2	96	**8**	**10**	**3**
CRC-12	40	45	10	5	**220**	0	0	0	100	**0**	**110**	**1548**

Table S3. Characteristics of panel of NSCLC samples, related to *Figure 3*.

Sample	Sex	Age	Type	Tumor location	Stage	Primary tumor/Metastasis	Biopsy/Resection
NSCLC-1	M	70	Adenocarcinoma	Lung	I	Primary tumor	Resection
NSCLC-2	M	57	Squamous cell carcinoma	Lung	I	Primary tumor	Resection
NSCLC-3	F	61	NOS	Lung	II	Primary tumor	Resection
NSCLC-4	M	62	Adenocarcinoma	Lung	IV	Primary tumor	Biopsy
NSCLC-5	M	62	Adenocarcinoma	Adrenal gland	IV	Metastasis	Biopsy
NSCLC-6	M	57	Squamous cell carcinoma	Lung	III	Primary tumor	Resection

F, female; and M, male.

Tumor organoids-T cells coculture systems

3

Cattaneo C.M.[1,3,*], Dijkstra K.K.[1,3,*], Fanchi L.F.[1], Kelderman S.[1], Kaing S.[1,3],, van Rooij N.[1], van de Brink S.[2,3], Schumacher T.N.[1,3], Voest E.E[1,3].

**These authors contributed equally*

[1]*Department of Molecular Oncology and Immunology, The Netherlands Cancer Institute, Antoni van Leeuwenhoek Hospital*

[2]*Hubrecht Institute for Developmental Biology and Stem Cell Research-KNAW, University Medical Center Utrecht*

[3]*Oncode Institute*

Nature Protocols. 2020 Jan, (15): 15-39

ABSTRACT

T cells are key players in cancer immunotherapy, but strategies to expand tumor-reactive cells and study their interactions with tumor cells at the level of an individual patient are limited. Here we describe the generation and functional assessment of tumor-reactive T cells based on cocultures of tumor organoids and autologous peripheral blood lymphocytes. The procedure consists of an initial coculture of 2 weeks, in which tumor-reactive T cells are first expanded in the presence of (IFNγ-stimulated) autologous tumor cells. Subsequently, T cells are evaluated for their capacity to carry out effector functions (IFNγ secretion and degranulation) after recognition of tumor cells, and their capacity to kill tumor organoids. This strategy is unique in its use of peripheral blood as a source of tumor-reactive T cells in an antigen- agnostic manner. In 2 weeks, tumor-reactive $CD8^+$ T-cell populations can be obtained from ~33–50% of samples from patients with non-small-cell lung cancer (NSCLC) and microsatellite-instable colorectal cancer (CRC). This enables the establishment of ex vivo test systems for T-cell-based immunotherapy at the level of the individual patient.

INTRODUCTION

T-cell-directed therapies, such as immune-checkpoint inhibition and adoptive T-cell transfer, have transformed the treatment landscape for solid tumors. Nevertheless, clinical efficacy is variable both between and within tumor types and the mechanisms that tumors use to escape elimination by the immune system are diverse[1–4] . Preclinical models that incorporate both endogenous T cells and tumor cells are scarce, especially for epithelial cancers. Moreover, the expansion of tumor-infiltrating lymphocytes (TILs) has been more challenging for epithelial tumors compared with melanoma[5] .

We have recently developed a coculture system of tumor organoids and peripheral blood lymphocytes[6] . Tumor-reactive T cells can be efficiently expanded from peripheral blood and evaluated for tumor reactivity and tumoricidal capacity. Here, we extend and describe the procedure for establishment of this coculture system (Fig. 1).

Applications of the protocol

We anticipate that this protocol will be primarily applied as an investigational tool in three different settings: (i) as a tool to evaluate the efficacy of investigational drugs in the immuno-oncology space; (ii) for translational studies for specific patients of interest, for example, an exceptional responder within a clinical trial; or (iii) to identify or validate mechanisms of resistance in a physiologically relevant setting. As an example, samples could be obtained from patients who initially respond to immune-checkpoint inhibition but then progress[7] . Hypotheses for potential resistance mechanisms of those patients that are generated based on more descriptive datasets (for example, tumor DNA sequencing) may be validated using tumor organoids derived from pre- and post- therapy samples.

In addition to these research applications, this method offers a potential strategy for the generation of T-cell products for adoptive T-cell transfer. The clinical success of TIL therapy in melanoma has not been matched in other tumor types and there is a need for strategies that bypass the challenges of TIL therapy for epithelial cancers.

Comparison with other approaches

Several other strategies to generate tumor-reactive T-cell products have been developed.

First, expansion of TILs has been used for many years to generate T-cell products for adoptive T-cell transfer[8]. This strategy has been successfully applied for the treatment of metastatic melanoma, but clinical experience in other tumor types has remained limited (reviewed in ref. [9]). Advantages of using TILs as a source of tumor-reactive T cells are the straightforward protocol and relatively short time required to generate a cell product. Moreover, although it has recently become clear that a substantial fraction of TILs do not show tumor specificity[10,11], T cells that are present at the tumor site will nevertheless be enriched for tumor-specific cells relative to peripheral blood. In addition, strategies for the more-selective expansion of tumor-reactive T cells from TILs could be conceived, either by pre-selecting T-cell populations enriched for tumor reactivity[12–14] or by stimulation with tumor cells (for example, organoids). However, there are also limitations to this technology: the absolute number of TILs may be too low in sparsely infiltrated tumors, which is particularly problematic when a tumor biopsy (rather than a surgical resection) is the only available material. In addition, how circulating tumor-reactive T cells and TILs compare with respect to fitness and T-cell receptor repertoire and whether the most tumor-expressed (neo-)antigens have already induced a tumor-resident T-cell population remained unclear.

As a second strategy, neo-antigen-specific T cells have been generated by activating circulating T cells with antigen-presenting cells (APCs) that present (a) neo-antigen(s) of interest. Such strategies can be successful, especially when a pre-selected population of T cells (for example, PD1^{+}) is used[15]. Neo-antigens that are loaded onto APCs can be predicted on the basis of the exome- and RNA- sequencing data of the tumor[16]. Although prediction pipelines continue to improve, they are, at present, imperfect (especially for less-common HLA haplotypes) and there is a risk of missing relevant antigens[17]. Alternatively, mini-genes encoding potential neo-antigens can be introduced into APCs and used to screen T cells, including healthy donor T cells, for reactivity[15,18]. This bypasses the need for antigen prediction but is a laborious approach, certainly in tumor types with a high mutational load, such as mismatch-repair-deficient tumors. Instead, the use of tumor cells as a substrate for selection of tumor-reactive T cells is antigen-agnostic and can result in the establishment of a polyclonal tumor-reactive T-cell population[19]. Although the turnaround time of sequencing and antigen prediction may be similar to the time required to establish organoids, the cost of sequencing and the need for bioinformatic analysis can be a disadvantage. Importantly, the use of tumor organoids

does not only enable the expansion of tumor-reactive T cells, but also the analysis of the activity of the resulting T cells against matched tumor cells.

Other approaches that coculture organoids or organotypic cultures with allogeneic or autologous lymphocytes have been described[20–23]. These approaches typically make use of immune cells isolated from tumor fragments and are a very valuable tool to study immune cells from their native environment, in particular in their interaction with cells that are difficult to culture, such as macrophages. However, expansion of T cells and/or tumor cells is usually limited, and cryopreservation is not always possible, which limits their use for approaches that require high numbers of T cells or repeated experiments.

Limitations

Tumor and healthy organoids can be established from both needle biopsies and surgical resections. The success rate depends on tumor type, amount of starting material (for example, resection versus biopsy) and treatment history. Typically, organoid culture from resections of treatment-naive primary tumors is more successful than from biopsies from heavily pre-treated metastases. For example, the success rate of establishing organoids from resection specimens of untreated primary CRC is ~90%; whereas the success rate when using a biopsy of a metastasis ranges from ~70% for CRC to ~35% for NSCLC[24–27].The time required to establish a frozen biobank of at least 1×10^6 organoids takes on average 30–80 d for CRC or NSCLC samples, respectively (Fig. 1b,c). Because of this variability, the feasibility and cost-effectiveness of an organoid-based approach for both research purposes and adoptive T-cell transfer is expected to differ between tumor types and patient populations, and should be carefully evaluated.

The evaluation of $CD4^+$ T-cell reactivity is complicated by the potential for recognition of non-tumor epitopes present in the culture system (for example, Geltrex-derived epitopes)[6] . The current protocol describes an adaptation to our previous method that serves to prevent the development of such undesired T-cell responses. Further evaluation is required to determine the frequency with which true tumor-specific CD4+ T-cell responses can be induced using this optimized strategy.

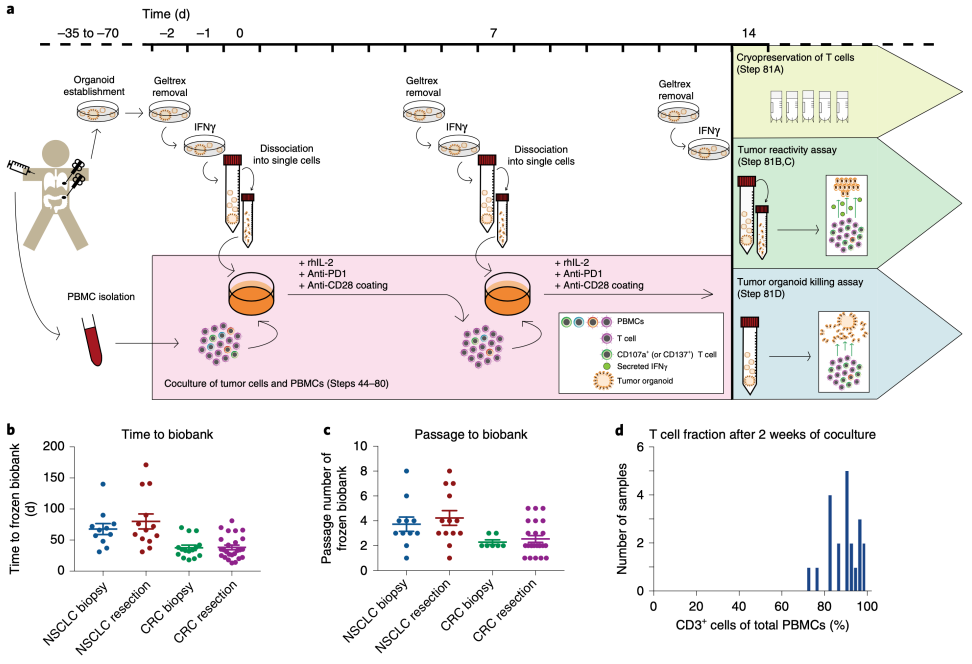

Fig. 1. Overview of the procedure.

a, Tumor organoids are established from tumor tissue and PBMCs are isolated from peripheral blood before the start of coculture. Organoids are isolated from Geltrex 2 d before coculture and stimulated with IFNγ 1 d before coculture. On the day of coculture, organoids are dissociated to single cells and plated together with PBMCs on an anti-CD28-coated plate, in the presence of IL-2 and anti-PD-1. After 1 week of coculture, PBMCs are restimulated with tumor cells. After 2 weeks of coculture with autologous tumor organoids (pink), T cells can be cryopreserved (yellow), T-cell reactivity against tumor cells is evaluated (green) or a tumor organoid killing assay is performed (blue).

b, Time from the start of organoid culture to establishment of a frozen biobank.

c, Passage number of organoids at time of freezing. d, Percentage CD3+ T cells in PBMCs after 2 weeks of coculture. Horizontal bars in b and c indicate average, error bars are s.e.m. Each symbol is an organoid culture from a separate tumor. NSCLC biopsy, n = 11; NSCLC resection, n = 13; CRC biopsy, n = 15; CRC resection, n = 25.

EXPERIMENTAL DESIGN

Overview

The following step-by-step procedure describes how to generate $CD8^+$ T cells that recognize and kill autologous tumor organoids (Fig. 1a). In the first part, we describe how to perform cocultures of peripheral blood lymphocytes and tumor cells, as well as methods to assess the reactivity of the resulting T-cell populations against tumor cells at the end of the procedure. In the second part, we focus on methods to test whether the obtained T-cell populations are able to kill the tumor organoids.

Coculture and reactivity assay

Before starting T cell–organoid cocultures, human peripheral blood mononuclear cells (PBMCs) are isolated from blood, and tumor organoids are generated and cultured as described previously[24,27,28] and in Steps 1–31 of this protocol. Tumor organoids are isolated from Geltrex (the basement membrane matrix) to avoid the presence of non-human protein material in the cultures. PBMCs are then stimulated weekly with dissociated autologous tumor organoids for a total time of 2 weeks. Tumor organoids are pre-stimulated with IFNγ to maximize antigen presentation. Cocultures are performed in the presence of anti-PD1 to counteract the induction of PD-L1 by IFNγ, IL-2 to support T-cell proliferation and plate-bound anti-CD28 antibodies to provide co-stimulation. T-cell reactivity is assessed by evaluating CD107a and IFNγ expression or CD137 expression in the presence or absence of tumor organoids.

Killing assay

Here we describe how to test whether the T-cell populations obtained after 2 weeks of coculture are able to kill autologous tumor organoids. Tumor organoids are cocultured for 72 h in the presence or absence of T cells, with the addition of anti-PD1 antibody, plate-bound anti-CD28 antibody, Y-27632 hydrochloride (to prevent anoikis) and a caspase dye (NucView488). Killing can be assessed by livecell imaging or a flow-cytometry-based

quantification that enables the analysis of the number of live tumor cells at the end of the experiment.

Controls

Evaluation of tumor reactivity is based on the quantification of different markers in the presence or absence of tumor organoids. As further controls to understand whether any observed reactivity is specific to the matched tumor cells, the following additional controls should be considered when material is available: (i) autologous healthy tissue organoids, to assess reactivity driven by any artifacts of organoid culture (prepared as described in Box 1), (ii) coculture with single-cell tumor digests, to test whether reactivity is also seen against tumor cells that have not been cultured in vitro, and (iii) coculture with single-cell digests of healthy tissue, to test for the specificity of the T cells for the tumor compared to healthy tissue. The killing assay is based on the quantification of the number of live tumor cells when organoids are cultured alone or in the presence of reactive T cells (for example, at a 5:1 T-cell:tumor cell ratio). The addition of T cells may lead to non-specific tumor cell death, for example, owing to competition for nutrients. For this reason, we think that the addition of a condition in which tumor cells and T cells are cocultured in the presence of MHC-blocking antibodies is essential.

PROTOCOL

Materials

Reagents

- B27 supplement without vitamin A (Gibco, cat. no. C12587-010)
- B27 supplement (Gibco, cat. no. 17504-044)
- N-Acetylcysteine (Sigma-Aldrich, cat. no. A9165-5G)
- Nicotinamide (Sigma-Aldrich, cat. no. N0636)
- Human recombinant EGF (Peprotech, cat. no. AF-100-15)
- A83-01 (Tocris, cat. no. 2939)
- SB202190 (Cayman Chemicals, cat. no. 10010399)
- Prostaglandin E2 (Cayman Cehmicals, cat. no. 14010-1)
- Y-27632 dihydrochloride (Sigma-Aldrich, cat. no. Y-0503)
- Human recombinant FGF-7 (Peprotech, cat. no. 100-19)
- Human recombinant FGF-10 (Peprotech, cat. no. 100-26)
- R-spondin 1-conditioned medium produced by R-spondin 1 producing cell line (available from the C. Kuo laboratory; instructions for preparation in Box 1 of refs. [28, 29, 30])
- Noggin-conditioned medium produced by Noggin producing cell line (available from the H. Clevers laboratory; instructions for preparation in Box 2)
- Wnt-3a-conditioned medium produced by L-Wnt-3a producing cell line (available from the H. Clevers laboratory; instructions for preparation Box 1 of refs. [29, 30])
- Geltrex LDEV-free reduced growth factor basement membrane (Gibco, cat. no. A1413202)
- PBS tablets (Gibco, cat. no. 18912-014)
- EDTA buffer, 0.5 M, disodium salt (Lonza, cat. no. 51234)
- FBS (Sigma-Aldrich, cat. no. F7524)
- Dimethyl sulfoxide (DMSO) (Sigma-Aldrich, cat. no. 34943)
- Bovine serum albumin fraction V (Sigma-Aldrich, cat. no. 10735078001)
- Dispase type II (Sigma-Aldrich, cat. no. D4693)
- Advanced DMEM-F12 (Gibco, cat. no. 12634-028)
- Penicillin/streptomycin (Gibco, cat. no. 15070063)
- Ultraglutamine type I (Lonza, cat. no. BE17-605E)
- HEPES (Gibco, cat. no. 15630-056)

- TrypLE Express (Gibco, cat. no. 12604-013)
- Trypsin-EDTA 0.05% (Gibco, cat. No. 25300054)
- Collagenase II (Sigma, cat. No. C6885)
- Hyaluronidase type IV-S (Sigma, cat. no. H4272)
- RPMI 1640 (Gibco, cat. no. 11875093)
- Human serum, from human male AB plasma (Sigma-Aldrich, cat. no. H3667)
- Benzonase (Merck, cat. no. 70746-3)
- Human recombinant interferon gamma (Peprotech, cat. no. 300-02)
- GolgiSTOP (Monensin) (BD, cat. no. 554724)
- GolgiPLUG (Brefeldin A) (BD, cat. no. 555029)
- Phorbol 12-myristate 13-acetate (PMA) (Sigma-Aldrich, cat. no. 19-144)
- Ionomycin (Sigma-Aldrich, cat. no. I9657)
- Mouse anti-human CD28 (eBioscience, CD28.2, cat. no. 16-0289-81, RRID:AB_468926)
- Interleukin-2 (Proleukin, Novartis)
- Anti-human PD1 / nivolumab (Merus / Selleckchem, cat. no. A2002, RRID:AB_2810223)
- Mouse anti-human CD107a (PE-conjugated) (BD, clone H4A3, cat. no. 555801, RRID:AB_396135)
- Mouse anti-human CD3 (PerCP-Cy5.5-conjugated) (eBioscience, clone SK7, cat. no. 332771, RRID:AB_1907379)
- Mouse anti-human CD4 (FITC-conjugated) (BD, clone RPA-T4, cat. no. 555346, RRID:AB_395751)
- Mouse anti-human CD8 (BV421-conjugated) (BD, clone RPA-T8, cat. no. 562429, RRID:AB_11153676)
- Mouse anti-human IFNγ (APC-conjugated) (BD, clone B27, cat. no. 554702, RRID:AB_398580)
- Mouse anti-human CD137 (APC-conjugated) (BD, clone 4B4-1, cat. no. 550890, RRID:AB_398477)
- Mouse anti-human HLA-ABC (MHC-I blocking antibody) (ThermoFisher, clone W6/32, cat. no. MA1-19027, RRID:AB_1076699)
- Mouse anti-human HLA-DR/DP/DQ (sodium azide free) (MHC-II blocking antibody) (BD, clone Tü39, cat. no. 555556, RRID:AB_395938)
- Mouse anti-human CD3 (Alexa Fluor 700-conjugated) (Invitrogen, cat. No. CD0329, RRID:AB_1470210)
- Mouse anti-human CD326 (EpCAM) (PE/Cy7-conjugated) (Biolegend, cat. No. 324222, RRID:AB_2561506)
- Live/dead fixable near-IR dead cell stain kit (Invitrogen, cat. no. L10119)

- Fixation/Permeabilization solution kit (BD, cat. no. 554714)
- Anti-mouse Ig, κ/negative control compensation particles set (BD, cat. no. 552843)
- Ammonium chloride (Sigma-Aldrich, cat. no. A9434)
- Sodium bicarbonate (Sigma-Aldrich, cat. no. S5761)
- Primocin (Invivogen, cat. no. PML-40-60)
- Lympholyte H (Tebu-bio, cat. no. CL5020)
- CellTrace Yellow Cell Proliferation Kit (Invitrogen, cat. No. C34567)
- CellTrace Far Red Cell Proliferation Kit (Invitrogen, cat. No. C34564)
- NucView488 Caspase-3 assay kit (Biotium, cat. No. 30029)
- AccuCount blank particles (7.0-7.9 µm) (Spherotech, cat. No. ACBP-70-10)
- Trypan Blue Solution (ThermoFisher, cat. no. 15250061)
- DAPI
- NaH_2PO_4 (Sigma-Aldrich, cat. no. S5011)
- KH_2PO_4 (Sigma-Aldrich, cat. no. P5655)
- NaCl (Sigma-Aldrich, cat. no. S7653)
- KCl (Sigma-Aldrich, cat. no. P9333)
- D-sorbitol (Sigma-Aldrich, cat. no. S1876)
- Sucrose (Sigma-Aldrich, cat. no. S7903)
- DL-dithiotreitol (Sigma-Aldrich, cat. no. D0632)

Equipment

- Falcon tubes, 15 mL (Sarstedt, cat. no. 62.554.502)
- Falcon tubes, 50 mL (Sarstedt, cat. no. 62.547.254)
- Plates, 6 well (Greiner, cat. no. 657165)
- Plates, 96 well, U-bottom (Greiner, cat. no. 650180)
- Plates, 24 well (Greiner, cat. no. 662160)
- Plates, 96 well, Flat bottom, Non-Tissue Culture Treated (Falcon, cat. no. 351172)
- Parafilm (Bemis, cat. no. PM-992)
- Hemocytometer (Labor Optik, cat. no. 1910000)
- Nunc Cryovials (ThermoFisher, cat. no. 375418)
- No 21 sterile carbon steel surgical scalpel blade (Swann-Morton, cat. no. 0207)
- Microlance needles 20G x 1 1/2", yellow (BD, cat. no. 301300)
- Culture dish, 100 x 20 mm (Greiner, cat. no. 664160)
- Flow cytometer (BD, Fortessa 1)
- -80 °C freezer (Panasonic, MOF-C8V1-PE)
- Mr Frosty freezing container (ThermoFisher, 5100-0036)
- Light microscope (Zeiss, Axiovert 25)
- 0.2 µm filter unit (Whatman, cat. no. 10462200)
- Syringe, 50 mL (Braun, cat. no. 8728844F-06)
- Water bath (37 °C)
- CO_2 incubator (5% CO_2, 37 °C)
- Centrifuge for 15- and 50-mL Falcon tubes and culture plates
- Biosafety cabinet
- Widefield microscope, recording PhaseContrast in combination with fluorescence and equipped with an AutoFocus system (Definite Focus – DF2), suitable for live cells
- ZeissZen Pro
- FIJI
- U-100 sterile insulin syringes (BD Micro-Fine, cat. no. 324891)
- Combitips advanced 5 mL (Eppendorf, cat. no. 0030089669)
- Combitips advanced 0.5 mL (Eppendorf, cat. no. 0030089634)
- Multipette E3x (Eppendorf, cat. no. 4987000029)

Reagent setup

Human material We have good experience with the use of cryopreserved human PBMC, stored at -80 °C. Tumor tissue can be obtained via surgical resection or a biopsy. The biopsy tissue can be stored in Ad-DF+++ with 1X Primocin at 4 °C for no longer than 24 hours prior to starting the procedure.

! CAUTION Informed consent must be obtained for the use of human material. Ethical approval must be obtained by and studies must conform to relevant institutional and national authorities.

! CAUTION It is strongly advised to authenticate human tissue (PBMC, organoid lines) using STR profiling or SNParrays and regularly test for contamination with Mycoplasma.

Ad-DF+++ Supplement Advanced-DMEM/F12 with 1% (vol/vol) penicillin/streptomycin, 1% (vol/vol) HEPES, and 1% (vol/vol) Ultraglutamine I. Store at 4 °C for up to 6 months.

Collagenase type II: Dissolve 150 mg collagenase type II in 10 mL PBS + 0.2% (wt/vol) BSA for a 15 mg/mL stock. Store in 1 mL aliquots at -20 °C for up to 1 year.

Hyaluronidase Type IV-S: Dissolve 30 mg hyaluronidase type IV-S in 3 mL distilled water to get a 10 mg/mL stock. Store in 1 mL aliquots at -20 °C for up to 1 year.

Wnt3a-conditioned medium Production of Wnt3a-conditioned medium has been described in Box 1 of refs. 29,30. Wnt3a-conditioned medium can be stored at 4 °C for up to 6 months.

R-spondin 1-conditioned medium Production of R-spondin 1-conditioned medium has been described in Box 1 of refs. 28,29,30. R-spondin 1-conditioned medium can be stored at -20 °C for up to 6 months or at 4 °C for up to 2 weeks.

Noggin-conditioned medium Production of Noggin-conditioned medium is described in Box 2. Noggin-conditioned medium can be stored in 50 mL aliquots at -20 °C for up to 6 months and for up to 2 weeks at 4 °C.

N-Acetylcysteine: dissolve 40.79 g into 500 mL PBS to have a 500 mM stock solution. Store at -20 °C for up to 1 year.

Nicotinamide: Dissolve 61.6 g into 500 mL PBS to have a 1 M stock solution. Store at -20 °C for up to 1 year.

Human recombinant EGF: Dissolve 1 mg into 2 mL 0.1% (wt/vol) BSA/PBS to have a 500 µg/mL stock solution. Store at -20°C for up to 1 year. Do not refreeze; aliquots of 20 µL are recommended.

A83-01: Dissolve 1.25 µg into 50 mL DMSO to have a 500 µM stock solution. Store at -20 °C for up to 1 year.

SB202190: Dissolve 25 mg into 7.546 mL DMSO to have a 10 mM stock solution. Store at -20 °C for up to 1 year.

Prostaglandine E2: Dissolve 1 mg into 28.36 mL to have a 100 µM stock solution. Store at -20 °C for up to 1 year.

Y-27632 dihydrochloride: Dissolve 32 mg into 10 mL DMSO to have a 10 mM stock solution. Store at -20 °C for up to 1 year.

Human recombinant FGF-7: Dissolve 0.1 mg into 2 mL 0.1% (wt/vol) BSA/PBS to have a 50 µg/mL stock solution. Store at -20 °C for up to 1 year. Do not refreeze; aliquots of 100 µL are recommended.

Human recombinant FGF-10: Dissolve 0.2 mg into 2 mL 0.1% (wt/vol) BSA/PBS to have a 100 µg/mL stock solution. Store at -20 °C for up to 1 year. Do not refreeze; aliquots of 100 µL are recommended.

Colorectal cancer organoid culture medium To prepare the medium, combine 5 mL Noggin-conditioned medium, 10 mL R-spondin 1-conditioned medium, 1 mL B27 minus vitamin A, 500 µL Nicotinamide (1 M in PBS), 125 µL N-Acetylcysteïne (500 mM in PBS), 5 µL EGF (500 µg/mL in PBS + 0.1% (wt/vol) BSA), 5 µL PGE2 (100 µM in PBS), 50 µL A83-01 (500 µM in DMSO), and 15 µL SB202190 (10 mM in DMSO). Add 5 µL Y-27632 (10 mM in DMSO) only for the first 3 days after thawing and passaging. Fill up to 50 mL with Ad-DF+++. Store at 4 °C for up to 2 weeks.

Colon organoid culture medium Same as colorectal cancer organoid medium, with an additional 25 mL of Wnt-3a-conditioned medium. Store at 4 °C for up to 2 weeks.

Non-small cell lung cancer and healthy airway epithelial medium To prepare the medium, combine 5 mL Noggin-conditioned medium, 5 mL R-spondin 1-conditioned medium, 1 mL B27, 500 µL Nicotinamide (1 M in PBS), 125 µL N-Acetylcysteine (500 mM in PBS), 6.25 µL FGF-7 (50 µg/mL in PBS + 0.1% (wt/vol) BSA), 12.5 µL FGF-10 (100 µg/mL in PBS + 0.1% (wt/vol) BSA), 50 µL A83-01 (500 µM in DMSO), 5 µL SB202190 (10 mM in DMSO), and 25 µL Y-27632 (10 mM in DMSO). Fill up to 50 mL with Ad-DF+++. Store at 4 °C for up to 2 weeks.

T cell culture medium Supplement RPMI 1640 with 1% (vol/vol) penicillin/streptomycin, 1% (vol/vol) Ultraglutamine I, and 10% (vol/vol) human serum. Store at 4 °C for up to 1 month.

T cell thawing medium Supplement RPMI 1640 with 1% (vol/vol) penicillin/streptomycin, 1% (vol/vol) Ultraglutamine I, and 10% (vol/vol) FBS. Store at 4 °C for up to 1 month.

FACS buffer Supplement 500 mL PBS with 5 mL EDTA (0.5 M) and 5 mg BSA. Store at 4 °C for up to 6 months.

Freezing medium Combine 45 mL FBS and 5 mL DMSO. Store at 4 °C for up to 6 months.

Non-small cell lung cancer digestion buffer Combine 1 mL collagenase type II (15 mg/mL in PBS + 0.2% (wt/vol) BSA), 500 µL dispase type II (10 mg/mL in ddH_2O), 20 µL Primocin, 10 µL Y-27632 (10 mM in DMSO) and 8.5 mL PBS. Use directly after preparation.

Colorectal cancer digestion buffer Combine 1 mL collagenase type II (15 mg/mL in PBS + 0.2% (wt/vol) BSA), 10 µL hyaluronidase type IV (10 mg/mL in ddH_2O), 20 µL Primocin, 10 µL Y-27632

(10 mM in DMSO) and 8.5 mL PBS. Use directly after preparation.

Red blood cell lysis buffer Add 8.26 g ammonium chloride, 1 g sodium bicarbonate and 200 µL EDTA (0.5 M) to 1 L of ddH2O. Stir for 30 minutes. Pass through 0.2 µm filter to sterilize. Store at 4 °C for up to 6 months.

NaH_2PO_4 Dissolve 28.39 g NaH_2PO_4 in 200 mL distilled water for a 1 M stock. Store at room temperature for up to 1 year.

KH_2PO_4 Dissolve 27.22 g KH_2PO_4 in 200 mL distilled water for a 1 M stock. Store at room temperature for up to 1 year.

NaCl Dissolve 58.44 g NaCl in 200 mL distilled water for a 5 M stock. Store at room temperature for up to 1 year.

KCl Dissolve 14.91 g KCl in 200 mL distilled water for a 1 M stock. Store at room temperature for up to 1 year.

D-sorbitol Dissolve 36.44 g D-sorbitol in in 200 mL distilled water for a 1 M stock. Store at room temperature for up to 1 year.

Sucrose Dissolve 68.46 g sucrose in 200 mL distilled water for a 1 M stock. Store at room temperature for up to 1 year.

DL-dithiotreitol Dissolve 1.54 g DL-dithiotreitol in 10 mL distilled water for a 1 M stock. Store at room temperature for up to 1 year.

Complete chelation solution Prepare 200 mL complete chelation solution by combining 1.12 mL of 1 M Na_2HPO_4 (for final concentration 5.6 mM), 1.6 mL of 1 M KH_2PO_4 (for final concentration 8.0 mM), 23.86 mL of 5 M NaCl (for final concentration 96.2 mM), 320 µL of 1 M KCl (for final concentration 1.6 mM), 6.68 mL of 1 M sucrose (for final concentration 43.4 mM) and 10.98 mL of 1 M D-sorbitol (for final concentration 54.9 mM) and 153.44 mL cold distilled water. Adjust to pH 7.0-7.3. Add 100 µL of 1 M DL-dithiothreitol (for final concentration 0.5 mM). Filter through 0.22 µm filter to sterilize. Store at 4 °C for maximum 1 day.

Box 1 | Establishment of healthy colon or airway organoids[25,26] • *Timing 2–3 h*

Procedure

1. Store tissue in Ad-DF+++ with 1× primocin at 4 °C for no longer than 24 h.
2. Remove the muscle layer and fat with forceps and razor blades.
3. Cut the tissue into small pieces.
4. Wash three times with CCS. Let the pieces sink to the bottom under normal gravity.
5. Add EDTA to a final concentration of 10 mM (200 µL of 0.5 M solution to 10 mL of CCS).
6. Incubate 45 min at 4 °C in a rotating wheel and shake vigorously to liberate crypts. The solution turns cloudy when crypts are liberated. If crypts are not liberated, replace EDTA–CCS with fresh solution and repeat step 6.
7. Allow tissue fragments to settle. Transfer the supernatant containing the crypts to a new tube and pipette up and down ten times.
8. Spin down the crypts (100g, for 5 min at 4 °C). Continue with Step 7 of the main protocol and culture similarly to tumor organoids. Use colon organoid medium for healthy colon organoids and NSCLC organoid medium for healthy airway organoids.

Box 2 | Production of Noggin-conditioned medium • *Timing 10 d*

Additional materials required

- DMEM (Gibco, cat. no. 41966). Store at 4 °C for up to 1 year.
- Geneticin (G418 sulfate, 50 mg/mL) (Gibco, cat. no. 10131035). Store at –20 °C in 500-µL aliquots for up to 1 year.
- HEK293-mNoggin-Fc cells (can be obtained from the laboratory of H. Clevers, Utrecht, The Netherlands). Store at –80 °C for up to 1 year or in liquid nitrogen, indefinitely.
- HEK293 culture medium: supplement DMEM with 1% (vol/vol) penicillin–streptomycin, 1% (vol/vol) ultraglutamine I and 10% (vol/vol) FBS. Store at 4 °C for up to 1 month.
- Selection medium: supplement 50 mL of HEK293 culture medium with 500 µL of 50 mg/mL geneticin (final concentration: 500 µg/mL). Store at 4 °C for up to 1 month.

Procedure

1. Preheat HEK293 growing medium to 37 °C.
2. Thaw a vial of HEK293-mNoggin-Fc cells in a 37 °C waterbath until a small clump of ice remains.
3. Transfer the cells to a 15-mL Falcon tube and add up to 10 mL of preheated HEK293 growing medium.
4. Centrifuge (300g, for 5 min at RT) and discard the supernatant.
5. Resuspend the cell pellet in 50 mL of selection medium and transfer to a T-175 culture flask.
6. Culture cells until confluency with the T-175 flask in a flat position.
7. Aspirate the medium and wash flask with 20 mL of PBS.
8. Collect cells by trypsinizing for up to 5 min with 5 mL of TrypLE Express at 37 °C.
9. Transfer cells to a 50-mL Falcon tube and add up 50 mL of PBS.
10. Centrifuge (300g, for 5 min at RT) and discard the supernatant.
11. Resuspend cells in HEK293 growing medium and split into 6× T-175 flasks. Culture five flasks in 50 mL of HEK293 growing medium and one flask in 50 mL of selection medium.
12. When cells reach confluency, replace medium with 50 mL of Ad-DF+++.

(*Continue next page*)

(From previous page)

13. Collect the conditioned medium after 1 week and centrifuge (300g, for 5 min at RT) to pellet cells.
14. Collect the supernatant and filter through a 0.2-µm filter unit.
15. Store the supernatant in aliquots of 50 mL at –20 °C. Conditioned medium can be stored for up to 6 months at –20 °C and for up to 2 weeks at 4 °C.
16. Use the cells cultured in the single flask with selection medium to repeat the procedure, or freeze the cells in small aliquots for later use. CRITICAL STEP Cells can be used for up to 12 passages to collect conditioned medium.

Box 3 | Preparation of compensation controls • *Timing 30 min*

For compensation, cells (option A) or compensation beads (option B) can be used. If cells are used, ensure that the relevant antigen is expressed. If necessary, stimulate cells to increase antigen expression. Compensation beads can only be used for antibody-based stains and not for dyes. A combination of compensation beads (for antibody-based stains) and cells (for dyes) is acceptable.

Procedure

(A) Preparation of compensation controls using cells

i. Prepare single-cell suspension of cells of interest and plate in a 96-well plate. The number of wells needed is equal to the number of different fluorochromes used in the staining panel plus one. CRITICAL STEP Work on ice from this step on and keep fluorochromes protected from light.
ii. Prepare stain dilutions for every fluorochrome used in the staining panel separately, at the same dilution as used in the staining panel.
iii. Wash cells in FACS buffer. Spin down at 330g, for 5 min at 4 °C and discard the supernatant.
iv. Add 20 µL of staining solution to separate wells for each stain. Leave one well unstained. For example, if the staining panel consists of anti-CD4–FITC and anti-CD8–BV421, stain one well with anti-CD4-FITC alone, one well with anti-CD8–BV421 alone and leave one well unstained. Mix well, without causing air bubbles.
v. Incubate for 30 min at 4 °C in the dark.
vi. Wash cells twice in FACS buffer. Spin down at 330g, for 5 min at 4 °C and discard the supernatant.
vii. Resuspend cells in 20–100 µL of FACS buffer and set up compensation on a suitable flow cytometer.
? TROUBLESHOOTING

(*Continue next page)*

(From previous page)

(B) Preparation of compensation controls using compensation beads

i. Vortex beads for 5 s.

ii. Mix one to three drops of negative and positive compensation beads.

iii. Pipette 20 µL of the beads mixture into as many wells as the number of antibody–fluorochrome conjugates that is used in the staining panel.

iv. Add 2 µL of antibody–fluorochrome conjugate per well. Use a different well for each different fluorochrome.

CRITICAL STEP Work on ice from this step on and keep fluorochromes protected from light.

v. Mix well by resuspending.

vi. Incubate for 5–60 min (at 4 °C in the dark).

vii. Set up compensation on a suitable flow cytometer.

? TROUBLESHOOTING

PROCEDURE

Establishment of tumor organoid culture from biopsy or resection material[24,25,26] ●
Timing 2-3 h

1. Dissect tissue with razor blade or needles on Petri dish to cubes of 1-2 mm^3.
2. Transfer tissue fragments to 15 mL Falcon tube and wash once in PBS. Centrifuge at 200g, for 5 minutes, at RT.
3. Discard supernatant and incubate tissue fragments for 15-60' at 37 °C in 10 mL colorectal or non-small cell lung cancer digestion buffer. Resuspend 10-15 times every 10 minutes and check the status of the digestion by evaluating using a microscope whether the tissue has dissociated into single cells.
   Δ CRITICAL STEP The total incubation time can vary depending on specimen size and tumor type: generally it can range from 15 to 30 minutes for biopsies, and from 45 to 60 minutes for resections.
4. Block the reaction by adding 2 mL of FBS when the tissue has dissociated so that >70% are single cells, or after 30 minutes for biopsies or 60 minutes for resections.
5. Pellet cells by centrifugation at 300g, 5', RT.
6. If the pellet is red, lyse erythrocytes by incubating for 5' in 5 mL red blood cell lysis buffer at room temperature. After lysis, fill up the 15 mL Falcon tube with PBS.
   Δ CRITICAL STEP This is not necessary if the pellet is not red.
7. Wash once more in PBS, centrifuge at 300g, 5', RT and discard the supernatant.
8. Count cells using a hemocytometer or automated cell counter.
9. Resuspend the pellet of cells in ice-cold complete organoid medium (roughly 1.5-3 * 10^4 cells/10 µL medium), and add 2 times the same volume of Geltrex.
   Δ CRITICAL STEP Geltrex needs to be kept ice cold at all times.
10. Plate digest/Geltrex drops in a 6-well culture plate (roughly 20 µL per drop).
11. Place the plate upside-down in a 37 °C incubator for 30 minutes, to let the Geltrex solidify.
12. Place plate in upright position and add complete organoid medium, supplemented with 1x Primocin.

Δ CRITICAL STEP Add Primocin to all medium until a frozen biobank is stored (step 20).

13. Replace medium with complete organoid medium twice per week.

Passaging organoids • *Timing 1 h*

Δ CRITICAL STEP Organoids can be passaged once every 1-2 weeks at a 1:2-1:6 split ratio. Split organoids when confluent or when their diameter exceeds 300 µm.

14. Remove complete organoid medium.
15. Resuspend organoid/Geltrex drops in pre-warmed TrypLE Express (1 mL/well).
16. Incubate at 37 °C for 5-15 minutes, resuspending with a p1000 pipette every 5 minutes.

    Δ CRITICAL STEP Avoid overtrypsinization. Check under microscope when organoids are dissociated into single cells: a mix of 70% single cells and 30% clusters of 7-10 cells is ideal.
17. Transfer TrypLE mix into a 15 mL Falcon tube.
18. Inhibit TrypLE by diluting 5-10 fold with cold Ad-DF+++.
19. Spin 300g, 5' and remove supernatant.
20. Repeat step 9-13.

Freezing organoids • *Timing 30 minutes*

Δ CRITICAL STEP Organoids are typically frozen after expansion to >5*10^5 organoids, which typically requires 5-11 weeks of culture with 2-4 passages (Fig. 1b-c).

Δ CRITICAL STEP Not all cells need to be frozen. If you so wish, retain some cells, these are ready for use in step 44.

21. Remove complete organoid medium and resuspend in ice cold Ad-DF+++ (1 mL Ad-DF+++ per well)

    Δ CRITICAL STEP Freezing (and thawing) steps are most efficient if organoids are frozen 3-5 days after passaging.
22. Transfer the suspension into a 15 mL Falcon tube and fill up tube with Ad-DF+++.
23. Spin 300g, 5', 4 °C.
24. Resuspend the pellet in ice cold 10% (vol/vol) DMSO/FCS. Use 1 mL of freezing medium per $5*10^4$ organoids.
25. Add 1 mL of the freezing mix per cryovial and quickly place the cryovials into a freezing container (e.g. Mr Frosty). Store at -80 °C overnight.

    Δ CRITICAL STEP Keep freezing medium ice cold during freezing and place the freezing container into a -80 °C freezer without delay.
26. Transfer cryovials to liquid nitrogen for long-term storage.

    ▫ PAUSE POINT Cells can be stored in liquid nitrogen indefinitely.

Thawing organoids • *Timing 1 hour*

27. Pre-heat 10 mL Ad-DF+++ at 37 °C.
28. Quickly thaw cryovials containing organoids in a 37 °C water bath.

    Δ CRITICAL STEP Do not completely thaw the frozen cells: a small clump of ice should remain when the vial is removed from the water bath.
29. Quickly transfer the content of the vial into a 15 mL Falcon tube and add 10 mL pre-warmed Ad-DF+++ in a dropwise manner.
30. Spin 300g, 5', room temperature. Remove supernatant.
31. Plate as described in steps 9-13.

Isolation of human peripheral blood mononuclear cells from blood • *Timing 2 h*

32. Prepare 0.1% (wt/vol) BSA in PBS (PBSA). Pass through 0.2 µm filter to sterilize.
33. Dispense blood into 50 mL Falcon tubes (15 mL per tube).
34. Add equal volume of 0.1% PBSA to each tube.
35. Transfer to 50 mL tubes containing 15 mL Lympholyte H. Lock the two tubes in a horizontal position and very carefully tilt the tubes so that a slow flow of blood starts and forms a layer on top of the Ficoll.
36. Spin 15', 1200g, no break, no acceleration, room temperature.
37. There will be a bottom layer of red blood cells, followed by a thin layer of PBMC and then a layer of plasma. Remove plasma to reach the PBMC.
    Δ CRITICAL STEP Minimize movement of tubes to maintain separation of the layers.
38. Collect PBMC in a separate tube by carefully pipetting up the cells from the layer.
39. Wash 2x with 0.1% PBSA (between washes spin at 1,000 g, 7', RT and discard the supernatant).
40. Wash once with PBSA followed by a spin at 200g, 7', RT to remove platelets. Discard supernatant.
41. If necessary, remove erythrocytes by incubating for 5 min in red blood cell lysis buffer at 37 °C. Wash again with PBSA and centrifuge (200g, 7', RT).
42. Count cells using hemocytometer or automated cell counter.
43. Cryopreserve cells for later use (as described in step 81A).

Organoid isolation for co-culture of tumor cells and peripheral blood mononuclear cells (day -2) • *Timing 30 min*

44. Aspirate medium from 6-well plate with organoids (containing 1-5*10^4 organoids per well, from step 12). Use one well for every 2 * 10^6 PBMC to be used for co-culture in step 71.
45. Add 1 mL/well of pre-heated (37 °C) dispase (2 mg/mL in PBS).
    Δ CRITICAL STEP Dispase treatment allows isolation of organoids from Geltrex. This step is essential to prevent recognition of Geltrex-derived epitopes by $CD4^+$ T cells.
46. Resuspend organoids by gently pipetting up and down with a P1000 pipette.
47. Incubate for 15' at 37 °C.
48. Transfer organoid suspension to a 15 mL Falcon tube.
49. Add 100 µL EDTA (0.5 M) for every 1 mL of dispase used and fill up tube up till 10 mL with PBS.
50. Pellet organoids (300g, 5', RT) and aspirate supernatant.
51. Resuspend organoids in complete organoid culture medium and plate 2-4 mL/well of a tissue culture-treated 6-well plate. Use 2 mL for every well used in step 44.
    Δ CRITICAL STEP Add 10 µM Y-27632 dihydrochloride to prevent cell death due to detachment from Geltrex.
52. Culture organoids for 24h at 37 °C.

Co-culture preparation (day -1) *Timing 1 h*

53. Add 200 ng/mL IFNγ to organoids to enhance antigen presentation.
54. Coat tissue culture-treated 96-well U-bottom plate with 5 µg/mL anti-CD28 in PBS (50 µL/well). Wrap plate in parafilm and incubate for 24 h at 4 °C. Anti-CD28 provides co-stimulatory signals during co-culture.
55. Quickly thaw cryopreserved PBMC at 37 °C.
56. Transfer PBMC to 15 mL Falcon tube and add up to 15 mL pre-heated (37 °C) T cell thawing medium in a drop-wise manner.

Δ CRITICAL STEP Cell loss during thawing can be up to 50%. Pre-heating of medium is essential for good recovery upon thawing.

57. Pellet cells (200g, 12', RT, intermediate deceleration).
58. Remove supernatant and incubate for 15' at 37 °C in 5 mL T cell thawing medium with 1:1,000 benzonase.

    Δ CRITICAL STEP Benzonase prevents cell clumping due to DNA released by dying cells. This is particularly important when thawing PBMC.
59. Fill up tube with T cell thawing medium and pellet cells (200g, 12', RT, intermediate deceleration). Discard supernatant.
60. Resuspend cells at 2 * 10^6/mL in T cell culture medium and add 150 u/mL of IL-2 and incubate overnight. To prevent adhesion of myeloid cells to the culture dish, leave cells in a 15 mL Falcon tube with a slightly opened lid wrapped in parafilm to allow gas exchange. Do not add >4 mL/tube to ensure sufficient oxygenation.

Co-culture (day 0) • *Timing 14 d*

61. Collect medium containing organoids in suspension that have been incubated with IFNγ overnight and spin down (300g, 5', RT). Remove supernatant.
62. Resuspend pellet in 1 mL/well TrypLE and combine with remaining cells that have adhered to the culture plate.
63. Incubate for 5-15' at 37 °C. Resuspend every few minutes and check using a microscope if organoids or big clusters of cells are still present. Stop when they have dissociated into single cells.

    Δ CRITICAL STEP Take care to prevent overtrypsinization. Some small cell clusters are acceptable.

    ? TROUBLESHOOTING
64. Transfer dissociated organoids to 15 mL Falcon tube and fill up with PBS.
65. Pellet dissociated organoids (300g, 5', RT).
66. Remove supernatant and resuspend pellet in 1 mL T cell culture medium.

67. Count cells using a hemocytometer.

    Δ CRITICAL STEP Resuspend well before taking a count sample to prevent dissociated organoids from sinking to the bottom of the tube.

68. Resuspend dissociated organoids at 5 * 10^4 cells/mL in T cell culture medium.
69. Resuspend PBMC from step 60 and count using hemocytometer or automated cell counter.
70. Wash PBMC in PBS (500g, 5', RT).
71. Resuspend PBMC at 1 * 10^6 cells/mL in T cell culture medium, supplemented with 300 U/mL IL-2 (2x concentrated) and 40 µg/ml anti-PD1 (2x concentrated).
72. Mix equal volume of dissociated organoids and PBMC for a PBMC:tumor cell ratio of 20:1.
73. Wash anti-CD28-coated plate 2x with PBS. Do not leave plate dry.
74. Plate 200 µL dissociated organoid / PBMC suspension per well and incubate at 37 °C.
75. Refresh or split co-culture every 2-3 days. If medium does not turn yellow after 2-3 days, follow option A. If medium turns yellow, follow option B.

(A) Refreshing co-culture

i. Gently remove 100 µL of culture medium per well.
ii. Add 100 µL T cell culture medium, supplemented with 300 U/mL IL-2 (2x concentrated) and 40 µg/ml anti-PD1 (2x concentrated).

(B) Splitting co-culture

i. Split cells 1:1 by resuspending cells and transferring 50% of volume to a new well. Note that there is no need to separate tumor cells from T cells at this stage.
ii. Add 100 µL T cell culture medium, supplemented with 300 U/mL IL-2 (2x concentrated) and 40 µg/ml anti-PD1 (2x concentrated).

Re-stimulation with tumor cells (day 7)

76. After 5 days of co-culture, repeat steps 44-52.
77. After 6 days of co-culture, repeat steps 53-54.
78. After 7 days of co-culture, resuspend co-cultured PBMC and transfer to 15 mL Falcon tube. Note that there is no need to separate tumor cells from PBMC at this stage; resuspension is sufficient to enrich for PBMC over tumor cells, since most tumor cells either adhered to the plastic, or have died during co-culture.
79. Repeat steps 61-75.
80. After 14 days of co-culture, collect PBMC and proceed with downstream assays. Note that after 2 weeks of co-culture, T cells should represent 90% of the total PBMC population (Fig. 1d).

Downstream assays

81. After co-culture, cells can be cryopreserved (option A), evaluated for tumor reactivity using IFNγ and CD107a as read-outs (option B), evaluated for tumor reactivity using CD137 as a read-out (option C), or can be used in tumor killing assays (option D). Typically, reactivity is assessed before cryopreservation, initially based on IFNγ and CD107a and if desired, confirmed using CD137 as a read-out.

(A) Cryopreservation of co-cultured T cells • *Timing 30 min*

(i) Count T cells using hemocytometer or automated cell counter.

(ii) Pellet T cells (500 g, 5', 4 °C).

(iii) Resuspend at 5-10 * 10^6/mL in ice cold freezing medium.

(iv) Quickly transfer 1 mL/vial to cryovials.

(v) Freeze immediately in Mr Frosty or comparable freezing container at -80 °C.
▫ PAUSE POINT Cells can be stored at -80 °C for 1 month. For long-term storage, transfer cells to liquid nitrogen.

(B) Tumor reactivity assay using IFNγ and CD107a as a read-out • *Timing 4 d, 24h required for reactivity assay*

(i) Two days before reactivity assay: repeat steps 44-52. If required for experimental design, prepare healthy tissue organoids as a control as described in Box 1 and processed as described above for tumour organoids.

(ii) One day before reactivity assay: repeat steps 53-54. If required for experimental design, prepare healthy tissue organoids as a control as described in Box 1 and processed as described above for tumour organoids.

(iii) Proceed with reactivity assay.
Repeat steps 61-67.

(iv) Resuspend dissociated organoids at 1 * 10^6 cells/mL in T cell culture medium.

(v) Count T cells using hemocytometer or automated cell counter.

(vi) Pellet T cells (500 g, 5', 4 °C).

(vii) Resuspend T cells at 2 * 10^6 cells/mL in T cell culture medium.

(viii) Prepare 3X anti-CD107a-PE/anti-PD1 master mix by adding 1:50 anti-CD107a-PE and 60 µg/mL anti-PD1 to T cell culture medium.

CD107a expression at the cell surface is transient due to recycling of cytotoxic granules and therefore the antibody is added throughout the co-culture.

Δ CRITICAL STEP Keep anti-CD107a-APC protected from light.

(ix) Prepare 3X PMA/Ionomycin solution by adding 150 ng/mL PMA and 3 µg/mL ionomycin to T cell culture medium.

(x) If using MHC-blocked organoids as controls, incubate dissociated organoids with 150 µg/mL of mouse anti-human HLA-ABC, clone W6/32, to block MHC-I and/or 30 µg/mL of mouse anti-human HLA-DR/DP/DQ, clone Tü39, to block MHC-II for 30' at 37 °C.

(xi) Wash anti-CD28-coated (step 54) tissue culture-treated 96-well U-bottom plate 2x with PBS.

Δ CRITICAL STEP Do not leave plate dry for >5 minutes.

We chose to use anti-CD28-coated plates also during the tumor reactivity assay to maintain co-stimulatory signals. If this is not desired, use a non-coated plate.

(xii) Plate 50 µL (= 1 * 10^5) T cells per well, and add 50 µL of anti-CD107a-APC/anti-PD1 master mix per well.

(xiii) Add 50 µL (= 5 * 10^4) tumor cells (test condition), 50 µL of T cell culture medium (negative control), or 50 µL of PMA/Ionomycin solution (positive control). Additional controls can include dissociated healthy organoids, tumor cells incubated with MHC-I/II blocking antibodies, from step (x), or single cell digests of tumor or healthy tissue (for preparation, follow steps 1-8).

(xiv) Mix well and spin (200g, 1', RT) to loosely pellet cells.

(xv) Incubate for 1 h at 37 °C.

(xvi) Prepare 4x GolgiStop/GolgiPlug solution by adding 1:375 GolgiStop (BD) and 1:250 GolgiPlug (BD) to T cell culture medium.

(xvii) Add 50 µL GolgiStop/GolgiPlug to each well.

(xviii) Mix well and spin (200g, 1', RT) to loosely pellet cells.

(xix) Incubate for 4 h at 37 °C.

(xx) Pellet cells (330g, 5', 4 °C) and remove supernatant.

Δ CRITICAL STEP Work on ice from this step on and keep fluorochromes protected from light.

(xxi) Wash cells in 200 µL/well FACS buffer. Centrifuge at 330g, 5', 4 °C and remove supernatant.

(xxii) Prepare cell surface staining solution with 1:20 anti-CD3-PerCP-Cy5.5, 1:20 anti-CD4-FITC, 1:200 anti-CD8-BV421 and 1:2,000 near-IR viability dye in FACS buffer.

(xxiii) Add 20 uL of the solution of step (xxii) to each well. For preparation of compensation controls, see Box 3.

(xxiv) Mix well without causing air bubbles.

(xxv) Incubate for 30' at 4 °C, protected from light.

(xxvi) Wash 2x with 200 µL FACS buffer (after each wash spin down cells at 330g, 5', 4 °C and then remove supernatant).

(xxvii) Fix cells in 80 µL Fix/Perm buffer (BD) on ice. Mix immediately.

(xxviii) Incubate for 20' at 4 °C, protected from light.

▫ PAUSE POINT After fixation, cells can be stored for 24h. Wash cells 1x with 200 µL FACS buffer to remove fixative and store in 20-100 µL FACS buffer. If desired, continue with the following steps the following day.

(xxix) Wash 2x with 200 µL Perm/Wash buffer (Fixation/Permeabilization kit, BD) (after each wash, spin down cells at 500g, 5', 4 °C and remove supernatant).

(xxx) Prepare intracellular staining solution with 1:40 anti-IFNγ-APC in Perm/Wash buffer (Fixation/Permeabilization kit, BD).

(xxxi) Add 20 uL of the solution made in step (xxx) to each well.

(xxxii) Mix well without causing air bubbles.

(xxxiii) Incubate for 30' at 4 °C, protected from light.

(xxxiv) Wash 2x with 200 µL Perm/Wash buffer (after each wash spin down at 500g, 5', 4 °C and discard supernatant).

(xxxv) Resuspend cells in 50 -100 µL FACS buffer and record on a suitable flow cytometer.

▫ PAUSE POINT It is possible to store the samples in 50-100 µL FACS buffer overnight at 4 °C in the dark and continue with the recording the morning after.

Examples of flow cytometry plots are shown in Figure 2a.

? TROUBLESHOOTING

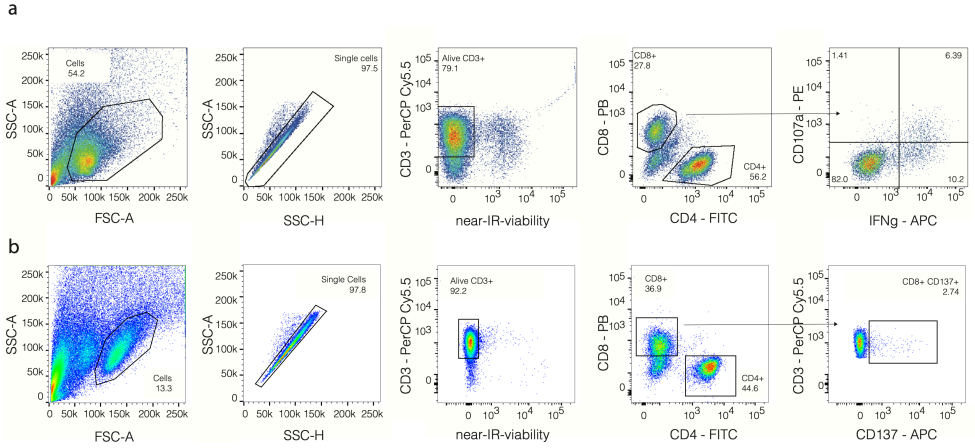

Fig. 2. Examples of flow cytometry plots showing tumor reactivity of CD8⁺ T cells.

After 2 weeks of coculture, T cells were restimulated with tumor organoids as described in Step 81B or 81C of this protocol.

a,b, Intracellular IFNγ and cell surface CD107a **(a)** or CD137 **(b)** are used as a read-out of reactivity. Gating strategy is shown. FSC-A, forward scatter–area; SSC-A, side scatter–area; SSC-H, side scatter–height.

(C) Tumor reactivity assay using CD137 as a read-out • *Timing 4 d, including 24h for reactivity assay*

(i) Two days before reactivity assay: repeat steps 44-52. If required for experimental design, prepare healthy tissue organoids as a control as described in Box 1 and processed as described above for tumour organoids.

(ii) One day before reactivity assay: repeat steps 53-54. If required for experimental design, prepare healthy tissue organoids as a control as described in Box 1 and using the same steps as used for tumor organoids.

(iii) Proceed with reactivity assay by repeating steps 61-67.

(iv) Resuspend dissociated organoids at 5 * 10^5 cells/mL in T cell culture medium.

(v) Count T cells using hemocytometer or automated cell counter.

(vi) Pellet T cells (500 g, 5', 4 °C) and discard supernatant.

(vii) Resuspend T cells at 1 * 10^6 cells/mL in T cell culture medium. Add 40 µg/mL anti-PD1 (2X final concentration).

(viii) Prepare 2X PMA/Ionomycin solution by adding 100 ng/mL PMA and 2 µg/mL ionomycin to T cell culture medium.

(ix) If using MHC-blocked organoids as controls, incubate dissociated organoids with 150 µg/mL of mouse anti-human HLA-ABC, clone W6/32, to block MHC-I and/or 30 µg/mL of mouse anti-human HLA-DR/DP/DQ, clone Tü39, to block MHC-II for 30' at 37 °C.

(x) Wash anti-CD28-coated (step 54) tissue culture-treated 96-well U-bottom plate 2x with PBS.

Δ CRITICAL STEP Do not leave plate dry for >5 minutes.

We chose to use anti-CD28-coated plates also during the tumor reactivity assay to maintain co-stimulatory signals. If this is not desired, use a non-coated plate.

(xi) Plate 100 µL (= 1 * 10^5) T cells per well, and add 100 µL (=5 * 10^4) tumor cells (test condition), 100 µL of T cell culture medium (negative control), or 100 µL of PMA/Ionomycin solution (positive control). Additional controls can include healthy organoids, organoids incubated with MHC-I/II blocking antibodies, or single cell digests of tumor or healthy tissue (for preparation, follow steps 1-8).

(xii) Mix well and spin (200g, 1', RT) to loosely pellet cells.

(xiii) Incubate for 24 h at 37 °C.

(xiv) Pellet cells (330g, 5', 4 °C) and remove supernatant.
Δ CRITICAL STEP Work on ice from this step on and keep fluorochromes protected from light. Wash cells in 200 µL/well FACS buffer (330g, 5', 4 °C).

(xv) Prepare cell surface staining solution with 1:20 anti-CD3-PerCP-Cy5.5, 1:20 anti-CD4-FITC, 1:200 anti-CD8-BV421, 1:2,000 near-IR viability dye and 1:30 anti-CD137-APC in FACS buffer.

(xvi) Add 20 uL of the solution of step (xv) to each well. For preparation of compensation controls, see Box 3.

(xvii) Mix well without causing air bubbles.

(xviii) Incubate for 30' at 4 °C, protected from light.

(xix) Wash 2x with 200 µL FACS buffer (after each wash, spin at 330g, 5', 4 °C and discard supernatant).

(xx) Resuspend cells in 50 -100 µL FACS buffer and record on a suitable flow cytometer. Examples of flow cytometry plots are shown in Figure 2b.
? TROUBLESHOOTING
▫ PAUSE POINT Cells can be rested for up to 4 hours before recording on a flow cytometer if kept at 4 °C, protected from light.

(D) Tumor organoid killing assay * TIMING 5 d

(xxi) Organoid isolation (day -2). Aspirate medium from 6-well plate with organoids.
Δ CRITICAL STEP Two wells of a 6-well plate (1-5*10^4 organoids per well) is sufficient to perform the experiment.

(xxii) Add 1 mL/well of pre-heated (37 °C) dispase (2 mg/mL in PBS).

(xxiii) Resuspend organoids by gently pipetting up and down with a P1000 pipette

(xxiv) Incubate for 5-15' at 37 °C.
Δ CRITICAL STEP Take care to prevent over incubation with dispase II. Dispase can lead to dissociation of organoids into single cells for a small fraction of organoid lines. Monitor organoids closely, and when detachment of single cells is observed, stop the reaction and continue with the following step.

(xxv) Transfer organoid suspension to a 15 mL Falcon tube.

(xxvi) Add 100 µL EDTA (0.5 M) for every 1 mL of dispase used and fill up tube up till 10 mL with PBS.
Pellet organoids (300g, 5', RT) and aspirate supernatant.

(xxvii) Resuspend organoids in complete organoid culture medium and plate 2-4 mL/well of a tissue culture-treated 6-well plate. Use 2 mL for every well used in step (i).
Δ CRITICAL STEP Add 10 µM Y-27632 dihydrochloride to prevent cell death due to detachment from Geltrex.

(xxviii) Culture organoids for 24h at 37 °C.

(xxix) Co-culture preparation (day -1). Add 200 ng/mL IFNγ to organoids to enhance antigen presentation.

(xxx) Coat a non-tissue culture-treated 96-well flat-bottom plate with 5 µg/mL anti-CD28 in PBS (50 µL/well). Wrap plate in parafilm and incubate for 24 h at 4 °C. Anti-CD28 provides co-stimulatory signals during co-culture.

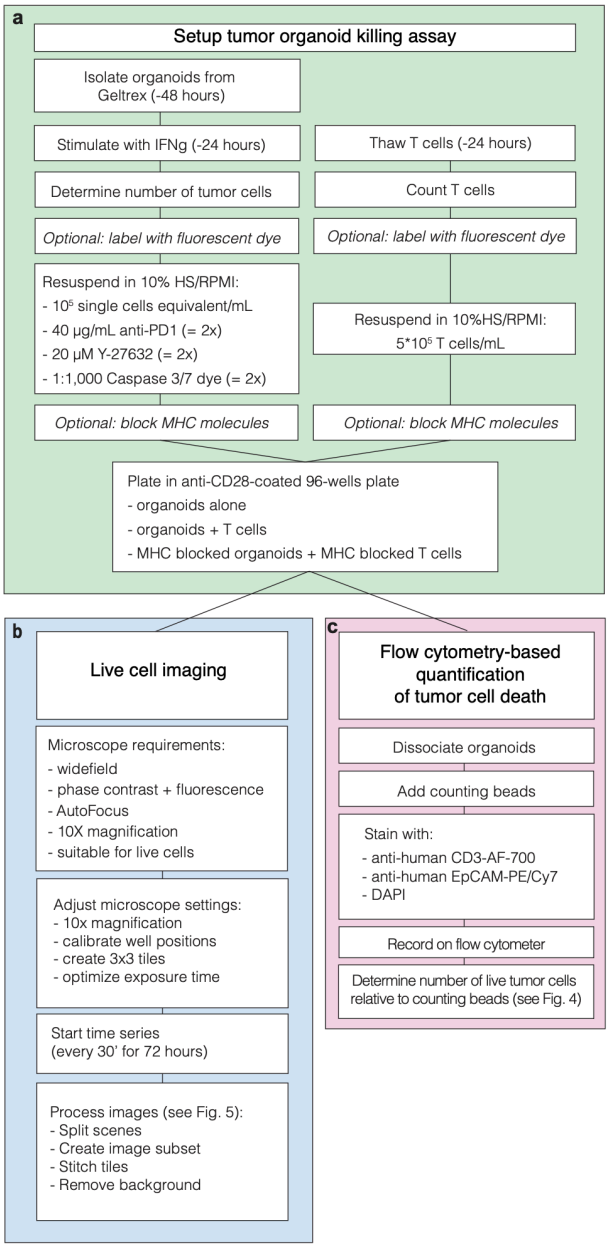

Fig. 3. Killing experiment overview.

a, Experimental setup.

b, Flow-cytometry-based quantification of the amount of alive tumor organoids.

c, Live-cell imaging setup and processing.

(xxxi) Killing assay (day 0). Collect organoids from the 6-well plate. Most organoids will either be in suspension or are loosely attached to the culture plate, and can be collected by resuspending the solution several times. Transfer the suspension of organoids and medium into a 15 mL tube. Split the total volume into two aliquots: 1/11 of the total volume will be used for dissociation into single cells and counting; 10/11 of the total volume will be used as fully formed organoids for the experiment.

? TROUBLESHOOTING

(xxxii) Pellet the 1/11 aliquot (300g, 5', RT). Resuspend the pellet in 500 uL TrypLE. Incubate 5-15' minutes at 37 °C. Resuspend every few minutes and check if organoids have dissociated. Stop when they have dissociated into single cells.

Δ CRITICAL STEP Take care to prevent overtrypsinization. Some small cell clusters are acceptable.

(xxxiii) Count cells using a hemocytometer.

Δ CRITICAL STEP Resuspend well before taking a count sample to prevent dissociated organoids from sinking to the bottom of the tube.

(xxxiv) The 10/11 aliquot will contain 10 times the number of cells that was counted in the 1/11 aliquot, but in the form of organoids ("single cell equivalents")

(xxxv) Wash organoids in PBS (300g, 5', RT) to remove IFNγ (added in step 81D(x)) from the medium.

(xxxvi) If desired, label organoids with fluorescent dyes by resuspending organoids in 1 mL 1:1,000 CellTrace FarRed or 1:10,000 CellTrace Yellow (in PBS). If T cells are also labelled with a fluorescent dye, make sure to use different dyes for T cells and organoids. Mix immediately. Incubate 20' at 37 °C, dark. Resuspend well every 5-10'. Block the labelling with 10 mL 10% (vol/vol) FBS/PBS (5', RT). Wash twice with 10 mL PBS (300g, 5', RT).

Δ CRITICAL STEP Organoids can be distinguished from T cells by labelling with fluorescent dyes as an alternative to staining with fluorescent antibodies. This may be preferred if separation by flow cytometry is difficult after staining with antibodies.

Δ CRITICAL STEP Before starting staining, take aside an aliquot of organoids to be used as unstained control during compensation (see Box 3).

Δ CRITICAL STEP Before continuing, take aside an aliquot of organoids to be used as single stained control during compensation (see Box 3).

(xxxvii) Resuspend organoids at 10^5 single cell equivalents/mL in T cell culture medium. Add:

anti-PD1 at 40 µg/mL concentration (2X final concentration); Y-27632 dihydrochloride at 20 µM concentration (2X final concentration); and 1:1,000 NucView488 caspase 3/7 dye (2X final concentration)

(xxxviii) Block MHC molecules on tumor organoids by taking aside three aliquots and incubating for 30' at 37 °C with the following: in the first, 50 µg/mL of mouse anti-human HLA-ABC, clone W6/32, to block MHC-I; in the second 10 µg/mL of mouse anti-human HLA-DR/DP/DQ, clone Tü39, to block MHC-II; and in the third 50 µg/mL of mouse anti-human HLA-ABC, clone W6/32, and 10 µg/mL of mouse anti-human HLA-DR/DP/DQ, clone Tü39, to block both MHC-I and MHC-II. Resuspend all three aliquots well every 5-10'.

(xxxix) Resuspend T cells and count using hemocytometer or automated cell counter.

(xl) Pellet T cells (300g, 5', RT)

(xli) If required, label T cells with fluorescent dyes by resuspending T cells in 1 mL 1:10,000 CellTrace FarRed or 1:100,000 CellTrace Yellow (in PBS). If organoids are also labelled with a fluorescent dye, make sure to use different dyes for T cells and organoids.. Mix immediately. Incubate 20'at 37 °C, dark. Resuspend well every 5-10'. Block the labelling with 10 mL 10% (vol/vol) FBS/PBS (5', RT). Wash twice with 10 mL PBS (300g, 5', RT)

Δ CRITICAL STEP Before starting, take aside an aliquot of T cells to be used as unstained control during compensation (see Box 3).

Δ CRITICAL STEP Before continuing to the next step, take aside an aliquot of T cells to be used as single stained control during compensation (see Box 3).

(xlii) Resuspend T cells at 5 * 10^5 cells/mL in T cell culture medium.

This results in a 5:1 T cell:tumor cell ratio. Other ratios can be used to measure dose dependent effects.

(xliii) Block MHC molecules on T cells by taking aside three aliquots and incubating the first with 50 ug/mL of of mouse anti-human HLA-ABC, clone W6/32, to block MHC-I for 30' at 37 °C; the second with 10 ug/mL of of mouse anti-human HLA-

DR/DP/DQ, clone Tü39, to block MHC-II for 30' at 37 °C; and the third with 50 ug/mL of mouse anti-human HLA-ABC, clone W6/32, and 10 µg/mL of mouse anti-human HLA-DR/DP/DQ, clone Tü39, to block both MHC-I and MHC-II for 30' at 37 °C. Resuspend all three aliquots well every 5-10'.

(xliv) Wash the anti-CD28-coated plate twice with 200 µL PBS per well. Do not leave the wells dry.

We chose to use anti-CD28-coated plates also during the tumor killing assay to maintain co-stimulatory signals. If this is not desired, use a non-coated plate.

(xlv) Plate each of the following in triplicate:

Organoids alone: 100 µL (= 1 * 10^4) tumor organoids + 100 µL T cell culture medium per well;

Organoids + T cells: 100 µL (= 1 * 10^4) tumor organoids + 100 µL (= 5 * 10^4) T cells per well;

Organoids + T cells + MHC-I block: 100 µL (= 1 * 10^4) MHC-I blocked organoids + 100 µL (= 5 * 10^4) MHC-I blocked T cells per well;

Organoids + T cells + MHC-II block: 100 µL (= 1 * 10^4) MHC-II blocked organoids + 100 µL (= 5 * 10^4) MHC-II blocked T cells per well;

Organoids + T cells + MHC-I/II block: 100 µL (= 1 * 10^4) MHC-I/II blocked Organoids + 100 (= 5 * 10^4) µL MHC-I/II blocked T cells per well;

Unstained and single stained controls for compensation setup: 100 µL (= 1 * 10^4) of unstained or single stained organoids + 100 µL T cell culture medium per well.

(xlvi) Take picture with regular microscope and incubate 72 h at 37 °C or proceed to next step with live cell imaging.

(xlvii) This and the following steps provide specific instructions for live cell imaging using ZeissPro imaging software. These can be taken as guidance for use with alternative software. General steps are indicated. First insert the plate in the appropriate location at the microscope. Remove lid, place the protection cover on top, and attach the CO_2 cover.

Δ CRITICAL STEP Keep the plate in the dark during the setup of the experiment

Δ CRITICAL STEP A widefield microscope, allowing recording of phase contrast in

combination with fluorescence, suitable for live cells, and equipped with AutoFocus system is necessary for this step.

(xlviii) For any software used, set magnification to 10X

(xlix) For any software used, calibrate plate and optimize exposure time. When using ZeissPro, load ZeissZenPro program, acquisition mode. Check all the following parameters:

Δ CRITICAL STEP Ensure there will be enough storage space on the hard drive.

Camera: HDCam full 10X

Carrier setup: 96 wells plate

Calibration: 7-points method. Follow the instructions provided by the software.

Focus strategy: absolute fixed. Check "use z-position from tiles set up"

Tiles: create a 3x3 tile for each scene you want to record, fix the z position for each position

Setup exposure time for bright-field and fluorochromes: ensure to maximize the signal without reaching saturation levels

For any software used: set time series to desired frequency (30 minutes)

Enable autosave to a specified folder

Start experiment and record for 72 hours.

(l) Killing quantification (day 3). Take endpoint pictures using regular microscope or finish live imaging.

(li) Wash cells twice with 200 µL PBS per well to remove serum from the medium.

(lii) Resuspend and transfer cell suspension into a 96-well U-bottom plate. Spin 500g, 5', RT. Decant supernatant.

(liii) During the spinning of the U-bottom plate, add 150 µL TrypLE per well to the empty 96-well flat-bottom plate, to be sure to detach any remaining cells from the bottom of the plate. Incubate 5' at 37 °C.

(liv) Combine TrypLE from flat-bottom plate with U-bottom plate to dissociate both the organoids that were in suspension and those that attached to the plate.

(lv) Incubate 5'-15' at 37 °C. Resuspend well every 5'.

Δ CRITICAL STEP Carefully check very often under the microscope whether organoids have dissociated into single cells. When dissociated, immediately proceed to step (xxxvii).

? TROUBLESHOOTING

(lvi) After cells are dissociated, inhibit TrypLE with 50 µL FBS per well. In this case, FBS is used to inhibit TrypLE because the volume in the well is too low to sufficiently dilute and wash out TrypLE.

(lvii) Add 5 µL per well of counting beads.

Δ CRITICAL STEP Ensure the number of beads per well is the same. If available, use a repetitive automated pipette.

(lviii) Pellet the cells (500g, 5', RT). Discard supernatant.

(lix) Wash the cells twice with 200 µL PBS per well (after each wash spin at 500g, 5', RT and then discard supernatant).

(lx) If cells have been stained with CellTrace dyes, skip this step and proceed directly to step 82D(xlii). Otherwise add 20 µL of staining mix containing 1:20 anti-CD3-AF700 and 1:200 anti-EpCAM-PE-Cy7 to each well. Incubate 30', 4 °C, dark. Wash the plate twice with 200 µL FACS buffer per well.

(lxi) Resuspend each well in 50 µL FACS buffer.

(lxii) Add DAPI (1:50) prior to recording on flow cytometer.

(lxiii) Prepare compensation controls as described in Box 3

(lxiv) Record on flow cytometer.

Δ CRITICAL STEP It is very important to resuspend cells right before recording to prevent cells from settling on the bottom of the tube.

(lxv) Calculate the amount of alive tumor cells per bead per well. An example of the gating strategy using antibodies or CellTrace dyes is shown in Fig. 4 and Suppl. Fig. 1, respectively.

? TROUBLESHOOTING

a

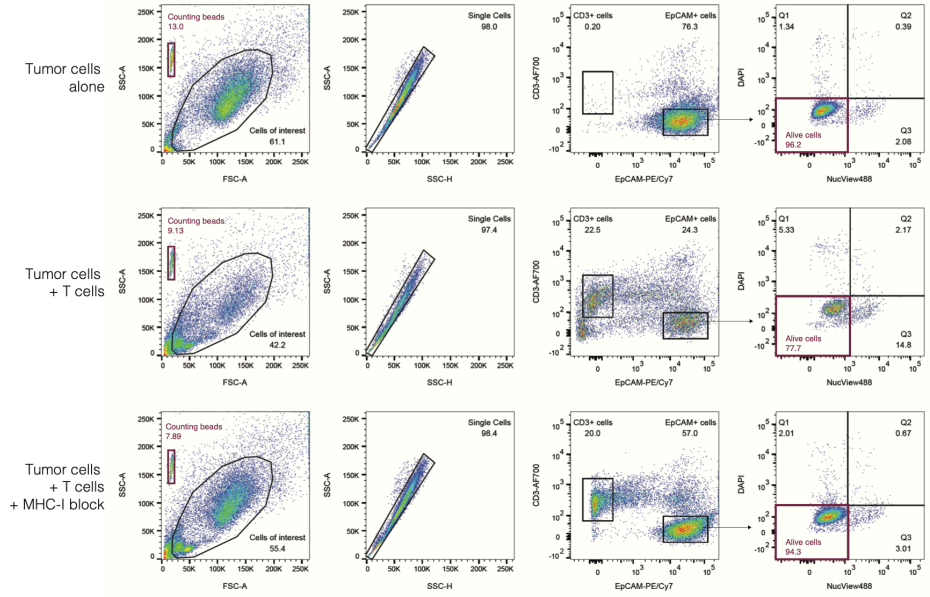

b

	Beads (count)	Alive tumor cells (count)	Alive tumor cells per bead
Tumor cells alone	3231	10949	3.4
Tumor cells + T cells	2403	2040	0.8
Tumor cells + T cells + MHC block	3009	11181	3.7

c

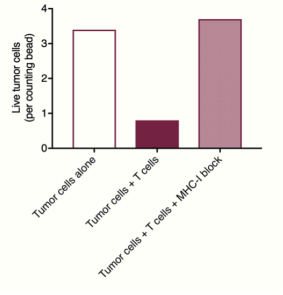

Fig. 4. Quantification of the tumor organoid killing assay.

a, Examples of flow cytometry plots showing tumor cells after a 72-h incubation with or without previously obtained autologous T-cell populations, in the presence or absence of MHC-I-blocking antibodies. The number of live tumor cells, defined as EpCAM+, DAPI– and NucView488–, is evaluated. Gating strategy is shown.
b, The absolute count of events in the alive cells gate is divided by the number of events in the counting beads gate (red box in a).
c, Bar graph of the number of live cells, normalized to counting beads

(lxvi) Optional: processing of live imaging data. Open the file with Zeiss ZenPro, processing mode. It will be a large file that has two dimensions: scenes (the well or condition) and time points (if one image was taken every 30 minutes for 72 hours, there will be 144 different time points).

Δ CRITICAL STEP Here, specific instructions are provided for ZeissPro imaging software. These can be taken as guidance for use with alternative software.

(lxvii) Use the function "split scenes" of the program to split scenes: instead of a large unique file, it will create several files (one per scene).

Δ CRITICAL STEP It is an important step to reduce the size of the file to be able to work with the recorded data.

(lxviii) Create region of interest. If not all tiles are needed, it is possible to further reduce the size of each scene by creating a smaller area of interest. If using Zeiss ZenPro, use the function "create image subset". Check the following parameters: All channels, to extract data on all the different channels used for the experiment; Extract all time points (unless you want to focus on a particular time frame; in that case, select time of interest); and rectangular region. Select and apply spatial rectangular region of interest.

Δ CRITICAL STEP It is possible to perform this step in batch, for all scenes at the same time. To do this select batch analysis on the program, and select all the different files of interest.

(lxix) Stitch tiles by using the function "Stitch" to fuse the 3x3 tiles in a unique file. Check "fuse tiles" and unselect the automatic function. In the "Channel to stitch" field select "bright field" because it is the channel that contains most of the data, making the stitch function more accurate. Choose to stitch multiple dimensions: c-dimension (channel) = reference, to stitch all the different channels in accordance with the bright field; and t-dimension (time) = reference, it is easier if a time point in the middle of experiment is selected (organoids may have moved in the field since the beginning of the experiment). Check and apply "create a new output".

Δ CRITICAL STEP If you do not select a new output it will overwrite the original data.

Δ CRITICAL STEP It is possible to perform this step in batch, for all scenes at the

same time. To do this, select batch analysis on the program, and select all the different files of interest.

(lxx) If you need to remove background, for example if for some of the fluorochromes the background signal is too intense, use background removal function for that channel (function available also in other programs, such as FiJi or Imaris). An example of the processing of live imaging data is shown in Fig. 5.

? TROUBLESHOOTING

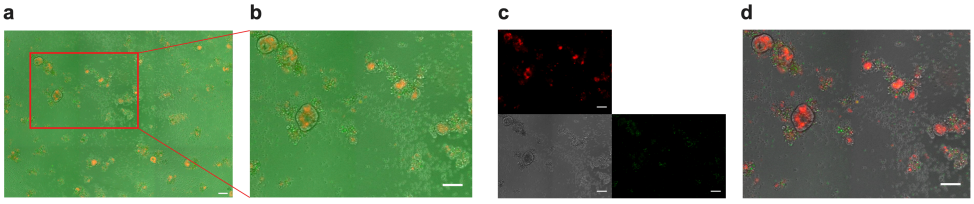

Fig. 5. Example of processing of live-cell imaging data.

a,b, After tiles have been fused with the stitching function of ZenPro **(a),** an image subset containing the region of interest is created **(b).**

c,d, Background is then removed from each channel **(c)** and a merged composite picture is created **(d)**. Red, mCherry-labeled tumor organoids; green, NucView488 Caspase 3/7 dye. In this example, T cells are surrounding mCherry+ tumor organoids, associated with tumor organoid dissociation, release of debris and NucView488+ apoptotic cells. Scale bar, 100 µm.

TROUBLESHOOTING

Troubleshooting advice can be found in Table 1 *(next page)*.

TIMING

- Steps 1-26: generation of frozen biobank of tumor organoids: variable, average 5 (CRC) to 10 weeks (NSCLC), Fig. 1b-c.
- Steps 32-43, isolation of human PBMC from peripheral blood: 2 hours.
- Steps 44-80, co-culture of tumor cells and peripheral blood mononuclear cells: 16 days. Assays are best started on Mondays or Wednesdays for optimal timing of medium refreshing.
- Step 81A, cryopreservation of cultured T cells: 30 minutes.
- Step 81B, tumor reactivity assay using IFNγ and CD107a as a read-out: 4 days. This consists of 2 days for isolation of organoids from Geltrex, followed by 24 hours for reactivity assay, staining, and flow cytometry.
- Step 81C, tumor reactivity assay using CD137 as a read-out: 4 days. This consists of 2 days for isolation of organoids from Geltrex, followed by 24 hours for reactivity assay, staining, and flow cytometry.
- Step 81D, tumor organoid killing assay: 5 days. This consists of 2 days for isolation of organoids from Geltrex, followed by 3 days co-culture, and flow cytometry on the fifth day.

Table 1. Troubleshooting guidance

Step	Problem	Possible reason	Solution
63, 81D(xxxvi)	Organoids do not dissociate into single cells	Human serum is inhibiting the reaction	Wash the plate two more times with 200 µL of PBS per well
		TrypLE is not effective in reducing organoids into single cells	Remove TrypLE and use Trypsin/EDTA 0.05% instead
		Trypsin/EDTA 0.05% is not effective in reducing organoids into single cells	Use mechanical methods: pass organoid suspension through a 29G needle, pipetting 5-7 times with gentle pressure
		Tumor organoids were too large at the end of the experiment	Start with smaller organoids
81B(xxxv), 81C(xx)	Few cells recorded	Cell loss during washing steps	Plate more cells, prevent air bubbles during staining, or use V-bottom plates
81B(xxxv), 81C(xx)	Low-intensity signal	Laser settings on flow cytometer suboptimal	Optimize laser settings on flow cytometer
		Decrease in fluorescence	Protect from light and keep on ice during staining procedure
81D(xii)	Organoids have attached to culture plate	The degree of attachment differs between samples	Use dispase to collect attached organoids (step 45-50)

Step	Problem	Possible reason	Solution
81D(xlvi)	Too few cells recorded	Organoids may suffer from absence of Geltrex during the experiment, and only a few of them may survive	Plate more cells (maintain T cell: tumor cell ratio)
	Poor separation between CD3 positive and EpCAM positive cells	Difficult dissociation into single cells: long exposure to TrypLE or Trypsin can affect expression of surface markers	Label organoids and/or T cells with dyes before starting experiment (see optional step 81D(xvii) and 81D(xxii))
		Low expression of surface markers	
81D(li)	High background despite performing background removal	Background intensity is not even over time	Background needs to be subtracted at each time point individually.
Box 2, A(vii)	No positive signal for dead cell dye	No dead cells in sample	Kill 50% of cells prior to staining by incubating at 95 °C for 45s
Box 2, A(vii)	No positive signal for antibody-fluorochrome conjugate	Antigen not expressed on cells used for compensation	Use compensation beads for compensation
Box 2, B(vi)	No positive signal	Compensation beads used for non-antibody-coupled fluorochromes	Use cells for compensation

ANTICIPATED RESULTS

This protocol describes an efficient method to generate tumor-reactive T cells from peripheral blood for a patient (population) of interest. After 2 weeks of coculture, we observed an ~90% enrichment of $CD3^+$ cells in the PBMC population (Fig. 1d). Furthermore, we observe induction of tumor-reactive $CD8^+$ T cells in 33–50% of cases[6] . The proportion of $CD8^+$ T cells that are tumor reactive can vary substantially between samples, ranging from 1 to 40% (ref. [6]). Given the high variability and the proportion of reactive cells, methods to enrich for tumor-reactive cells can be considered (for example, FACS-based sorting of the reactive population).

Note that the loss of MHC class I expression can be frequent in some tumor types (for example, up to 50% in microsatellite-instable CRC) and that omission of MHC-I-deficient samples may help to increase the proportion of successful cases. The evaluation of $CD4^+$ T-cell reactivity is limited by the potential for recognition of foreign epitopes that are present during culture, in particular Geltrex- derived epitopes. The current protocol describes an adaptation to our previously described method that serves to prevent such reactivity. The frequency with which tumor-specific $CD4^+$ T-cell reactivity can be observed using the current strategy still needs to be evaluated more thoroughly.

Cocultures can be initiated with as little as 10 mL of blood (containing 2–10 × 10^6 T cells). To avoid sampling bias, it is recommended to start cocultures with at least 1 × 10^6 PBMCs. T-cell expansion during coculture can range from 3- to 20- fold. After coculture, T cells can be used for downstream assays as described in this protocol, or further expanded using protocols established for TIL expansion[31].

In T-cell–organoid killing assays, variable levels of cytotoxicity can be observed, but typically range between 20 and 80%. Changes in target:effector ratio can substantially alter the extent of tumor killing observed. Non-specific cell death of up to 20% can be seen (depending on the target:effector ratio) and, to control for this, MHC blocking antibodies are strongly recommended.

ACKNOWLEDGMENTS

We would like to thank Martijn van Baalen, Anita Pfauth and Frank van Diepen for assistance in flow cytometry. We thank Marjolijn Mertz, Lenny Brocks and Bram van den Broek for help in live imaging experiments. We thank Marc van de Wetering, Norman Sachs, Hans Clevers and Hubrecht Organoid Technology (HUB) for advice on organoid cultures. We would like to thank Merus for the provision of anti-PD-1.

This work was supported by the NWO gravitation program (NWO 2012-2022) (to E.V. on behalf of CancerGenomics.nl), KWF grant HUBR2014-7006 (to E.V.), the KWF Queen Wilhelmina Award (NKI 2013-6122, to T.S.) and ERC AdG SENSIT (to T.S.).

AUTHOR CONTRIBUTIONS

C.M.C. and K.K.D. designed the protocol, performed the experiments, and wrote the manuscript. L.F.F., S.Ke., S.Ka., and N.v.R. provided critical input in the design of the protocol. S.v.d.B. provided the protocol for Noggin conditioned medium. T.S. and E.V. supervised the study.

COMPETING FINANCIAL INTERESTS

There are no competing financial interests to report.

DATA AVAILABILITY STATEMENT

The data that provide examples of the results that can be generated with this protocol are available from the corresponding author on reasonable request.

REFERENCES

1. Blank, C.U., Haanen, J.B., Ribas, A., & Schumacher, T.N. The "cancer immunogram". Science 352, 658-660 (2016).
2. Dijkstra, K.K., Voabil, P., Schumacher, T.N., & Voest E.E. Genomics- and transcriptomics-based patient selection for cancer treatment with immune checkpoint inhibitors: a review. JAMA Oncol. 2, 1490-1495. (2016).
3. Pitt, J.M., et al. Resistance mechanisms to immune-checkpoint blockade in cancer: tumor-intrinsic and –extrinsic factors. Immunity 44, 1255-1269. (2016).
4. Sharma, P., Hu-Lieskovan, S., Wargo, J.A. & Ribas, A. Primary, adaptive, and acquired resistance to cancer immunotherapy. Cell 168, 707-723. (2017).
5. Turcotte, S. et al. Phenotype and function of T cells infiltrating visceral metastases from gastrointestinal cancers and melanoma: implications for adoptive cell transfer therapy. J. Immunol. 191, 2217-2225. (2013).
6. Dijkstra, K.K. et al. Generation of tumor-reactive T cells by co-culture of peripheral blood lymphocytes and tumor organoids. Cell 174, 1586-1598. (2018).
7. Zaretsky, J.M. et al. Mutations associated with acquired resistance to PD-1 blockade in melanoma. N. Engl. J. Med. 375, 819-829. (2016).
8. Rosenberg, S.A. & Restifo, N.P. Adoptive cell transfer as personalized immunotherapy for human cancer. Science 348, 62-68. (2015).
9. Geukes Foppen, M.H., Donia, M., Svane, I.M. & Haanen, J.B. Tumor-infiltrating lymphocytes for the treatment of metastatic cancer. Mol. Oncol. 9, 1918-1935. (2015).
10. Scheper, W. et al. Low and variable tumor reactivity of the intratumoral TCR repertoire in human cancers. Nat. Med. 25, 89-94. (2018).
11. Simoni, Y. et al. Bystander $CD8^+$ T cells are abundant and phenotypically distinct in human tumors. Nature 557, 575-579. (2018).
12. Gros, A. et al. PD-1 identifies the patient-specific $CD8^+$ tumor-reactive repertoire infiltrating human tumors. J. Clin. Invest. 124, 2246-2259. (2014).
13. Strønen, E. et al. Targeting of cancer neoantigens with donor-derived T cell repertoires. Science 352, 1337-1441. (2016).
14. Yossef, R. et al. Enhanced detection of neoantigen-reactive T cells targeting unique and shared oncogenes for personalized cancer immunotherapy. JCI Insight 3, pii:122467. (2018).
15. Ye, Q. et al. CD137 accurately identifies and enriches for naturally-occurring tumor-reactive T cells in tumor. Clin. Cancer. Res. 20, 44-55. (2014).

16. Gros, A. et al. Prospective identification of neoantigen-specific lymphocytes in the peripheral blood of melanoma patients. Nat. Med. 22, 433-438. (2016).

17. Cohen, C.J. et al. Isolation of neoantigen-specific T cells from tumor and peripheral lymphocytes. J. Clin. Invest. 125, 3981-991. (2015).

18. Schumacher, T.N., Scheper, W., & Kvistborg, P. Cancer neoantigens. doi: 10.1146/annurev-immunol-042617-053402. (2018).

19. Verdegaal, E.M. et al. Successful treatment of metastatic melanoma by adoptive transfer of blood-derived polyclonal tumor-specific CD4+ and CD8+ T cells in combination with low-dose interferon-alpha. Cancer Immunol. Immunother. 60, 953-963. (2011).

20. Nozaki, K. et al. Co-culture with intestinal epithelial organoids allows efficient expansion and motility analysis of intraepithelial lymphocytes. J Gastroenterol 52, 206-213. (2016).

21. Tsai, S. et al. Development of primary human pancreatic cancer organoids, matched stromal and immune cells and 3D tumor microenvironment models. BMC Cancer 18, 335. (2018).

22. Jenkins, R.W. et al. Ex vivo profiling of PD-1 blockade using organotypic tumor spheroids. Cancer Discov 8, 196-215. (2018).

23. Neal, J.T. et al. Organoid modeling of the tumor immune microenvironment. Cell 175, 1972-1988. (2018).

24. Weeber, F. et al. Preserved genetic diversity in organoids cultured from biopsies of human colorectal cancer metastases. Proc. Natl. Acad. U S A 112, 13308-13311. (2015).

25. Van de Wetering, M. et al. Prospective derivation of a living biobank of colorectal cancer patients. Cell 161, 933-945. (2015).

26. Sachs, N. et al. Long-term expanding human airway organoids for disease modeling. EMBO J. 38, e100-300. (2019).

27. Schütte, M. et al. Molecular dissection of colorectal cancer in pre-clinical models identifies biomarkers predicting sensitivity to EGFR inhibitors. Nat. Commun. 8, 14262. (2017).

28. Drost, J. et al. Organoid culture systems for prostate epithelial and cancer tissue. Nat. Protoc. 11, 347-358. (2016).

29. Broutier, L. et al. Culture and establishment of self-renewing human and mouse adult liver and pancreas 3D organoids and their genetic manipulation. Nat. Protoc. 11, 1724-1743. (2016).

30. Fujii, M., Matano, M., Nanki, K. & Sato, T. Efficient genetic engineering of human intestinal organoids using electroporation. Nat. Protoc. 10, 1474-1485. (2015).

31. Dudley, M.E., Wunderlich, J.R., Shelton, T.E., Even, J. & Rosenberg, S.A. Generation of tumor-infiltrating lymphocyte cultures for use in adoptive transfer therapy for melanoma patients. J. Immunother. 26, 332-342. (2003).

SUPPLEMENTARY FIGURE

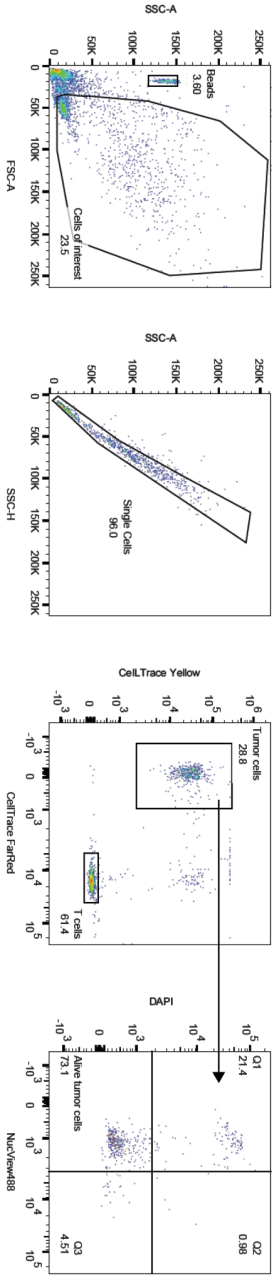

Supplementary Figure 1.

Example of flow cytometry plots showing labelling of tumor cells with CellTrace Yellow and T cells with CellTrace Far Red.

The physiological value of the co-culture platform

4

Cattaneo C.M.[1,2], Schipper L.[1,2], Dijkstra K.K.[1,2], Voest E.E[1,2].

[1]Department of Molecular Oncology and Immunology, The Netherlands Cancer Institute, Antoni van Leeuwenhoek Hospital

[2]Oncode Institute

ABSTRACT

Although immunotherapy has made great impact on the prognosis of advanced cancer patients, there still is a large fraction of patients who do not respond. To stratify patients between potential responders and non-responders, several biomarkers, such as tumor mutational load, the proficiency of the antigen presenting machinery or the expression levels of immune checkpoints, have been investigated. Nevertheless, the predictive capacity of these markers remains limited. We recently showed that co-culture of autologous tumor organoids and peripheral blood lymphocytes (PBMC) allows the generation of tumor reactive T cells for the individual patient. In this work, we hypothesized that the co-culture platform may be used as a new prediction method for immunotherapy responses. In a cohort of 12 different patients we identify a 100% correlation between the generation of tumor reactive T cells and the response to anti-PDL-1 blocking therapy. We then show the ability of the platform to detect the effect of anti-PDL-1 blocking antibodies. Furthermore, our data indicate that via the coculture platform we can monitor response to immunotherapy over time. Although limited by the small sample size, these fundings validate the physiological value of the platform.

INTRODUCTION

The widespread use of immunotherapy has made great impact on the prognosis of advanced cancer patients (Sharma et al., 2015). Blocking antibodies against immune checkpoints are now used for treatment of advanced melanoma, non small cell lung cancer (NSCLC), mismatch repair deficient colorectal cancer (dMMR-CRC), head and neck squamous cell carcinoma, renal cell carcinoma, gastric cancer, hepatocellular cancer and cervical cancer (Meric-Bernstam et al., 2020). Response to immune checkpoints blockade varies greatly among individuals, with response rates of 11-43% for monotherapy, and of 58% when anti-CTLA4 and anti-PD-1/PDL-1 inhibitors are combined (Larkin et al., 2015; Garon et al., 2015; Borghaei et al., 2015; Le et al., 2015; Le et al., 2017; Overman et al., 2017; Overman et al., 2018; Shadendorf et al., 2015; Robert et al., 2015). Despite these encouraging data, there still is a large fraction of patients who do not respond, highlighting the need of developing strategies to identify patients with higher chances of response ultimately to both avoid side effects and limit the costs of an ineffective treatment.

Several biomarkers have been investigated in an attempt to stratify patients between potential responders and non-responders. For example, tumor foreignness can be determined via genomic approaches (Alexandrov et al., 2013). However, although a correlation between nonsynonymous mutational burden and clinical benefit from anti-CTLA-4 and anti-PD-1/PDL-1 therapies in melanoma, NSCLC and CRC has been shown (Le et al., 2015; Rizvi et al., 2015; Snyder et al., 2014; Van Allen et al., 2015; Gubin et al., 2015; Osipov et al., 2019), the predictive capacity of mutational load as a biomarker for immunotherapy response remains unfortunately limited. The complexity of this approach is illustrated by the fact that non-responders can be found in the high mutational load group, as well as responders in the low mutational group (Rizvi et al., 2015; Van Allen et al., 2015; Gubin et al., 2015). Other biomarkers focus on the Identification of *a priori* immune evasion mechanisms to select the non-responders population. Obvious candidates, such as the proficiency of the antigen processing and presentation machinery or the expression levels of CTLA-4 or PDL-1, have been widely investigated as potential biomarkers for (non-)response (Davis et al., 2019; Restifo et al., 1996; Paulson et al., 2018). Numerous studies linked mutations in Beta-2 microglobulin

(B2m) or human leukocyte antigen (HLA) molecules to evasion mechanisms; other studies associated tumors with high expression levels of surface PDL-1 molecules with better response. Unfortunately, the predictive capacity of these markers remains limited (Leone et al., 2013; Rooney et al., 2015; Shukla et al., 2015; Dierssen et al., 2007; Van Allen et al., 2015; Herbst et al., 2014).

The complexity that characterizes the study of biomarkers for immunotherapy response can, at least partially, be explained by the intricate interaction between tumor cells and their microenvironment. Dissecting the interplay between cancer, stromal, endothelial and immune cells is key to understand how a specific tumor reacts to a specific therapy. Platforms to allow the analysis of such an extended interaction, on the level of individual patients are currently lacking. However, our autologous tumor organoids - Peripheral Blood Lymphocytes (PBMC) coculture system has, for the first time, allowed the analysis of interactions between cancer cells and different immune cells. We believe this model may contribute to individualized immunotherapy for epithelial cancers (Dijkstra et al., 2018; Cattaneo et al., 2020).

Here, we hypothesized that such a platform may be used as a new prediction method for immunotherapy response. We therefore investigated how data obtained from this autologous coculture platform correlates with clinical outcome of patients treated with immunotherapy.

RESULTS

To test whether the coculture platform would be suitable as a prediction tool for immunotherapy responses, we first selected a cohort of 8 patients treated with immunotherapy for whom pre-treatment tumor biopsies or resection material and blood specimens were available (Fig. 1A). Tumor organoids cultures were established for each patient according to our previously described method (Cattaneo et al., 2020; Dijkstra et al., 2020). Next, we screened for surface expression of MHC class I and class II (MHC-I and MHC-II) after stimulation with interferon-gamma (IFNg). With the exception of one patient (ITO-068, not used for follow up experiments), all tumor organoids expressed MHC-I and/or MHC-II upon stimulation with IFNg (Fig. 1B).

We then proceed by coculturing patient derived PBMC with the autologous MHC proficient tumor organoids (Cattaneo et al., 2020; Dijkstra et al., 2018). At the end of the coculture, tumor cells recognition by $CD8^+$ or $CD4^+$ T cells was evaluated by staining for IFNg (Fig. 1C). Tumor recognition was detected for all responders; conversely, no tumor reactivity was detected for those patients who did not respond to immunotherapy (Fig. 1D).

Figure 1. Coculture of tumor organoids and PBMC derived from pre-immunotherapy specimens shows correlation with clinical responses. ***(next page)***

(A) Description of the 8 cancer patients cohort used in the experiments.
(B) Cell-surface MHC class I and MHC class II expression as determined by flow cytometry. Organoids were stimulated with 200 ng/mL IFNg for 24 hr (grey) or were left unstimulated (white). Top: Bar graphs indicate median fluorescence intensity (MFI) of anti-HLA-A, -B, and -C-PE minus MFI of isotype control. Bottom: Bar graphs indicate median fluorescence intensity (MFI) of anti-HLA-DR, -DQ, -DP- FITC minus MFI of isotype control. Tumor organoids with MFI < 100 above isotype control (dashed line) were classified as MHC class I or MHC class II deficient. Error bars represent SEM of at least two independent experiments.
(C) Representative flow cytometry plots of PBMC at the end of the 2 weeks coculture with autologous tumor organoids. Top: gating strategy. Bottom: Tumor recognition was assessed by measuring IFNg expression of $CD8^+$ or $CD4^+$ T cells after re-stimulation of week 2-PBMC with autologous tumor organoids, compared to unstimulated week2-PBMC. A reactive and a non-reactive example is depicted.
(D) Quantification of organoid-induced IFNg production of $CD8^+$ (left) and $CD4^+$ (right) T cells obtained after 2-week co-culture with autologous tumor organoids. The background (spontaneous IFNg production) is subtracted from the signal. Error bars represent SEM of at least two biological replicates. Coculture results for patient not responding to immunotherapy are shown in grey; coculture results for patients responding to immunotherapy are shown in purple.

A

Sample	Tumor	Lesion	Immunotherapy
ITO-042	NSCLC	Metastasis	Nivolumab
ITO-068	MSI-CRC	Primary	Nivolumab
ITO-108	MSS-CRC	Metastasis	Pembrolizumab
ITO-109	NSCLC	Metastasis	Nivolumab
ITO-110	MSI-CRC	Primary	Nivolumab
ITO-111	MSI-CRC	Metastasis	Nivolumab
ITO-120	NSCLC	Metastasis	Pembrolizumab
ITO-127	NSCLC	Metastasis	Pembrolizumab

B

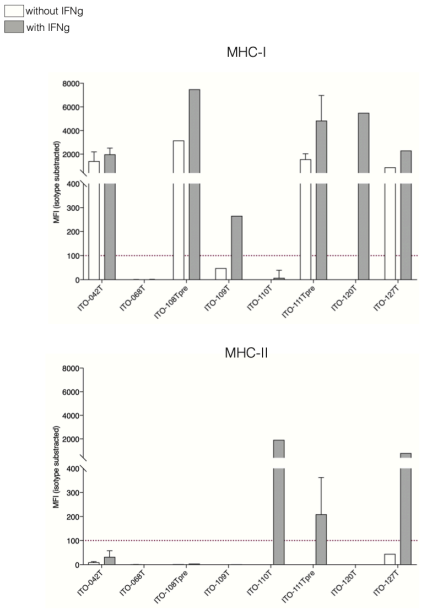

C

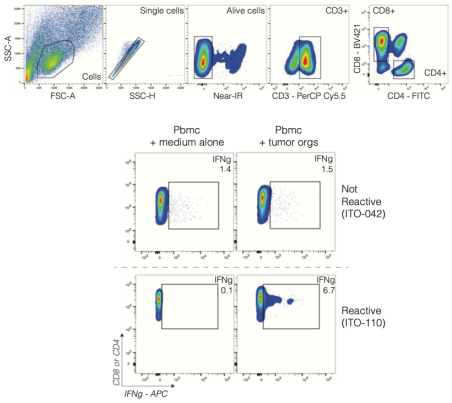

D

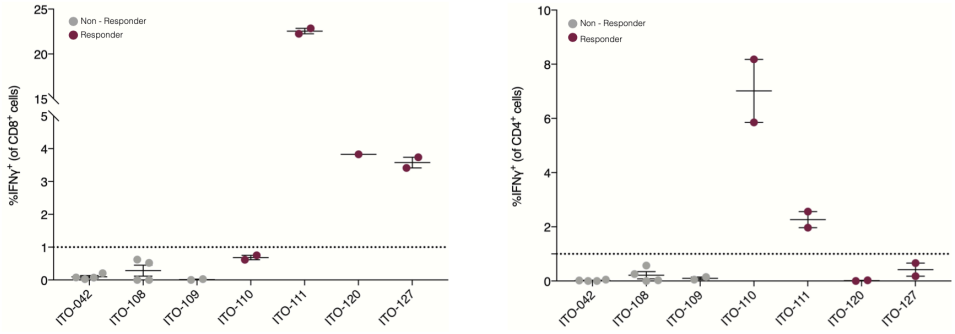

Next, to expand the cohort, we randomly selected 6 additional patients treated with immunotherapy for whom blood and tumor specimens were collected at various timepoints during treatment (Fig. 2A). After coculturing patient-derived PBMC with autologous MHC proficient tumor organoids (Fig. 2B), tumor recognition by T cells was evaluated for both responders and non-responders (Fig. 2C).

Collectively, out of 14 patients treated with immunotherapy, we were able to analyze 12 MHC proficient tumors. In this limited set of patients, we show a 100% correlation between the ability to generate tumor reactive T cells via the coculture system and responses to immunotherapy (Fig. 1 and 2).

Figure 2. Coculture of tumor organoids and PBMC derived from specimens collected at different timepoints during immunotherapy shows correlation with clinical responses. ***(next page)***

(A) Characterization of the additional set of patients treated with immunotherapy.
(B) Cell-surface MHC class I and MHC class II expression as determined by flow cytometry. Organoids were stimulated with 200 ng/mL IFNg for 24 hr (grey) or were left unstimulated (white). Left: Bar graphs indicate median fluorescence intensity (MFI) of anti-HLA-A, -B, and -C-PE minus MFI of isotype control. Right: Bar graphs indicate median fluorescence intensity (MFI) of anti-HLA-DR, -DQ, -DP- FITC minus MFI of isotype control. Tumor organoids with MFI < 100 above isotype control (dashed line) were classified as MHC class I or MHC class II deficient. Error bars represent SEM of at least two independent experiments.
(C) Quantification of organoid-induced IFNg production of $CD8^+$ (left) and $CD4^+$ (right) T cells obtained by 2-week co-culture with autologous tumor organoids. The background (spontaneous IFNg production) is subtracted from the signal. Error bars represent SEM of at least two biological replicates. Coculture results for patient not responding to immunotherapy are shown in grey; coculture results for patients responding to immunotherapy are shown in purple.

A

				Time point during IT	
Patient	Tumor	Lesion	Immunotherapy	Blood	Tumor
ITO-066	MSI-CRC	Metastasis	Atezolizumab+OX40	On	On
ITO-106	MSS-CRC	Metastasis	Pembrolizumab	On	Pre
ITO-108	MSS-CRC	Metastasis	Pembrolizumab	Pre-Post	Pre-Post
ITO-114	MSI-CRC	Metastasis	Nivolumab	Pre	Post
ITO-116	MSI-CRC	Metastasis	Nivolumab	Pre	Post
ITO-124	MSI-CRC	Metastasis	Nivolumab	On	Pre

B

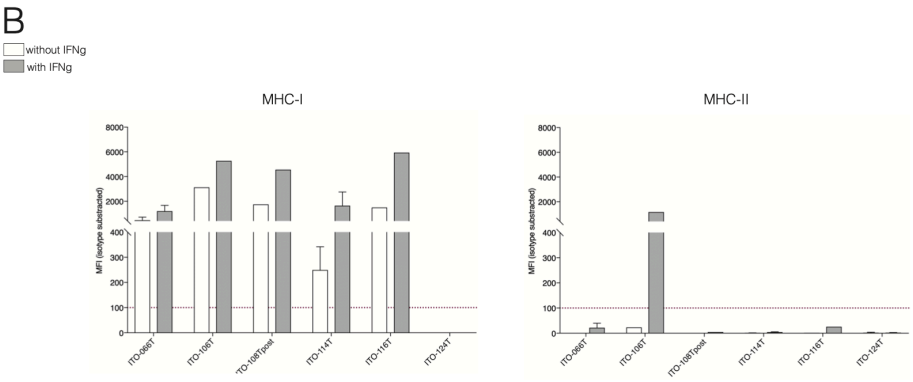

C

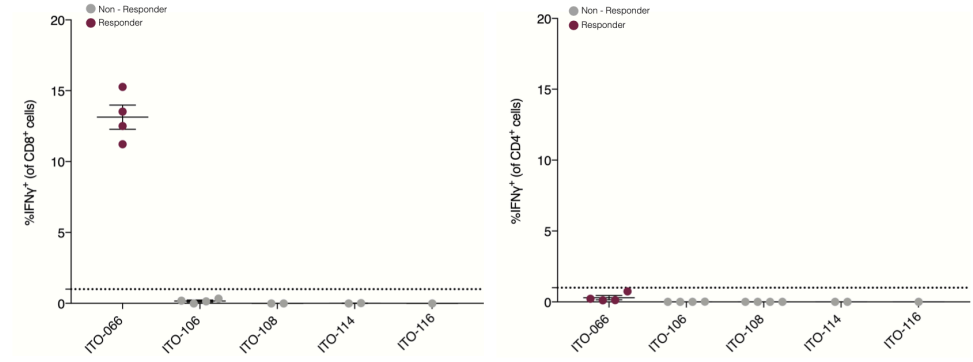

Since IFNg exposure has been described not only to upregulate the antigen presentation machinery, but also the expression of PDL-1 on the surface of tumor cells (Dijkstra et al., 2018), our co-cultures have always been performed in the presence of anti-PDL-1 blocking antibody. We then decided to investigate whether the coculture platform would allow to study the effect of anti-PD-1/PDL-1 blocking antibodies on the interaction between tumor and immune cells. For this purpose, we tried to induce tumor reactive T cells in the presence or absence of anti-PDL-1 blocking antibodies. In all three cases tested (Fig. 3 A), we detected a major difference in the tumor response pattern: co-culturing patient-derived PBMC and autologous tumor organoids in the absence of anti-PDL-1 failed to generate tumor reactive $CD8^+$ and $CD4^+$ T cells (Fig. 3 B-C). This data suggests that the co-culture platform is suitable for the analysis of anti-PDL-1 mediated responses.

A

				Time point during IT	
Patient	Tumor	Lesion	Immunotherapy	Blood	Tumor
ITO-110	MSI-CRC	Primary	Nivolumab	Pre	Pre
ITO-120	NSCLC	Metastasis	Pembrolizumab	Pre	Pre
ITO-120	NSCLC	Metastasis	Pembrolizumab	On	Pre

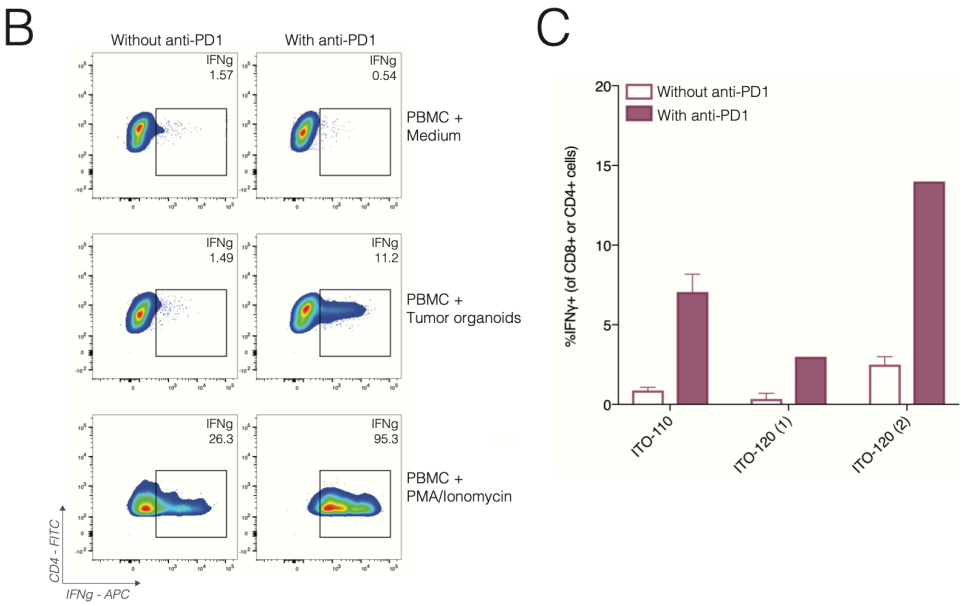

Figure 3. The coculture platform allows the analysis of anti-PDL-1-mediated responses

(A) Characterization of the patients used for the experiments.
(B) Representative flow cytometry plots of CD4+ T cells at the end of two week coculture with autologous tumor organoids, in the presence or absence of anti-PDL-1 blocking antibody.
(C) Quantification of organoid-induced IFNg production of CD4+ or CD8+ T cells obtained by 2-week coculture with autologous tumor organoid, in the presence (purple) or not (white) of anti-PDL-1 blocking antibodies. The background (spontaneous IFNg production) is subtracted from the signal. Error bars represent SEM of at least two biological replicates.

Next, we used our co-culture platform to monitor the response to immunotherapy over time. For a MSI-CRC patient who initially responded to nivolumab, we isolated PBMC before and after 8 months of treatment. We also generated organoids from two separate lesions, pre-treatment (Lesion 1) and at progression (Lesion 2) (Fig. 4 A-B). We then co-cultured both pre- and on- treatment PBMC with either Lesion 1- or Lesion 2-derived organoids, and evaluated $CD8^+$ T cell-mediated tumor reactivity. Co-culturing of both pre- and on- treatment PBMC with lesion 1 tumor organoids enabled us to generate a massive tumor specific T cell response: ~30% of the induced $CD8^+$ T cells secreted IFNg (Fig. 3 C-D), mimicking the pattern of good response seen in the clinic (Fig. 3 A-B). However, co-culture of the same PBMCs with lesion 2 (which was progressive)-derived tumor organoids, failed to generate a tumor reactive T cell population (Fig. 3 C-D). Collectively, this data shows the potential of the platform to not only correlate with the clinical outcome, but also to monitor treatment response over time.

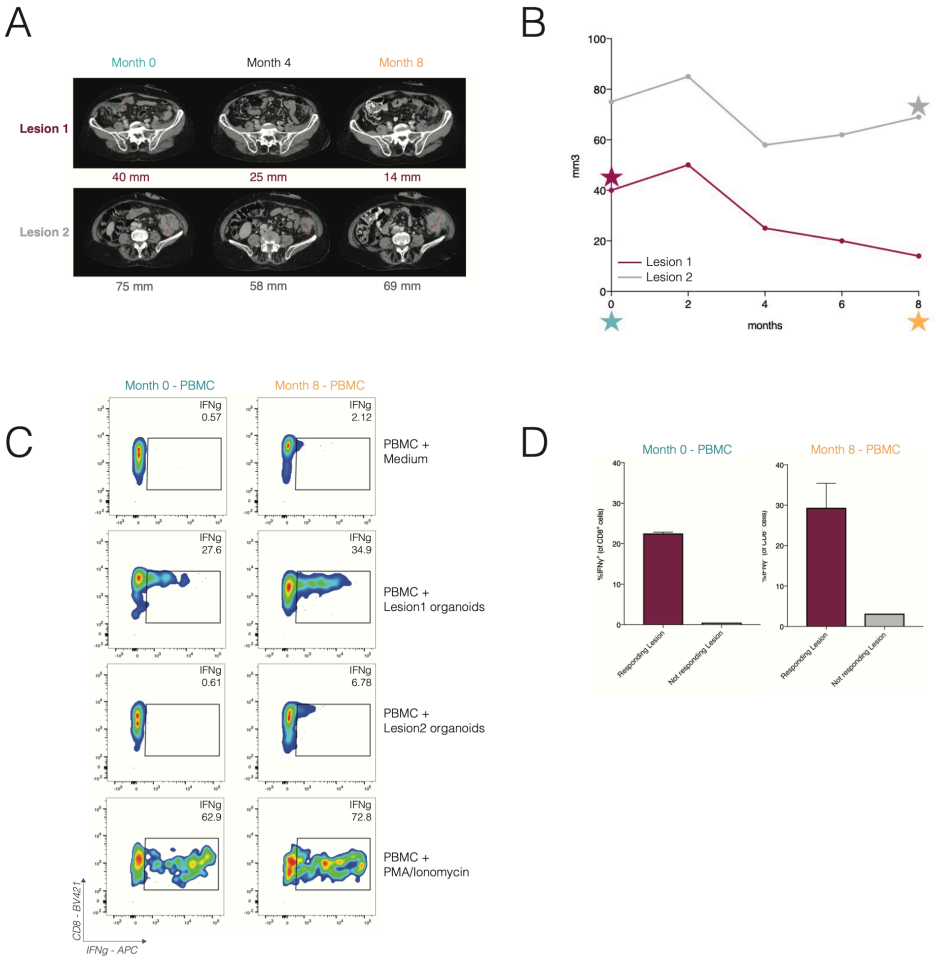

Figure 4. The coculture platform allows to monitor responses to immunotherapy over time during treatment.

(A) Computer tomography scans over an 8-month period of the peritoneal metastasis lesion and the primary tumor of patient ITO-111, treated with nivolumab

(B) Line graph representing the clinical response of patient ITO-111 diagnosed with MSI-CRC to nivolumab. Y axis: lesions measured in mm3. Lesion 1 is shown in purple. Lesion 2 is shown in grey. X axis: time after start of nivolumab treatment (months). Star symbol represents the moment of sample collection for lesion 1 (purple), lesion 2 (grey), pre-treatment blood (blue) and on-treatment blood (orange).

(C) Representative flow cytometry plots of CD8+ T cells, derived form pre-treatment (blue) or on-treatment (orange) PBMC, at the end of two week coculture with autologous tumor organoids, derived from either lesion 1 or lesion 2.

(D) Quantification of organoid-induced IFNg production of CD8* T cells obtained by 2-week coculture of pre-treatment (left and blue) and on-treatment (right and orange) PBMC with lesion 1 (purple) or lesion 2 (grey) derived tumor organoids. The background (spontaneous IFNg production) is subtracted from the signal. Error bars represent SEM of at least two biological replicates.

DISCUSSION

In this study we explored the potential of our coculture platform as a tool to predict and monitor immunotherapy responses. We demonstrated that, after 2 weeks co-culture of PBMC with autologous tumor organoids, the presence (or absence) of tumor reactive T cell populations strongly correlated with clinical responses to anti-PDL-1 blocking therapy. Although our findings were obtained in a small set of only 12 patients, we believe they may serve as a starting point for confirmatory studies in a larger group of patients. Another interesting finding was the ability of the platform to detect the effect of anti-PDL-1 blocking antibodies in the interaction between tumor cells and PBMC. Furthermore, we showed that co-culturing tumor organoids and PBMC offers the potential to monitor responses over time, opening the road to the opportunity to identify and investigate resistance mechanisms that may occur upon treatment and to test potential strategies to overcome resistance.

However, although we obtained very interesting results, there are several intrinsic limitations to our approach. First, the number of patients in which we tested the predictive value of the co-culture platform was small and needs to be expanded to be able to determine its true predictive value. Secondly, in the setting of personalized medicine, establishment and culture of tumor organoids from each individual patient can be a real challenge. The establishment success rate varies greatly between different tumor types: it is around 50-70% for colorectal cancer organoids, it drops to only 17% for NSCLC organoids, and it is even lower for other tumor types, such as breast or gastric cancer. Furthermore, other difficulties may occur when working with tumor organoids, such as the contamination from autologous healthy (non-tumoral) cells in the culture. Thirdly, when thinking of a large scale clinical test, time becomes a critical parameter. Unfortunately, starting from a surgical specimen, an average of 50-70 days are required for the establishment of a patient specific tumor organoids biobank.

Taken together, our findings showed significant challenges that prohibit the present use of this model system as a predictive tool for the success of immunotherapy. We currently position our platform therefore more as a research tool.

Nevertheless, the results we show here highlight the potential of the co-culture platform to better understand the development of resistance to immunotherapy. We

foresee applications of the co-culture system as a physiological test platform to identify novel mechanism of (non-) response, to develop novel strategies to overcome resistance, and to select combination therapies for better success of current immunotherapies.

METHODS

Human subjects

The study (NL48824.031.14) was approved by the Medical Ethical Committee of the Netherlands Cancer Institute – Antoni van Leeuwenhoek hospital and written informed consent was obtained from all patients. Peripheral blood and tumor tissue were obtained from patients with a confirmed diagnosis of colorectal or non-small cell lung cancer. Mismatch repair deficiency was confirmed by immunohistochemical staining for the mismatch repair proteins MSH2, MSH6, MLH1 and PMS2 in routine assessment by a pathologist (see Immunohistochemistry).

Organoid culture

Tumor tissue was obtained either by 18G core needle biopsy or by surgical resection. Tumor tissue was processed for organoid culture within 24 hr. CRC organoids were established essentially as described in van de Wetering et al., 2015. NSCLC organoids were cultured using similar methods; a detailed protocol is accessible at bioRxiv (Sachs et al., 2018). Briefly, tumor tissue derived from needle biopsies was mechanically dissociated into small tumor pieces using needles and embedded in Geltrex (Geltrex LDEV-free reduced growth factor basement membrane extract, GIBCO). Tumor tissue derived from surgical resections was cut into small pieces and enzymatically digested using 1.5 mg/mL collagenase II (Sigma-Aldrich), 10 mg/mL hyaluronidase type IV (Sigma-Aldrich) and 10 mM Y-27632 (Sigma-Aldrich) before embedding in Geltrex. After Geltrex solidification for 20 min at 37 C, cells were overlaid with human CRC or non-small cell lung cancer (NSCLC) organoid medium (van de Wetering et al., 2015; Sachs et al., 2018). Human CRC organoids medium is composed of Ad-DF+++ (Advanced DMEM/F12 (GIBCO) supplemented with 2 mM Ultra- glutamine I (Lonza), 10 mM HEPES (GIBCO), and 100/100 U/ml Pencillin/Streptomycin (GIBCO)), 10% Noggin-conditioned medium, 20% R-spondin1-conditioned medium, 1x B27 supplement without vitamin A (GIBCO), 1.25 mM N-Acetylcysteine (Sigma-Aldrich), 10 mM nicotinamide (Sigma-Aldrich), 50 ng/mL human recombinant EGF (Peprotech), 500 nM A83-01 (Tocris), 3 mM

SB202190 (Cayman Chemicals) and 10 nM prostaglandin E2 (Cayman Chemicals). Human wild-type colon organoid medium is identical to CRC medium, except that 50% Wnt3a-conditioned medium is added. Human NSCLC and normal airway organoid medium is composed of Ad-DF+++, 10% Noggin-conditioned medium, 10% R-spondin1-conditioned medium, 1x B27 supplement, 1.25 mM N-Acetylcystein, 10 mM nicotinamide, 25 ng/mL human recombinant FGF-7 (Peprotech), 100 ng/mL human recombinant FGF-10 (Peprotech), 500 nM A83-01, 1 mM SB202190, 5 mM Y-27632. R-spondin1-conditioned medium was produced from 293T-HA-Rspol-Fc producer cell lines (obtained from C. Kuo, Stanford), Wnt3a-conditioned medium from L-Wnt3a cells and Noggin-conditioned medium from HEK293-mNoggin-Fc cell lines (both kind gift from J. den Hertog, Utrecht). In the first two weeks of organoid culture, 1x Primocin (Invivogen) was added to prevent microbial contamination. Organoids were passaged approximately every week by incubating in TrypLE Express (GIBCO) for 5-10 min at 37 C to dissociate organoids to single cells and replating in fresh Geltrex. After passaging, 10 mM Y-27632 was added to CRC medium for the first 2-3 days. Organoids were cryopreserved in 10% FCS/DMSO or Recovery Cell Culture Freezing Medium (ThermoFisher) as master and working biobanks. Organoids < passage 30 were used in experiments. To rule out overgrowth by healthy lung organoids for NSCLC organoids derived from intrapulmonal lesions, hematoxylin and eosin stained sections of tumor organoids (see Immunohistochemistry) were evaluated by a pathologist to determine tumor status of organoids. To prevent overgrowth by healthy lung organoids, for patient NSCLC-3, p53 mutant organoids were selected by culturing in the presence of 5 mM Nutlin-3 (Cayman Chemicals). Organoids were regularly checked for mycoplasma contamination using the MycoAlert Mycoplasma Detection Kit (Lonza).

Peripheral blood lymphocytes

The peripheral blood mononuclear cells (PBMC) fraction was isolated from peripheral blood by Ficoll-Paque density gradient separation and cryopreserved until later use.

Organoid line authentication

DNA was isolated from master and working biobanks of organoids and patient-matched peripheral blood using a DNEasy kit (QIAGEN). Samples were genotyped using a Taqman-based SNParray targeting 26 SNPs (Hartwig Medical Foundation, Amsterdam). An identity score was calculated as described by (Tanabe et al., 1999) and (Liang-Chu et al., 2015). When comparing two samples, for each locus where both samples had called alleles, the number of distinct alleles in each individual sample, as well as the number of shared alleles was computed. These were summed across all loci and an identity score was computed defined as

$$\frac{2x \text{ the number of shared alleles}}{\text{total distinct alleles sample 1} + \text{total distinct alleles sample 2}}$$

A threshold of 0.9 of the summed identity score was defined as a cut-off and organoid lines that did not match to autologous blood were discarded.
If samples showed identity scores < 0.9 in comparison with autologous blood, but showed exclusively heterozygous to homozygous changes in the tumor, suggesting loss of heterozygosity due to copy number aberrations. We authenticated these lines by performing HLA-typing by PCR (Sanquin, Amsterdam) or based on whole genome sequencing data by Optitype (Szolek et al., 2014).

Flow cytometry

For evaluation of MHC-I and MHC-II expression by tumor organoids, organoids were dissociated to single cells using TrypLE Express, with or without overnight pre-incubation with 200 ng/mL IFNg. Tumor cells were washed in FACS buffer (PBS + 5 mM EDTA + 1% bovine serum antigen) and stained with mouse anti-human HLA-A,B,C-PE (BD Bioscience) or anti-HLA-DP,DQ,DR-FITC (eBioscience) anti- bodies, or isotype controls (PE mouse IgG1, kappa (BD) and FITC mouse IgG1 kappa (eBioscience)) for 30 min at 4 C. Cells were washed twice with FACS buffer and DAPI was added to exclude dead cells prior to recording at a Becton Dickinson Fortessa or LSRII flow cytometer.

Organoid and T cell co-culture

Peripheral blood lymphocytes (PBL) and tumor organoids were generated and co-cultured as previously described (Dijkstra et al., 2018; Cattaneo et al., 2020). Briefly, PBLs were isolated from peripheral blood using Ficoll–Paque and cryopreserved for later use. Culture media for PBMC was composed of RPMI 1640 (GIBCO), supplemented with 2 mM Ultraglutamine I, 1:100 penicillin/streptomycin and 10% male human AB serum (Sigma-Aldrich; cat. no. H3667) (''T cell medium''). One day before co-culture, PBMC were thawed in pre-warmed (37°C) T cell medium (human serum was replaced with FCS during thawing) and incubated for 15 min with 25 U/mL benzonase (Merck; cat. no. 70746-3) at 37 C. After washing, cells were resuspended at 2-3 x 10^6 cells/mL in T cell medium supplemented with 150 U/mL IL-2 and cultured overnight at 37°C . 48 hours prior to co-culture, tumor organoids were isolated from Geltrex by incubation with 2 mg/mL dispase II and cultured in CRC medium. Prior to co-culture, tumor organoids (isolated from Geltrex) were stimulated for 24 hours with 200 ng/mL human recombinant IFNg (Peprotech; cat. no. 300-02). 96-well U-bottom plates were coated with 5 µg/mL anti-CD28 (clone CD28.2, eBioscience; cat. no. 16-0289-81) and kept overnight at 4 °C . The next day, tumor organoids were dissociated to single cells with TrypLE Express and resuspended in T cell medium. Anti-CD28-coated plates were washed twice with PBS and PBMC were seeded at a density of 10^5 cells/well and stimulated with single cell dissociated organoids at a 20:1 effector:target ratio. Co-cultures were performed in the presence of 150 U/mL IL-2 and, when needed, 20 µ/mL anti-PD-1-blocking antibody (kindly donated by Merus, Utrecht; cat. no. 5C4). Half of the medium, including IL-2 and anti-PD-1, was refreshed two to three times per week. Every week, PBMC were collected, counted, and replated at 10^5 cells/well, and re-stimulated with fresh tumor organoids, for a total of 2 weeks co-culture.

Tumor recognition assay

For evaluation of tumor reactivity, 10^5 PBMC were restimulated with tumor organoids (isolated from Geltrex and stimulated with IFNg, as described before) at a 2:1 effector:target ratio and seeded in anti-CD28-coated plates in the presence, when needed, of 20 µ/mL anti-PD-1 and co-cultured for 5 hr for IFNg evaluation. Golgi-Plug

(1:1000, BD; cat. no. 555029) and Golgi-Stop (1:1500, BD, cat. no. 554724) was added after 1 hr and co-culture continued for an additional 4 hr. Cells were washed twice in FACS buffer and stained with the following antibodies: anti-CD3-PerCP-Cy5.5 (BD; cat. no. 332771), anti-CD4-FITC (BD; cat. no. 555346), anti-CD8-BV421 (BD; cat. no. 562429), and near-IR viability dye (Life technologies) for 30 min at 4°C in the dark. Cells were washed twice in FACS buffer, fixed using the Cytofix/Cytoperm kit (BD, according to manufacturer's instructions), and stained for intracellular IFNg (anti-IFNg-APC, BD; cat. no. 554702). PBMC stimulated with 50 ng/mL phorbol 12-myristate 13-acetate (PMA, Sigma-Aldrich; cat. no. 19-144) and 1 mg/mL ionomycin (Sigma-Aldrich; cat. no. I9657) served as positive controls and PBMC cultured without tumor stimulation as negative controls. Cells were then washed twice with FACS buffer and recorded at a Becton Dickinson Fortessa or LSRII flow cytometer.

REFERENCES

- Alexandrov L.B., Nik-Zainal S., Wedge D.C., et al. (2013). Australian Pancreatic Cancer Genome Initiative; ICGC Breast Cancer Consortium; ICGC MMML-Seq Consortium; ICGC PedBrain. Signatures of mutational processes in human cancer. Nature 500, 415-421.
- Borghaei H., Paz-Ares L., Horn L., Spigel D.R., Steins M., Ready N.E., Chow L.Q., Vokes E.E., Felip E., Holgado E., et al. (2015). Nivolumab versus docetaxel in advanced nonsquamous non-small-cell lung cancer. N. Engl. J. Med. 373, 1627–1639.
- Cattaneo C.M., Dijkstra K.K., Fanchi L.F., et al. (2020) Tumor organoid-T cell coculture systems. Nature Protocol 15, 15-39.
- Davis A.A. and Patel V.G. (2019). The role of PD-L1 expression as a predictive biomarker: an analysis of all US Food and Drug Administration approvals of immune checkpoint inhibitors. J. Immunother. Cancer 7, 278
- Dierssen J.W., de Miranda N.F., Ferrone S., van Puijenbroek M., Cornelisse C.J., Fleuren G.J., van Wezel T., and Morreau H. (2007). HNPCC versus sporadic microsatellite-unstable colon cancers follow different routes toward loss of HLA class I expression. BMC Cancer 7, 33–43.
- Dijkstra K.K., Cattaneo C.M., Weeber F., Chalabi M., et al. (2018) Generation of tumor-reactive T cells by coculture of peripheral blood lymphocytes and tumor organoids. Cell 174, 1-13
- Dijkstra K.K., Monkhorst K., Schipper L.J., Hartemink K.J., Smit E.F., et al. (2020). Challenges in Establishing Pure Lung Cancer Organoids Limit Their Utility for Personalized Medicine. Cell Reports 31, 107588
- Garon E.B., Rizvi N.A., Hui R., Leighl N., Balmanoukian A.S., Eder J.P., Patnaik A., Aggarwal C., Gubens M., Horn L., et al.; KEYNOTE-001 Investigators (2015). Pembrolizumab for the treatment of non-small-cell lung cancer. N. Engl. J. Med. 372, 2018–2028.
- Gubin M.M., Zhang X., Schuster H., et al. (2014) Checkpoint blockade cancer immunotherapy targets tumour-specific mutant antigens. Nature 515, 577-581.
- Herbst R.S., Soria J.C., Kowanetz M., et al. (2014) Predictive correlates of response to the anti-PD-L1 antibody MPDL3280A in cancer patients. Nature 515, 563-567.
- Larkin J., Chiarion-Sileni V., Gonzalez R., Grob, J.J., Cowey C.L., Lao C.D., Schadendorf D., Dummer R., Smylie M., Rutkowski P., et al. (2015). Combined nivolumab and ipilimumab or monotherapy in untreated melanoma. N. Engl. J. Med. 373, 23–34.
- Le D.T., Uram J.N., Wang H., Bartlett B.R., Kemberling H., Eyring A.D., Skora A.D., Luber B.S., Azad N.S., Laheru D., et al. (2015). PD-1 blockade in tumors with mismatch-repair deficiency. N. Engl. J. Med. 372, 2509–2520.

- Le D.T., Durham J.N., Smith K.N., Wang H., Bartlett B.R., Aulakh L.K., Lu S., Kemberling H., Wilt C., Luber B.S., et al. (2017). Mismatch repair deficiency predicts response of solid tumors to PD-1 blockade. Science 357, 409–413.
- Leone P., Shin E.C., Perosa F., Vacca A., Dammacco F., Racanelli V. (2013) MHC class I antigen processing and presenting machinery. J Natl Cancer Inst 105, 1172-1187.
- Liang-Chu M.M.Y., Yu M., Haverty P.M., Koeman J., Ziegle J., Lee M., Bourgon R., and Neve R.M. (2015). Human biosample authentication using the high-throughput, cost-effective SNPtrace(TM) system. PLoS ONE 10, e0116218.
- Meric-Bernstam F., Larking J., Tabernero J. and Bonini C. (2020). Enhancing anti-tumour efficacy with immunotherapy combinations. The Lancet. https://doi.org/10.1016/S0140-6736(20)32598-8.
- Osipov A., Popovic A., Hopkins A., et al. (2019). Tumor mutational burden and response rates to immune checkpoint inhibitors targeting PD-1, CTLA-4 and combination. J. Clin. Oncol. 27, 2578
- Overman M.J., McDermott R., Leach J.L., Lonardi S., Lenz H.J., Morse M.A., Desai J., Hill A., Axelson M., Moss R.A., et al. (2017). Nivolumab in patients with metastatic DNA mismatch repair-deficient or microsatellite instability-high colorectal cancer (CheckMate 142): an open-label, multicentre, phase 2 study. Lancet Oncol. 18, 1182–1191.
- Overman M.J., Lonardi S., Wong K.Y.M., Lenz H.J., Gelsomino F., Aglietta M., Morse M.A., Van Cutsem E., McDermott R., Hill, A., et al. (2018). Durable clinical benefit with nivolumab plus ipilimumab in DNA mismatch repair-deficient/microsatellite instability-high metastatic colorectal cancer. J. Clin. Oncol. 36, 773–779.
- Paulson K.G., Voillet V., McAfee M.S. et al. (2018). Acquired cancer resistance to combination immunotherapy from transcriptional loss of class I HLA. Nat. Commun. 9, 2968
- Restifo N.P., Marincola F.M., Kawakami Y., Taubenberger J., Yannelli J.R. and Rosenber S.A. (1996). Loss of functional beta2-microglobulin in metastatic melanomas from five patients receiving immunotherapy. J. Natl. Cancer Inst. 88, 100-08
- Rizvi N.A., Hellmann M.D., Snyder A., et al. (2015) Cancer immunology. Mutational landscape determines sensitivity to PD-1 blockade in non-small cell lung cancer. Science 348,124-128.
- Robert C., Schacher J., Long G.V., Arance A., Grob JJ., Mortier L., Daud A., Carlino M.S., McNeil C., Lotem M et al. (2015). KEYNOTE-006 investigators. Pembrolizumab vs ipilimumab in advanced melanoma. N Engl J Med. 372, 2521-2532.
- Rooney M.S., Shukla S.A., Wu C.J., Getz G., Hacohen N. (2015) Molecular and genetic properties of tumors associated with local immune cytolytic activity. Cell 160, 48-61.

- Shadendorf D., Hodu F.S., Robert C., Weber J.S., Margolin K., Hamid O., Patt D., Chen T., Berman D.M., Wolchock J.D. (2015). Pooled analysis of long-term survival data from phase II and phase III clinical trials of ipilimumab in unresectable or metastatic melanoma. J Clin Oncol. 33,1889-1894.
- Sharma P., Allison J.P. (2015) Immune checkpoint targeting in cancer therapy. Cell 161, 205-214.
- Shukla S.A., Rooney M.S., Rajasagi M., et al. (2015) Comprehensive analysis of cancer-associated somatic mutations in class I HLA genes. Nat Biotechnol. 33, 1152-1158.
- Snyder A., Makarov V., Merghoub T., et al. (2014) Genetic basis for clinical response to CTLA-4 blockade in melanoma. N Engl J Med. 371, 2189-2199.
- Szolek A., Schubert B., Mohr C., Sturm M., Feldhahn M., and Kohlbacher O. (2014). OptiType: precision HLA typing from next-generation sequencing data. Bioinformatics 30, 3310–3316.
- Tanabe H., Takada Y., Minegishi D., Kurematsu M., Masui T., and Mizusawa H. (1999). Cell line individualization by STR multiplex system in the cell bank found cross-contamination between ECV304 and EJ-1/T24. Tiss. Cult. Res. Commun. 18, 329–338.
- Van Allen E.M., Miao D., Schilling B., et al. (2015) Genomic correlates of response to CTLA-4 blockade in metastatic melanoma. Science 350, 207-211.

5

Werner helicase is a synthetic-lethal vulnerability in mismatch repair–deficient colorectal cancer refractory to targeted therapies, chemotherapy and immunotherapy

Picco G.[1], **Cattaneo C.M.[2,5]**, van Vliet E.[1], Crisafulli G.[3,4], Rospo G.[3,4], Consonni S.[1], Vieira S.F.[1], Rodriguez I.S.[2,5], Cancelliere C.[3], Banerjee R.[1], Schipper L.[2,5], Oddo D.[3,4], Dijkstra K.K.[2,5], Cinatl J.[6], Michaelis M.[7], Yang F.[1], di Nicolantonio F.[3,4], Sartore Bianchi A.[8], Siena S.[8,9], Arena S.[3,4], Voest E.[2,5,#], Bardelli A.[3,4,#], Garnett M.J.[1,#]

[#] *These authors contributed equally*

[1]Wellcome Sanger Institute, Cambridge, UK

[2]Department of Molecular Oncology and Immunology, the Netherlands Cancer Institute, Antoni van Leeuwenhoek Hospital, the Netherlands

[3]Candiolo Cancer Institute, FPO–IRCCS, Italy

[4]Department of Oncology, University of Torino, Italy

[5]Oncode Institute

[6]Institute for Medical Virology, Goethe-University, Germany

[7]School of Biosciences, University of Kent, UK

[8]Niguarda Cancer Center, Grande Ospedale Metropolitano Niguarda, Italy

[9]Dipartimento di Oncologia ed Emato-Oncologia, Università degli Studi di Milano, Italy

Cancer Discovery, 2021 March

ıy

ABSTRACT

Targeted therapies, chemotherapy, and immunotherapy are used to treat patients with mismatch repair-deficient (dMMR)/microsatellite instability-high (MSI-H) colorectal cancer (CRC). The clinical effectiveness of targeted therapies and chemotherapy is limited by primary or secondary resistance, as well as by drug toxicities, and about half of immunotherapy patients are refractory to immune checkpoint inhibitors. Loss of Werner syndrome ATP-dependent helicase (WRN) is a synthetic-lethality in dMMR/MSI-H cells. To inform the development of WRN as a therapeutic target, we performed WRN knockout or knockdown in over 60 heterogeneous dMMR CRC preclinical models, demonstrating that WRN dependency is an almost universal feature, and a robust marker for patient selection. Furthermore, models of primary and acquired resistance to clinically-relevant targeted therapy, chemotherapy, and immune checkpoint blockade retain WRN dependency. These data show the potential of therapeutically targeting WRN in most dMMR/MSI-H CRC patients, and support the development of WRN as a therapeutic option for patients with dMMR/MSI-H cancers refractory to current treatment strategies.

INTRODUCTION

DNA mismatch repair (MMR) is an evolutionarily conserved process that recognizes and repairs spontaneously mis-incorporated bases during DNA replication. Microsatellite instability (MSI) is caused by impaired MMR and is a ubiquitous feature in cancer, observed in >20 different tumor types and frequently present in colon, ovarian, endometrial, and gastric cancer, with hundreds of thousands of estimated MSI cancer diagnoses worldwide each year. Lynch syndrome is caused by inherited MMR defects [1]. Approximately 10 - 15% of sporadic CRC display dMMR/MSI, with important prognostic and therapeutic implications for patients [2].

Molecularly targeted therapies and chemotherapy agents are used to treat patients with dMMR CRC. Tumor evolution and resistance are major causes of treatment failure and mortality in CRC patients [3,4]. For instance, activating KRAS mutations lead to primary and secondary resistance to epidermal growth factor receptor (EGFR)-targeted therapies [5,6]. Combination therapies based on vertical suppression of the EGFR - mitogen-activated protein kinase (MAPK) pathway are effective in BRAF-mutated CRC tumors [7,8,9,10], but again resistance occurs in preclinical models and the clinical setting [11,12,13]. Rearrangements in ROS1, ALK, or NTRK are also enriched in dMMR tumors [14,15] and lead to hypersensitivity to matched kinase inhibitors [16]. Resistance to these matched targeted agents can emerge due to NTRK1 mutations or by genomic alterations that converge to activate the MAPK pathway [17,18,19]. Immunotherapy with checkpoint inhibitors to PD-1 and PD-L1 are effective against dMMR CRC tumors due to their high mutational burden and increased numbers of neoantigens [20,21,22]. While response rates to checkpoint inhibitors are high and durable for many dMMR CRC patients, around half have primary resistance and are refractory to treatment [22,23,24,25], and secondary resistance is a problem [21,26,27]. Thus, while advances in precision medicine have led to improved treatment options for dMMR/MSI-H CRC patients, a range of mechanisms can confer resistance and there remains an unmet clinical need for new therapeutic options for patients that are refractory to currently available therapies.

We and others recently identified Werner helicase (WRN) as a synthetic-lethal target in dMMR/MSI-H cancers, with a large proportion of sensitivities in CRC cancer cell lines [28,29,30,31]. WRN is a member of the RecQ family of DNA helicases and has important but

poorly understood roles in maintaining genome stability, DNA repair, replication, transcription, and telomere maintenance (32,33). WRN is selectively essential for dMMR/MSI-H cell viability both in vitro and in vivo, and WRN knockout in dMMR/MSI-H cells induces double-stranded DNA breaks and widespread genome instability, promoting apoptosis [32,33]. A previously unappreciated genetic feature of dMMR/MSI-H cancer cells, DNA (TA)n-dinucleotide repeat expansions, have recently been reported to cause the selective vulnerability to WRN depletion [34]. Given these promising results, translational efforts are needed to comprehensively evaluate the efficacy of WRN inactivation and the performance of dMMR/MSI status as a biomarker of response for patient stratification. In this context, targeting WRN potentially represents an effective option as first-line treatment in monotherapy or combinatorial regimens. Additionally, WRN dependency has not been evaluated in advanced or therapy-refractory tumors, such as in the context of primary and acquired resistance to targeted agents, chemotherapy, and/or immunotherapy.

In the present study, we determined the spectrum of WRN dependency in a broad collection of dMMR/MSI-H CRC models, including those derived from patients refractory to targeted agents and chemotherapy, or that displayed limited benefit from immune checkpoint inhibitors. We demonstrate that WRN dependency is widespread in a heterogeneous collection of dMMR models, supporting the use of MSI status for patient stratification. Additionally, we provide evidence that WRN synthetic-lethality is retained in diverse models of primary and acquired resistance to targeted therapy, chemotherapy, and checkpoint inhibitor therapy, expanding the cohort of patients potentially benefiting from WRN-targeted therapies.

RESULTS

WRN dependency in heterogeneous dMMR CRC preclinical models.

WRN helicase is a promising candidate drug target for dMMR cancers. A limited number of CRC cell lines have been used to evaluate WRN inhibition efficacy, and an in- depth evaluation of WRN dependency in a diverse set of preclinical models is missing. To assess the robustness of the WRN-dMMR association, we assembled the largest collection of dMMR CRC preclinical models to date, including 60 unique models (each from a different individual) derived from primary tumors and metastatic lesions, and comprised of both cancer cell lines and newly-generated patient-derived 3D organoid cultures (Fig. 1A and Supplementary Table S1). This collection reflects the genetic/molecular diversity observed in dMMR/MSI-H CRC patients (Supplementary Fig. S1A). Pathogenic missense mutations in KRAS occurred in 35% (n = 21) of models, while BRAF V600E mutations were present in 33% (n=20). Cell lines with oncogenic driver gene fusions in the NTRK gene (n = 2), as well as ALK and RSPO3 genes (n = 1 of each), were represented [35,36].

Of the 60 dMMR CRC models, we curated published WRN dependency data for 22 cell lines previously measured by genome-wide CRISPR-Cas9 screens or siRNA-mediated WRN knockdown [28,29,37]. Profiles of WRN dependency were generated by CRISPR- Cas9 and/or RNA interference for an additional 38 dMMR CRC preclinical models not included in previous studies, including models derived from metastatic lesions (Fig. 1A). Cell lines (n = 29) were tested by RNA interference (Fig. 1B), while patient-derived organoids (n = 5) were tested by either CRISPR-Cas9-based dropout screening or viability and co-competition assays (Supplementary Fig. S1B-D). Five additional difficult-to-transfect cell lines and models displaying an intermediate response by RNA interference were confirmed to be sensitive using CRISPR-Cas9-based clonogenic assays (Fig. 1C). Strikingly, altogether 92% (55 of 60) of dMMR/MSI CRC models were dependent on WRN for viability, irrespective of the presence of different cancer driver mutations or gene rearrangements (Fig. 1A). As expected, MMR-proficient models were not affected by WRN knockout (Supplementary Fig. S1B). Interestingly, five outlier dMMR models were not dependent on WRN, retaining >75% viability following depletion (Fig. 1B). We independently confirmed the lack of WRN dependency in these

models by CRISPR-Cas9 clonogenic assays and efficient WRN downregulation and knockout by Western Blot (Fig. 1D and Supplementary Fig. S1E- F). Moreover, in WRN-independent MSI-H cells, less than 10% of metaphases are affected by double-strand breaks (DSBs) after WRN knockout, similar to what is detected in MSS cells (Supplementary Fig. S1G-H).

Integration of multiple mutation, gene, and protein expression datasets for the models confirmed that all had one or more alterations in a gene encoding a protein involved in MMR (Fig. 1E). WRN dependency was not associated with mutational burden ($p = 0.88$; Student's t-test). Interestingly, we observed a statistically significant enrichment for MSH2 ($p = 0.0048$ or 0.0357 excluding cell lines with missing data; Fisher's exact test) and MLH1 ($p = 0.0096$ or 0.0625) alterations in WRN-dependent versus independent cell models. We re- assessed MSI status by PCR and independently evaluated MLH1, MSH2, and MSH6 protein expression by Western Blot for WRN independent lines (Supplementary Fig. S2A). All the models were confirmed MSI-H except GEO, which was classified as MSI-low, explaining WRN independence and the absence of alterations in canonical MMR pathway genes in this model. An analogous analysis in an independent set of cancer models from non-CRC dMMR/MSI-H-predominant tissue lineages confirmed an enrichment for MSH2 alterations (p- value = 0.0391) in WRN dependent models, but not MLH1 (Supplementary Fig. S2B). We then performed PCR-based and WGS sequencing coverage analysis to assess MSI cell lines for expanded TA-repeats, a recently identified feature of MSI cells contributing to WRN synthetic-lethality (33). WGS sequencing data were available for a subset of cell lines. We confirmed the presence of expanded TA-repeats in MSI WRN-dependent cell lines compared to MSS cells, as evidenced by a failure to PCR amplify some broken repeat regions and reduced WGS sequencing coverage across broken repeats ($p\text{-value} < 0.001$) (Supplementary Fig. S2C-D). Strikingly, MSI-H WRN-independent cells were most similar to MSS cells, with little or no evidence of expanded TA-repeats with either analysis. The expanded TA-repeat phenotype was variable in cell lines within the MSI subgroups, but nonetheless our results suggest that repeat length is not altered, or at least not to the same extent, in WRN-independent MSI-H cell lines.

Overall, employing a heterogeneous collection of dMMR/MSI-H CRC models, including a large cohort of previously untested models, our results indicate that inhibiting WRN has a nearly universal synthetic-lethal effect, strongly supporting WRN as a target

and dMMR as a therapeutic biomarker for patient selection. There exists however a rare subset of dMMR/MSI-H CRC, characterised by the absence of MLH1 and MSH2 alterations and expanded TA-repeat phenotype, which are not dependent on WRN and would presumably be refractory to WRN targeted therapies.

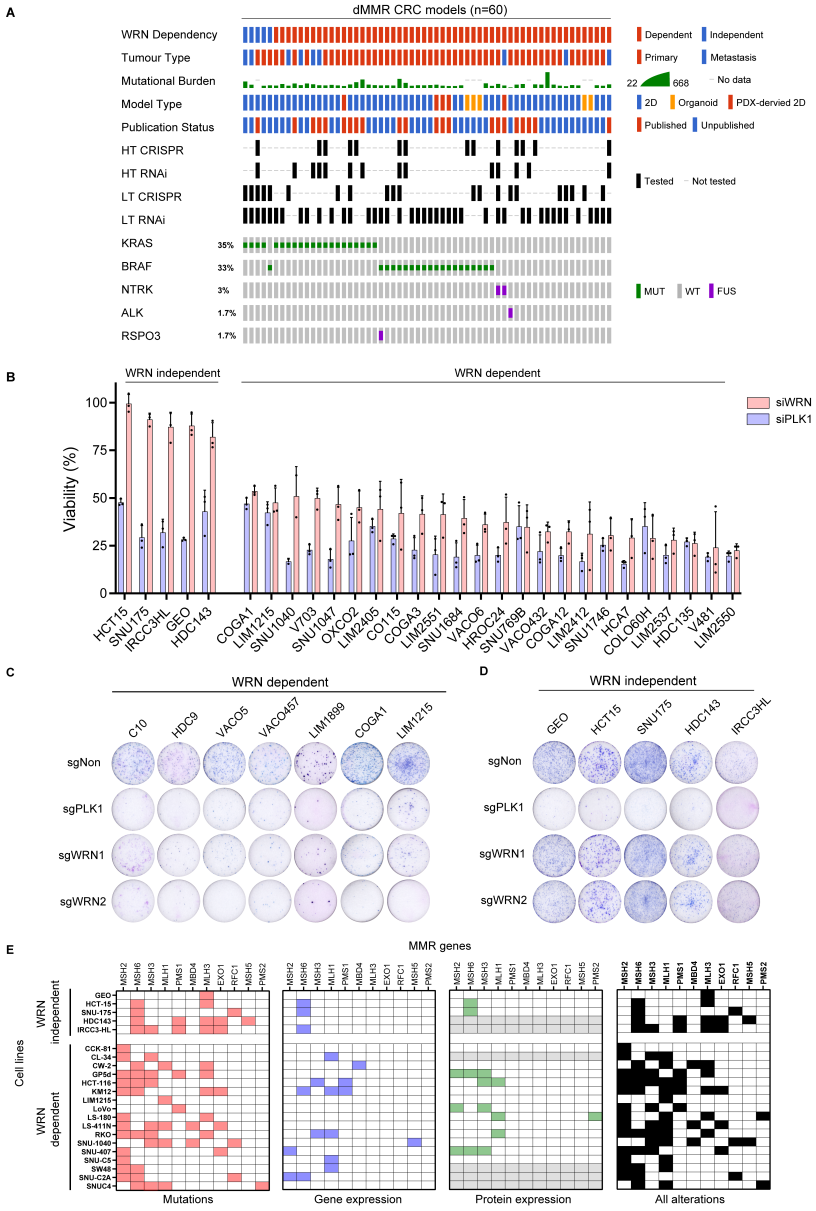

Figure 1: Landscape of WRN dependency in dMMR CRC preclinical models. *(previous page)*

A, Oncoprint representation of WRN dependency and oncogenic driver mutations in dMMR CRC models. For each model, WRN dependency status, type of model, tumor type, mutational burden, model type, publication status of WRN dependency data, and assay types are annotated. Missense mutations in KRAS and BRAF, and oncogenic rearrangements in NTRK1, ALK, and RSPO3 are indicated.
B, WRN depletion assay in 29 dMMR CRC cell lines. Bars are normalized viability upon siRNA-mediated WRN depletion in WRN-dependent cell lines and WRN-independent cell lines, as indicated. Non-targeting siRNA or PLK1 siRNAs (blue bars) were used as negative and positive controls, respectively. Dots represent mean and SD of 3 independent experiments with 5 technical replicates each. SNU1040 was tested twice.
C, WRN dependency in hard to transfect cell lines and models displaying an intermediate response by RNA interference evaluated by CRISPR-cas9-based clonogenic assays (14 days).
D, Clonogenic assays of dMMR CRC models insensitive to WRN knockout. Clonogenic assays are representative of three independent experiments.
E, Genomic and proteomic profile of MMR-pathway gene alterations in dMMR CRC cancer models. Coloured (red, blue, green, and light black) boxes indicate the presence of the alteration. Light grey boxes represent data unavailable.

WRN inhibition is effective in dMMR CRC models of acquired resistance to targeted therapies and chemotherapy

New treatment options for patients with advanced and treatment-refractory disease represents an unmet clinical need. Given the diverse genetic background of tumors dependent on WRN, we hypothesized that dMMR tumors with acquired resistance to targeted therapies and chemotherapy may retain WRN dependency. To investigate this, we began by using isogenic dMMR CRC cell models of acquired resistance to clinically-relevant single agent or combination therapies (Fig. 2A) [11,18,38]. Specifically, cells were made resistant in vitro to the anti-EGFR monoclonal antibody cetuximab, the combination of cetuximab and the BRAF inhibitor (BRAFi) dabrafenib (D+C), or the NTRK inhibitor entrectinib. We confirmed drug sensitivity of the parental cell lines and corresponding resistance of the derivative line (Supplementary Fig. S3A). Upon RNAi-mediated silencing of WRN, all models showed a marked reduction in fitness (Fig. 2B). To confirm these results, we independently performed CRISPR-Cas9 knockout of WRN and observed a marked reduction in cell fitness in all drug-sensitive and drug-resistant lines (Fig. 2C). Downregulation or knockout of the WRN protein was confirmed by Western blot (Supplementary Fig. S3B-C).

Triple therapy based on EGFR, BRAF, and MEK inhibitors recently demonstrated

efficacy in metastatic CRC patients with the BRAF V600E mutation (9). To validate WRN dependency in this setting, we selected drug-resistant BRAF-mutated VACO432 cells in the presence of dabrafenib and cetuximab (D+C) double therapy, and dabrafenib, trametinib, and cetuximab (D+C+T) triple therapy (Fig. 2A). The resulting resistant cells had a KRAS G13D mutation, which is a common mechanism of acquired resistance to this therapy regimen in CRC patients [10] (Supplementary Fig. S3D). Remarkably, cell lines resistant to double or triple therapy retained notable sensitivity to the loss of WRN (Fig. 2B-C). Lastly, we used cell lines derived from a patient-derived xenograft (PDX) model generated from a CRC patient positive for LMNA-NTRK1 rearrangement, treated in vivo with entrectinib in a mouse-human co-clinical trial [18]. An NTRK1 G595R mutation led to entrectinib resistance both in the patient and in the resistant cell line generated from the tumor that acquired resistance in vivo (Supplementary Fig. S3E-F). Again, both the entrectinib-sensitive and resistant cell lines showed a strong dependency on WRN (Fig. 2D-F). WRN knockout in LMNA-NTRK1 cells led to numerous chromosomal abnormalities, including chromatid and chromosome breaks and rearrangements (Fig. 2G-H and Supplementary Fig. S3G).

Figure 2. WRN dependence in models of acquired resistance to targeted agents. *(next page)*

A, Representation of in vitro dMMR CRC models of acquired resistance to EGFR, NTRK1, and BRAF- target therapies.

B and D, Cell viability in models of acquired resistance upon transfection of WRN- targeting siRNAs. PLK1 (siPLK1) siRNA were used as positive control. MMR-proficient (pMMR) cell line SW620 was included as a negative control. Data are the mean ± standard deviation (SD) of three independent experiments with five technical replicate each and were analyzed with two-tailed Student's t-test comparing siWRN to non-targeting control: ns, not significant; * $p \leq 0.05$, ** $p \leq 0.01$ and *** $p \leq 0.001$.

C and E, Normalized viability data in models of acquired resistance upon WRN knockout. Non-essential (sgNon) and PLK1 (sgPLK1) sgRNAs were used as negative and positive controls, respectively. The pMMR SW620 cell line was a negative control. Data are mean and SD of 3 independent experiments with 5 technical replicates each. Statistical significance was evaluated comparing WRN sgRNAs versus non-essential gene sgRNA (sgNon) performing a two-tailed Student's t-test: ns, not significant; $P \leq 0.05$, ** $P \leq 0.01$ and *** $P \leq 0.001$.

F, WRN reduction verified by Western blot. siRNA non-targeting controls (siNTC), siRNA targeting WRN (siWRN). Tubulin is a loading control. Representative of two independent experiments.

G, Quantification of metaphase chromatid breaks in IRCC1-XL-ENTR-R cells 96h after transduction with WRN sgRNA ($n \geq 20$ randomly selected metaphases analyzed).

H, Representative metaphase karyotype of IRCC-1-XL- ENT-R cells after 96h transduction with WRN-targeting sgRNA2. Red arrows indicate chromosome (chrb) and chromatid (chtb) breaks.

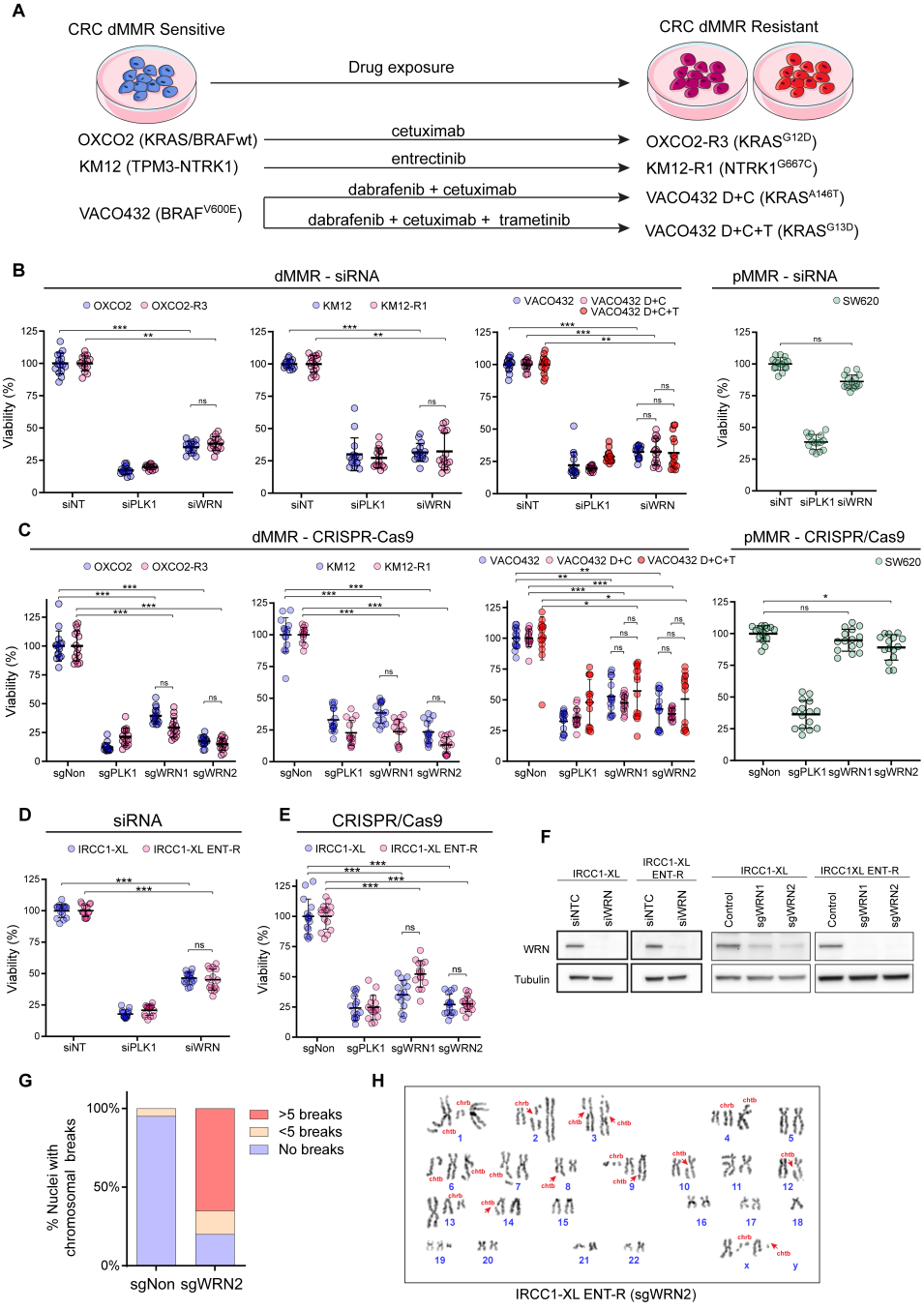
A
CRC dMMR Sensitive
Drug exposure
CRC dMMR Resistant
OXCO2 (KRAS/BRAFwt)
cetuximab
OXCO2-R3 (KRAS^{G12D})
KM12 (TPM3-NTRK1)
entrectinib
KM12-R1 (NTRK1^{G667C})
VACO432 (BRAF^{V600E})
dabrafenib + cetuximab
VACO432 D+C (KRAS^{A146T})
dabrafenib + cetuximab + trametinib
VACO432 D+C+T (KRAS^{G13D})
B
dMMR - siRNA
pMMR - siRNA
OXCO2
OXCO2-R3
KM12
KM12-R1
VACO432
VACO432 D+C
VACO432 D+C+T
SW620
Viability (%)
siNT
siPLK1
siWRN
C
dMMR - CRISPR-Cas9
pMMR - CRISPR/Cas9
sgNon
sgPLK1
sgWRN1
sgWRN2
D
siRNA
IRCC1-XL
IRCC1-XL ENT-R
E
CRISPR/Cas9
F
siNTC
siWRN
Control
WRN
Tubulin
G
% Nuclei with chromosomal breaks
100%
50%
0%
>5 breaks
<5 breaks
No breaks
H
IRCC1-XL ENT-R (sgWRN2)

We next evaluated WRN dependency in the setting of acquired resistance to standard of care chemotherapeutic agents. We treated the MSI CRC cell line HCT116 with increasing doses of oxaliplatin (two independent selections) until resistant cells emerged. We also generated MSI CRC SW48, RKO and LoVo cells resistant to irinotecan, oxaliplatin, or 5-FU (Fig. 3A-B and Supplementary Fig. S4A). Additionally, we established a cell line (IRCC-114-XL) from the PDX of a patient with a clinical history of Lynch syndrome, who relapsed after treatment with mFOLFOX (folinic acid, 5-fluorouracil, and oxaliplatin) for 6 months after surgery, displaying no objective response and rapid progression of disease (Fig. 3C-D). Notably, WRN knockout or depletion markedly reduced the viability of all twelve chemotherapy-resistant dMMR/MSI-H CRC sublines, and IRCC-114-XL cells (Fig. 3E-H, Supplementary Fig. S4B-D). WRN knockout in IRCC-114-XL cells promoted DSBs formation and marked chromosomal defects (Fig. 3I-J and Supplementary Fig. S4E-G).

Figure 3. WRN dependency in chemo-resistant dMMR/MSI-H CRC sublines and patient-derived model. ***(next page)***

A, dMMR CRC models of acquired resistance to chemotherapeutic agents.
B, Proliferation assays of cell line models of acquired resistance to chemotherapies and parental counterparts. Data are average ± SD of three technical replicates and are representative of three independent experiments.
C, The IRCC-114-XL cell line established from a PDX model of a Lynch syndrome patient treated with mFOLFOX for 6 months after surgery.
D, Computed tomography (CT) scan of the IRCC-114 patient displaying drug resistance and early tumor progression after chemotherapy.
E, F, G, Normalized viability of upon siRNA-mediated WRN depletion in HCT116 and SW48 chemotherapy-resistant sublines and IRCC-114-XL cells. Non-targeting siRNA (siNT) and siPLK1 were used as negative and positive controls, respectively. Data are mean and SD of 3 independent experiments with 5 technical replicates each. Statistical significance was evaluated using a Student's t-test: ns, not significant; * P ≤0.05, ** P ≤0.01 and *** P≤0.001
H, Normalized viability for IRCC-114-XL cells upon WRN knockout. Non-essential (sgNon) and PLK1 (sgPLK1) sgRNAs were negative and positive controls, respectively. Data are mean and SD of 2 independent experiments with 5 technical replicates each. Statistical significance was calculated using a two-tailed Student's t- test: ns, not significant; P ≤0.05, ** P ≤0.01, and *** P≤0.001.
I, Chromosome breaks in IRCC-114-XL cell line 96h after WRN depletion (≥20 metaphase spreads assayed).
J, Representative images of IRCC-114-XL metaphases (left) and a pulverized metaphase (right) after 96h of transduction with a sgWRN. Red arrows indicate chromosome (chrb) and chromatid (chtb) breaks.

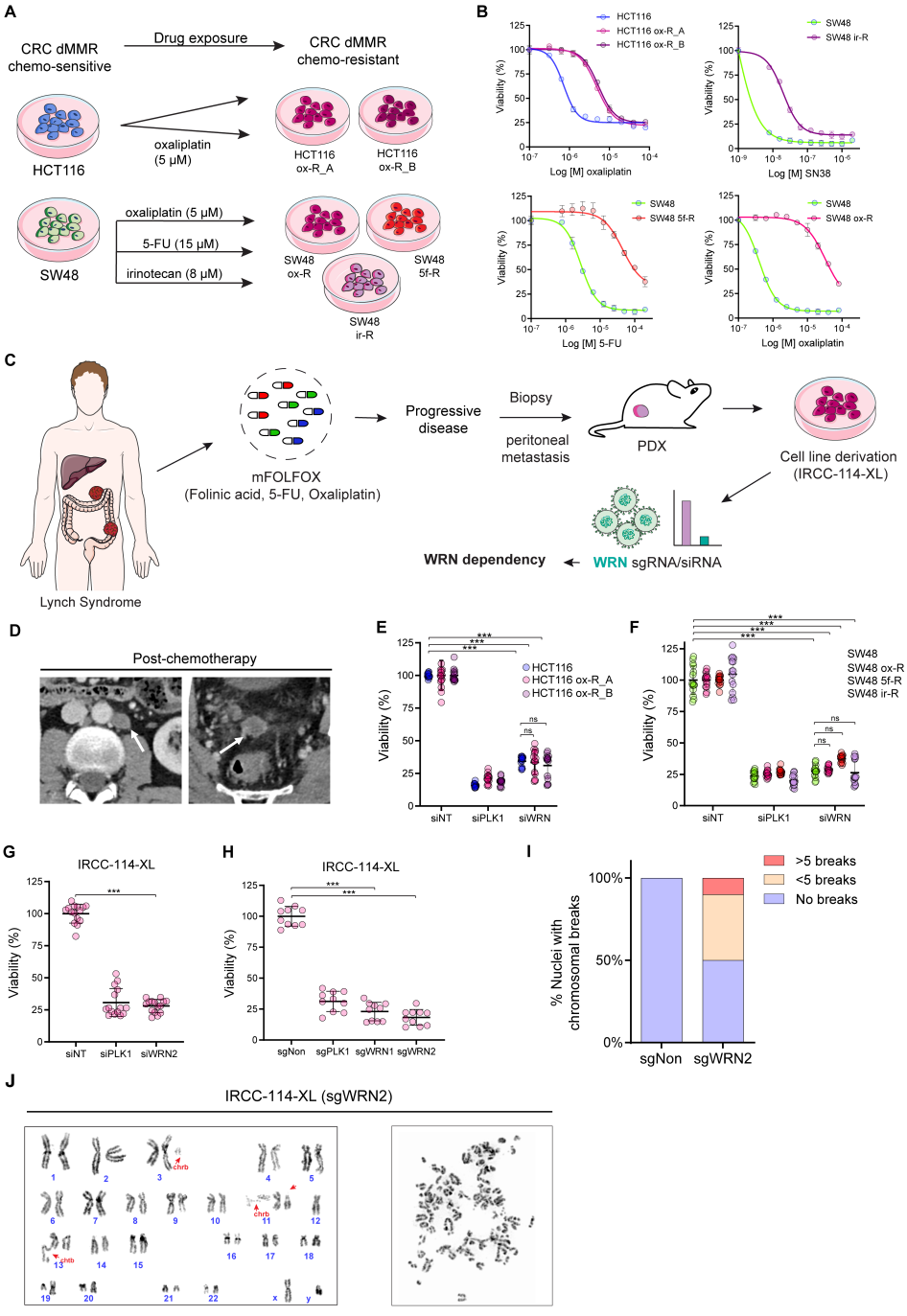
A
CRC dMMR chemo-sensitive
Drug exposure
CRC dMMR chemo-resistant
HCT116
oxaliplatin (5 µM)
HCT116 ox-R_A
HCT116 ox-R_B
SW48
oxaliplatin (5 µM)
5-FU (15 µM)
irinotecan (8 µM)
SW48 ox-R
SW48 5f-R
SW48 ir-R
B
HCT116
HCT116 ox-R_A
HCT116 ox-R_B
Viability (%)
Log [M] oxaliplatin
SW48
SW48 ir-R
Log [M] SN38
SW48 5f-R
Log [M] 5-FU
SW48 ox-R
C
Lynch Syndrome
mFOLFOX
(Folinic acid, 5-FU, Oxaliplatin)
Progressive disease
Biopsy
peritoneal metastasis
PDX
Cell line derivation (IRCC-114-XL)
WRN dependency
WRN sgRNA/siRNA
D
Post-chemotherapy
E
HCT116
HCT116 ox-R_A
HCT116 ox-R_B
siNT
siPLK1
siWRN
F
SW48
SW48 ox-R
SW48 5f-R
SW48 ir-R
G
IRCC-114-XL
siWRN2
H
sgNon
sgPLK1
sgWRN1
sgWRN2
I
% Nuclei with chromosomal breaks
>5 breaks
<5 breaks
No breaks
J
IRCC-114-XL (sgWRN2)

Altogether, these results demonstrate that dMMR CRC cells resistant to clinically-relevant targeted therapies or chemotherapy retain a synthetic-lethal dependency on WRN, irrespective of the mutational background of the tumor and the therapeutic regimen to which resistance was acquired.

Patient-Derived dMMR CRC Models Refractory to Immunotherapy are WRN Dependent

We next used multiple patient-derived organoid models to investigate whether dMMR CRC tumors responding poorly to immunotherapy are dependent on WRN. First, we evaluated WRN dependency in the setting of resistance to T cell-mediated tumor cell killing using an autologous tumor organoid and peripheral blood lymphocyte co-culture system [39,40]. We made use of a previously established organoid model from a dMMR CRC patient (CRC-12) together with matched tumor-reactive T cells generated by two weeks of co-culturing peripheral blood mononuclear cell (PBMCs) with tumor organoids [39] (Fig. 4A left panel). CRC-12 cells were killed by autologous tumor-reactive T cells in a dose- dependent manner. Killing was rescued by the addition of a MHC class I blocking antibody, confirming an antigen-specific CD8+ T cell mediated response (Supplementary Fig. S5A). To generate a model of resistance, we in vitro selected a sub-population of CRC-12 organoids resistant to T cell killing (CRC-12-RES). In addition, as a positive control for resistance, we knocked out the B2M gene to create an isogenic CRC-12 line (CRC-12-B2M), and confirmed loss of MHC-I expression (Supplementary Fig. S5B). CD137 surface expression was used as a marker for T cell activation. Autologous CD8+ T cells were reactive to CRC-12 tumor organoids, whereas no CD8-mediated reactivity was detected in the presence of CRC-12-RES or CRC-12-B2M organoids; CD4+ T cell reactivity remained unaffected (Fig. 4B and Supplementary Fig. S5C-D). Accordingly, while CRC-12 parental organoids were killed by autologous tumor-reactive T cells, CRC-12-RES and CRC-12-B2M KO organoids were unaffected by the presence of the reactive population (Fig. 4C). Resistance in CRC-12-RES organoids was not due to the loss of MHC-I or IFNγ receptor (Supplementary Fig. S5B and E), and B2M mutations were absent. Next, we used these advanced models to investigate WRN dependency.

Strikingly, WRN knockout inhibited viability in the parental CRC-12 organoid, as well as CRC-12-RES, demonstrating that strong WRN dependency is retained in a model refractory to autologous T cell-mediated cytotoxicity (Fig. 4D).

To corroborate our findings, we investigated WRN dependency in two organoids derived from a sporadic dMMR CRC patient with variable clinical response to immunotherapy. CRC-14a and CRC-14b were derived from biopsies obtained from a peritoneal metastasis and primary tumor of a patient with a clinical treatment history of capecitabine, oxaliplatin, and bevacizumab, then treated with nivolumab monotherapy (Fig. 4A, right panel). The CRC-14a metastasis biopsy was taken before the start of the checkpoint blockade, and this lesion regressed on nivolumab, whereas the biopsy for CRC- 14b was taken from the primary tumor upon progression on nivolumab (Fig. 4E). To induce (or enrich for) a tumor reactive T cell population, both organoids were individually co-cultured with autologous PBMCs obtained before treatment with nivolumab [39,40]. After 2 weeks of co-culture with CRC-14a (from the responsive metastatic lesion), we observed marked and selective CD8+ T cell reactivity against CRC-14a (but not CRC-14b) organoids (Fig. 4F). In contrast, when CRC-14b organoids (derived from the non-responding primary tumor) were used in the co-culture, no T cell reactivity was detected against any of the organoid lines. Of note, CD4+ T cell reactivity remained unaltered (Supplementary Fig. S5F). Interestingly, loss of MHC-I expression was found in CRC-14b, potentially explaining the failure to generate tumor reactive T cells from PBMCs, and lack of clinical response to nivolumab treatment (Supplementary Fig. S5G). B2M protein expression in CRC-14b was confirmed by flow cytometry (Supplementary Fig. S5H) and no frameshift or nonsense mutations were detected, suggestive of a B2M-independent resistance mechanism, although a non- synonymous variant of unknown significance (Y30C) was present. These results support CRC-14b as an ex vivo model to evaluate WRN dependency in an immune refractory setting. Viability assays after CRISPR-based knock-out of WRN in CRC-14b organoids revealed a strong dependency on the WRN helicase (Fig. 4G-H). Altogether, these data provide multiple lines of evidence that WRN dependency is retained in patient-derived dMMR CRC preclinical models of resistance to immunotherapy.

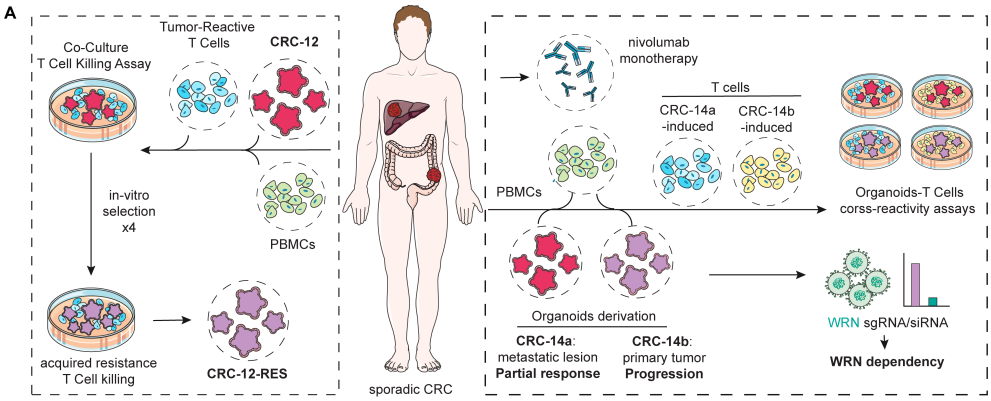
A
Co-Culture
T Cell Killing Assay
Tumor-Reactive
T Cells
CRC-12
in-vitro
selection
x4
PBMCs
acquired resistance
T Cell killing
CRC-12-RES
sporadic CRC
nivolumab
monotherapy
T cells
CRC-14a
-induced
CRC-14b
-induced
PBMCs
Organoids-T Cells
corss-reactivity assays
Organoids derivation
CRC-14a:
metastatic lesion
Partial response
CRC-14b:
primary tumor
Progression
WRN sgRNA/siRNA
WRN dependency

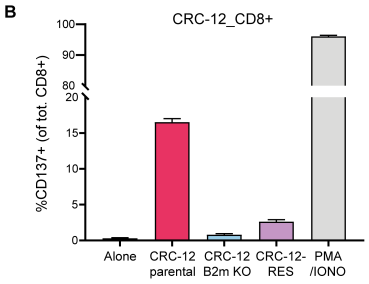
B
CRC-12_CD8+
%CD137+ (of tot. CD8+)
Alone
CRC-12
parental
CRC-12
B2m KO
CRC-12-
RES
PMA
/IONO

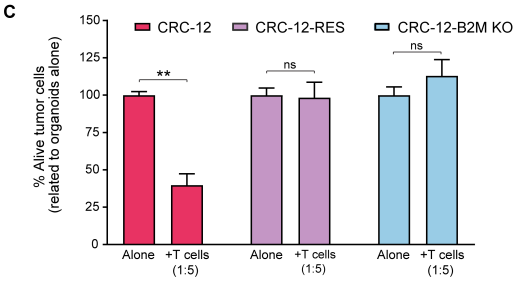
C
CRC-12
CRC-12-RES
CRC-12-B2M KO
% Alive tumor cells
(related to organoids alone)
**
ns
ns
Alone
+T cells
(1:5)

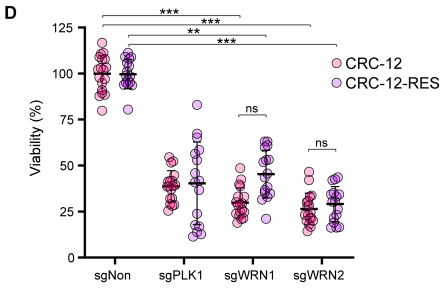
D
Viability (%)
CRC-12
CRC-12-RES
***
**
ns
sgNon
sgPLK1
sgWRN1
sgWRN2

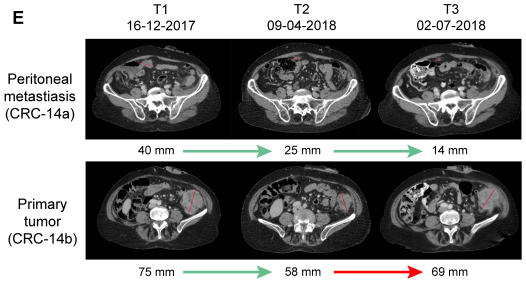
E
T1
16-12-2017
T2
09-04-2018
T3
02-07-2018
Peritoneal
metastiasis
(CRC-14a)
40 mm
25 mm
14 mm
Primary
tumor
(CRC-14b)
75 mm
58 mm
69 mm

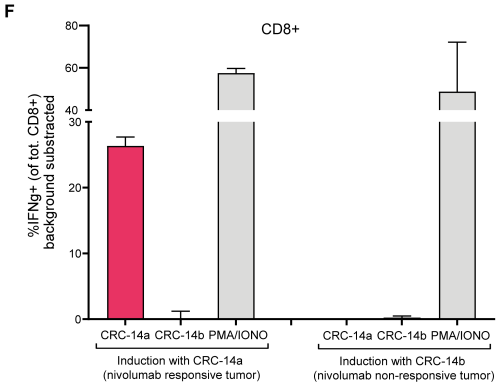
F
CD8+
%IFNg+ (of tot. CD8+)
background substracted
CRC-14a
CRC-14b
PMA/IONO
Induction with CRC-14a
(nivolumab responsive tumor)
Induction with CRC-14b
(nivolumab non-responsive tumor)

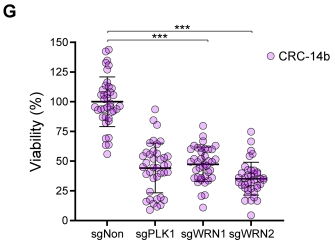
G
CRC-14b
Viability (%)
***
***
sgNon
sgPLK1
sgWRN1
sgWRN2

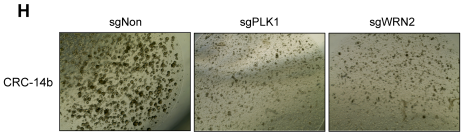
H
sgNon
sgPLK1
sgWRN2
CRC-14b

Figure 4. Patient-derived CRC dMMR organoid models refractory to immunotherapy are WRN dependent. ***(previous page)***

A, dMMR CRC tumor organoid-T cell co-cultures from a sporadic dMMR primary tumor (left panel) or two lesions in a patient with a heterogeneous clinical response to nivolumab (right panel).
B, CD137 expression of CD8+ T cells upon stimulation with different CRC-12-derived organoids lines. Values are background corrected, and bars represent mean and SEM of two independent experiments.
C, Organoid killing after 3 days of T cell co-culture. Error bars represent SEM of at least two biological replicates.
D, Viability in CRC-12 and CRC-12-RES upon WRN knockout. Non-essential (sgNon) and PLK1 (sgPLK1) sgRNAs were negative and positive controls, respectively. Data are the mean ± standard deviation (SD) of three independent experiments with 6 technical replicates each.
E, Computer tomography scans over an 8-month period of the peritoneal metastasis lesion and the primary tumor of CRC-14 patient treated with nivolumab. Red and green arrow indicates a size increase and reduction, respectively.
F, IFNγ expression of CD8+ T cells upon exposure to CRC-14a (responsive) or CRC-14b (non responsive) organoids. Stimulation with PMA/ionomycin is a positive control. Background IFN-γ-positive cells (in unstimulated condition) was subtracted from the signal. Data are the mean and SEM of at least 2 independent experiments.
G, Viability of CRC-14b organoids upon WRN knockout. sgNon and sgPLK1 were used as negative and positive controls, respectively. Data are the mean ± standard deviation (SD) of four independent experiments (10 technical replicates each).
H, Representative images of CRC-14b (10x magnification) 10 days after transduction with indicated sgRNAs.
C, D, G: Significance was evaluated by two-tailed Student's t test. ns, not significant; ** P ≤0.01 and *** P≤0.001.

DISCUSSION

We have investigated the potential of therapeutically targeting WRN in preclinical models of dMMR CRC, including in the setting of resistance to targeted therapies, chemotherapy and immunotherapy. We used the largest collection of dMMR CRC preclinical models characterized to date, nearly tripling the number assessed for WRN dependency. Greater than 90% of models were WRN dependent, including models with diverse genetic backgrounds, molecular contexts, and oncogenic alterations, suggesting WRN dependency is an almost universal feature of dMMR/MSI CRC cells. This reinforces dMMR/MSI status as a robust biomarker for WRN synthetic-lethality and to stratify patients for the clinical development of WRN-targeted therapies. Notably, for the ~7% of dMMR CRC models that were WRN independent, functional expression of MSH2 and MLH1 was retained, suggesting that WRN dependency is influenced by the underlying MMR-pathway genes altered. Moreover, TA-repeats are differentially altered compared to MSI-H WRN dependent lines, suggesting that loss of MSH2 or MLH1 might be of particular importance to generate TA- dinucleotide repeat expansions reported to confer WRN addiction [34]. This observation warrants confirmation in larger cohorts but, if validated, could provide mechanistic insight into the WRN-MSI synthetic lethal interaction and help refine patient selection strategies based on novel biomarkers of sensitivity.

Inhibition of WRN leads to genome instability in dMMR cells. This may be due to a catastrophic failure to process TA-dinucleotide expansions that accumulate in MSI cells [34]. This is distinctive from targeted agents which inhibit specific oncogenic alterations in cancer cells and immunotherapies which suppress immune evasion and tolerance. Consistent with an orthogonal therapeutic activity, WRN is a synthetic-lethality in preclinical models of resistance to molecular targeted therapies, including models addicted to a diverse set of oncogenic alterations and that acquire different genetic mutations to promote therapy escape. In addition, WRN is synthetic-lethal in patient-derived models from dMMR CRC patients with limited clinical benefit from chemotherapy and PD-1 inhibitors, or resistant to autologous T-cell mediated cancer cell killing. Resistance to targeted therapies can occur through a range of mechanisms, including through reactivation of the targeted pathway, while for immunotherapies, several mechanisms of resistance are emerging including loss of antigen processing and presentation [41]. Our finding suggests that WRN inhibitors could be effective as a second

or third-line monotherapy for dMMR patients. Indeed, WRN sensitivity was not correlated with mutational load in dMMR tumors, whereas low mutability in dMMR tumors is negatively associated with response to immune checkpoint blockade [25,42]. Because of their independent modes of action, combining a checkpoint inhibitor, chemotherapy or a targeted therapy with a WRN inhibitor may suppress cross-resistance and promote tumor eradication. Moreover, WRN inhibition may also be synergic with immunotherapy as loss of DNA repair modulates the neoantigen landscape and increases mutational burden, leading to an enhanced immune response [43]. DNA damage resulting from loss of WRN could likewise potentiate the effects of immunotherapy, similar to combining chemotherapeutics with immune-modulating agents [44]. Investigations into the effects of WRN inhibition on immune recognition and surveillance to increase therapeutic efficacy for patients with dMMR CRC refractory to immunotherapy regimens are warranted. Collectively, our findings provide a rationale for the clinical development of WRN-targeted medicines in advanced CRC patients, and potentially in combination with existing therapies.

For our study, we exploited a tumor organoid T cell co-culture system as a preclinical tool to assess WRN dependence. We used for the first time an organoid co-culture system to model in vitro acquired resistance to T cell killing. Mechanisms driving resistance to immunotherapy and tumor reactive T-cells in these model are currently unverified, but loss of MHC-I expression in organoids derived from an anti-PD-1 resistant tumor points to a loss of antigenicity and immunogenicity due to immune selection pressure, favouring the growth of tumor cell clones with a non-immunogenic phenotype, similar to what has been described clinically [45].

WRN has a role in maintenance of genome stability and Werner syndrome is an autosomal recessive disorder associated with premature ageing caused by mutation in the WRN gene. Nonetheless, WRN mutations are compatible with human development well into the fourth decade of life, and disease-associated complications take decades to manifest, suggesting a therapeutic window of activity could be achieved using WRN-targeted medicines in appropriately selected patients. WRN is the focus of ongoing drug discovery programs. Small molecule WRN helicase inhibitors have been reported [46,47], but their efficacy is impaired by lack of selectivity against dMMR cells, off-target effects, and cytotoxicity to normal cells [48]. Our study provides new information to support the continued development of WRN-targeted medicines. Furthermore, as potent and

selective WRN drugs are developed, our findings will inform patient selection strategies and provide a strong rationale for their clinical development in patients with dMMR tumors not benefiting from current therapeutics alone.

METHODS

Cell models

A full description of cell models (cell lines and organoids) used in this study is provided in Supplementary Table 1. The majority of cell lines were curated from the Genomics of Drug Sensitivity 1000 cell line collection and are annotated in the Cell Model Passports database (https://cellmodelpassports.sanger.ac.uk/) (49), or are from previously reported collection [35,50]. The LIM1215 parental cell line has been described previously (ADD REF: R. H. Whitehead, F. A. Macrae, D. J. St John, J. Ma, A colon cancer cell line (LIM1215) derived from a patient with inherited nonpolyposis colorectal cancer. J. Natl. Cancer Inst. 74, 759– 765 (1985)) and was obtained together with LIM2405, LIM2412 and LIM2537 from Prof. Robert Whitehead, Vanderbilt University, Nashville, with permission from the Ludwig Institute for Cancer Research, Zurich, Switzerland. LIM2550 and LIM2551 were obtained from CellBank Australia. Cell lines were maintained in their original culturing conditions according to supplier guidelines or as previously described [51]. Cells were supplemented with 10% FBS, 2 mM L-glutamine, and antibiotics (100 U/mL penicillin and 100 mg/mL streptomycin) and grown at 37 °C and 5% CO2 air incubator. Cells were routinely screened for the absence of mycoplasma contamination using the VenorGeM Classic kit (Minerva Biolabs). The identity of each cell line was checked before starting each experiment and after every genomic DNA extraction by PowerPlex16 HS System (Promega), through Short Tandem Repeats (STR) at 16 different loci (D5S818, D13S317, D7S820, D16S539, D21S11, vWA, TH01, TPOX, CSF1PO, D18S51, D3S1358, D8S1179, FGA, Penta D, Penta E, and amelogenin). Amplicons from multiplex PCRs were separated by capillary electrophoresis (3730 DNA Analyzer, Applied Biosystems) and analyzed using GeneMapper v 3.7 software (Life Technologies). The MSI status of the cell lines and organoids in Fig. 1 was previously reported [35,39,52] and/or publicly available (Cell Model Passports database (https://cellmodelpassports.sanger.ac.uk/) [49]. The PDX-derived cell line IRCC-114-XL was generated following previously described procedures [37] approved by the Italian Ministry of the Health and the Local Ethics Committee (Protocol n. 1014/2009 and 194/2010 of Grande Ospedale Metropolitano Niguarda, Milano, Italy) in accordance with generally accepted guidelines for the use of human material. Organoids were derived at the Sanger Institute by the Cell Model Network UK consortium (CMN-UK) as part of the

Human Cancer Model Initiative (HCMI), and genomic characteristics, such as microsatellite stability status, were downloaded from the Cell Model Passports website[49].

Patient-derived organoids for immuno-oncology studies were derived at the Netherlands Cancer Institute as previously reported (Dijkstra et al. 2018; Cattaneo et al. 2020). Briefly, tumor tissue was mechanically dissociated and digested with 1.5 mg/mL of collagenase II (Sigma-Aldrich),10 µg/mL of hyaluronidase type IV (Sigma-Aldrich), and 10 µM Y-27632 (Sigma-Aldrich). Cells were embedded in Geltrex (Geltrex LDEV-free reduced growth factor basement membrane extract, Gibco) and placed in a 37 °C incubator for 20 min. Human CRC organoids medium is composed of Ad-DF+++ (Advanced DMEM/F12 (GIBCO) supplemented with 2 mM Ultraglutamine I (Lonza), 10 mM HEPES (GIBCO), and 100/100 U/mL Penicillin/Streptomycin (GIBCO), 10% Noggin-conditioned medium, 20% R-spondin1- conditioned medium, 1x B27 supplement without vitamin A (GIBCO), 1.25 mM N- acetylcysteine (Sigma-Aldrich), 10 mM nicotinamide (Sigma-Aldrich), 50 ng/mL human recombinant EGF (Peprotech), 500 nM A83-01 (Tocris), 3 µM SB202190 (Cayman Chemicals) and 10 nM prostaglandin E2 (Cayman Chemicals). Organoids were passaged every 1–2 weeks by incubating in TrypLE Express (Gibco) for 5–10 min followed by embedding in Geltrex. Organoids and cell lines were authenticated by SNP array and regularly tested for Mycoplasma using Mycoplasma PCR43 and the MycoAlert Mycoplasma Detection Kit (catalog no. LT07-318). In the first two weeks of organoid culture, 1x Primocin (Invivogen) was added to prevent microbial contamination. All the procedures performed with patient specimens were conducted under the approval of the institutions' local Ethical Committee, after the written informed consent of the patients. The study (NL48824.031.14) was approved by the Medical Ethical Committee of the Netherlands Cancer Institute – Antoni van Leeuwenhoek hospital and written informed consent was obtained from all patients. Peripheral blood and tumor tissue were obtained from patients with a confirmed diagnosis of colorectal cancer.

Generation of subline resistant to chemotherapy.

Colorectal cancer cell lines SW48, LoVo, RKO and HCT116 were obtained from ATCC. SW48, LoVo and RKO drug-resistant sublines were derived from the resistant cancer cell

line (RCCL) collection (https://research.kent.ac.uk/industrial-biotechnology-centre/the-resistant-cancer-cell-line-rccl-collection/) [53] and established by continuous exposure to stepwise increasing drug concentrations as previously described [54]. SW48, LoVo and RKO resistant sublines were adapted to growth in the presence of 5-fluorouracil (5-FU) (8, 1.5 and 3μM; 5f-R), irinotecan (8, 0.34 and 1.7 μM; ir-R), or oxaliplatin (5, 5 and 3.8 μM; ox- R), respectively. SW48, LoVo and RKO cells were propagated in DMEM/F-12 supplemented with 10 % FBS, 100 IU/mL penicillin and 100 μg/mL streptomycin at 37°C. Similarly, HCT116 resistant sublines (HCT116 ox-R_A and B) were adapted to growth in the presence of 5 μM of oxaliplatin.

Molecular characterization of WRN-independent dMMR cell lines

The MSI status of WRN independent dMMR models (GEO, HCT15, HDC143, SNU175, and IRCC3HL) was re-assessed and confirmed with the MSI Analysis System kit (Promega). The analysis requires a multiplex amplification of seven markers, including five mononucleotide repeat markers (BAT-25, BAT-26, NR-21, NR-24, and MONO-27) and two pentanucleotide repeat markers (Penta C and Penta D). The products were analyzed by capillary electrophoresis in a single injection (3730 DNA Analyzer, ABI capillary electrophoresis system (Applied Biosystems). Results were analyzed using GeneMapper V5.0 software. Mutations in MMR-pathway genes were downloaded from The Cell Model Passport or Dependency Map (DepMap) websites. Mutations in IRCC3-HL and HDC143 cell lines were obtained by whole-exome sequencing data generated at the Candiolo Cancer Institute. Mutational burden of cancer cell lines was computed analyzing NGS data previously published [55–57] and available at the European Nucleotide Archive (ENA; accession codes PRJEB33045 and PRJEB33640). Genetic analysis was performed as described in the [55– 57]. Mutations in VACO432 C+D+T cell model were detected though Sequenom analysis by using Myriapod Colon status kit (Diatech Pharmacogenetics, Italy). SNP were excluded except if predicted as damaging. For gene expression, we used RNAseq (RPKM) data previously generated [58]. For GEO and HDC143 we used gene expression data obtained previously [35]. Proteomics data were already available [59,60]. To identify which MMR- pathway gene displayed altered gene or protein expression, we computed the Z-score by gene across all the cell lines in the

respective dataset and considered genes with Z-score or normalized values less than negative 2 to identify genes downregulated in a particular sample. WRN dependency was obtained mining essentiality data obtained from multiple sources: Project Score (https://score.depmap.sanger.ac.uk/) and Dependency Map (DepMap; https://depmap.org/portal/) websites or additionally available datasets [61]. Cell lines were considered WRN dependent if WRN essentiality reached threshold values of significance in at least one of the CRISPR (Sanger or DepMap Public 20Q2) or combined RNAi (Broad, Novartis, Marcotte) datasets. Statistical significance was computed by performing Fisher's exact comparison for the presence of cumulative alterations (mutation, gene expression, and protein expression) detected in WRN-dependent versus WRN- independent cell lines. For TA-dinucleotide repeat expansion analysis whole genome sequencing data for cancer cell lines were downloaded from SRA study SRP186687 (https://trace.ncbi.nlm.nih.gov/Traces/study/?acc=SRP186687). Fastq files were mapped to human genome reference GRCh38 using bwa-mem alignment algorithm [62] and then PCR duplicates were marked using MarkDuplicates tool (http://broadinstitute.github.io/picard). The genomic coordinates of broken and unbroken regions were downloaded from Wietmarschen et al. Nature, 2020 [34], and then converted into the GRCh38 assembly version using the LiftOver tool [63]. A total of 5362 and 59926 broken and unbroken regions were analysed, respectively. For all WGS the fragments per base per million (FPBM) were calculated in each interval as reported in Wietmarschen et al. Nature, 2020 [34], and, lastly, the median values of broken and unbroken regions were estimated in each sample. PCR- based analysis of TA-repeats were performed as previously reported [34], using the same PCR primer sequences. Samples were denatured at 95 °C for 3 min and underwent 28 cycles of denaturation at 95 °C for 30s, annealing/extension at 60 °C for 3 min, followed by an extension at 60 °C for 10 min. PCR products were separated on a 2% agarose gel and visualized by ethidium bromide staining.

Immunohistochemistry

Immunohistochemistry assessment of MMR status in patient-derived organoids derived at the Netherlands Cancer Institute was performed as follows. Formalin-fixed, paraffin-

embedded (FFPE) sections were obtained from both pretreatment biopsies and resection specimens. Baseline tumor biopsies were used to assess MMR status using IHC for MLH1, PMS2, MSH2 and MSH6 according to standard protocols for the Ventana automated immunostainer (MLH1 Ready-to-Use, M1, 6472966001, lot no. G07286, Roche; MSH2, Ready-to-Use, G219-1129, 5269270001, lot no. 1616008C, Roche; MSH6, 1/50 dilution, EP49, AC-0047, lot no. EN020910, Abcam; PMS2, 1/40 dilution, EP51, M3647, lot no. 1012289, Agilent Technologies).

Generation of Cas9 expressing cell lines

Between 2-3 x 10^5 cells were transduced overnight with lentivirus containing Cas9 (Addgene, 68343) in a T25 flask, in the presence of polybrene (8 µg/mL). Lentivirus-containing medium was refreshed the following day with complete medium. Tumoral organoids were dissociated into single cells and incubated overnight in suspension and complete media. The following day cells were seeded in matrigel and grown as organoids. Positively transduced cells were selected for with blasticidin (20 µg/mL, Thermo Fisher Scientific, A1113903) starting 48 hours after transduction. Cas9 activity was determined as described previously (64). Briefly, cells or organoids were transduced with Cas9 reporter virus (pKLV2-U6gRNA(gGFP)- PGKBFP2AGFP-W), as described above. The number of BFP+ and GFP-BFP double-positive cells were determined by flow cytometry on a BD LSR Fortessa instrument (BD), and data were subsequently analysed using FlowJo to determine the percentage of BFP+ cells. All cell lines and organoid lines displayed Cas9 activity over 75%.

Organoid genome editing and genome-wide CRISPR-Cas9 screens

The genome-wide sgRNA library transduction was adapted from a previous protocol recently reported to screen cancer cell lines [64]. Briefly, tumor organoids were dissociated into single cells, and a total of 3.3x10^7 cells were transduced overnight, in suspension, with an appropriate volume of the lentiviral-packaged whole-genome sgRNA library to achieve 30% transduction efficiency (100x library coverage) and polybrene (8 µg/mL).

The following day, cells were seeded in matrigel and grown as organoids. After 48h organoids were selected with Puromycin (2 µg/mL). After 14 days, approximately $2x10^7$ cells were collected, pelleted and stored at –80 °C for DNA extraction. Genomic DNA was extracted using the Qiagen, Blood & Cell Culture DNA Maxi Kit, 13362, as per the manufacturer's instructions. PCR amplification, Illumina sequencing (19-bp single-end sequencing with custom primers on the HiSeq2000 v.4 platform) and sgRNA counting were performed as described previously [64]. To generate B2M knockout organoids lines, we used sgRNA targeting B2M (GGCCGAGATGTCTCGCTCCG), cloned into LentiCRISPR v2 plasmid and the virus was produced by standard method. To express luciferase in the organoids, we used pLenti CMV Puro LUC (w168-1) (Plasmid #17477; Addgene).

CRISPR-Cas9 viability and co-competition assay

Approximately 1.5-3 x 10^3 Cas9 expressing cells per well, of a 96-well plate were transduced overnight in the presence of polybrene (8 µg/mL) with lentiviral constructs containing sgRNAs against:
a non-essential gene (CYP2A13, GTCACCGTGCGTGCCCCGG),
an essential gene (PLK1, GCGGACGCGGACACCAAGG),
and two sgRNAs against WRN (#1, GAGCATGAGTCTATCAGAT) and
(#2, GTCCTGTGGAACATACCATG).
Medium was refreshed for fresh complete medium the following day, and cells were treated with blasticidin (20 µg/mL) and puromycin (2 µg/mL, Thermo Fisher Scientific, A1113803) to select for Cas9 expressing cells carrying the sgRNAs. Cells were allowed to grow for approximately 7-10 days before cell viability was determined using the CellTiter-Glo 2.0 Assay (Promega, G9241). For the co-competition assay, organoids were transduced as above to achieve 50% of BFP-positive cells and seeded in six-well plates the day after to form organoids. A co-competition score was determined as the ratio of the percentage of BFP-positive (sgRNA trasduced) cells on day 14 compared to day 3, as measured by flow cytometry.

RNA interference-based sensitivity assay

Approximately 1.5-3.5 x 10^3 cells per well, of a 96-well plate, were reverse transfected with ON-TARGETplus siRNA, to a final concentration of 20 nM, using RNAiMAX (Invitrogen) as per manufacturer instructions. Each experiment included transfection reagent only as mock control, a non-targeting pool as negative control (Dharmacon, D-001810-10-05), polo-like kinase 1 (PLK1) pool as positive control (Dharmacon, L-003290-00-0010), and the targeting pool against WRN (Dharmacon, L-010378-00-0005).
siRNA sequences:
Non-targeting Control Pool
UGGUUUACAUGUCGACUAA
UGGUUUACAUGUUGUGUGA
UGGUUUACAUGUUUUCUGA
UGGUUUACAUGUUUUCCUA
PLK1
GCACAUACCGCCUGAGUCU
CCACCAAGGUUUUCGAUUG
GCUCUUCAAUGACUCAACA
UCUCAAGGCCUCCUAAUAG
WRN
GAUCCAUUGUGUAUAGUUA
GCACCAAAGAGCAUUGUUA
AUACGUAACUCCAGAAUAC
GAGGGUUUCUAUCUUACUA
Cells were grow for 5-7 days. Cell viability was assessed using the CellTiter-Glo 2.0 Assay (Promega, G9241) as described below.

Drug sensitivity assay

Drug sensitivity assays were performed to confirm the resistance of each cell line. For each pair of cell lines of interest, approximately 1.5-2.5 x 10^3 cells per well of a 96-well plate were seeded and grown for both the drug-sensitive and drug-resistant lines. The

following day, a concentration range of the respective drug was added to the cells, in triplicate per concentration per line, and cells were allowed to grow for 7-10 days. Cell viability was assessed using the CellTiter-Glo 2.0 Assay (Promega, G9241).

Cell viability assay

Cell viability was determined using the CellTiter-Glo 2.0 Assay (Promega, G9241), as per manufacturer instructions. Briefly, 25 µL of Celltiter-Glo 2.0 reagent was added to each well of a 96 well plate and incubated for at least 20 minutes at room temperature in the dark. After incubation, the luminescent signal was read out using an Envision Multiplate Reader.

Western blotting

Western blotting was performed to confirm the absence of WRN in siRNA and CRISPR treated cells. For siRNA-based knockdown, approximately 0.5-1 x 10^6 cells were seeded in a 6-well plate in OptiMem and treated as described above. This assay included siRNA pools targeting WRN and a non-targeting pool as negative control. For CRISPR-based knockdown, approximately 1 x 10^6 cells were seeded in a 10cm cell culture dish and treated as described above. This assay included two sgRNAs against WRN and a negative control without virus. Protein was isolated 72-96h after seeding with 100-150 uL RIPA buffer supplemented with proteinase and phosphatase inhibitors. Lysate concentration was determined using the BCA Assay. Per sample, 20-30 µg of lysate was loaded onto a 4-12 % Bis-Tris gel (Invitrogen) for SDS-PAGE followed by protein transfer from the gel onto a PVDF membrane. Membranes were blocked in 5% milk (in TBST) and incubated overnight with the appropriate antibodies. Blots were washed in TBST and incubated with secondary antibody for 1h at room temperature. Blots were washed in TBST before the signal was enhanced with Super Signal Dura and visualized. The following primary antibodies were used for immunoblot analysis: anti-WRN antibody (Cell Signalling Technologies, 4666, 1:2000), and anti-β-tubulin (Sigma-Aldrich, T4026: 1:5000) as loading control. Anti-Mouse IgG HRP-linked secondary antibody (GE Healthcare, #NA931) was used as a secondary antibody. Precision Plus Protein Standards (BioRad, 161-0373) was used as a molecular weight marker.

Karyotype analysis with human M-FISH (multiplex fluorescence in situ hybridisation) probes.

WRN was knocked out using CRISPR-Cas9 as described above. Puromycin selection (2 µg/mL) was initiated 48h after transduction, and cells were harvested for metaphases 96h after transduction from control and WRN knockout cell lines followed a standard protocol with modifications. Briefly, cells growing in T150 flasks were treated with colcemid (KaryoMaxTM ColcemidTM Solution in PBS, 10 g/mL, ThermoFisher Scientific), to a final concentration of 0.1 g/mL for 1.5h. TrypLE Express Enzyme (ThermoFisher Scientific) was used to dissociate adherent cells to obtain a single cell suspension, which was pelleted down and resuspened in a hypotonic solution (0.56% KCl in H2O) for 12 -14 minutes and subsequently fixed with Carnoy's fixative, 3:1 (v/v) methanol: acetic acid. FISH analysis was performed as previously reported (65). Metaphase slides were prepared and fixed in acetone (Sigma Aldrich) for 10 min followed by baking at 62°C for 30 min. Denaturation of metaphase spreads was carried out by immersing slides in an alkaline denaturation solution (0.5 M NaOH,1.0 M NaCl) for 7 1⁄2 - 8 minutes followed by two subsequent washes in 1 M Tris-HCl (pH 7.4) and 1×PBS, 4 min each. Slides were dehydrated in a 70%, 90% and 100% ethanol series. The probe mix (24 colour human M-FISH paint) was denatured at 65°C for 10 min before applying onto the denatured slide. Hybridisation was carried out at 37°C for two nights. Post hybridisation steps included a 30 min (approx.) wash in 2×SSC at 37°C, to remove coverslips, followed by a 5 min stringent wash in 0.5×SSC at 75°C, a 5 min rinse in 2×SSC containing (0.05% Tween-20 (VWR) and another 5 min rinse in 1×PBS, both at room temperature. Slides were finally mounted in Vectashield® VibranceTM Antifade Mounting medium with DAPI (4', 6-diamidino-2-phenylindole), Vector Laboratories. Metaphases were imaged using AxioImager D1 microscope equipped with appropriate narrow-band pass filters for DAPI, Aqua, FITC, Cy3, Texas Red and Cy5 fluorescence. Digital images were captured using the SmartCapture software (Digital Scientific, UK) and 20 randomly selected metaphase cells were karyotyped and analysed with particular interest in chromatid and chromosome breaks including complex rearrangements based on Multiplex FISH and DAPI banding pattern using the SmartType Karyotyper (Digital Scientific, UK).

Organoid and T cell co-culture

Peripheral blood mononuclear cells (PBMCs) and tumor organoids were generated and co-cultured as previously described (39,40). Briefly, PBMCs were isolated from peripheral blood using Ficoll–Paque and cryopreserved for later use. For patient CRC-14, blood was drawn before the first cycle of nivolumab. Culture media for PBMCs was composed of RPMI 1640 (GIBCO), supplemented with 2 mM Ultraglutamine I, 1:100 penicillin/streptomycin and 10% male human AB serum (Sigma-Aldrich; cat. no. H3667) (''T cell medium''). One day before co-culture, PBMCs were thawed in pre-warmed (37°C) T cell medium (human serum was replaced with FCS during thawing) and incubated for 15 min with 25 U/mL benzonase (Merck; cat. no. 70746-3) at 37C. After washing, cells were resuspended at 2-3 x 10^6 cells/mL in T cell medium supplemented with 150 U/mL IL-2 and cultured overnight at 37C. 48 hours prior to co-culture, tumor organoids were isolated from Geltrex by incubation with 2 mg/mL dispase II and cultured in CRC medium. Prior to co-culture, tumor organoids (isolated from Geltrex) were stimulated for 24 hours with 200 ng/mL human recombinant IFNγ (Peprotech; cat. no. 300-02). 96-well U-bottom plates were coated with 5 µg/mL anti-CD28 (clone CD28.2, eBioscience; cat. no. 16-0289-81) and kept overnight at 4C. The next day, tumor organoids were dissociated to single cells with TrypLE Express and resuspended in T cell medium. Anti-CD28-coated plates were washed twice with PBS and PBMC were seeded at a density of 10^5 cells/well and stimulated with single cell dissociated organoids at a 20:1 effector:target ratio. Co-cultures were performed in the presence of 150 U/mL IL-2 and 20 µg/mL anti-PD-1-blocking antibody (kindly donated by Merus, Utrecht; cat. no. 5C4). Half of the medium, including IL-2 and anti-PD-1, was refreshed two to three times per week. Every week, PBMCs were collected, counted, and replated at 10^5 cells/well, and re-stimulated with fresh tumor organoids, for a total of 2 weeks co-culture.

Tumor recognition assay, killing assay, and generation of organoids resistant to autologous reactive T cells

For evaluation of tumor reactivity, 10^5 PBMCs were restimulated with tumor organoids (isolated from Geltrex and stimulated with IFNγ, as described before) at a 2:1 effector: target ratio and seeded in anti-CD28-coated plates in the presence of 20 µg/mL anti-

PD-1 and co- cultured for 5 hours for IFNγ evaluation. Golgi-Plug (1:1000, BD; cat. no. 555029) and Golgi- Stop (1:1500, BD, cat. no. 554724) was added after 1 hour and co-culture continued for an additional 4 hours. Cells were washed twice in FACS buffer and stained with the following antibodies: anti-CD3-PerCP-Cy5.5 (BD; cat. no. 332771), anti-CD4-FITC (BD; cat. no. 555346), anti-CD8-BV421 (BD; cat. no. 562429), and near-IR viability dye (Life technologies) for 30 min at 4°C in the dark. Cells were washed twice in FACS buffer, fixed using the Cytofix/Cytoperm kit (BD, according to manufacturer's instructions), and stained for intracellular IFNγ (anti-IFNγ-APC, BD; cat. no. 554702). PBMCs stimulated with 50 ng/mL phorbol 12-myristate 13-acetate (PMA, Sigma-Aldrich; cat. no. 19-144) and 1 mg/mL ionomycin (Sigma-Aldrich; cat. no. I9657) served as positive controls and PBMCs cultured without tumor stimulation as negative controls. Cells were then washed twice with FACS buffer and recorded at a Becton Dickinson Fortessa or LSRII flow cytometer.

For CD137 expression evaluation, 10^5 PBMCs were restimulated with tumor organoids (isolated from geltrex and stimulated with IFNγ, as described before) at a 2:1 effector: target ratio and seeded in anti-CD28-coated plates in the presence of 20 µg/mL anti-PD-1 and co- cultured for 24 hours. Cells were washed twice in FACS buffer and stained with the following antibodies: anti-CD3-PerCP-Cy5.5 (BD), anti-CD4-FITC (BD), anti-CD8-BV421 (BD), anti- CD137-APC (BD; cat. no. 550890) and near-IR viability dye (Life technologies) for 30 min at 4C in the dark. PBMCs stimulated with 50 ng/mL phorbol 12-myristate 13-acetate (PMA, Sigma-Aldrich) and 1 µg/mL ionomycin (Sigma-Aldrich) served as positive controls and PBMCs cultured without tumor stimulation as negative controls. Cells were then washed twice with FACS buffer and recorded with a Becton Dickinson Fortessa or LSRII flow cytometer.

To determine the sensitivity of tumor organoids to T cell-mediated killing, flat- bottom non-tissue culture-treated plates were coated with 5 mg/mL anti-CD28 and kept at 4°C overnight prior to co-culture. Tumor organoids were previously transduced with luciferase reporter gene. Organoids were isolated from Geltrex 48 hours prior to co-culture and stimulated with 200 ng/mL IFNγ for 24 hours prior to co-culture. The next day, part of the organoids were dissociated to single cells and counted using a hemocytometer. This was used to infer the number of tumor cells per tumor organoid to allow coculture of organoids and T cells at a 5:1 effector:target ratio. Next, tumor organoids were resuspended in the T cell medium. T cells were collected after two weeks of co-culture

with tumor organoids and resuspended in the T cell medium. Anti-CD28-coated plates were washed twice with PBS and 1 x 10^4 organoids were seeded for 72 hours in triplicate without T cells or with 5 x 10^4autologous T cells obtained by two weeks of organoid co-culture. To block MHC class I and II, organoids were pre-incubated for 30 min with 50 µg/mL pan-MHC-I blocking antibody W6/32, or pan-MHC-II blocking antibody T39 (blocking antibody remained present throughout the co-culture; BD; cat no. 555556). At the end of the 72 hours, tumor cells viability in the different conditions was measured by luciferase reporter assay using 3 µg/mL luciferin (Promega; cat. no. E1605). Luminescence was measured with a Tecan reader (1000 ms exposure).

Flow cytometry

For evaluation of MHC-I, tumor organoids were dissociated to single cells using TrypLE Express, with or without overnight pre-incubation with 200 ng/mL IFNγ. Tumor cells were washed in FACS buffer (PBS, 5 mM EDTA, 1% bovine serum antigen) and stained with mouse anti-human HLA-A,B,C-PE (BD Bioscience; cat. no. 555553), or isotype controls (PE mouse IgG1, kappa (BD Bioscience; cat. No 556650) for 30 min at 4C. Cells were washed twice with FACS buffer and DAPI was added to exclude dead cells prior to recording at a Becton Dickinson Fortessa or LSRII flow cytometer.

AUTHORS CONTRIBUTIONS

Conception and design: Gabriele Picco, Mathew J. Garnett, Alberto Bardelli, Emile Voest

Development of methodology: Gabriele Picco, Chiara Cattaneo, Krijn Dijkstra, Sarah Consonni, Sabrina Arena, Federica di Nicolantonio, Daniele Oddo, Ruby Banerjee.

Acquisition of data (provided animals, acquired and managed patients, provided facilities, etc.): Gabriele Picco, Chiara Cattaneo, Esmée van Vliet, Carlotta Cancelliere, Sara Vieira, Krijn Dijkstra, Iñigo Sánchez Rodríguez , Ruby Banerjee, Luuk Schipper, Andrea Sartore Bianchi, Salvatore Siena, Federica di Nicolantonio, Fengtang Yang, Martin Michaelis, Jindrich Cinatl.

Analysis and interpretation of data (e.g., statistical analysis, biostatistics, computational analysis): Gabriele Picco, Chiara Cattaneo, Esmée van Vliet, Giovanni Crisafulli, Giuseppe Rospo, Krijn Dijkstra, Inigo Matteo, Daniele Oddo, Sara Consonni, Ruby Banerjee, Luuk Schipper, Fengtang Yang.

Writing, review, and/or revision of the manuscript: Gabriele Picco, Mathew J. Garnett, Chiara Cattaneo, Esmée van Vliet, Alberto Bardelli, Emile Voest, Sabrina Arena, Federica di Nicolantonio, Krijn Dijkstra.

COMPETING INTERESTS

M.J.G. receives research funding from GlaxoSmithKline. A.B. is an advisory board member for Roche, Biocartis, Third Rock, Neophore, Phoremost, Illumina and Horizon Discovery. S.A. acted as consultant for MSD Italia. The other authors declare no potential conflicts of interest.

ACKNOWLEDGMENTS

We thank the Garnett laboratory, Cellular Genetics and Phenotyping facility, and drug screening teams at the Sanger Institute for data generation and assistance. We thank Annalisa Lorenzato (University of Torino) for technical help with sequenom analysis, Pamela Arcella (University of Torino) and Monica Montone (Candiolo Cancer Institute, FPO–IRCCS) for preclinical models establishment. We thank Michael Linnebacher (university of rostock, Germany) for providing the HROC cell models. The M.J.G. laboratory is supported by SU2C (SU2C-AACR-DT1213) and Wellcome Trust (206194). The research leading to these results has received funding from FONDAZIONE AIRC under 5 per Mille 2018 - ID. 21091 program – P.I. (A.B., F.D.N. and S.S.), AIRC under MFAG 2017 -ID 20236 (S.A.), European Community's Seventh Framework Programme under grant agreement no. 602901 MErCuRIC (A.B.); H2020 grant agreement no. 635342-2 MoTriColor (A.B.); AIRC IG 2018 - ID. 21923 project (A.B.), AIRC IG n. 17707 and IG n. 21407 (F.D.N.), Therapy in Colorectal Cancer Ministero della Salute, Project n. NET 02352137 (A.S.B., A.B., F.D.N. and S.S.). TRANSCAN-2 JTC 2014 contract no. TRS-2015-00000060 INTRACOLOR (S.A.); FPRC 5xmille 2017 Ministero Salute PTCRC-Intra 2020 (REGENERATION-YIG 2020 project) (S.A.); AIRC-CRUK-FC AECC Accelerator Award contract 22795 (A.B.); Fondazione Piemontese per la Ricerca sul Cancro-ONLUS 5 per mille 2015 Ministero della Salute (A.B. and F.D.N.); Ministero Salute, RC 2019 (A.B. and F.D.N.); Ministero Salute, RC 2019 (A.B. and F.D.N.). Hilfe für krebskranke Kinder Frankfurt e.V., Frankfurter Stiftung für krebskranke Kinder (J.C.). Kent Cancer Trust (M.M.). We thank Kong Xiangjun (Daniel Peeper lab) for providing the B2m-KO virus; and Catrin Lutz (Jos Jonkers lab) for providing the luciferase virus. We thank Arno Velds (NKI) and Shriram Bhosle (Sanger Institute) for bioinformatic support. We thank Matthew Coelho, Hayley Fracies for their helpful advice. We thank Cibele Sotero-Caio and Kirsy Roberts (Sanger Institute) for technical help with karyotyping and PCR analysis.

REFERENCES

1. Latham A, Srinivasan P, Kemel Y, Shia J, Bandlamudi C, Mandelker D, et al. Microsatellite Instability Is Associated With the Presence of Lynch Syndrome Pan- Cancer. J Clin Oncol. 2019;37:286–95.
2. Vilar E, Gruber SB. Microsatellite instability in colorectal cancer-the stable evidence. Nat Rev Clin Oncol. 2010;7:153–62.
3. Xie Y-H, Chen Y-X, Fang J-Y. Comprehensive review of targeted therapy for colorectal cancer. Signal Transduct Target Ther. 2020;5:22.
4. Amirouchene-Angelozzi N, Swanton C, Bardelli A. Tumor Evolution as a Therapeutic Target. Cancer Discov [Internet]. 2017; Available from: http://dx.doi.org/10.1158/2159-8290.CD-17-0343
5. Misale S, Yaeger R, Hobor S, Scala E, Janakiraman M, Liska D, et al. Emergence of KRAS mutations and acquired resistance to anti-EGFR therapy in colorectal cancer. Nature. 2012;486:532–6.
6. Misale S, Di Nicolantonio F, Sartore-Bianchi A, Siena S, Bardelli A. Resistance to anti- EGFR therapy in colorectal cancer: from heterogeneity to convergent evolution. Cancer Discov. 2014;4:1269–80.
7. Prahallad A, Sun C, Huang S, Di Nicolantonio F, Salazar R, Zecchin D, et al. Unresponsiveness of colon cancer to BRAF(V600E) inhibition through feedback activation of EGFR. Nature. 2012;483:100–3.
8. Corcoran RB, Ebi H, Turke AB, Coffee EM, Nishino M, Cogdill AP, et al. EGFR- mediated re-activation of MAPK signaling contributes to insensitivity of BRAF mutant colorectal cancers to RAF inhibition with vemurafenib. Cancer Discov. 2012;2:227–35.
9. Kopetz S, Grothey A, Yaeger R, Van Cutsem E, Desai J, Yoshino T, et al. Encorafenib, Binimetinib, and Cetuximab in BRAF V600E-Mutated Colorectal Cancer. N Engl J Med. 2019;381:1632–43.
10. Corcoran RB, André T, Atreya CE, Schellens JHM, Yoshino T, Bendell JC, et al. Combined BRAF, EGFR, and MEK Inhibition in Patients with BRAFV600E-Mutant Colorectal Cancer. Cancer Discov. 2018;8:428–43.
11. Oddo D, Sennott EM, Barault L, Valtorta E, Arena S, Cassingena A, et al. Molecular Landscape of Acquired Resistance to Targeted Therapy Combinations in BRAF-Mutant Colorectal Cancer. Cancer Res. 2016;76:4504–15.
12. Hazar-Rethinam M, Kleyman M, Han GC, Liu D, Ahronian LG, Shahzade HA, et al. Convergent Therapeutic Strategies to Overcome the Heterogeneity of Acquired Resistance in BRAFV600E Colorectal Cancer. Cancer Discov. 2018;8:417–27.

13. Pietrantonio F, Oddo D, Gloghini A, Valtorta E, Berenato R, Barault L, et al. MET-Driven Resistance to Dual EGFR and BRAF Blockade May Be Overcome by Switching from EGFR to MET Inhibition in BRAF-Mutated Colorectal Cancer. Cancer Discov. 2016;6:963–71.

14. Pietrantonio F, Di Nicolantonio F, Schrock AB, Lee J, Tejpar S, Sartore-Bianchi A, et al. ALK, ROS1, and NTRK Rearrangements in Metastatic Colorectal Cancer. J Natl Cancer

15. Cocco E, Benhamida J, Middha S, Zehir A, Mullaney K, Shia J, et al. Colorectal Carcinomas Containing Hypermethylated MLH1 Promoter and Wild-Type BRAF/KRAS Are Enriched for Targetable Kinase Fusions. Cancer Res. 2019;79:1047–53.

16. Drilon A, Laetsch TW, Kummar S, DuBois SG, Lassen UN, Demetri GD, et al. Efficacy of Larotrectinib in TRK Fusion-Positive Cancers in Adults and Children. N Engl J Med. 2018;378:731–9.

17. Cocco E, Schram AM, Kulick A, Misale S, Won HH, Yaeger R, et al. Resistance to TRK inhibition mediated by convergent MAPK pathway activation. Nat Med. 2019;25:1422–7.

18. Russo M, Misale S, Wei G, Siravegna G, Crisafulli G, Lazzari L, et al. Acquired Resistance to the TRK Inhibitor Entrectinib in Colorectal Cancer. Cancer Discov. 2016;6:36–44.

19. Misale S, Arena S, Lamba S, Siravegna G, Lallo A, Hobor S, et al. Blockade of EGFR and MEK intercepts heterogeneous mechanisms of acquired resistance to anti-EGFR therapies in colorectal cancer. Sci Transl Med. 2014;6:224ra26.

20. Le DT, Uram JN, Wang H, Bartlett BR, Kemberling H, Eyring AD, et al. PD-1 Blockade in Tumors with Mismatch-Repair Deficiency. N Engl J Med. 2015;372:2509–20.

21. Le DT, Durham JN, Smith KN, Wang H, Bartlett BR, Aulakh LK, et al. Mismatch repair deficiency predicts response of solid tumors to PD-1 blockade. Science. 2017;357:409– 13.

22. Overman MJ, Lonardi S, Wong KYM, Lenz H-J, Gelsomino F, Aglietta M, et al. Durable Clinical Benefit With Nivolumab Plus Ipilimumab in DNA Mismatch Repair- Deficient/ Microsatellite Instability-High Metastatic Colorectal Cancer. J Clin Oncol. 2018;36:773–9.

23. Le DT, Kim TW, Van Cutsem E, Geva R, Jäger D, Hara H, et al. Phase II Open-Label Study of Pembrolizumab in Treatment-Refractory, Microsatellite Instability- High/Mismatch Repair-Deficient Metastatic Colorectal Cancer: KEYNOTE-164. J Clin Oncol. 2019;JCO1902107.

24. Gurjao C, Liu D, Hofree M, AlDubayan SH, Wakiro I, Su M-J, et al. Intrinsic Resistance to Immune Checkpoint Blockade in a Mismatch Repair-Deficient Colorectal Cancer. Cancer Immunol Res. 2019;7:1230–6.

25. Mandal R, Samstein RM, Lee K-W, Havel JJ, Wang H, Krishna C, et al. Genetic diversity of tumors with mismatch repair deficiency influences anti-PD-1 immunotherapy response. Science. 2019;364:485–91.

26. Hu ZI, Hellmann MD, Wolchok JD, Vyas M, Shia J, Stadler ZK, et al. Acquired resistance to immunotherapy in MMR-D pancreatic cancer. J Immunother Cancer. 2018;6:127.

27. Sahin IH, Akce M, Alese O, Shaib W, Lesinski GB, El-Rayes B, et al. Immune checkpoint inhibitors for the treatment of MSI-H/MMR-D colorectal cancer and a perspective on resistance mechanisms. Br J Cancer. 2019;121:809–18.

28. Behan FM, Iorio F, Gonçalves E, Picco G, Beaver CM, Santos R, et al. Prioritisation of oncology therapeutic targets using CRISPR-Cas9 screening [Internet]. bioRxiv. 2018

29. Chan EM, Shibue T, McFarland JM, Gaeta B, Ghandi M, Dumont N, et al. WRN helicase is a synthetic lethal target in microsatellite unstable cancers. Nature. 2019;568:551–6.

30. Lieb S, Blaha-Ostermann S, Kamper E, Rippka J, Schwarz C, Ehrenhöfer-Wölfer K, et al. Werner syndrome helicase is a selective vulnerability of microsatellite instability-high tumor cells. Elife [Internet]. 2019;8. Available from: http://dx.doi.org/10.7554/eLife.43333

31. Kategaya L, Perumal SK, Hager JH, Belmont LD. Werner Syndrome Helicase Is Required for the Survival of Cancer Cells with Microsatellite Instability. iScience. 2019;13:488–97.

32. Brosh RM Jr. DNA helicases involved in DNA repair and their roles in cancer. Nat Rev Cancer. 2013;13:542–58.

33. Chu WK, Hickson ID. RecQ helicases: multifunctional genome caretakers. Nat Rev Cancer. 2009;9:644–54.

34. van Wietmarschen N, Sridharan S, Nathan WJ, Tubbs A, Chan EM, Callen E, et al. Repeat expansions confer WRN dependence in microsatellite-unstable cancers. Nature [Internet]. 2020; Available from: http://dx.doi.org/10.1038/s41586-020-2769-8

35. Medico E, Russo M, Picco G, Cancelliere C, Valtorta E, Corti G, et al. The molecular landscape of colorectal cancer cell lines unveils clinically actionable kinase targets. Nat Commun. 2015;6:7002.

36. Picco G, Petti C, Centonze A, Torchiaro E, Crisafulli G, Novara L, et al. Loss of AXIN1 drives acquired resistance to WNT pathway blockade in colorectal cancer cells carrying RSPO3 fusions. EMBO Mol Med. 2017;9:293–303.

37. Lazzari L, Corti G, Picco G, Isella C, Montone M, Arcella P, et al. Patient-Derived Xenografts and Matched Cell Lines Identify Pharmacogenomic Vulnerabilities in Colorectal Cancer. Clin Cancer Res. 2019;25:6243–59.

38. Arena S, Bellosillo B, Siravegna G, Martínez A, Cañadas I, Lazzari L, et al. Emergence of Multiple EGFR Extracellular Mutations during Cetuximab Treatment in Colorectal Cancer. Clin Cancer Res. 2015;21:2157–66.

39. Dijkstra KK, Cattaneo CM, Weeber F, Chalabi M, van de Haar J, Fanchi LF, et al. Generation of Tumor-Reactive T Cells by Co-culture of Peripheral Blood Lymphocytes and Tumor Organoids. Cell. 2018;174:1586–98.e12.

40. Cattaneo CM, Dijkstra KK, Fanchi LF, Kelderman S, Kaing S, van Rooij N, et al. Tumor organoid-T-cell coculture systems. Nat Protoc. 2020;15:15–39.

41. Schoenfeld AJ, Hellmann MD. Acquired Resistance to Immune Checkpoint Inhibitors. Cancer Cell. 2020;37:443–55.

42. Schrock AB, Ouyang C, Sandhu J, Sokol E, Jin D, Ross JS, et al. Tumor mutational burden is predictive of response to immune checkpoint inhibitors in MSI-high metastatic colorectal cancer. Ann Oncol. 2019;30:1096–103.

43. Germano G, Lamba S, Rospo G, Barault L, Magrì A, Maione F, et al. Inactivation of DNA repair triggers neoantigen generation and impairs tumour growth. Nature.

44. Langer CJ, Gadgeel SM, Borghaei H, Papadimitrakopoulou VA, Patnaik A, Powell SF, et al. Carboplatin and pemetrexed with or without pembrolizumab for advanced, non- squamous non-small-cell lung cancer: a randomised, phase 2 cohort of the open-label KEYNOTE-021 study. Lancet Oncol. 2016;17:1497–508.

45. Rosenthal R, Cadieux EL, Salgado R, Bakir MA, Moore DA, Hiley CT, et al. Neoantigen-directed immune escape in lung cancer evolution. Nature. 2019;567:479–85.

46. Aggarwal M, Sommers JA, Shoemaker RH, Brosh RM Jr. Inhibition of helicase activity by a small molecule impairs Werner syndrome helicase (WRN) function in the cellular response to DNA damage or replication stress. Proc Natl Acad Sci U S A. 2011;108:1525–30.

47. Aggarwal M, Banerjee T, Sommers JA, Iannascoli C, Pichierri P, Shoemaker RH, et al. Werner syndrome helicase has a critical role in DNA damage responses in the absence of a functional fanconi anemia pathway. Cancer Res. 2013;73:5497–507.

48. Bou-Hanna C, Jarry A, Lode L, Schmitz I, Schulze-Osthoff K, Kury S, et al. Acute cytotoxicity of MIRA-1/NSC19630, a mutant p53-reactivating small molecule, against human normal and cancer cells via a caspase-9-dependent apoptosis. Cancer Lett. 2015;359:211–7.

49. van der Meer D, Barthorpe S, Yang W, Lightfoot H, Hall C, Gilbert J, et al. Cell Model Passports-a hub for clinical, genetic and functional datasets of preclinical cancer models. Nucleic Acids Res. 2019;47:D923–9.

50. Russo M, Lamba S, Lorenzato A, Sogari A, Corti G, Rospo G, et al. Reliance upon ancestral mutations is maintained in colorectal cancers that heterogeneously evolve during targeted therapies. Nat Commun. Nature Publishing Group; 2018;9:1–12.

51. Iorio F, Knijnenburg TA, Vis DJ, Bignell GR, Menden MP, Schubert M, et al. A Landscape of Pharmacogenomic Interactions in Cancer. Cell. 2016;166:740–54.

52. Garnett MJ, Edelman EJ, Heidorn SJ, Greenman CD, Dastur A, Lau KW, et al. Systematic identification of genomic markers of drug sensitivity in cancer cells. Nature. 2012;483:570–5.

53. Michaelis M, Wass MN, Cinatl J. Drug-adapted cancer cell lines as preclinical models of acquired resistance. Cancer Drug Resistance [Internet]. OAE; 2019; Available from: https://kar.kent.ac.uk/76175/1/3127.pdf

54. Michaelis M, Rothweiler F, Barth S, Cinatl J, van Rikxoort M, Löschmann N, et al. Adaptation of cancer cells from different entities to the MDM2 inhibitor nutlin-3 results in the emergence of p53-mutated multi-drug-resistant cancer cells. Cell Death Dis. 2011;2:e243.

55. Rospo G, Lorenzato A, Amirouchene-Angelozzi N, Magrì A, Cancelliere C, Corti G, et al. Evolving neoantigen profiles in colorectal cancers with DNA repair defects. Genome Med. 2019;11:42.

56. Corti G, Bartolini A, Crisafulli G, Novara L, Rospo G, Montone M, et al. A Genomic Analysis Workflow for Colorectal Cancer Precision Oncology. Clin Colorectal Cancer. 2019;18:91–101.e3.

57. Crisafulli G, Mussolin B, Cassingena A, Montone M, Bartolini A, Barault L, et al. Whole exome sequencing analysis of urine trans-renal tumour DNA in metastatic colorectal cancer patients. ESMO Open [Internet]. 2019;4. Available from: http://dx.doi.org/10.1136/esmoopen-2019-000572

58. Garcia-Alonso L, Iorio F, Matchan A, Fonseca N, Jaaks P, Peat G, et al. Transcription Factor Activities Enhance Markers of Drug Sensitivity in Cancer. Cancer Res. 2018;78:769–80.

59. Roumeliotis TI, Williams SP, Gonçalves E, Alsinet C, Del Castillo Velasco-Herrera M, Aben N, et al. Genomic Determinants of Protein Abundance Variation in Colorectal Cancer Cells. Cell Rep. 2017;20:2201–14.

60. Nusinow DP, Szpyt J, Ghandi M, Rose CM, McDonald ER 3rd, Kalocsay M, et al. Quantitative Proteomics of the Cancer Cell Line Encyclopedia. Cell. 2020;180:387– 402.e16.

61. Pacini C, Dempster JM, Gonçalves E, Najgebauer H, Karakoc E, van der Meer D, et al. Integrated cross-study datasets of genetic dependencies in cancer [Internet]. bioRxiv. 2020 [cited 2020 Jun 29]. page 2020.05.22.110247. Available from: https://www.biorxiv.org/content/10.1101/2020.05.22.110247v2

62. Li H. Aligning sequence reads, clone sequences and assembly contigs with BWA-MEM [Internet]. arXiv [q-bio.GN]. 2013. Available from: http://arxiv.org/abs/1303.3997

63. Hinrichs AS, Karolchik D, Baertsch R, Barber GP, Bejerano G, Clawson H, et al. The UCSC Genome Browser Database: update 2006. Nucleic Acids Res. 2006;34:D590–8.

64. Behan FM, Iorio F, Picco G, Gonçalves E, Beaver CM, Migliardi G, et al. Prioritization of cancer therapeutic targets using CRISPR-Cas9 screens. Nature. 2019;568:511–6.

65. Picco G, Chen ED, Alonso LG, Behan FM, Gonçalves E, Bignell G, et al. Functional linkage of gene fusions to cancer cell fitness assessed by pharmacological and CRISPR-Cas9 screening. Nat Commun. 2019;10:2198.

SUPPLEMENTARY MATERIAL

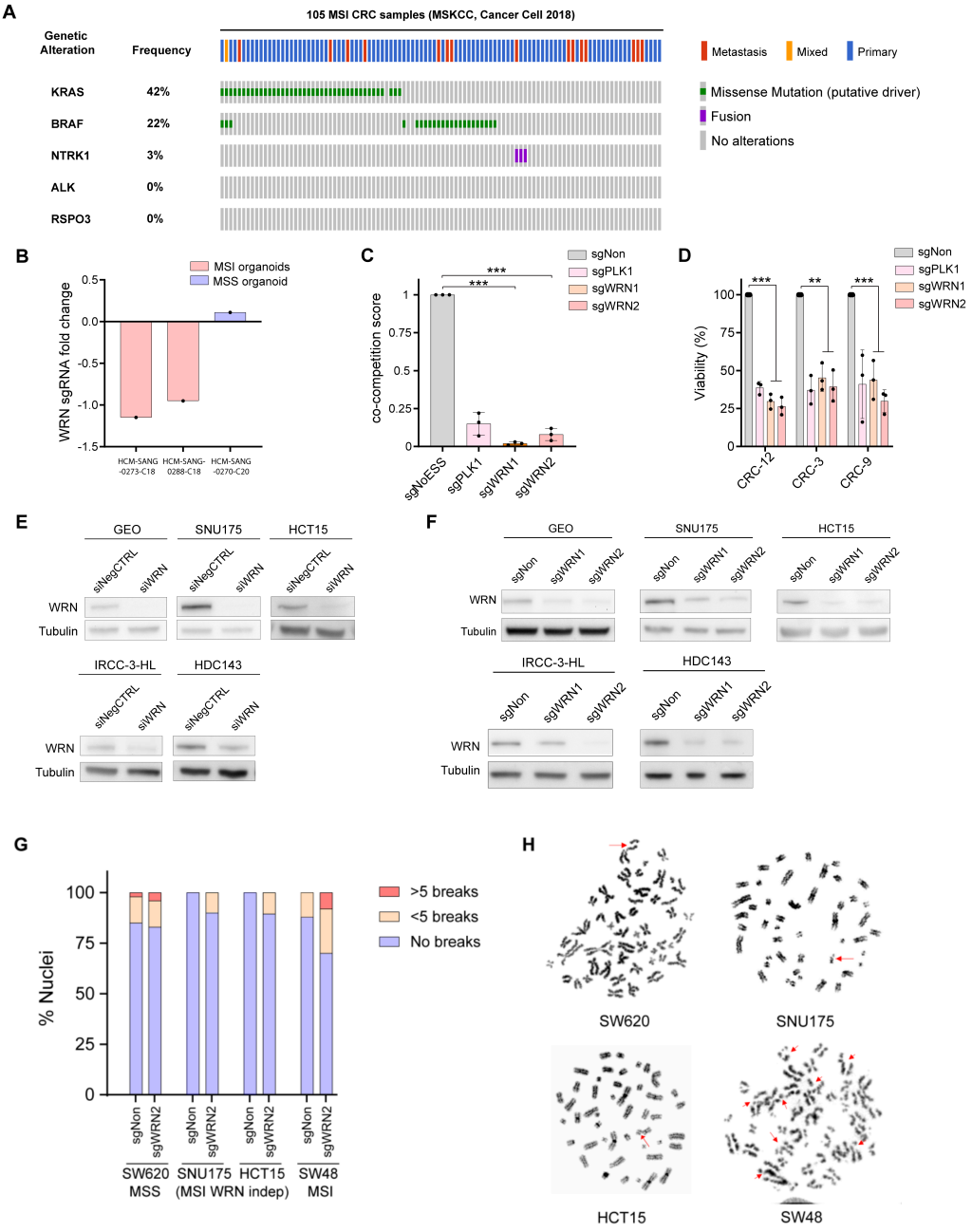

Supplementary Figure 1. WRN dependency validation experiments in dMMR CRC preclinical models. ***(previous page)***

A, Alterations of KRAS, BRAF, NTRK1, ALK and RSPO3 genes in 105 dMMR/MSI CRC samples (MSKCC, Cancer Cell 2018).

B, WRN essentiality values from whole- genome CRISPR-cas9 dropout screening in two dMMR (red bar) and one MMR-proficient (blue bar) CRC organoids. Fold changes are the average of three technical replicates.

C, Validation of WRN dependency in HCM-SANG-0273-C18 organoid by CRISPR-based co-competition assay. Data are mean ± SD of three independent experiments. A co-competition score of less than 1 indicates a relative reduction in BFP-positive cells, resulting from targeting of a loss-of-fitness gene.

D, Normalized viability in dMMR organoids upon transduction of WRN sgRNAs. Non-essential (sgNon) and PLK1 (sgPLK1) sgRNAs were used as negative and positive controls, respectively. Data represent the mean and SD of 3 independent experiments with 10 technical replicates each. Statistical significance was evaluated comparing WRN sgRNA versus non essential gene sgRNA (sgNon): ns, not significant; $P < 0.05$; $P < 0.01$; $P < 0.001$ (two-tailed Student't test).

E, siRNA-mediated depletion of WRN verified by Western blot (images are representative of two independent experiments). siRNA non-targeting controls (siNTC), siRNA targeting WRN (siWRN).

F, WRN knockout with WRN-targeting sgRNAs confirmed by Western blot (images are representative of two independent experiments).

G, Chromatid breaks in SW620 (MSS), SNU175 and HCT15 (MSI WRN independent) and SW48 (MSI WRN dependent) cell line 96h after WRN depletion (≥20 metaphase spreads analysed).

H, Representative images of metaphases affected by chromatid breaks (red arrows) after 96h of transduction with sgWRN2.

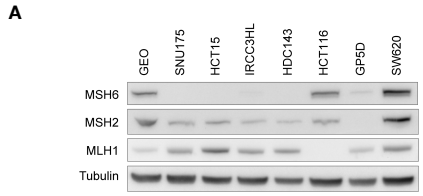
A
GEO
SNU175
HCT15
IRCC3HL
HDC143
HCT116
GP5D
SW620
MSH6
MSH2
MLH1
Tubulin

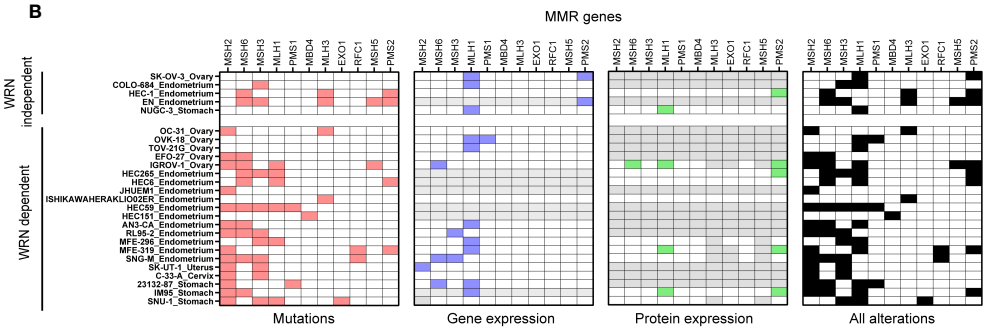
B
MMR genes
WRN independent
WRN dependent
Mutations
Gene expression
Protein expression
All alterations

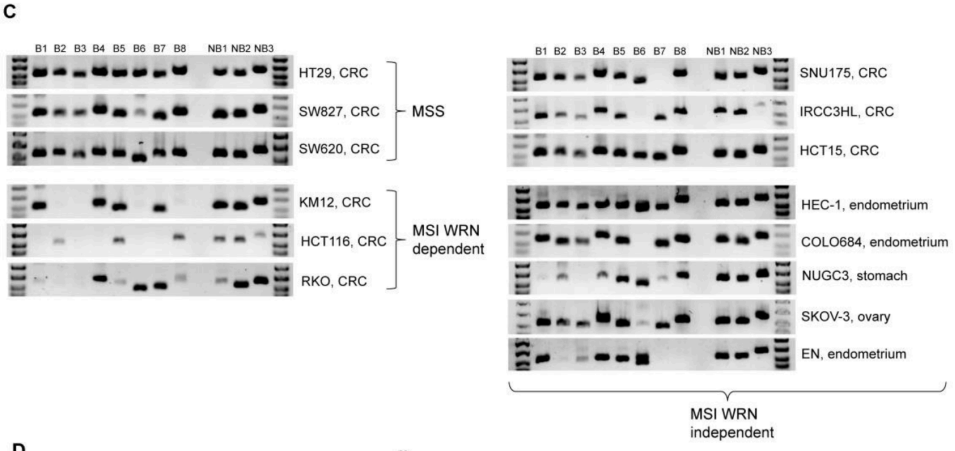
C
HT29, CRC
SW827, CRC
SW620, CRC
MSS
KM12, CRC
HCT116, CRC
RKO, CRC
MSI WRN dependent
SNU175, CRC
IRCC3HL, CRC
HCT15, CRC
HEC-1, endometrium
COLO684, endometrium
NUGC3, stomach
SKOV-3, ovary
EN, endometrium
MSI WRN independent

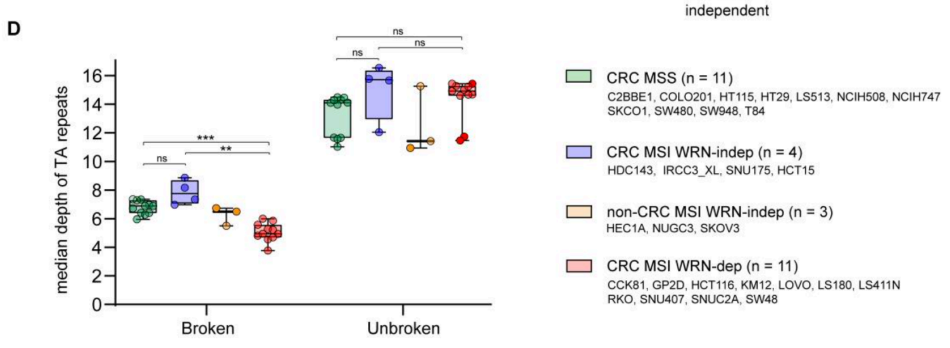
D
median depth of TA repeats
Broken
Unbroken
CRC MSS (n = 11)
C2BBE1, COLO201, HT115, HT29, LS513, NCIH508, NCIH747
SKCO1, SW480, SW948, T84
CRC MSI WRN-indep (n = 4)
HDC143, IRCC3_XL, SNU175, HCT15
non-CRC MSI WRN-indep (n = 3)
HEC1A, NUGC3, SKOV3
CRC MSI WRN-dep (n = 11)
CCK81, GP2D, HCT116, KM12, LOVO, LS180, LS411N
RKO, SNU407, SNUC2A, SW48

Supplementary Figure 2. Molecular and TA-repeats coverage analysis in MSI-H WRN independent cell lines. ***(previous page)***

A, Validation of MLH1, MSH2 and MSH6 protein expression measured by Western blot in a set of WRN independent MSI dMMR CRC cancer cell lines (images are representative of two independent experiments). SW620 (pMMR/MSS), HCT116 (MLH1 loss) and GP5D (MSH2 and MSH6 loss) were included as positive controls for protein expression.
B, Mutations, gene expression and protein expression alterations of MMR-pathway genes in cancer models from non-CRC dMMR/MSI-predominant lineages. Coloured (red, blue, green and light black) box indicates the presence of the alteration, light grey boxes represent data unavailable.
C, Agarose gels of PCR fragments (or lack thereof) at (TA)n repeats in CRC and non-CRC cell lines as indicated. B1–B8 sites were reported as recurrently broken after WRN downregulation in KM12 and HCT116 cells, NB1–NB3 regions did not display any breakage and are included as a negative control for expanded repeats. Data are representative of two independent experiments.
D, Box and whisker plots displaying the median sequencing depth of broken and not-broken (TA)-repeat loci in WGS data from MSS and MSI cancer cell lines, as indicated. For coverage analysis, WGS data were unavailable for IRCC3_HL and so we used WGS sequencing data for IRCC3-XL, which is a primary cell line derived from a patient-derived xenograft generated from the same biopsy as IRCC3_HL.

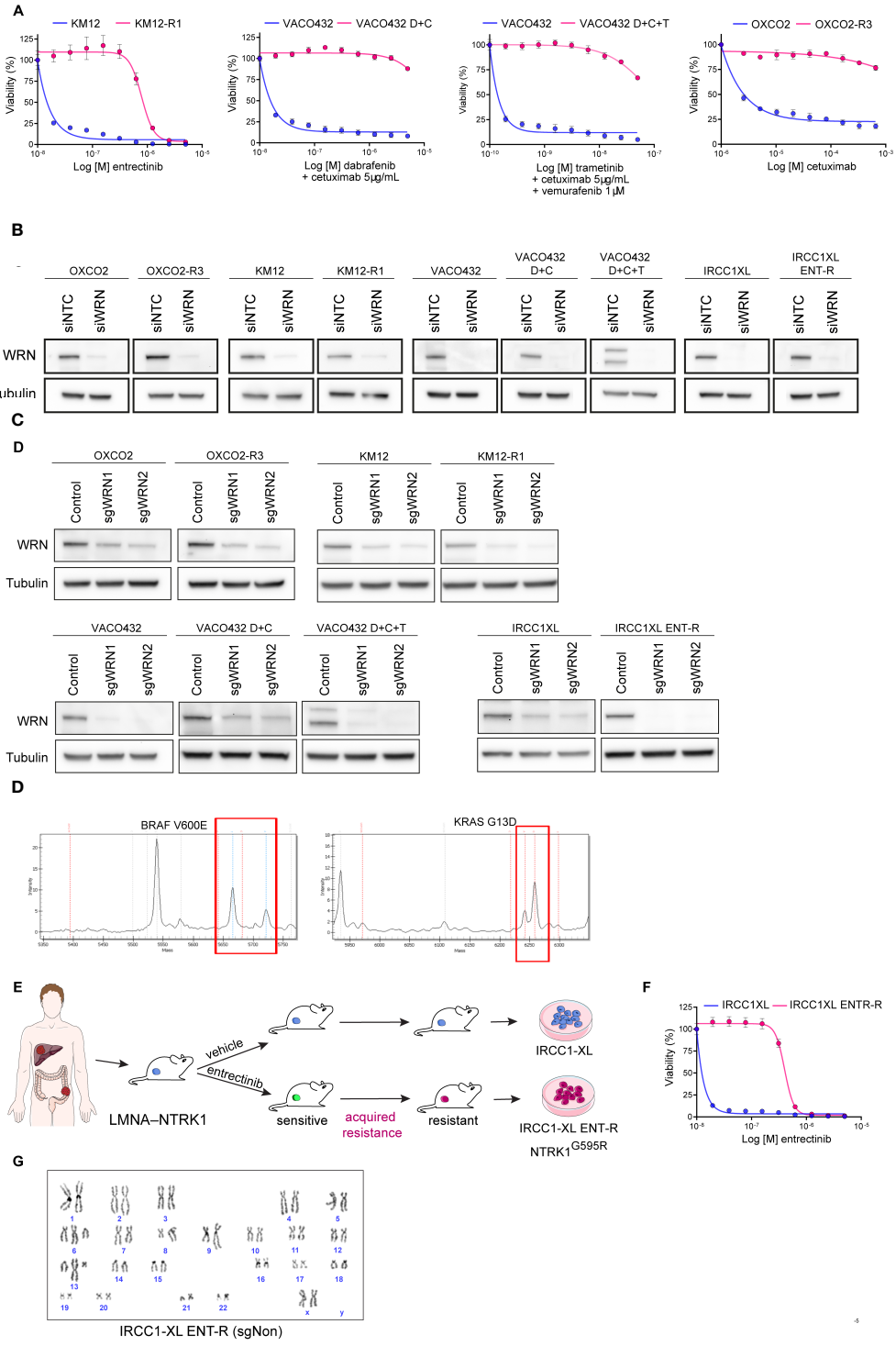
A
KM12
KM12-R1
Viability (%)
Log [M] entrectinib
VACO432
VACO432 D+C
Log [M] dabrafenib
+ cetuximab 5µg/mL
VACO432
VACO432 D+C+T
Log [M] trametinib
+ cetuximab 5µg/mL
+ vemurafenib 1 µM
OXCO2
OXCO2-R3
Log [M] cetuximab
B
OXCO2
OXCO2-R3
KM12
KM12-R1
VACO432
VACO432 D+C
VACO432 D+C+T
IRCC1XL
IRCC1XL ENT-R
siNTC
siWRN
WRN
Tubulin
C
D
Control
sgWRN1
sgWRN2
WRN
Tubulin
D
BRAF V600E
KRAS G13D
E
vehicle
entrectinib
LMNA–NTRK1
sensitive
acquired resistance
resistant
IRCC1-XL
IRCC1-XL ENT-R
NTRK1G595R
F
IRCC1XL
IRCC1XL ENTR-R
Viability (%)
Log [M] entrectinib
G
IRCC1-XL ENT-R (sgNon)

Supplementary Figure S3. Validation experiments in preclinical models of acquired resistance to targeted agents. (*previous page)*

A, Proliferation assays of cell line models of acquired resistance and parental counterparts in response to targeted therapies. Data are average ± SD of three technical replicates and are representative of three independent experiments.
B, siRNA-mediated depletion of WRN was verified by Western blot (images are representative of two independent experiments). siRNA non-targeting controls (siNTC), siRNA targeting WRN (siWRN). Tubulin is a loading control.
C, Reduction in WRN protein levels with two independent WRN-targeting sgRNAs confirmed by Western blot (images are representative of two independent experiments).
D, Sequenom sequencing spectrum of VACO432 C+D+T cell model revealing an acquired KRAS G13D mutation in addition to the BRAF V600E mutation shared with the parental counterpart.
E, Schematic representation of a patient-derived NTRK1-rearranged in vivo model of acquired resistance to entrectinib.
F, Proliferation assays of IRCC- 1-XL and IRCC1-XL-ENT-R cell lines treated with entrectinib. Data are average ± SD of three technical replicates and are representative of three independent experiments.
G, Representative images of IRCC-1-XL-ENT-R line after 96h from transduction with non-essential gene targeting sgRNA (sgNon). Metaphases were karyotyped based on DAPI-banding patterns and visualized by microscopy. No alterations were detected.

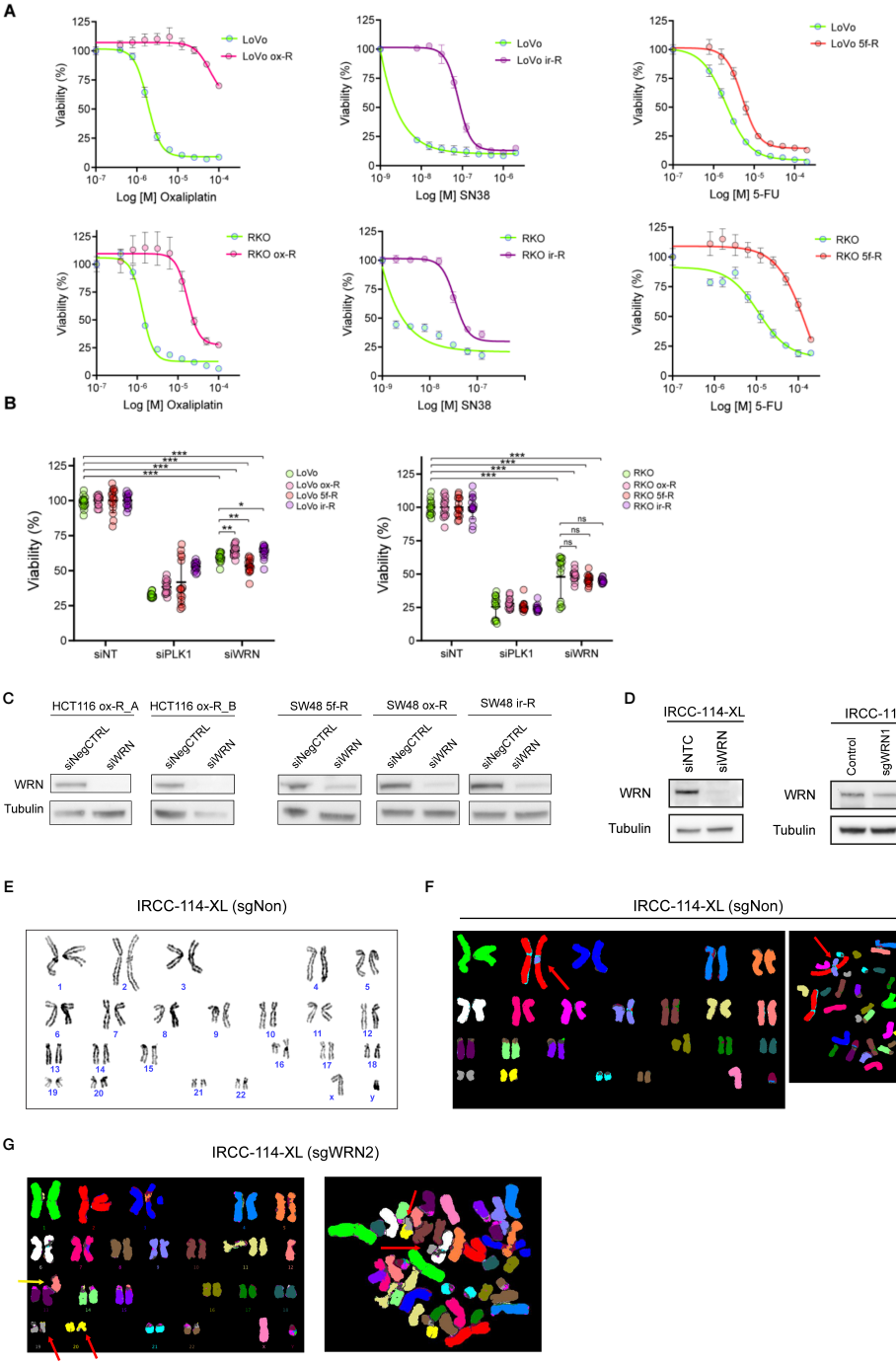
A
LoVo
LoVo ox-R
LoVo ir-R
LoVo 5f-R
RKO
RKO ox-R
RKO ir-R
RKO 5f-R
Viability (%)
Log [M] Oxaliplatin
Log [M] SN38
Log [M] 5-FU
B
siNT
siPLK1
siWRN
C
HCT116 ox-R_A
HCT116 ox-R_B
SW48 5f-R
SW48 ox-R
SW48 ir-R
siNegCTRL
siWRN
WRN
Tubulin
D
IRCC-114-XL
siNTC
siWRN
Control
sgWRN1
sgWRN2
E
IRCC-114-XL (sgNon)
F
IRCC-114-XL (sgNon)
G
IRCC-114-XL (sgWRN2)

Supplementary Figure S4. Validation experiments in chemotherapy resistant models and IRCC-114_XL cells following WRN depletion. ***(previous page)***

A, Proliferation assays in Lovo and RKO models of acquired resistance to chemotherapies and parental counterparts. Data are average ± SD of three technical replicates and are representative of three independent experiments.

B, Normalized viability of upon siRNA-mediated WRN depletion in LoVo and RKO chemotherapy-resistant sublines. Non-targeting siRNA (siNT) and siPLK1 were used as negative and positive controls, respectively. Data are mean and SD of 2 independent experiments with 4 technical replicates each. Statistical significance was evaluated using a Student's t-test: ns, not significant; ** P≤0.01 *** P≤0.001.

C-D, Reduction in WRN protein levels in HCT116 and SW48 sublines and IRCC-114-XL cells confirmed by Western blot after siRNA-mediated depletion of WRN (left) or with two WRN-targeting sgRNAs (right) (representative of two independent experiments).

E, Representative image of an IRCC-114-XL metaphase harvested 96h after transduction with non-targeting sgRNA (sgNon), karyotyped based on DAPI-banding patterns and visualized by microscopy. No chromosomal defects were detected.

F and G, Metaphases of IRCC- 114-XL cell line transduced with non-targeting sgRNA **(F)** and WRN-targeting sgRNA **(G).** Overlaps and complex rearrangements are indicated by red and yellow arrows, respectively. Metaphases have been imaged using SmartCapture and karyotyped using SmartType Karyotyper based on M-FISH and DAPI banding patterns.

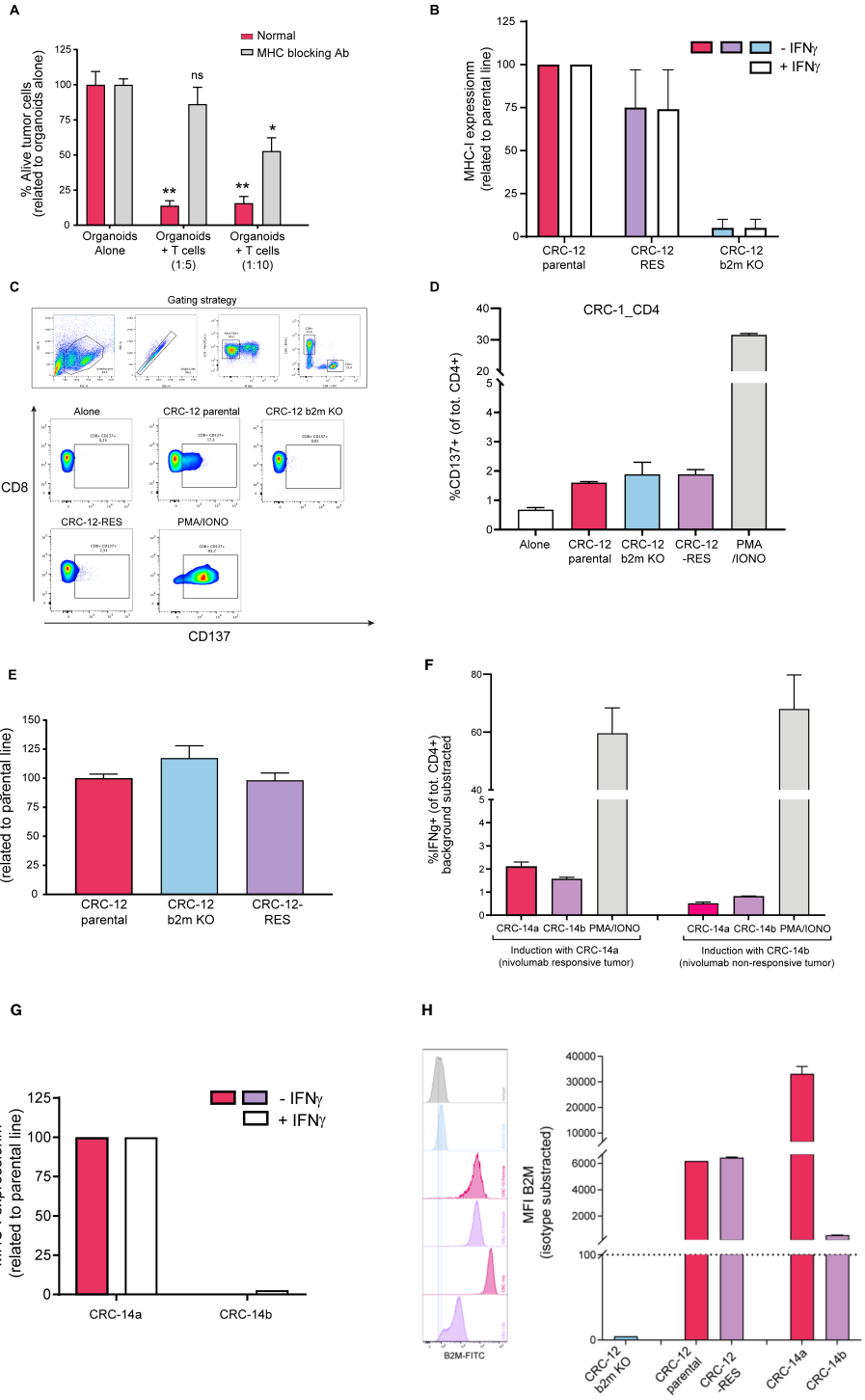
A
Normal
MHC blocking Ab
% Alive tumor cells (related to organoids alone)
ns
**
**
*
Organoids Alone
Organoids + T cells (1:5)
Organoids + T cells (1:10)
B
- IFNγ
+ IFNγ
MHC-I expressionm (related to parental line)
CRC-12 parental
CRC-12 RES
CRC-12 b2m KO
C
Gating strategy
Alone
CRC-12 parental
CRC-12 b2m KO
CRC-12-RES
PMA/IONO
CD8
CD137
D
CRC-1_CD4
%CD137+ (of tot. CD4+)
Alone
CRC-12 parental
CRC-12 b2m KO
CRC-12 -RES
PMA /IONO
E
MFI IFNg-R (related to parental line)
CRC-12 parental
CRC-12 b2m KO
CRC-12-RES
F
%IFNg+ (of tot. CD4+) background substracted
CRC-14a
CRC-14b
PMA/IONO
Induction with CRC-14a (nivolumab responsive tumor)
Induction with CRC-14b (nivolumab non-responsive tumor)
G
- IFNγ
+ IFNγ
MHC-I expressionm (related to parental line)
CRC-14a
CRC-14b
H
B2M-FITC
MFI B2M (isotype substracted)
CRC-12 b2m KO
CRC-12 parental
CRC-12 -RES
CRC-14a
CRC-14b

Supplementary Figure S5. Validation experiments in patient-derived dMMR/MSI tumor organoid- T cell co-culture system. ***(previous page)***

A, CRC-12 parental organoids viability upon T cell co-culture with luciferase reporter assay. Error bars represent the mean and SEM of at least two biological replicates. Significance was determined by two-tailed Student's t test. ns, not significant; ** P ≤0.01 and *** P≤0.001.
B, Cell surface MHC class I expression in CRC-12, CRC-12-RES and CRC-12-B2M knockout cells as determined by flow cytometry. Organoids were stimulated with 200 ng/mL IFNγ for 24 hr or were left unstimulated. Bar graphs indicate median fluorescence intensity (MFI) of anti-HLA-A, -B, and -C-PE minus MFI of isotype control, normalized to the parental line. Error bars represent SEM of at least two independent experiments.
C, Flow cytometry gating strategies and representative plots of CD8+ T cells tested for tumor reactivity after 2 weeks of co-culture with autologous CRC-12 organoids. T cells were re-stimulated with CRC-12 organoids and evaluated for cell surface staining of CD137. PMA/ionomycin stimulation was included as a positive control.
D, CD137 expression by CD4+ T cells obtained by 2- week co-culture with autologous CRC-12 tumor organoids, on stimulation with CRC-12 organoids. Bars represent the mean and SEM of two biologically independent experiments.
E, Cell surface IFNγ receptor expression of CRC-12, CRC-12-RES and CRC-12-B2M KO organoid lines as determined by flow cytometry. Error bars represent the mean and SEM of at least two biological replicates.
F, Quantification of IFNγ-positive CD4 T cells induced by 2-week co-culture of PBMCs with CRC-14a (responsive) or CRC-14b (non-responsive) organoids derived from the CRC-14 patient. T cells were re-stimulated with CRC-14a (left) or CRC-14b (right) organoids and evaluated for intracellular staining of IFNγ. Background IFNγ-positive cells (in unstimulated condition) were subtracted from the signal. Data represent the mean and SEM of at least 2 independent experiments.
G, Cell surface MHC class I expression in CRC-14a and CRC-14b determined by flow cytometry. Organoids were stimulated with 200 ng/mL IFNγ for 24 hr or were left unstimulated. Bar graphs indicate median fluorescence intensity (MFI) of anti-HLA-A, -B, and -C-PE minus MFI of isotype control, normalized to the parental line. Error bars represent SEM of at least two independent experiments.
H, Cell surface B2M expression of CRC- 12-B2M KO, CRC-12, CRC-12-RES, CRC-14a and, CRC-14b organoid lines as determined by flow cytometry. Error bars represent the mean and SEM of at least two biological replicates.

6

Identification of patient-specific T cell neoantigens through HLA-agnostic genetic screens

Cattaneo C.M.[1,2], Battaglia T.[1,2,*], Urbanus J.[1,2,*], Haanen J.[1,3], Voest E.E.[1,2,#], Schumacher T.N.[1,2,#], Scheper W.[1,#].

*,# These authors contributed equally

[1]Department of Molecular Oncology and Immunology, The Netherlands Cancer Institute, Antoni van Leeuwenhoek Hospital

[2]Oncode Institute

[3]Department of Medical Oncology, The Netherlands Cancer Institute, Antoni van Leeuwenhoek Hospital

Manuscript in revision, Nature Biotechnology

ABSTRACT

Cancer neoantigens that arise from tumor mutations are drivers of tumor-specific T cell responses, but identification of the T cell-recognized neoantigen repertoire of individual patients is complicated by their patient-specific nature. Here we develop the first genetic neoantigen discovery platform that allows identification of both $CD4^+$ and $CD8^+$ T cell-recognized neoantigens with high sensitivity and across complete HLA genotypes. This technology should facilitate the development of personalized neoantigen-based cancer immunotherapies.

INTRODUCTION

Cancer immunotherapies that aim to harness the anti-tumor activity of T cells, such as immune checkpoint blockade or adoptive transfer of tumor-reactive T cells, have shown impressive clinical results in a subset of cancer patients. Accumulating evidence suggests that the efficacy of these therapies is to a large extent driven by T cells that recognize cancer neoantigens – T cell antigens that arise as a result of patient-specific nonsynonymous tumor mutations [1]. Based on these data, a major effort has been initiated to develop approaches that can be used to specifically boost the activity of neoantigen-reactive T cells in individual patients. However, tumor mutations and their associated neoantigens are, with few exceptions, unique to individual cancer patients [2], underscoring the need for technologies that allow the comprehensive discovery of T cell-recognized neoantigens in a truly personalized fashion. Moreover, while the role of MHC class I-restricted $CD8^+$ T cells in anti-tumor immunity is well-established [3-5], recent data highlight important roles for MHC class II-restricted $CD4^+$ T cells in tumor control and response to immunotherapy, both through direct anti-tumor cytotoxicity and by boosting the activity of tumor-specific $CD8^+$ T cells [6-9]. Thus, experimental tools that enable the identification of both $CD4^+$ and $CD8^+$ T cell-recognized tumor antigens on a per-patient basis are required.

To date, the antigenic targets of T cells have mostly been identified through the use of fluorescently labelled peptide-MHC (pMHC) multimers [10,11], or functional assays that rely on coincubation of T cells and antigen-presenting cells (APC) modified to present candidate epitopes [12,13]. However, pMHC-based methods are limited by the fact that candidate antigenic peptides are selected using imperfect ***in silico*** predictions of peptide presentation on selected MHC alleles and by the fact that recombinant production has proven difficult for certain MHC alleles, and both these issues are particularly challenging for MHC class II-restricted antigens. Notably, in recent work a number of novel functional assays has been developed that rely on concepts developed in functional genomics, and in which APCs engineered to express large libraries of candidate T cell antigens are screened using T cell pools as a selective pressure [14-18]. While these approaches offer considerable throughput with respect to the antigen space that can be assayed, the methods developed to date rely on artificial APCs that are modified to express single

MHC (class I) alleles of choice. Given that any individual expresses up to twelve distinct MHC class I and II alleles, these methods are not straightforwardly compatible with the identification of T cell antigens across the complete MHC-I and -II haplotype of cancer patients. Thus, additional technologies are required to enable the unbiased, HLA-agnostic discovery of T cell antigens in individual patients.

Here, we present a high-throughput genetic platform for the personalized identification of $CD4^+$ and $CD8^+$ T cell-recognized (neo)antigens (Fig. 1A). In this method, which we term ***HANSolo*** (HLA-Agnostic Neoantigen Screening), patient-matched, Bcl-6/xL-immortalized B cell lines are engineered to express large libraries of minigenes that encode candidate T cell antigens. As the resulting B cells are fully MHC class I and class II proficient, this enables the unbiased screening of T cell specificities across the complete MHC class I and class II genotypes of individual patients. To this purpose, antigen library-expressing B cells are co-incubated with patient T cells (e.g. tumor-infiltrating lymphocytes (TIL), or T cells engineered to express patient-derived T cell receptors [19]) and antigen hits are identified by next-generation sequencing to measure the depletion of those B cells that express T cell-recognized epitopes.

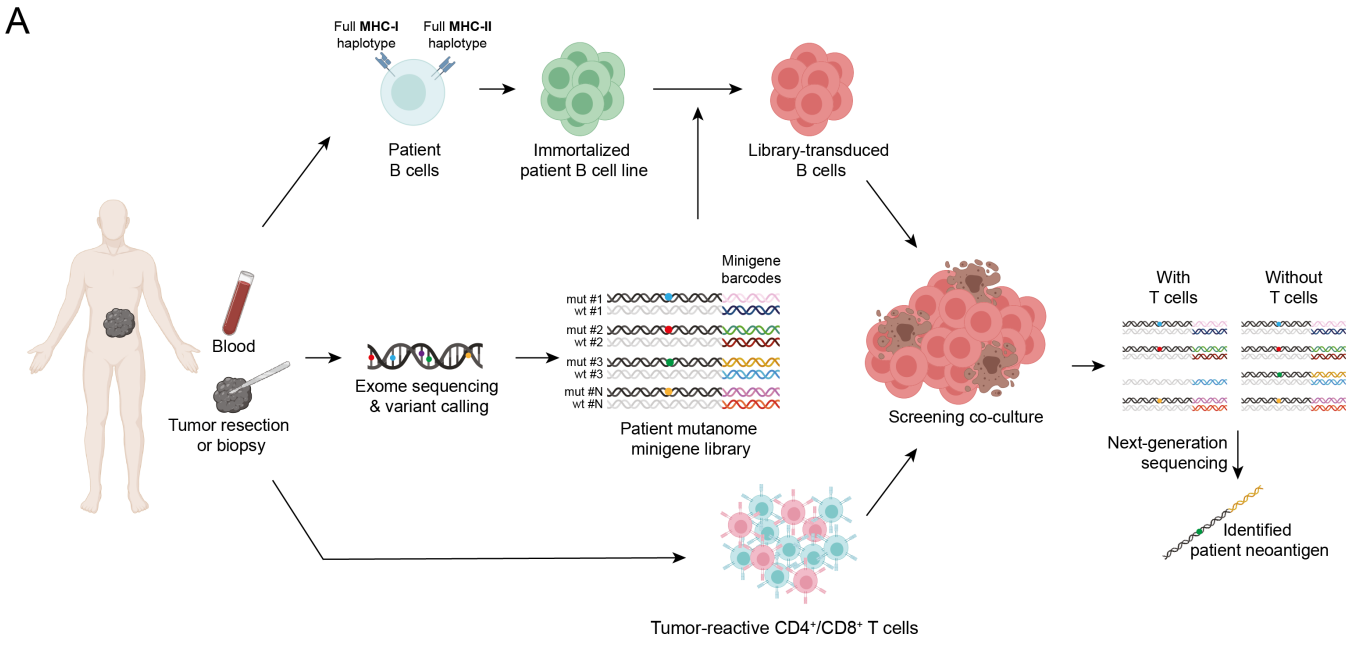

Figure 1 (part 1). Overview and validation of neoantigen discovery technology.

(A) Schematic overview of the methodology.

RESULTS

To first evaluate the feasibility and sensitivity of our method, we took advantage of two well-described HLA-A*02:01-restricted TCRs specific for either the $CDK4_{R24L}$ neoantigen (TCR #53) [20], or for the melanocyte differentiation antigen-derived $MART1_{26-35}$ epitope, a self antigen with low affinity for MHC (TCR 1D3) [21] (Supplementary Fig. 1). Activity of the $CDK4_{R24L}$ neoantigen-specific TCR should result in strong depletion of B cells expressing the mutant, but not the wild-type, CDK4 sequence. In addition, analysis of the activity of the $MART1_{26-35}$ self antigen-specific TCR should allow one to assess the sensitivity of the method in the context of weak T cell–target cell interactions. Furthermore, as a high affinity variant of the $MART1_{26-35}$ epitope has previously been identified (the $MART1_{26-35*A27L}$ analog, from here on referred to as MART1-ELA) [22], use of the 1D3 TCR also makes it possible to determine whether the strength of TCR-pMHC interactions can be gauged from screening data. To provide first proof-of-concept, we designed a model antigen library with a complexity (4,764 minigenes) that would be sufficient to enable the screening of the entire mutational repertoire of human tumors with the highest mutational burden, such as microsatellite-instable tumors [23]. Individual MHC class I-restricted antigens, including well-described tumor-associated T cell antigens, such as $CDK4_{R24L}$ and MART1, and immunodominant epitopes of EBV, CMV and influenza (Supplementary Table 1; Supplementary Fig. 1) as well as MHC class II-restricted neoantigens were expressed as minigenes, each coupled to two unique barcode identifiers to provide internal replicate measurements. Subsequently, HLA-A*02:01-positive immortalized B cells were created and modified with the epitope library.

Screening of this library with T cells expressing the $CDK4_{R24L}$-specific TCR resulted in significant depletion of $CDK4_{R24L}$-expressing B cells, but crucially not B cells expressing the wild-type CDK4 minigene (Fig. 1B). Furthermore, B cells expressing either the native or affinity-enhanced $MART1_{26-35}$ epitope were selectively depleted after exposure to T cells transduced with the MART1-specific TCR. Notably, depletion was more pronounced in the case of B cells expressing the MART1 analogue. These data demonstrate the feasibility of our genetic screening method, and furthermore indicate

that it enables the distinction between T cell epitopes that are recognized with different efficiencies.

Next, to test whether this platform allows the profiling of the antigen-specificities of T cell populations in which T cells specific for a given neoantigen make up only a minority of the total T cell pool (such as patient TIL cultures, or donor T cells expressing libraries of patient-derived TCRs), we mixed T cells expressing either the MART1-specific or $CDK4_{R24L}$-specific TCR with mock-transduced T cells, such that MART1- and $CDK4_{R24L}$-specific T cells represented 10%, 1%, 0.3%, or 0.1% of total T cells. Analysis of depleted T cell epitopes after exposure to these different T cell populations demonstrated that substantial depletion of the low affinity native MART1 epitope was only achieved when using a homogeneous MART1-specific T cell pool. In contrast, the MART1-ELA and $CDK4_{R24L}$ epitopes were robustly identified when cognate TCR-expressing T cells comprised as little as 0.3-1% of all T cells (Fig. 1C). Together, these data demonstrate that our genetic screening methodology allows the efficient discovery of MHC class I-restricted T cell (neo)antigens from large antigen libraries. Furthermore, the technology allows one to distinguish high and low avidity TCR-pMHC interactions and, in case of high avidity TCR-pMHC interactions, genetic screens may be performed with clonally diverse T cell populations.

A substantial fraction of T cell-recognized cancer neoantigens is restricted by MHC class II molecules, and $CD4^+$ T cells recognizing such MHC class II-restricted neoantigens contribute to tumor control [6-9]. To assess whether our autologous APC immortalization strategy may also be utilized for the discovery of MHC class II-restricted neoantigens, we generated an antigen expression system in which each putative neoantigen is fused to the sorting signal of the invariant chain (CD74), with the aim to route such antigens into the MHC class II presentation pathway (Supplementary Fig. 2). We next took advantage of two MHC class II-restricted neoantigen-specific TCRs that were isolated from tumor-infiltrating T cells of a melanoma patient (Supplementary Fig. 2), transduced both TCRs into donor $CD4^+$ T cells, and expressed our model antigen library in patient-matched immortalized B cells. Screening of library-expressing B cells with T cells expressing either MHC class II-restricted TCR resulted in the significant depletion of B cells that expressed the cognate neoantigen, but not its wild-type counterpart (Fig. 1D), demonstrating the versatility of the platform to enable identification of both MHC class I and class II-restricted neoantigens.

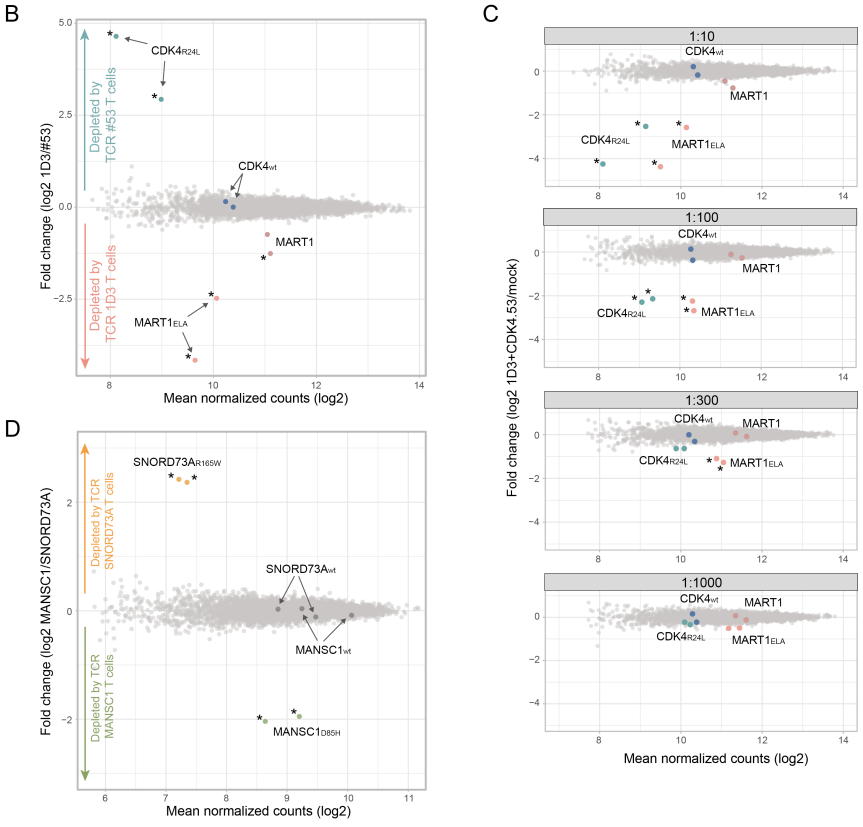

Figure 1 (part 2). Overview and validation of neoantigen discovery technology.

(B) Immortalized HLA-A*02:01 B cells were transduced with a library of 4,764 minigenes that included minigenes encoding the $CDK4_{R24L}$ neoantigen, its wild-type counterpart, the $MART1_{26-35}$ epitope (MART1) and the affinity-enhanced $MART1_{26-35*A27L}$ epitope (MART1-ELA). Library-expressing B cells were co-incubated with donor $CD8^+$ T cells engineered to express the $CDK4_{R24L}$-specific TCR #53, or the $MART1_{26-35}$-specific TCR 1D3. After 72 hours, minigenes from remaining B cells were amplified and quantified by deep sequencing. Dots represent individual minigenes. Fold change, defined as the relative abundance of minigenes in the presence of either 1D3 T cells or CDK4 T cells, and mean normalized read counts are plotted for each individual minigene. Minigenes encoding model MART1 and CDK4 epitopes are highlighted. Asterisks indicate screen hits, defined as minigenes with FDR-corrected p-values < 0.05 and log2 fold change > |1|. $CDK4_{R24L}$ $P = 6.9x10^{-48}$, $P = 2.5x10^{-65}$; MART1 $P = 1.2x10^{-26}$; MART1-ELA $P = 7.6x10^{-157}$, $P = 1.7x10^{-48}$.

(C) $CD8^+$ T cells expressing either the #53 or 1D3 TCR were diluted 10-, 100-, 300- or 1,000-fold with mock-transduced T cells to simulate T cell pools with low abundance antigen-reactive T cell populations, and were incubated with library-expressing B cells. Data are plotted as in (B) with fold change showing relative minigene abundance when exposed to either 1D3 or #53 TCR T cells as compared to mock T cells.

(D) Patient-derived TCRs specific for the MHC class II-restricted $MANSC1_{D85H}$ and $SNORD73A_{R165W}$ neoantigens were expressed in donor $CD4^+$ T cells and used to screen patient-matched immortalized B cells transduced with the CD74 signal-fused minigene library. Data are plotted as in (B) with fold change showing relative minigene abundance in the presence of MANSC1 TCR or SNORD73A TCR T cells.

As compared to previously developed genetic screening technologies, HANSolo has the advantage of allowing the identification of T cell epitopes restricted by any of the class I or II alleles of an individual patient. To demonstrate the utility of such unbiased screening, we focused on a patient with microsatellite-instable colorectal cancer (MSI-CRC). Given that microsatellite-instable tumors are characterized by mutational loads that exceed those of other human cancers [23], we reasoned that this analysis would serve as a useful test for the broader feasibility of our approach. A T cell product with enriched tumor-reactivity was first generated by ex vivo culture of peripheral blood mononuclear cells (PBMCs) of this patient with matched tumor organoids [24,25], and expanded tumor-reactive T cells consisted primarily of $CD8^+$ T cells (Supplementary Fig. 3). In parallel, nonsynonymous mutations in protein-coding genes were identified by exome sequencing (Supplementary Table 2), and a library of 1,834 minigenes that covered all mutations was generated and expressed in autologous immortalized B cells. Screening of the patient mutanome library with organoid-expanded tumor-reactive T cells revealed T cell reactivity against two neoantigens – $ABT1_{R139C}$ and $EEF1A1_{F280V}$ (Fig. 2A). Furthermore, the selective recognition of these neoantigens, and not their wild-type counterparts, was confirmed upon expression of the individual sequences in patient B cells (Fig. 2B). To understand whether the identified neoantigen-specific T cell responses make up a major or minor part of the T cell product, tumor organoid-reactive T cells were sorted based on CD137 surface expression and subjected to single-cell paired TCRα/β sequencing (Fig. 2C, Supplementary Fig. 3). The three top ranking TCRs were then expressed in donor $CD8^+$ T cells, and their specificity towards both identified neoantigens was tested. This yielded two $EEF1A1_{F280V}$-specific TCRs, each comprising 0.5% and 0.6% of the total patient T cell product (Fig. 2C,D). Thus, our method enables the personalized profiling of neoantigen-specificities of patient-derived T cell populations, even in a setting in which neoantigen-specific T cells represent only a minor fraction of the T cell population.

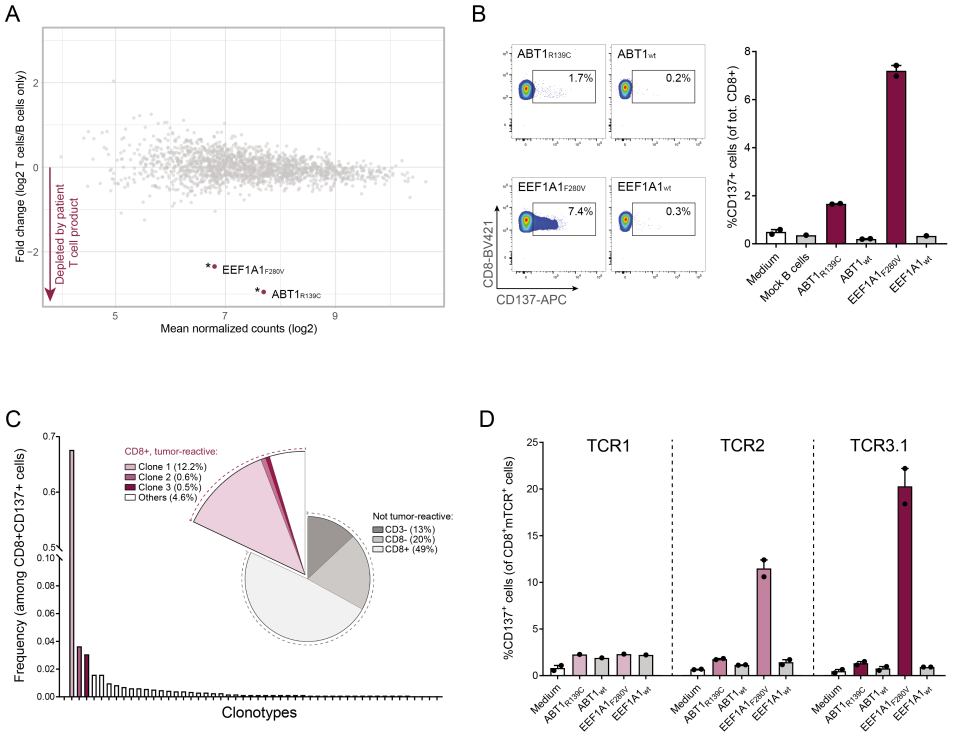

Figure 2. Personalized and HLA-agnostic neoantigen screening of patient-derived T cells.

(A) Nonsynonymous tumor mutations in mismatch repair-deficient colorectal cancer tissue of patient CRC-9 were identified by exome and RNA sequencing, and used to design a personalized mutanome minigene library consisting of 1,834 unique minigenes. Patient B cells were immortalized, transduced with the mutanome library, and incubated with patient PBMCs that had been co-cultured with matched tumor organoids for two weeks. Fold change represents relative minigene abundance in cultures with or without patient PBMCs. Screen hits, defined as minigenes with FDR-corrected p-value < 0.05 and log2 fold change > |1|, are marked by asterisks.

(B) Neoantigen hits identified in (A) were validated by expressing EEF1A1$_{F280V}$, ABT1$_{R139C}$ or the respective wild-type sequences as single minigenes in patient B cells and incubating transduced B cells with organoid-induced patient PBMCs. CD8$^+$ T cell activation was subsequently assessed by measuring CD137 surface expression. Data depict representative flow cytometry plots (left) and mean CD137 levels of technical replicates (error bars indicate S.D.).

(C) The organoid-induced PBMC product was incubated with autologous organoids and activated (CD137$^+$) CD8$^+$ T cells were subsequently isolated and subjected to single-cell paired TCRαβ sequencing. Bars indicate the frequency of the 50 most abundant clonotypes, with the three TCRs selected for downstream analysis indicated in purple. The pie chart indicates the abundance of these three TCRs as a proportion of the entire organoid-induced PBMC product.

(D) Organoid-reactive TCRs identified in (C) were gene-synthesized, expressed in donor CD8$^+$ T cells and incubated with patient B cells expressing the EEF1A1$_{F280V}$ or ABT1$_{R139C}$ neoantigens, or the corresponding wild-type control minigenes. TCR3.2 lacked reactivity towards patient tumor organoids (see Supplementary Fig. 3) and was therefore omitted from analysis. Bars indicate mean CD137 levels of technical replicates, error bars indicate S.D.

DISCUSSION

Collectively, these data demonstrate the feasibility of personalized and HLA-agnostic discovery of $CD4^+$ and $CD8^+$ T cell neoantigens from large genetic libraries. Identified neoantigens may be used to select TCRs for use in next-generation TCR gene therapies, or may be utilized in patient-specific cancer vaccines [26-29]. Of note, state-of-the-art algorithms that predict the immunogenicity of tumor mutations for use in personalized neoantigen vaccines failed to rank the patient $ABT1_{R139C}$ neoantigen as an actionable vaccination target (Supplementary Table 3), underlining the value of approaches that allow the unbiased identification of patient neoantigens. Importantly, with the current next-generation sequencing and DNA synthesis technologies and dedicated screening workflows, our platform enables patient neoantigen discovery within ten weeks, a timespan that is compatible with the production of personalized immunotherapies [27].

METHODS

Antibodies

The following antibodies were used for flow cytometry:
CD3-PerCP-Cy5.5 (clone SK7; eBioscience);
CD4-FITC (clone RPA-T4; BD Biosciences),
CD8-BV421 (clone RPA-T8; BD Biosciences),
CD14-APC-H7 (clone MoP9),
CD16-APC-H7 (clone 3G8),
CD19-FITC (clone 4G7),
CD137-BV421 (clone 4B4-1; Biolegend),
CD137-APC (clone 4B4-1; BD Biosciences),
PE-conjugated anti-mouse TCRβ constant domain (clone H57-597; BD Biosciences). The viability stain IR-Dye (Thermo Fisher) was used to identify live cells.

Patient tumor organoids, PBMC and B cell lines

Tumor tissue and peripheral blood mononuclear cells (PBMCs) were collected from patients treated at the NKI-AVL (Amsterdam, the Netherlands) with written informed consent and in accordance with guidelines of the Medical Ethical Committee. The study protocol (study nr. NL48824.031.14) was approved by the Medical Ethical Committee of the NKI-AVL. For patient CRC-9, tumor organoids were established as described previously [25]. In brief, tumor tissue was obtained by surgical resection, manually cut into ~1 mm^3 pieces and enzymatically digested using 1.5 mg/mL collagenase II, 10 mg/mL hyaluronidase type IV and 10 mM Y-27632. Tumor cells were subsequently embedded in Geltrex matrix (Gibco) and cultured in Ad-DF+++ (Advanced DMEM/F12 supplemented with 2 mM Ultraglutamine I, 10 mM HEPES, and 100/100 U/ml penicillin/streptomycin) medium containing 10% Noggin-conditioned medium, 20% R-spondin1-conditioned medium, 1x B27 supplement without vitamin A, 1.25 mM N-Acetylcysteine, 10 mM nicotinamide, 50 ng/mL human recombinant EGF, 500 nM A83-01, 3 mM SB202190 and 10 nM prostaglandin E2. In the first two weeks of organoid culture, 1x Primocin (Invivogen) was added to prevent microbial contamination. Organoids were

passaged every 1–2 weeks by incubating in TrypLE Express (Gibco) for 5–10 min followed by embedding in Geltrex. Immediately after passaging, when organoids were in single cell suspension, human CRC organoids medium was supplemented with 10 µM Y-27632. Organoids and cell lines were authenticated by SNP array and routinely tested for Mycoplasma contamination.

PBMCs were isolated from peripheral blood by Ficoll-Paque density gradient separation and cryopreserved in a 10% DMSO/FBS solution in liquid nitrogen, or cultured in RPMI 1640 medium supplemented with 2 mM Ultraglutamine I, 10% human AB serum (Life Technologies), penicillin/streptomycin (Roche), and 150 U/ml IL-2 (Proleukin, Novartis).

Immortalized patient B cell lines were generated by retroviral transduction with Bcl-6/Bcl-xL, as previously described [30]. Briefly, patient PBMCs were stained with IR-Dye and antibodies against CD3, CD14, CD16 and CD19. Single IR-Dye$^-$CD3$^-$CD14$^-$CD16$^-$CD19$^+$ cells were sorted using a FACSAria Fusion cell sorter (BD Biosciences) and stimulated for 36 hours in the presence of irradiated (55 Gy) CD40L$^+$ mouse L cells in B cell medium (IMDM medium (Gibco) supplemented with penicillin-streptomycin (Roche), 10% heat-inactivated fetal bovine serum (Sigma-Aldrich) and 50 ng/ml IL-21 (Peprotech)), followed by retroviral transduction of Bcl-6 and Bcl-xL. The Bcl-6/Bcl-xL-encoding vector also encodes GFP, to allow evaluation of transduction efficiency. Bcl-6/Bcl-xL-immortalized (GFP$^+$) B cells were cultured in B cell medium and were stimulated every week by addition of irradiated CD40L$^+$ L cells.

Retroviral transduction of T cell receptors

Codon-optimized TCR α and β variable sequences (encompassing V-CDR3-J domains) of selected TCRs were gene-synthesized (Twist Biosciences) and subcloned into a modified pMP71 retroviral vector [19]. This vector contains mouse TCR constant regions to reduce mispairing of introduced and endogenous TCR chains, as well as the puromycin N-acetyltransferase resistance gene. Retrovirus was produced by transfecting FLY-RD18 packaging cells with pMP71-TCR plasmid DNA using Xtremegene 9 transfection reagent (Roche). In parallel, healthy donor PBMCs (Sanquin Blood Bank, the Netherlands) were separated into CD8$^+$ (for transduction with MHC class I-restricted TCRs) and CD8$^-$ (for transduction with MHC class II-restricted TCRs) cells using the CD8$^+$ T Cell Isolation Kit

(Miltenyi Biotec). Isolated cell fractions were stimulated with CD3/CD28 Dynabeads (Life Technologies) in RPMI 1640 medium supplemented with 10% human AB serum (Life Technologies), penicillin/streptomycin (Roche), and 150 U/ml IL-2 (Proleukin, Novartis). After 48 hours, retroviral supernatants were collected and used to infect prestimulated $CD8^-/CD8^+$ PBMCs by spinoculation (400 g for 60 min) in Retronectin (Takara)-coated 24-well plates. Transduction efficiency was measured 72 hours later by staining TCR-transduced cells with an anti-mouse TCRβ constant domain antibody and analysis by flow cytometry. TCR-transduced T cells were then selected with 2.5 μg/ml puromycin for 48 hours and received fresh medium and IL-2 every 3-4 days. After 12-14 days of culture, transduced T cells were expanded using the rapid expansion protocol (REP), using 30 ng/ml anti-CD3 antibody (clone OKT-3; eBioscience) and 3,000 U/ml IL-2 in a 1:1 mixture of RPMI 1640 and AIM-V medium (Gibco) supplemented with 5% human AB serum (Life Technologies), in the presence of irradiated (40 Gy) allogeneic PBMCs (200:1 feeder/T cell ratio). After 7 days of REP culture, medium was refreshed with medium and IL-2 every 2 days.

Generation of tumor organoid-reactive T cells

Tumor-reactive patient T cells were generated by coculturing PBMCs and autologous tumor organoids as described previously [24,25]. In brief, following incubation with 200 ng/mL IFNγ (Peprotech) for 24 hours, patient tumor organoids were dissociated into single cell suspensions using TripLE Express (Gibco). Tumor organoid cells were mixed with patient PBMCs (20:1 PBMC/tumor cell ratio) and $1x10^5$ cells were seeded in each well of a U-bottom 96-well plate precoated with 5ug/mL anti-CD28 antibody (clone CD28.2; eBioscience). Coculture medium consisted of RPMI 1640 supplemented with 2 mM Ultraglutamine I, penicillin/streptomycin (Roche), 10% human AB serum (Life Technologies), 150 U/mL IL-2 (Proleukin, Novartis) and 20 μg/ml anti-PD1 blocking antibody (clone 5C4; kindly provided by Merus, The Netherlands). Medium, IL-2 and anti-PD1 were refreshed every 2-3 days. PBMCs were harvested and restimulated every 7 days by replating with fresh tumor organoid cells.

T cell activation assays

Reactivity of patient T cells and TCR-transduced donor T cells was determined by co-incubating T cells and target cells for 18-24 hours in U-bottom 96-well plates (1:1 T cell/target cell ratio) in RPMI 1640 supplemented with penicillin/streptomycin (Roche) and 10% human AB serum (Life Technologies). Incubation of T cells without target cells, and in the presence or absence of 50 ng/ml phorbol 12-myristate 13-acetate (Sigma-Aldrich) and 1 µg/ml ionomycin (Sigma-Aldrich) served as negative and positive controls, respectively. Following incubation, cells were stained with IR-Dye and antibodies against CD3, CD4, CD8 and CD137, and analyzed by flow cytometry. When T cell reactivity towards tumor organoids was tested, IFNγ-pretreated organoids were incubated with T cells in the presence of 20 µg/ml anti-PD1 blocking antibody (Merus) in U-bottom 96-well plates that were precoated with 5 µg/ml anti-CD28 antibody.

The cytotoxic capacity of T cells was assessed by co-incubating T cells and target cells for 72 hours in flat-bottom 96-well plates at a T cell/target cell ratio of 5:1. Target cells cultured in the absence of T cells served as negative control. Following incubation, 7.46 µm AccuCount blank counting beads (Spherotech) were added to individual cultures to enable quantification of remaining live target cells. Cells were subsequently harvested, stained with DAPI and anti-CD3 antibody, and measured by flow cytometry. When cytotoxicity against tumor organoids was assessed, IFNγ-pretreated organoids were incubated with T cells in the presence of 20 µg/mL anti-PD1 blocking antibody (Merus) and 10 µM Y-27632 in flat-bottom 96-well plates that were previously coated with 5 µg/ml anti-CD28 antibody. Where indicated, target cells were incubated with 50 µg/ml MHC class I blocking antibody (clone W6/32) for 30 min at 37 °C prior to incubation with T cells. Represented data are derived from single experiments, unless indicated otherwise.

Exome and RNA sequencing

Genomic DNA was extracted from CRC-9 tumor organoids and PBMCs using the DNeasy Blood and Tissue kit (Qiagen), and tumor RNA was extracted from CRC-9 organoids using the RNeasy Mini kit (Qiagen). Whole-exome and RNA sequencing was performed as previously described [19,24].

Antigen library design

To design the antigen library used to validate the screening platform, protein sequences of genes encoding known human non-mutated cancer regression antigens, as well as selected immunodominant genes of Epstein-Barr virus, cytomegalovirus and influenza, were collected from the Uniprot database (www.uniprot.org) (Supplementary Table 1). Protein sequences were reverse-translated and codon-optimized, and resulting nucleotide sequences were segmented into 93 nt minigenes with 45 nt overlap between neighbouring minigenes. In addition, a set of previously characterized neoantigens was included, all encoded by 93 nt minigenes in which the mutant codon was flanked on either side by 45 nt of the relevant non-mutant gene sequence. Minigene sequences encoding non-mutated peptides were included for each model neoantigen. Each 93 nt sequence was subsequently duplicated for a total of 4764 sequences, internal BbsI recognition sites were removed without altering encoded peptide sequences, and minigenes were flanked by sequences to enable PCR amplification and subcloning by BbsI into the pMSCV retroviral vector (see Supplementary Fig. 1). In addition, a unique 12 nt barcode sequence was incorporated into each individual library oligo sequence. The final oligo library was synthesized by Twist Biosciences.

To design the CRC-9 patient library, all single nucleotide variants (SNVs) and frameshifting indels with confirmed RNA expression within tumor cells were encoded as 63 nt minigenes. For SNVs, minigenes were designed that encoded peptides in which the mutant residue was flanked on either side by 10 amino acids of the relevant non-mutant protein sequence. In the case of frameshifting indels, or when SNVs resulted in loss of a stop codon, the newly formed open reading frame (ORF) was segmented in 63 nt minigenes with 30 nt overlap between adjacent minigenes. Minigenes encoding the $MART1_{26\text{-}35}$ and $CDK4_{R24L}$ epitopes were included in the library as internal controls. Internal BbsI recognition sites were removed without altering encoded peptide sequences, and minigenes were flanked by sequences for PCR amplification and subcloning as described above. The final library of 1,834 unique oligos was synthesized by Twist Biosciences.

Library cloning

Oligo libraries were amplified by 12 cycles of PCR using Phusion High-Fidelity DNA Polymerase (New England Biolabs) and primers Preamp Forward (5'-ACTGTCAGAAGACTGCAAGC-3') and primers Preamp Reverse (5'-TGACAGCGAAGACCATAGTG-3'). For screening experiments using $CD8^+$ T cells, the amplified library was cloned by Golden Gate assembly using BbsI (New England Biolabs) into a pMSCV retroviral vector that also encodes the puromycin N-acetyltransferase resistance gene and mCherry. To target minigene-encoded peptides to the MHC class II processing pathway for screens using $CD4^+$ T cells, the pMSCV-puro-mCherry vector was first modified to include the sorting sequence of the invariant chain CD74 (residues 17-98) as an N-terminal fusion to the minigene-encoded epitope sequences [31], after which the amplified library was inserted using Golden Gate assembly. Subcloned libraries were amplified using Endura electrocompetent cells (Lucigen) and library DNA was extracted using the PureLink HiPure Maxiprep kit (Invitrogen). During all cloning steps, a library representation of at least 100x was maintained.

Libraries were retrovirally transduced in duplicate into immortalized B cell lines at an infection rate of <10%, as described above. One day after transduction, B cells were transferred to B cell culture medium in the presence of irradiated $CD40L^+$ L cells and 50 ng/ml IL-21. Transduction efficiency was assessed 3 days post-transduction by measuring mCherry expression by flow cytometry, followed by selection with 2.5 µg/ml puromycin for 3 days and expansion of the B cell cultures until used in screens.

Antigen discovery screens

For proof-of-concept screens using MHC class I-restricted TCRs, the antigen library encoding known cancer regression antigens was transduced into a previously immortalized, HLA-A*02:01$^+$ patient B cell line (OVC21) [19]. Library-expressing B cells were co-incubated in duplicate with donor $CD8^+$ T cells transduced with the $MART_{26-35}$-specific TCR 1D3 or $CDK4_{R24L}$-specific TCR #53 (both HLA-A*02:01-restricted) in RPMI 1640 medium supplemented with 10% human AB serum, penicillin-streptomycin and 25 U/ml IL-2 at a T cell/B cell ratio of 5:1 and at a density of 1.5 x 10^6 total cells/cm^2.

Cultures were resuspended on day 1 and 2 of the experiment. To simulate screening conditions using clonally diverse T cell populations, 1D3 and #53 TCR-expressing T cells were mixed with donor-matched mock-transduced T cells at indicated ratios. For screens using patient-derived MHC class II-restricted TCRs, the model library - subcloned into the $CD74_{17\text{-}98}$-modified pMSCV vector - was transduced into patient-matched immortalized B cells (patient NKIRTIL017), and library-expressing B cells were cocultured with donor $CD4^+$ T cells transduced with either the $MANSC1_{D85H}$- or $SNORD73A_{R165W}$-specific patient TCR as described above. Library coverage of at least 150x was maintained in all experiments. After 72 hours of co-incubation, cells were washed in PBS, and cell debris was removed by Ficoll-Paque density gradient separation. Isolated cells were subsequently resuspended in DirectPCR Lysis Reagent (Viagen) containing 500 µg/ml proteinase K and lysed by incubation at 55 °C for 60 min, 85 °C for 30 min and 94 °C for 5 min. Minigene sequences were then amplified by PCR using NEBNext Ultra II Q5 Master Mix (New England Biolabs), using the following primers:

Prep-I Forward (for screens with $CD8^+$ T cells):
5'-CAAGCAGAAGACGGCATACGATGGAGGAGAACCCTGGACCTACAAGC-3'
Prep-II Forward (for screens with $CD4^+$ T cells):
5'-CAAGCAGAAGACGGCATACGACCTGCGGATGAAGCTGCCCG-3'
Prep Reverse:
5'-
AATGATACGGCGACCACCGAGATCTACACTCTTTCCCTACACGACGCTCTTCC
GATCTNNNNNNNG ATCCGACTCGGTGCCACTTTTTCAAC-3'

The 7 nt stretch of N nucleotides indicates a unique barcode sequence used to enable the multiplexed preparation of sequencing libraries. Following PCR, samples were pooled equimolarly and run on a 1% agarose gel in order to separate minigene amplicons from potential primer dimers. Minigene amplicons were extracted from gel using the Monarch DNA Gel Extraction Kit (New England Biolabs) and deep sequenced on an Illumina HiSeq 2500 Sequencing system (single read 65 bp).

For the patient CRC-9 neoantigen screen, the tumor variant-encoding library was transduced into autologous immortalized B cells, cells were selected with

puromycin, and cocultured in duplicate with tumor organoid-reactive patient T cells at a T cell/B cell ratio of 5:1. Library-expressing B cells cultured in the absence of patient T cells served as a negative control. After 48 hours of coculture, cells were washed in PBS, stained with DAPI (Sigma-Aldrich), and live B cells ($DAPI^{-}GFP^{+}$) were sorted by flow cytometry. Genomic DNA was extracted from sorted B cells using the DNeasy Blood and Tissue kit (Qiagen), and minigene sequences were amplified and sequenced as described above. To validate identified patient neoantigens, minigenes encoding the screen hits, as well as their wild-type counterparts, were synthesized as individual gBlocks (IDT), cloned into the pMSCV-puro-mCherry vector and transduced into immortalized patient B cells. Following selection with puromycin, minigene-transduced B cells were cocultured with organoid-reactive patient T cells as described above.

Sequence analysis

Initial sequence quality profiles were quantified by FastQC and de-multiplexed using fastq-multx with 1 mismatch allowed. Vector sequences were trimmed from sequence reads using fastq-mcf against the UniVec database and samples were subsequently quality filtered using cutadapt. For the proof-of-concept screens, the unique 12 nt barcodes that were added to individual minigene sequences were extracted using seqkit and mapped using Bowtie2 with no multi-matched hits allowed. For the patient neoantigen screen, high quality reads were mapped against the full minigene sequences of the patient library using BBMap with ambiguously mapped reads removed and only perfect mappings allowed. Per-sample count tables were differentially compared and normalised using DESeq2. Minigenes with an average abundance below the 4th percentile and a coefficient of variation >1 were removed from analyses. Statistical testing was performed using DESeq2's Wald's test using an FDR-corrected p-value cutoff < 0.05 and a log2 fold change $>|1|$.

Single-cell TCR sequencing

CRC-9 patient T cells were cocultured with matched tumor organoids for 24 hours, and stained with IR-Dye and antibodies against CD3, CD4, CD8 and CD137. Tumor-reactive $CD8^{+}$ T cells (live $CD3^{+}CD4^{-}CD8^{+}CD137^{+}$) were then isolated by flow cytometry and

loaded into a Chromium single cell sorting system (10X Genomics). TCR library preparation was performed using the Chromium Single Cell VDJ Library protocol (10X Genomics) according to the manufacturer's instructions, and the library was subsequently sequenced on a Illumina Miseq sequencing system.

In silico selection of neoantigen vaccine targets

The computational tools Vaxrank [32] and pVACseq [33] were used to rank tumor mutations of patient CRC-9 for use in a putative personalized cancer vaccine. HLA typing of patient CRC-9 was performed using OptiType for HLA-A, -B and –C alleles. For Vaxrank, the set of CRC-9 somatic variant calls and aligned RNA reads were used as input, with parameters set to a peptide length of 25, an epitope length of 8-11 and utilization of the MHCFlurry prediction algorithm. For pVACtools, variants were annotated with VEP, gene expression was determined using Salmon and DNA/RNA coverage was quantified by bam-readcount. Epitope length was set to 8-11 and the prediction algorithms MHCflurry and MHCnuggets were used.

Code availability

Scripts used for analyzing sequencing data from antigen discovery screens are stored at https://github.com/twbattaglia/amplicon-nf. Script output for the presented analyses are stored at https://github.com/twbattaglia/HANSolo-manuscript. Access to both repositories can be obtained from the corresponding author on request.

Data availability

DNA sequencing data of antigen discovery screens have been deposited in the NCBI Sequence Read Archive under accession code PRJNA707215.

ACKNOWLEDGMENTS

We would like to thank Maarten Slagter for bioinformatic support, Krijn Dijkstra for support with single-cell TCR sequencing, Anne van de Leun for support with isolation of neoantigen-specific TCRs, Kaspar Bresser and David Vredevoogd for helpful discussions on library design, Ziva Moravec and Rhianne Voogd for technical assistance, the NKI-AVL Flow Cytometry Facility for flow cytometric support, and the NKI-AVL Genomics Core Facility for support with next generation sequencing. This work was supported by the Dutch Cancer Society Young Investigator Grant (grant No. 2020-1 / 12977) (to W.S.), ZonMw Translational Research Program 2 (grant No. 446002001) (to W.S. and J.B.A.G.), the Queen Wilhelmina Cancer Research Award and ERC AdG SENSIT (grant agreement No. 742259) (to T.N.S.), the NWO Gravitation program (NWO 2012-2022) (to E.E.V.) and by Oncode Institute (to T.N.S. and E.E.V.).

AUTHOR CONTRIBUTIONS

C.M.C., J.U., and W.S. designed, performed, analyzed, and interpreted experiments. T.B. analyzed sequencing data of screens. C.M.C., J.B.A.G., E.E.V., T.N.S. and W.S. wrote the manuscript. All authors reviewed the manuscript.

COMPETING INTERESTS

T.N.S. is advisor for Adaptive Biotechnologies, Allogene Therapeutics, Merus, Neogene Therapeutics, and Scenic Biotech; is a recipient of research support from Merck KgaA; is a stockholder in Allogene Therapeutics, Merus, Neogene Therapeutics, and Scenic Biotech; and is venture partner at Third Rock Ventures, all outside of the current work. All other authors declare no competing interests.

REFERENCES

1. Schumacher, T.N., Scheper, W. & Kvistborg, P. Cancer Neoantigens. Annu Rev Immunol (2018).
2. Schumacher, T.N. & Schreiber, R.D. Neoantigens in cancer immunotherapy. Science 348, 69-74 (2015).
3. Gros, A., et al. Prospective identification of neoantigen-specific lymphocytes in the peripheral blood of melanoma patients. Nat Med 22, 433-438 (2016).
4. Gubin, M.M., et al. Checkpoint blockade cancer immunotherapy targets tumour-specific mutant antigens. Nature 515, 577-581 (2014).
5. Rizvi, N.A., et al. Cancer immunology. Mutational landscape determines sensitivity to PD-1 blockade in non-small cell lung cancer. Science 348, 124-128 (2015).
6. Alspach, E., et al. MHC-II neoantigens shape tumour immunity and response to immunotherapy. Nature 574, 696-701 (2019).
7. Oh, D.Y., et al. Intratumoral CD4(+) T Cells Mediate Anti-tumor Cytotoxicity in Human Bladder Cancer. Cell 181, 1612-1625 e1613 (2020).
8. Tran, E., et al. Cancer immunotherapy based on mutation-specific CD4+ T cells in a patient with epithelial cancer. Science 344, 641-645 (2014).
9. Borst, J., Ahrends, T., Babala, N., Melief, C.J.M. & Kastenmuller, W. CD4(+) T cell help in cancer immunology and immunotherapy. Nat Rev Immunol 18, 635-647 (2018).
10. Bentzen, A.K., et al. Large-scale detection of antigen-specific T cells using peptide-MHC-I multimers labeled with DNA barcodes. Nat Biotechnol 34, 1037-1045 (2016).
11. Hadrup, S.R., et al. Parallel detection of antigen-specific T-cell responses by multidimensional encoding of MHC multimers. Nat Methods 6, 520-526 (2009).
12. Lu, Y.C., et al. Efficient identification of mutated cancer antigens recognized by T cells associated with durable tumor regressions. Clin Cancer Res 20, 3401-3410 (2014).
13. Tran, E., et al. Immunogenicity of somatic mutations in human gastrointestinal cancers. Science 350, 1387-1390 (2015).
14. Kula, T., et al. T-Scan: A Genome-wide Method for the Systematic Discovery of T Cell Epitopes. Cell 178, 1016-1028 e1013 (2019).
15. Joglekar, A.V., et al. T cell antigen discovery via signaling and antigen-presenting bifunctional receptors. Nat Methods 16, 191-198 (2019).
16. Li, G., et al. T cell antigen discovery via trogocytosis. Nat Methods 16, 183-190 (2019).
17. Kisielow, J., Obermair, F.J. & Kopf, M. Deciphering CD4(+) T cell specificity using novel MHC-TCR chimeric receptors. Nat Immunol 20, 652-662 (2019).

18. Sharma, G., Rive, C.M. & Holt, R.A. Rapid selection and identification of functional CD8(+) T cell epitopes from large peptide-coding libraries. Nat Commun 10, 4553 (2019).

19. Scheper, W., et al. Low and variable tumor reactivity of the intratumoral TCR repertoire in human cancers. Nat Med 25, 89-94 (2019).

20. Stronen, E., et al. Targeting of cancer neoantigens with donor-derived T cell receptor repertoires. Science 352, 1337-1341 (2016).

21. Jorritsma, A., et al. Selecting highly affine and well-expressed TCRs for gene therapy of melanoma. Blood 110, 3564-3572 (2007).

22. Valmori, D., et al. Vaccination with a Melan-A peptide selects an oligoclonal T cell population with increased functional avidity and tumor reactivity. J Immunol 168, 4231-4240 (2002).

23. Chalmers, Z.R., et al. Analysis of 100,000 human cancer genomes reveals the landscape of tumor mutational burden. Genome Med 9, 34 (2017).

24. Dijkstra, K.K., et al. Generation of Tumor-Reactive T Cells by Co-culture of Peripheral Blood Lymphocytes and Tumor Organoids. Cell 174, 1586-1598 e1512 (2018).

25. Cattaneo, C.M., et al. Tumor organoid-T-cell coculture systems. Nat Protoc 15, 15-39 (2020).

26. Sahin, U., et al. Personalized RNA mutanome vaccines mobilize poly-specific therapeutic immunity against cancer. Nature 547, 222-226 (2017).

27. Ott, P.A., et al. An immunogenic personal neoantigen vaccine for patients with melanoma. Nature 547, 217-221 (2017).

28. Hilf, N., et al. Publisher Correction: Actively personalized vaccination trial for newly diagnosed glioblastoma. Nature 566, E13 (2019).

29. Keskin, D.B., et al. Neoantigen vaccine generates intratumoral T cell responses in phase Ib glioblastoma trial. Nature 565, 234-239 (2019).

30. Kwakkenbos, M.J., et al. Generation of stable monoclonal antibody-producing B cell receptor-positive human memory B cells by genetic programming. Nat Med 16, 123-128 (2010).

31. Bonehill, A., et al. Messenger RNA-electroporated dendritic cells presenting MAGE-A3 simultaneously in HLA class I and class II molecules. J Immunol 172, 6649-6657 (2004).

32. Rubinsteyn, A., Hodes, I., Kodysh, J. & Hammerbacher, J. Vaxrank: A computational tool for designing personalized cancer vaccines. (bioRxiv, 2017).

33. Hundal, J., et al. pVACtools: A Computational Toolkit to Identify and Visualize Cancer Neoantigens. Cancer Immunol Res 8, 409-420 (2020).

SUPPLEMENTARY MATERIAL

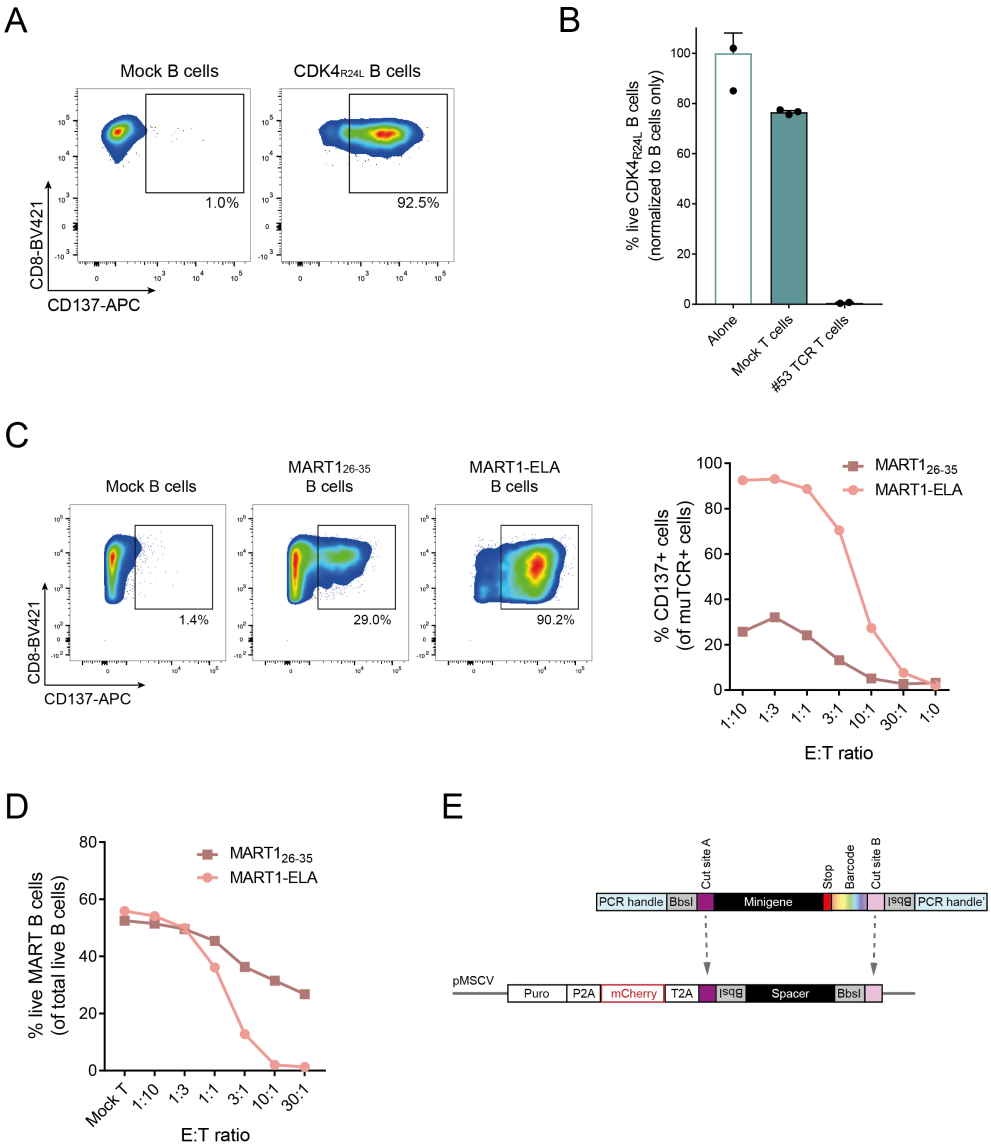

Supplementary Figure 1. *(previous page)*

(A) Specificity of TCR clone #53 for the $CDK4_{R24L}$ neoantigen. TCR #53 was transduced into donor $CD8^+$ T cells and resulting cells were incubated with mock-transduced or $CDK4_{R24L}$ minigene-transduced HLA-$A2^+$ B cells. T cell activation was assessed by measuring CD137 surface expression.
(B) Quantification of killing of B cells expressing $CDK4_{R24L}$ minigenes after a 72 hour co-culture with TCR #53-transduced donor $CD8^+$ T cells. Incubation of B cells in the presence of mock-transduced $CD8^+$ T cells served as a negative control, and data were normalized to the fraction of live B cells that were measured in the absence of T cells. Bars indicate mean values of technical replicates, error bars indicate S.D
(C) Specificity of TCR clone 1D3 for the native $MART1_{26-35}$ epitope and its MHC affinity-enhanced variant MART1-ELA. Donor $CD8^+$ T cells expressing TCR 1D3 were incubated with HLA-$A2^+$ B cells that were transduced to express either MART1 epitope at the indicated effector: target ratios. Incubation of T cells with mock-transduced B cells served as a negative control. Data depict representative flow cytometry plots (left) and mean CD137 levels of technical replicates (right).
(D) Quantification of killing of B cells expressing $MART1_{26-35}$ or MART1-ELA minigenes after co-culture with 1D3 TCR-transduced donor $CD8^+$ T cells. Incubation of B cells in the presence of mock-transduced T cells served as a negative control. Data depict mean percentages of live B cells of technical replicates.
(E) Schematic overview of library minigene design and cloning strategy.

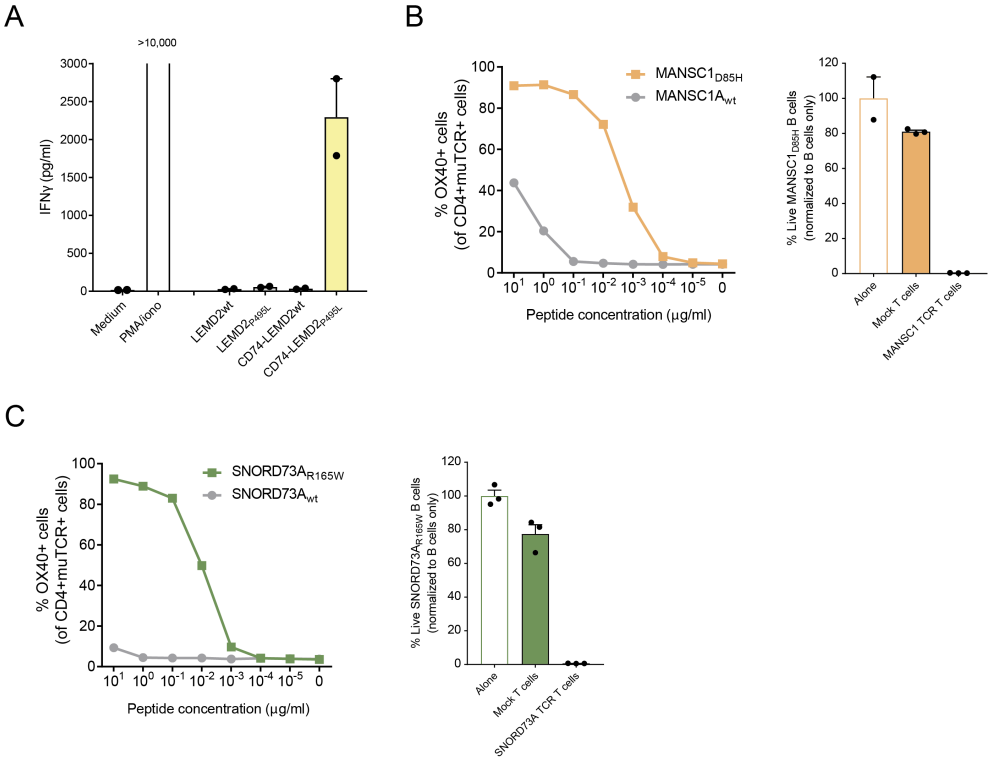
A
>10,000
IFNγ (pg/ml)
3000
2500
2000
1500
1000
500
0
Medium
PMA/iono
LEMD2wt
LEMD2p.I69L
CD74-LEMD2wt
CD74-LEMD2p.I69L
B
% OX40+ cells (of CD4+muTCR+ cells)
MANSC1D85H
MANSC1Awt
Peptide concentration (µg/ml)
% Live MANSC1D85H B cells (normalized to B cells only)
Alone
Mock T cells
MANSC1 TCR T cells
C
% OX40+ cells (of CD4+muTCR+ cells)
SNORD73AR165W
SNORD73Awt
Peptide concentration (µg/ml)
% Live SNORD73AR165W B cells (normalized to B cells only)
Alone
Mock T cells
SNORD73A TCR T cells

Supplementary Figure 2. *(previous page)*

(A) TIL were expanded from a melanoma tumor with previously identified MHC II-restricted neoantigen reactivity[1] by incubation of single-cell suspensions of tumor tissue in the presence of high dose IL-2. $CD4^+$ T cells were subsequently isolated by flow cytometry and incubated with autologous immortalized B cells that were transduced to express a minigene encoding the patient neoantigen $LEMD2_{P495L}$, or the same minigene coupled to the $CD74_{17\text{-}98}$ sorting signal (as described in Methods). $CD4^+$ T cell activation was assessed by analysis of IFNγ secretion . Patient B cells expressing the corresponding wild-type LEMD2 minigene, either coupled to $CD74_{17\text{-}98}$ or not, served as negative controls. Data represent mean IFNγ levels of technical duplicates, errors bars indicate S.E.M.

(B, C) Characterization of $MANSC1_{D85H}$- and $SNORD73A_{R165W}$-specific TCRs. Left: TCRs were expressed in donor $CD4^+$ T cells and resulting cells were incubated with patient-matched B cells pulsed with the indicated concentrations of $MANSC1_{D85H}$ or $SNORD73A_{R165W}$ peptides, or the respective wild-type control peptides. T cell activation was subsequently assessed by measuring OX40 surface expression. Data depict mean OX40 levels of technical replicates. Right: Quantification of killing of B cells expressing $MANSC1_{D85H}$- or $SNORD73A_{R165W}$ minigenes after a 72 hour co-culture with donor $CD4^+$ T cells transduced to express the indicated TCRs. Incubation of B cells in the presence of mock-transduced T cells served as a negative control, and data were normalized to the fraction of live B cells that were detected in the absence of T cells. Bars indicate mean values of technical replicates, error bars indicate S.D.

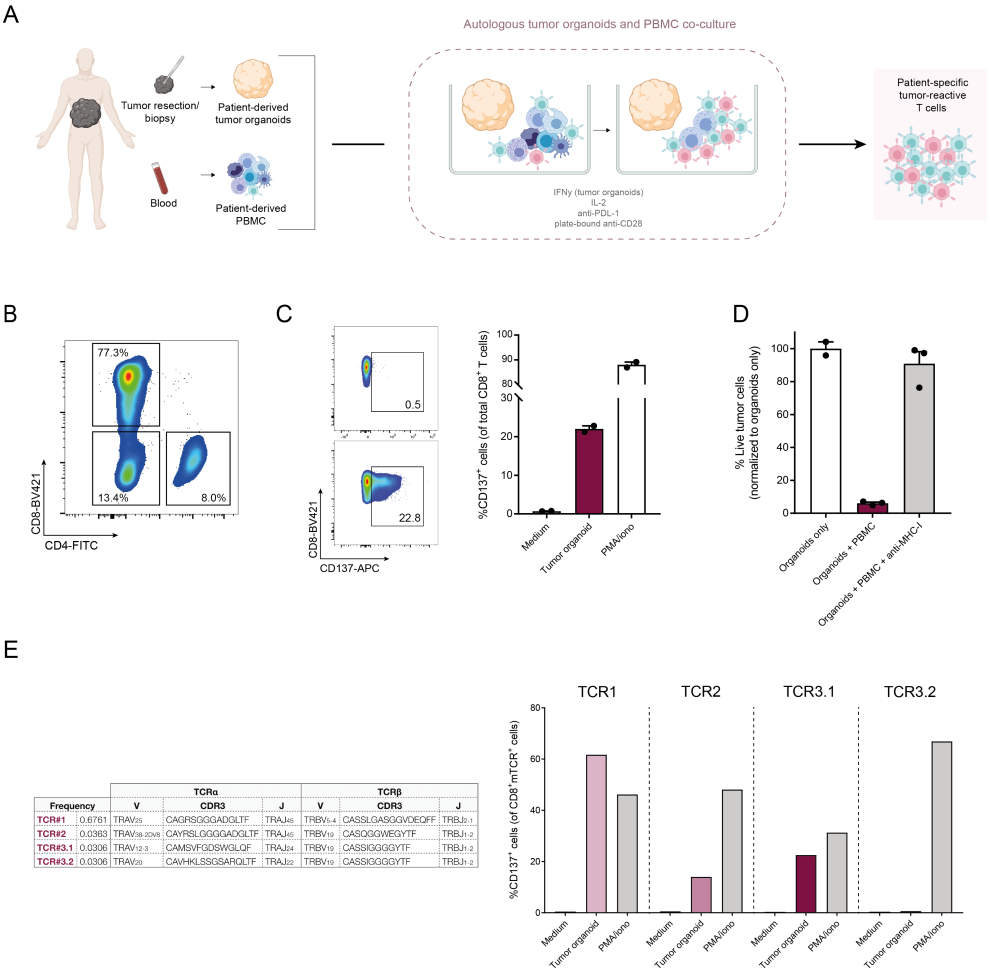

		TCRα			TCRβ		
Frequency		V	CDR3	J	V	CDR3	J
TCR#1	0.6761	TRAV25	CAGRSGGGADGLTF	TRAJ45	TRBV5-4	CASSLGASGGVDEQFF	TRBJ2-1
TCR#2	0.0363	TRAV38-2DV8	CAYRSLGGGGADGLTF	TRAJ45	TRBV19	CASQGGWEGYTF	TRBJ1-2
TCR#3.1	0.0306	TRAV12-3	CAMSVFGDSWGLQF	TRAJ24	TRBV19	CASSIGGGGYTF	TRBJ1-2
TCR#3.2	0.0306	TRAV20	CAVHKLSSGSARQLTF	TRAJ22	TRBV19	CASSIGGGGYTF	TRBJ1-2

Supplementary Figure 3. *(previous page)*

(A) Schematic overview of the generation of personalized tumor-reactive T cell products by coculture of patient PBMCs with matched tumor organoids (see refs. [2,3]).

(B) Tumor organoid-specific T cells were obtained by co-incubation of PBMCs of patient CRC-9 with matched tumor organoids for two weeks. The fractions of $CD4^+$, $CD8^+$ and $CD4^-CD8^-$ T cells were analyzed by flow cytometry. Depicted data are gated on live single $CD3^+$ cells.

(C) Reactivity of organoid-induced patient PBMCs. Organoid-reactivity of the CRC-9 cell product was assessed by incubation of cells with tumor organoids and analysis of CD137 surface expression. Data depict representative flow cytometry plots (left) and mean CD137 levels of technical replicates (right; error bars indicate S.D.).

(D) Quantification of patient PBMC cytotoxicity towards matched tumor organoids. Data were normalized to the fraction of live B cells that were detected in the absence of T cells. To assess the contribution of MHC class I-restricted T cells to organoid killing, patient PBMCs and organoids were co-incubated in the presence or absence of an MHC class I-blocking antibody. Data depict mean values of technical replicates, error bars indicate S.D.

(E) Left: TCRα and β sequence information of the top three ranking clonotypes of Fig. 2C. Right: Organoid reactivity of the selected TCRs. TCRs were expressed in donor $CD8^+$ T cells and incubated with patient tumor organoids. $CD8^+$ T cell activation was assessed by measuring CD137 surface expression.

Supplementary references

1. Linnemann, C., et al. High-throughput epitope discovery reveals frequent recognition of neo-antigens by CD4+ T cells in human melanoma. Nat Med 21, 81-85 (2015).
2. Cattaneo, C.M., et al. Tumor organoid-T-cell coculture systems. Nat Protoc 15, 15-39 (2020).
3. Dijkstra, K.K., et al. Generation of Tumor-Reactive T Cells by Co-culture of Peripheral Blood Lymphocytes and Tumor Organoids. Cell 174, 1586-1598 e1512 (2018).

Summary and general discussion

7

Cancer immunotherapy has shown great clinical successes in the treatment of advanced cancers. However, a large fraction of patient do not respond to current immunotherapies and, even in the more immune-responsive tumor types, durable responses remain rare events. Treatment failure could be explained by many different mechanisms: defects in the tumor antigen processing and presenting machinery, expression of immune checkpoint molecules, low level of tumor foreignness, general immune status and T-cell receptors (TCRs) repertoire, only to cite a few, all contribute in the interaction between tumor and immune cells (Blank et al., 2016). Understanding the specific interactions between tumor and immune cells, predicting possible immune evasion mechanisms and finding solutions to overcome these mechanisms, for the individual patient, are the current challenges of the immuno-oncology field.

The implementation of personalized medicine in the field of immunotherapy is substantial; to achieve that, we strongly believe a pre-clinical *in vitro* model for the analysis of (different) aspects of the interactions between tumor and immune cells is urgently needed. A personalized *in* vitro model needs an autologous source of immune and tumor cells. Tumor organoids are a three-dimensional culture system that enables the indefinite propagation of normal and tumor epithelial cells for a variety of tissues. Tumor organoids can be established from needle biopsy or resection material, and most importantly, they retain histological and molecular features of the original tumor they are derived from. (Weeber et al., 2015; van de Wetering et al., 2015). On the other side, the peripheral blood compartment represents an interesting source of immune cells. First, Compared to tumor-infiltrating lymphocytes (TILs), peripheral blood mononuclear lymphocytes (PBMCs) are a relative easy accessible source of immune cells, and have been previously investigate as a potential source for tumor-reactive T cells (Verdegaal et al., 2011). Second, peripheral blood represents a source of T cells with a lower degree of exhaustion. We built our model for precision immune-oncology by combining autologous tumor organoids and PBMCs.

In chapter 2 we demonstrate that by co-culturing PBMCs and autologous tumor organoids we are able to generate a tumor-reactive T cell population for a subset of

colorectal cancer (CRC) and non-small cell lung cancer (NSCLC) patients; in chapter 3 we present an improved version of the co-culture platform protocol. We show that the obtained tumor-reactive T cells are specifically able to recognize and kill tumor organoids, while ignoring autologous healthy colon or airway organoids. Furthermore, to control for any intrinsic artifact of the organoids cultures, we compare reactivity against organoids and single cells digest of the original tumor, as well as between tumor and healthy tissue. We provide proof of concept that tumor organoids can be used to establish individualized *ex vivo* model systems to support T cell-based therapies and to study the interactions between T cells and tumor cells. We speculate the established co-culture platform could be of extreme relevance for three major applications: the development of a personalized prediction tool for immunotherapy responses; the mechanical dissection of different aspects of tumor-immune cells interactions in a physiological setting; the generation of an unbiased personalized T cells product for adoptive T cell transfer purposes.

By comparing the results of our co-cultures with clinical responses to immunotherapy in chapter 4, we demonstrate that the ability to generate a tumor reactive T cell population via our platform perfectly correlates with long term clinical responses to anti-PD-1 blocking therapy, in a subset of 12 different CRC and NSCLC patients. We also show the feasibility of using the platform to monitor responses over time, during treatment: for one CRC patient we were indeed able to mimic response to nivolumab of two different lesions, reacting differently to the treatment, at two different timepoints. However, even though those data suggest in favor of using the co-culture results as biomarker of (non-) response to checkpoint inhibitors, we quickly realised the intrinsic limitations of the approach. Time and success rates involved into the establishment of tumor organoids culture strongly argue against the use of such a model for treatment decision purposes.

Nevertheless, these correlation data highlight once more the value of the co-culture platform as a physiologically-relevant investigational tool: for example, efficacy of new (combination of) candidate drugs in the immuno-oncology scenario can be easily assessed; or, mechanisms of primary (or acquired) resistance to immunotherapy can be identified, analysed and potentially overcome.

In chapter 5 we use the co-culture system to generate and analyze models of primary and acquired resistance to immunotherapy. To be specific, Werner helicase (WRN) was previously identified as a specific synthetic-lethal target in mismatch repair-deficient (dMMR)/microsatellite instability-high (MSI-H) cancers. We demonstrate that WRN dependency is retained in diverse models of primary and acquired resistance to targeted, chemo- and checkpoint inhibitor therapy, providing a strong rationale for the clinical development of specific small-molecule inhibitors targeting WRN. The generation of acquired resistance was obtained by prolonged exposure of tumor organoids to the pressure of tumor-reactive T cells: this method, while laborious, shows for the first time, the feasibility of using an organoid co-culture system to model in vitro acquired resistance to T cells activity.

With respect to the last potential application of the co-culture platform, the ability to obtain specific tumor-reactive T cells offers a potential strategy for the generation of T-cell products for adoptive T-cell transfer. The clinical success of TIL therapy in melanoma has not been matched in other tumor types and there is a need for strategies that bypass the challenges of TIL therapy for epithelial cancers.

To fully explore this hypothesis, several important steps need to be taken. Most importantly, it is fundamental to know what are the targets of the actions of the induced tumor-reactive T cells. Systems that allow the unbiased analysis of T cell-mediated tumor recognition, such as the identification of their antigenic targets, in the personalized setting are currently lacking. Accumulating evidence suggests that cancer neoantigens are important drivers of both spontaneous and therapy-induced anti-tumor T cell responses (Schumacher et al., 2018). Experimental tools that enable the analysis of both $CD4^+$ and $CD8^+$ T cell-recognized tumor antigens on a per-patient basis are urgently needed .

In chapter 6 we present HANSolo, HLA-Agnostic Neoantigen Screening, a high-throughput genetic platform for personalized discovery of $CD4^+$ and $CD8^+$ T cell-recognized (neo)antigens. By using patient-matched immortalized B cells, encoding

for all non-synonymous tumor-specific mutations, as APCs, we demonstrate that we can enable the unbiased screening of T cell specificities across all MHC-I and -II alleles of individual patients, in a fully autologous manner.

Taken together, the data we generate show that the co-culture platform represents a new solution to investigate the complex interactions between tumor cells and T cells. However, cancer is a complex disease, reducing it to the study of only two elements would mean being extremely simplistic. Tumor cells and T cells do not stand alone; instead they are immersed in a specific microenvironment, consisting of a large variety of different cell types: the interplay and the equilibrium between cancer, stromal, endothelial, and multiple different immune cells are the keys to understand how a tumor develops, and how it would react to a specific therapy.

On the road to precision immunotherapy, the co-culture platform “only” marks a step; future steps directed towards the expansion of the actual co-culture model to more diverse cell types will be needed to explore the full potential of what we created so far.

REFERENCES

- Blank C.U., Haanen J.B., Ribas A. and Schumacher T.N. (2016) CANCER IMMUNOLOGY. The "cancer immunogram". Science 352:658-60
- Hanahan D. and Weiberg R.A. (2000) The hallmarks of cancer. Cell 100:57-70
- Hanahan D. and Weiberg R.A. (2011) The hallmarks of cancer: the next generation. Cell 144:646-74
- Schumacher, T.N., Scheper, W. & Kvistborg, P. (2019) Cancer Neoantigens. Annu. Rev. Immunol. 37:173-200
- Van de Wetering M., Francies H.E., Francis J.M. et al. (2015) Prospective derivation of a living organoid biobank of colorectal cancer patients. Cell 161:933-45
- Verdegaal E.M.E., Visser M., Ramwadhodoebé T.H. et al. (2011) Successful treatment of metastatic melanoma by adoptive transfer of blood-derived polyclonal tumor-specific CD4+ and CD8+ T cells in combination with low-dose interferon-alpha. Cancer Immunol. Immunother. 60:953-63
- Weeber F., van de Wetering M., Hoogstrat M., et al. (2015) Preserved genetic diversity in organoids cultured from biopsies of human colorectal cancer metastases. PNAS 112:13308-11.

Addendum

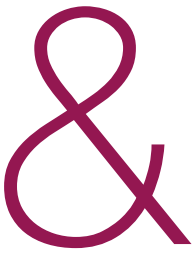

NEDERLANDSE SAMENVATTING

Immuuntherapie voor kanker heeft de behandeling van vergevorderde kankers sterk veranderd. In het afgelopen decennium zijn de successen van immuuntherapie van buitengewone anekdotes tot een solide en stabiele werkelijkheid geworden. Checkpointremmers zijn succesvol ingezet als behandeling voor verschillende tumoren: melanomen, niet-kleincellige longkankers, hoofd en nek plaveiselcarcinomen, niercelcarcinomen, Hodgkin lymfoom, urotheelcarcinomen, maagcarcinomen, primair mediastinaal B-cellymphoom, Merkelcelcarcinoom, hepatocellulair carcinoom, baarmoederhalskanker en colorectale kanker, om er een aantal te noemen. Echter, zelfs in de meest immuun-reactieve tumortypen zijn langdurige responsen op checkpointremmers zeldzame gebeurtenissen en de succespercentages variëren sterk, van ~15% wanneer toegepast in monotherapie, tot ~60% wanneer toegepast in combinatie.

Om de effectiviteit van de huidige kanker immuuntherapieën te verbeteren, is het noodzakelijk om manieren te vinden om te voorspellen welke patiënten de grootste kans hebben om goed te reageren op de behandeling, welke patiënten waarschijnlijk een terugval zullen krijgen, welke resistentiemechanismen er op zullen komen en, het belangrijkst, hoe deze mechanismen overkomen kunnen worden. Deze uitdagingen onderstrepen de noodzaak voor een preklinisch model dat gebruikt kan worden om de interactie tussen tumorcellen en immuuncellen te bestuderen op een onbevooroordeelde manier, voor individuele patiënten.

In dit proefschrift omarmen we deze uitdagingen, op zoek naar een uitgebreide oplossing.

In **hoofdstuk 2** presenteren we een nieuw model voor het bestuderen van directe interacties tussen tumor- en immuuncellen voor individuele patiënten. Door een co-cultuur van mononucleaire lymfocyten uit perifeer bloed (PBMC's) and autologe tumor organoïden konden we tumor-reactieve T-cellen genereren voor een subgroep van colorectale kanker (CRC) en niet-kleincellige longkanker (NSCLC) patiënten. Ook demonstreren we dat deze T-cellen in staat zijn om specifiek tumor organoïden te

herkennen en te doden, terwijl autologe gezonde darm of luchtweg organoïden genegeerd werden. Wij speculeren dat dit nieuwe platform gebruikt kan worden als een technologie om de verschillende aspecten van tumor-immuun interacties te ontleden en voor het genereren van een patiënt-specifiek T-cel product.

In **hoofdstuk 3** beschrijven we het co-cultuur platform in detail en benadrukken we de voor- en nadelen van onze methode om tumorreactieve T-cellen te genereren ten opzichte van de bestaande methoden.

In **hoofdstuk 4** onderzoeken we de fysiologische waarde van het platform, waarbij we de hypothese onderzoeken dat het kan worden gebruikt om de respons van patiënten op immuuntherapie te voorspellen. We laten een perfecte correlatie zien tussen het vermogen om patiëntspecifieke tumorreactieve T-cellen te genereren en de klinische uitkomst van anti-PD-1-blokkeertherapie voor een subgroep van colorectale kanker (CRC) en niet-kleincellige longkanker (NSCLC) patiënten. We demonstreren ook de mogelijkheid van het gebruik van het co-cultuursysteem om de respons op immuuntherapie gedurende de behandeling te volgen. We bieden ook een kritisch standpunt en benadrukken de intrinsieke beperkingen van het gebruik van tumororganoïden als modelsysteem voor een dergelijk voorspellend doel.

In **hoofdstuk 5** gebruiken we het co-cultuur systeem om modellen van primaire of verworven resistentie tegen immuuntherapie te genereren en analyseren. Om precies te zijn, is Werner-helicase (WRN) geïdentificeerd als een specifiek synthetisch-letaal doelwit bij mismatch-reparatie-deficiënte (dMMR) / microsatelliet-instabiele (MSI-H) kankers. We tonen aan dat WRN-afhankelijkheid behouden blijft in diverse modellen van primaire en verworven resistentie tegen doelgerichte, chemo- en checkpointremmertherapie, wat een sterk motief biedt voor de klinische ontwikkeling van specifieke remmers van kleine moleculen die gericht zijn op WRN.

In **hoofdstuk 6** focussen we ons op een beter begrip van de tumor-reactieve T-cellen die we hebben geïnduceerd door het samen kweken van tumororganoïden en autologe PBMC's. We presenteren HANSolo, HLA-Agnostic Neoantigen Screening, een high-

throughput genetisch platform voor gepersonaliseerde ontdekking van (neo)antigenen herkend door CD4+ en CD8+ T-cellen. We demonstreren dat we een onbevooroordeelde screening van T-celspecificiteiten in alle MHC-I- en -II-allelen mogelijk kunnen maken van individuele patiënten, door patiënt-gekoppelde geïmmortaliseerde B-cellen als APC's te gebruiken die coderen voor een bibliotheek die bestaat uit alle niet-synonieme tumorspecifieke mutaties.

Een algemene discussie van het in dit proefschrift gepresenteerde onderzoek kan gevonden worden in **hoofdstuk 7.**

PHD PORTFOLIO

Courses

October, 2016	Laboratory Animal Science (LAS) - Art. 9 certification	*Universiteit Utrecht*
March, 2017	Postgraduate course "ImageJ/FIJI imaging processing"	*OOA - Onderzoekenschool Oncologie Amsterdam*
November, 2017	Postgraduate course "Basic medical statistic"	*OOA - Onderzoekenschool Oncologie Amsterdam*
May, 2018	ENII Summer school in advanced immunology	*European Network of immunology Institutes*
November, 2018	Postgraduate course "Ethics and integrity in science"	*OOA - Onderzoekenschool Oncologie Amsterdam*

Supervision of students

August, 2019 - March, 2020	Supervision of 1st year PhD student	*Katholieke Universiteit Leuven, Belgium*
February, 2020 - November, 2020	Supervision of 1st year Master student, practical internship	*VUMC, Amsterdam, the Netherlands*
March,2020 - October, 2020	Supervision of 1st year Master student, literature study	*VUMC, Amsterdam, the Netherlands*

Conferences

October, 2017	OIO Retreat 2017	Poster presentation	*Renesse, The Netherlands*
May, 2018	XIII ENII summer school in advanced immunology	Poster Presentation	*Porto Cervo, Italy*
October, 2018	OIO Retreat 2018	Speaker	*Renesse, The Netherlands*
March, 2019	Keystone symposia "Cancer Immunotherapy: Mechanistic insights to improve clinical benefit"	Poster Presentation	*Whistler, Canada*
June, 2019	International PhD Student Cancer Conference (IPSCC)	Poster Presentation	*Amsterdam, The Netherlands*
September, 2019	META-CAN 2nd workshop	Speaker	*Leuven, Belgium*
November, 2019	NCRI Cancer Conference 2019	Speaker	*Glasgow, Scotland*
June, 2020	EACR 2020	Speaker	*(Virtual)*
October, 2020	32nd EORTC/NCI/AACR symposium	Speaker	*(Virtual)*

LIST OF PUBLICATIONS

Cattaneo C.M., Battaglia T.*, Urbanus J.*, Haanen J., Voest E.E.#, Schumacher T.N.#, Scheper W.#. **Identification of patient-specific T cell neoantigens through HLA-agnostic genetic screens.** Manuscript in revision, Nature Biotechnology.

Picco G., Cattaneo C.M., van Vliet E., Crisafulli G., Rospo G., Consonni S., Vieira S.F., Rodriguez I.S., Cancelliere C., Banerjee R., Schipper L., Oddo D., Dijkstra K.K., Cinatl J., Michaelis M., Yang F., di Nicolantonio F., Sartore Bianchi A., Siena S., Arena S., Voest E.#, Bardelli A.#, Garnett M.J.# **.Werner helicase is a synthetic-lethal vulnerability in mismatch repair–deficient colorectal cancer refractory to targeted therapies, chemotherapy and immunotherapy.** Cancer Discovery. 2021 March.

Cattaneo C.M.*, Dijkstra K.K.*, Fanchi L.F., Kelderman S., Kaing S., van Rooij N., van de Brink S., Schumacher T.N., Voest E.E. **Tumor organoids-T cells coculture systems.** Nature Protocols. 2020 Jan, (15): 15-39.

Dijkstra K.K.*, Cattaneo C.M.*, Weeber F., Chalabi M., van de Haar J., Fanchi L.F., Slagter M., van Der Velden D., Kaing S., Kelderman S., van Rooij N., van Leerdam M.E., Depla A., Smit E.F., Hartemink K.J., de Groot R., Wolders M.C., Sachs N., Snaebjornsson P., Monkhorst K., Haanen J., Clevers H., Schumacher T.N.#, Voest E.E.#. **Generation of tumor-reactive T cells by coculture of peripheral blood lymphocytes and tumor organoids.** Cell. 2018 Sept 6; (174): 1-13.

Gandaglia A., Brivio E., Carli S., Palmieri M., Bedogni F., Stefanelli G., Bergo A., Leva B., Cattaneo C.M., Pizzamiglio L., Cicerone M., Bianchi V., Kilstrup-Nielsen C., D'Annessa I., Di Marino D., D'Adamo P., Antonucci F., Frasca A., Landsberger N. **A novel Mecp2Y120D Knock-in Model Displays Similar Behavioral Traits But Distinct Molecular Features Compared to the Mecp2-Null Mouse Implying Precision Medicine for the Treatment of Rett Syndrome.** Molecular Neurobiology. 2018.

*, # *These authors contributed equally*

CURRICULUM VITAE

Chiara Maria Cattaneo was born on the 17th of October 1991, in Rho. She attended the Scientific Lyceum "Falcone e Borsellino", located in the province of Milano, obtaining her diploma on July 2010.

In the autumn of the same year she started her bachelor degree in Medical and Pharmaceutical Biotechnology at Vita-Salute San Raffaele University, in Milano. She graduated in 2013, with a bioinformatic thesis on the interplay between transcription factors and microRNA in regulatory gene expression networks. This research was performed under the supervision of Prof. L. Pattini and Prof. G. Casari, at Politecnico di Milano University and at Vita-Salute San Raffaele University, in Milano.

In 2013, she continued her education with a Master's degree in Molecular and Cellular Medical Biotechnology. She graduated in 2015, with an experimental thesis on the characterization of a new mouse model, carrying a newly discovered missense pathogenic mutation of the Mecp2 gene. This research was performed under the supervision of Prof. N. Lansdsberger and Prof. G. Ferrari, at Vita-Salute San Raffaele University, in Milano.

In 2016 she joined the group of Prof. E.E. Voest, at the division of Molecular Oncology and Immunology of the Netherlands Cancer Institute. Her major findings are described in this thesis.

In 2021, she will start her postdoc in Prof. A. Bardelli group, in Milano, Italy.

ACKNOWLEDGMENTS

… and finally, my last chance to add a few words to this book.

This thesis holds on paper the progresses of my scientific work, but this last four years have been much more than that. It has been a professional and personal journey: I learned what my strength and weaknesses are, I learned to cherish the happy moments, as well as how to face the difficulties; most importantly, I became aware of my value, acquiring a self-confidence I could only dream few years ago.

None of that would have been possible without the people I met along the way.

Emile, thank you. You gave me the mean and support to grow as an independent scientist. You stimulated me to always think ahead, to the next steps. You taught me when it is the right moment to step away from the details, and start looking at the bigger picture: a lesson that will always be part of me as a scientist. Thank you for your optimistic view, for making time for me every time I needed you, for rescuing me when I was going the wrong way. However, you also made me taste lasagna with bananas in it. That I will truly never forget.

Vivien and Wouter, my great paranymphs, thank you. **Vivien**, I am so happy you decided to come back to Amsterdam. I really valued you as a scientist: discussing ideas, projects and how to overcome problems just became natural with you around. I really treasured your opinion and suggestions. Most importantly, I valued you as a friend. In the working life, it was awesome having you to complain about everything, to share an incredible amount of snacks, to be the person I could always count on. But even more outside the lab: the baking, the online shopping, the calls, the wine drinking, the dinners, the complaining again, the gossiping, the sharing near-death-experiences… Thank you. You really made this crazy past year easier to handle.

Wouter, I am really happy we found each other in the department. The depth of your knowledge is amazing, the way you approach problems and how you solve them is really inspiring. Even more than that, the way you are always willing to help everyone made me wish, one day, to be as good of a scientist as you are. I have lovely memories of our meetings, with 90% of the time used for chit-chatting about everything, leaving

always only few minutes at the end for science. I loved working with you and I really hope we could keep doing it in the future. I grew to consider you not only as lab partner but also as a friend.

Chelsea and Christina, thank you. **Chelsea**, you are literally the first person I met when I arrived in Amsterdam. I loved you were also the last person I saw before leaving the Netherlands. I could spend hours talking about your talent as a scientist, or about how amazed I always am in front of your organization, your strength and your ability to solve any problems is on your way… But what I really thank you for is your friendship, your availability, your presence, your advice. You are a great example. I really value you as woman, as scientist and as mother.

Christina, how many good memories we shared at the beginning of our PhDs. I loved facing "the Dutch boys" with you, and making fun of them together (I still remember a particular google search I shall not repeat here!)! I think somewhere I still have the picture of the two of us, sitting very closely, working together in the same one-person-only-flowhood. I admire your attitude, both towards work and life. Your positivity and your fiercely facing the difficulties are really inspiring. And I can't wait to share another G&T with you.

Krijn, my first lab partner, thank you. In the first years of my PhD I learned so much, thank to you. You also introduced me to the beauty of immunology, even if - and I quote myself here - "I wanna do everything, except from immuno-stuff". We shared great laughs and great grumpiness together, and I will always cherish that.

The Voest (+1) group, thank you. Taken individually we are such a weird mix of A-type personalities, but together, somehow, we managed to success and have great fun. **Myriam**, your attention and care for the people around you always amazed me. In my mind, if I try to draw the perfect doctor, I get to a picture very similar to what you are. King **Joris**, we may sometimes have had fighting personalities, but I always valued your scientific opinion. I admire your ability to always ask the right questions, no matter the topic of discussion. Your social dominance and your humor will be missed! **Salo**, thank you for being The Salo. I have always been amazed by how your mind works in your organized chaos, and how successful and deep as a scientist you can be. Thank you for sharing great deep-into-the-internet videos with me, and thank you for all the snacks I

stole from you in the past years. **Sovann**, thank you for always been available to help and for sharing your parenting skills with us. Also, "smile from the inside" is now one of my most favorite sentences ever. **Tom**, from the first moment I met you I know you were going to be the perfect addition to the group. You are not only an insanely competent and reliable scientist, but you are most importantly real fun to work (and gossip) with. **Steven**, our adopted one. Thank you for bringing calm into the office during the most heated discussion. Thank you for your kindness, and for always be available to help and listen to my complaints. Thank you for all the non-politically correct discussions and jokes: "I think we should close the door". **Luuk**, you always surprised me with how fast you can generate crazy new interesting ideas. I think everyone should learn how to face life with the same enthusiasm you show everyday! **Pim**, the start of your PhD has not been the easiest, but I am sure you are going to do great. Thank you for saving me from Google Translate, thank you for not letting Vivien kill all of my plants, but most importantly, for being the voice of reason in the office in the past months. **Louisa**, I had so much fun working (and sharing a glass from time to time) with you. Thank you for bringing me to Italy the day of my birthday a couple of years ago. I really wish we can celebrate our PhDs together soon! **Laurien**, I appreciate your humor a lot. And thank you for introducing me to the best licorice in the world. Too bad that happened just few weeks before leaving the Netherlands, and I am now victim of a withdrawal syndrome! **Alice**, literally nothing in my PhD could have been completed without you. THANK YOU!
Thanks to all the other old and new Voesties, it was a pleasure to share part of my journey with you.

The B6(+1) department. The supportive and lively scientific atmosphere had a great impact on my formation. I have awesome memories of so many of you in the lab, at the PhD retreats and at the borrels. I will try to name a few. **Esmée**, I loved our updating moments. It was so nice to know that I could just pass by your office and share a laugh, a bad comment, a complaint, or a sweet with you. I know you are a brilliant scientist, but you are also an amazing and positive person to have around. Thank you. **Rhianne**, **Sanne** and **Saskia**, thank you for the chit-chatting, the gossip, the help and the "inappropriate skirt". I will miss your smiles when facing your office before going into the lab! **Jos** and **Mireille**, your infinite wisdom is a treasure. Thank you for sharing your knowledge with me. Thank you for all the advice, the teaching, the borrowing reagents I

forgot to order, for always sharing a smile. **Anne**, I had so much fun in Canada with you. It was the perfect conference. I learned I don't deal very well with fire ("Dangeroupts!"), and that I am clearly a city folk, madly scared by a stinkbug. It is also thank to you that now I can't spell anymore ~~preganananant~~ ~~prefnat~~ ~~pergonate~~… Oh well, I give up! **Meike**, I remember with so much fun the running very fast through all the posters at Renesse. It was so nice having you around in the lab, sharing some frustration and fashion advice. **Paulien**, **Ziva** and **Daniela**, you girls are so much fun. It was really a pleasure to share part of my journey with you. **Elselien**, I am so glad we randomly met at one of the PhD retreats. It was awesome to share frustration and lots of laugh with you. I can't wait for you (and Tom) to come visit!

To all the B6 PIs, thank you for being such a vast source of inspiration. **Daniel**, **Ton**, **John**, **Christian**, **Daniela** and **Pia**, I look up at you, hoping to follow your example. **Pia**, thank you for being so approachable and for all of your precious advice, I really treasure them all.

The core facilities, thank you. Your work has been fundamental for the completion of this thesis. **Martijn**, **Frank** and **Anita**, from the flow cytometry facility, thank you for always find the perfect solution to all of my problems; **Marjolijn**, **Lenny** and **Bram**, from the miscroscopy unit, to help me set the impossible organoids video; **Ron** and **Arno**, from the genomic facility, thank you for the speed and accuracy of your work.

Thank you to all the people, living close or far away, that contributed to make my life joyful outside the lab. **Valentina**, the other "Rhodense" in the Netherlands, and **Anna**, my first supervisor; **Simone**, **Francesca**, **Laura**, **Elena**, **Francesca**, and **Linda**, thank you for the support and for the life-long friendship. I can't wait for being back with you.

Thank you to my **family**. Sometimes, life has been very hard in the past four years. Knowing that, if the difficulties were getting unbearable, I could always come back, or ask for help, is what gave me freedom to always push a little harder, and achieve everything I wanted. Thank you for this opportunity.

Lastly, **Ale**. Thank you for giving me a new prospective. Thank you for being at my side and to love me, always, even when I am insane. Thank you for every single moment we spend together. I just cannot wait to spend the rest of my life with you.

The road goes ever on and on
Down from the door where it began.
Now far ahead the Road has gone,
And I must follow, if I can,
Pursuing it with eager feet,
Until it joins some larger way
Where many paths and errands meet.
And whither then? I cannot say.

J.R.R. Tolkien